UNIVERSITÀ DEGLI STUDI DI PALERMO
Dottorato in Scienze Molecolari e Biomolecolari
Dip. di Scienze e Tecnologie Biologiche, Chimiche e Farmaceutiche (STEBICEF)
Settore Scientifico Disciplinare CHIM06 (Chimica Organica)

PROPERTIES AND APPLICATIONS OF POLYAMINOCYCLODEXTRIN DERIVATIVES

(Proprietà e applicazioni di derivati poliamminociclodestrinici)

DOTTORANDO
Dott. MARCO RUSSO

COORDINATORE
Prof. PATRIZIA DIANA

TUTOR
Prof. MICHELANGELO GRUTTADAURIA

CO-TUTOR
Prof. PAOLO LO MEO

CICLO XXIX
ANNO CONSEGUIMENTO TITOLO 2017

Dedicated to my Parents

and Marisa

INDEX

Abstract

The potential applications of polyaminocyclodextrins were investigated in the present work. In particular, different polyaminocyclodextrin derivatives (**amCD**s) were obtained by exploiting a straightforward synthetic protocol based on the nucleophilic displacement reaction between *heptakis*-(6-deoxy)-(6-bromo)-βCD (**BrβCD**) and linear polyamines. Provided suitable NMR, ESI-MS and potentiometric characterization, different possible applications of these materials were investigated. First, the ability to give host-guest inclusion complexes with different organic guests was evaluated both for the free **amCD**s and for **amCD**-based nanosponge materials. The latter ones were synthesized by polymerization of **amCD**s with **BrβCD** and characterized by FT-IR, solid-state NMR, DSC, porosimetry and potentiometric titration techniques. In both cases, pH-tunable inclusion properties were found. The external binding abilities of **amCD**s, due to the presence of the polyamine arms, were also confirmed by using a model polyanion (alginate) and a plasmid DNA (pUC19). In the latter case, the ability to support possible DNA uptake and bacterial transformation was tested on a Ca-competent *E. coli* bacterial strain. Among the other possible applications, the already know ability of **amCD**s to stabilize silver nanoparticle (**AgNP**s) systems was exploited. Two different Ag/**amCD** nanoparticle systems were prepared and used as catalysts for the $NaBH_4$ reduction of aromatic nitrocompounds. The catalysts are characterized by a peculiar structure with the presence of a silver metal core, covered "onion-like" by different layers of **amCD**, which undergoes significant structural modifications during the reduction process (confirmed by TEM, DLS and UV-vis evidences). Analysis of the unexpected kinetic results using a modified Langmuir-Hinshelwood model, enabled to achieve a thorough elucidation of the reaction mechanism. The **amCD**s were also used for the synthesis of palladium nanoparticles, which were tested as catalysts for the Suzuki C-C coupling reaction. Once again, the results obtained show that the presence of the **amCD** plays a significant role in the reaction course.
The final section describes the activity carried on during a stage in the laboratories directed by prof. P. Shahgaldian of the FHNW University – Basel (Switzerland), on the photothermal activation of β-Galactosidase by means of cyclodextrin-capped gold nanoparticles.

*Nel presente lavoro sono state prese in esame le potenziali applicazioni delle poliamminociclodestrine. In particolare, diversi derivati poliamminociclodestrinici (**amCD**) sono stati ottenuti utilizzando un approccio sintetico diretto, tramite reazione di sostituzione nucleofila tra la heptakis-(6-deossi)-(6-bromo)-βCD (**BrβCD**) e poliammine lineari. Una volta effettuata l'opportuna caratterizzazione NMR, ESI-MS e potenziometrica, sono state investigate diverse possibili utilizzazioni di tali materiali. Anzitutto, sono state valutate le capacità di dare complessi di inclusione* host-guest *con diversi derivati organici sia delle **amCD** libere che di materiali costituiti da nanospugne a base di **amCD**. Questi ultimi sono stati sintetizzati per polimerizzazione di **amCD** con la **BrβCD**, e caratterizzati tramite tecniche FT-IR, NMR in stato solido, DSC, porosometriche e potenziometriche. In entrambi i casi sono state verificate proprietà di inclusione pH-modulabili. Le capacità di legame esterno delle **amCD** dovute alla presenza dei bracci poliamminici sono state anche confermate utilizzando un polianione modello (alginato) e un DNA plasmidico (pUC19). In quest'ultimo caso, le capacità di supportare l'eventuale trasporto del DNA e la trasformazione batterica sono state testate su cellule di E. coli Ca-competenti. Tra le altre possibili applicazioni, si sono sfruttate le già note capacità delle **amCD** di stabilizzare nanoparticelle di argento (**AgNP**). Due differenti sistemi nanoparticellari Ag/**amCD** sono stati preparati e usati come catalizzatori per la riduzione di nitrocomposti aromatici con $NaBH_4$. I catalizzatori risultano caratterizzati da una particolare struttura a cipolla, con un nucleo di argento ricoperto da diversi strati di **amCD**, la quale subisce significative modificazioni durante la reazione di riduzione (confermate da evidenze TEM, DLS e UV-vis). L'analisi degli inattesi risultati cinetici tramite un approccio tipo Langmuir-Hinshelwood modificato ha permesso di acquisire una approfondita*

elucidazione del meccanismo di reazione. Le ***amCD*** *sono state anche utilizzate per la sintesi di nanoparticelle di palladio, che sono state testate come catalizzatori per la reazione di* coupling *C-C di Suzuki. Di nuovo, i risultati ottenuti mostrano che la presenza della* ***amCD*** *gioca un ruolo significativo nel decorso della reazione.*

L'ultima parte della presente dissertazione descrive l'attività svolta in un periodo di stage presso il laboratorio di ricerca del prof. P. Shahgaldian della FHNW University di Basilea (Svizzera), riguardante l'attivazione fototermica di β-galattosidasi tramite nanoparticelle d'oro stabilizzate con ciclodestrine.

- 1 -

GENERAL OVERVIEW

1.1 - Cyclodextrins: structure, properties and applications

Since their discovery by Villiers in 1891,[1] ***Cyclodextrins*** (**CD**s) have known an increasing interest, as one of the most famous and studied class of supramolecular hosts. An impressive number of papers and reviews and an entire volume of "Comprehensive Supramolecular Chemistry" have been dedicated to them.[2] Dating from 1948, over 37000 publications (source: Scopus) focus on this subject, with a roughly linear increasing trend over the last thirty years (Figure 1.1). This accounts for the undoubted topicality and vitality of this research field, which may be confidently predicted to be even furtherly productive for long time in the future.

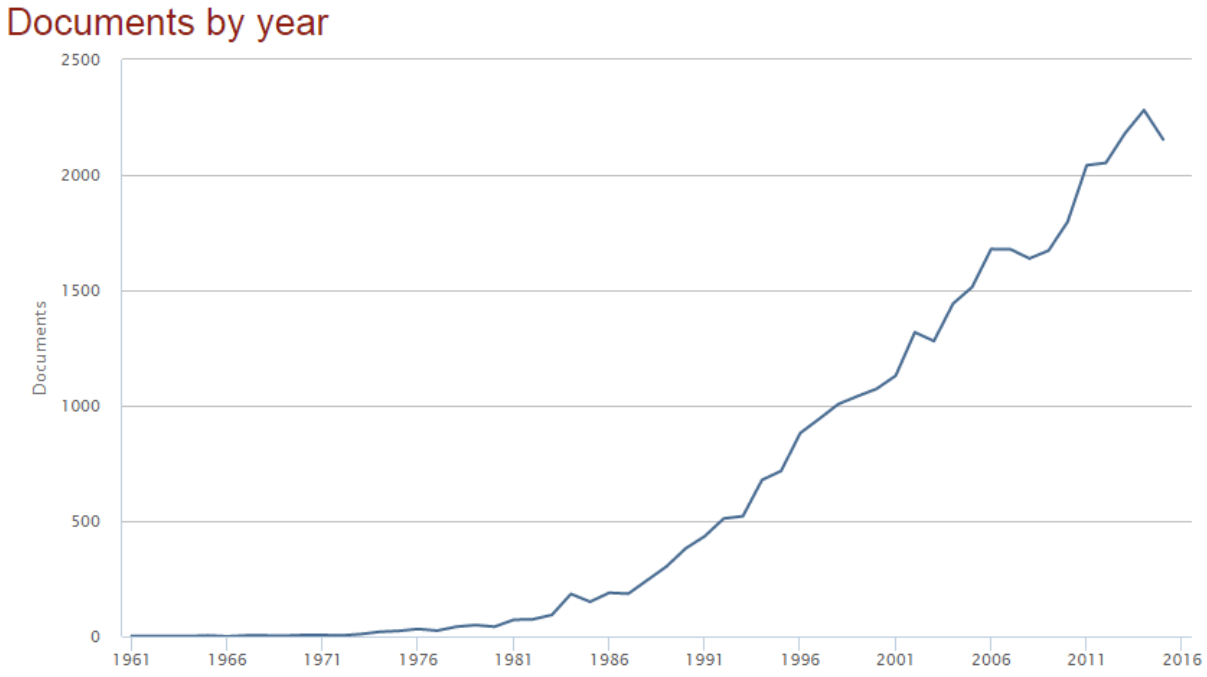

Figure 1.1 – Number of publications per year from 1961 on the topic "Cyclodextrin" (source: Scopus).

Cyclodextrins are cyclic oligosaccharides made up of α-glucopyranose units linked by 1,4 glycosidic bridges.[3,4] According to the number of glucopyranose units, the most important **CD**s known and studied are the **αCD** (six units), the **βCD** (seven units) and the **γCD** (eight units) (Figure 1.2). These are natural products deriving from enzymatic degradation of starch by means of the Cyclodextrin-Glucanotransferase enzyme (CGTase), produced by bacteria such as *Bacillus Amylobacter*[1] or *B. Macerans*.[5] Higher member **CD**s[6-8] (up to 26 glucose units, or even beyond), as well as the smallest five units member,[9] are known in literature, but they are mainly products of chemical synthesis and have been less extensively studied.

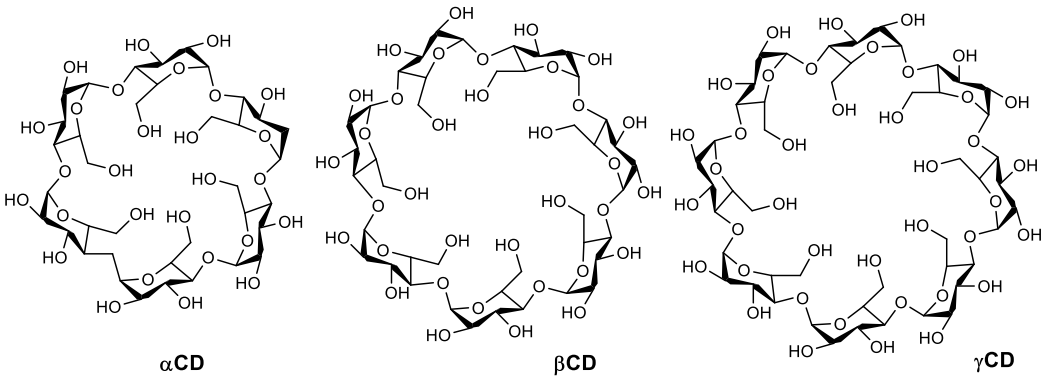

Figure 1.2 – Structures of Cyclodextrins.

CDs possess a torus-like structure with a cavity that is wider and wider in size as the number of glucopyranose units increases (Table 1.1) This kind of structure is characterized by the presence of a narrower edge (primary rim) and a wider edge (secondary rim). On the primary rim primary hydroxyl group on C6 reside, whereas in the secondary one reside the secondary hydroxyl group on C2 and C3. The inner wall of the cavity is featured by the presence of the H3 and H5 hydrogen atoms and of the ether-like oxygen of the glycosidic bridges. This confers an hydrophobic character to the cavity. Furthermore, the electron confinement of oxygen lone pair inside the **CD** cavity, gives rise to a local electric field. As a consequence, the primary and secondary rims respectively acquire a positive and negative polarity.[10-12]

The physical and chemical properties of **αCD**, **βCD** and **γCD** show quite regular trends, except for the water solubility that drop off in the case of **βCD** (Table 1.1).[4] The lesser solubility of **βCD** is related on one side to the odd number of primary hydroxyl groups, which break the hydrogen-bonded structure of water (having in turn an even number of hydrogen bond donors/acceptors groups).

Table 1.1 – Properties of Cyclodextrins

	αCD	**βCD**	**γCD**
Number of glucose unit	6	7	8
Molecular weight (g/mol)	972.85	1134.99	1297.14
Cavity diameter (Å)	4.7-5.2	6.0-6.4	7.5-8.3
External diameter (Å)	14.2-15.0	15.0-15.8	17.1-17.9
Depth (Å)	7.9-8.0	7.9-8.0	7.9-8.0
Internal cavity volume ($Å^3$)	174	262	472
Solubility in water (25°C, g/L)	145	18.5	232
Number of H2O molecules in the cavity	6	11	17
Melting point (°C)	250-260	255-265	240-245
pK at 25°C	12.332	12.202	12.081
[α_D](deg)	+150.5	+162.0	+177.4

On the other side, the presence of an effective homodromic intramolecular hydrogen bonds network between the secondary hydroxyl groups stiffens the overall structure and hampers the formation of hydrogen bonds with water. At this regard it is worth mentioning that the methylation of secondary hydroxyl groups increases the water solubility of **βCD**.[13] The lesser solubility of the title **βCD** in water is also the reason of the wider use of it with respect to the α and γ homologues: indeed, obtaining **βCD** by precipitation from aqueous solution is easier and cheaper.

The main reason why the chemistry of **CD**s is so much appealing is their ability to form host-guest inclusion complexes (which should more correctly addressed as "*cavitates*") with a wide range of diverse organic molecules,[14,15] together with their nontoxic and therefore biocompatible nature. As a matter of fact, the hydrophobic cavity of **CD**s provides a favorable microenvironment able to fit suitably sized and shaped molecular moieties, in such a way to form supramolecular host-guest complexes. The hydrophobic cavity, joined with the outer hydrophilic structure, allows also vehiculation and delivery of organic molecules in an aqueous environment.[16] For these reasons **CD**s have known a rapid diffusion in many application fields as: *i*) pharmaceutic used as drug delivery systems;[17,18] *ii*) cosmetic as main excipient of fresheners;[19,20] *iii*) food and agro industry as protecting agent for flavourings and nutrients;[21] *iv*) analytical chemistry as modified stationary phase in chromatographic separation[22] and so on[23,24]. Furthermore, the peculiar nature of **CD**s enables them to interact with biological membranes.[25,26] In particular, they can extract structural components as cholesterol[27,28] or phospholipids,[29] or alternatively, they can undergo internalization. In the last case, this allows the internalization of any possible included guest.

The formation of inclusion complexes with **CD**s has been thoroughly investigated in the last decades. Therefore, the thermodynamic aspects of the process and the driving forces implied at a microscopic level can to date considered quite well understood. Many energy contributions take part to the formation and stabilization of the inclusion complex, such as hydrogen bonding,

Van der Waals interactions, hydrophobic effects, electrostatic interactions.[14,15,30,31] Moreover, a crucial factor is the ability of the fairly flexible **CD** structure to undergo conformational change upon guest binding also known as "*induced fit effect*".[32,33] The latter process enables the host to maximize its interaction with the guest, enhancing the stability of the aggregate. Nevertheless, the main driving force of the complexation process is considered the release of high-energy water molecules from the hydrophobic cavity and the hydrophobic effects.[16] The release of water molecules provides a favourable enthalpy contribution, because these molecules are clustered and do not interact properly with the cavity walls, then upon re-join with the bulk solvent a number of hydrogen bonds are formed. The hydrophobic effect provides a mainly entropic favourable contribution. It is possible to illustrate this taking into account that presence of free **CD** and guest in solution implies the formation of two holes in the water framework, which force the water molecules to organize themselves and provide a solvation cage around the **CD**, or to minimize the contact with the usually non-polar guest molecules. After the formation of the complex has occurred, holes in the water structure are suppressed, with a net entropic gain due to the partially recovered dynamic nature of hydrogen bonding structure of water. Of course, upon complex formation a number of non-covalent interactions occur, according to the nature of **CD**, guest and solvent;[34,35] for this reasons it is not possible to docket each complexation process as enthalpy- or entropy-driven, and an enthalpy-entropy compensation effect is frequently observed.[15,36,37] The latter issue has been strictly debated in literature. Indeed, is necessary to consider that the formation of an inclusion complex is an equilibrium process, with an equilibrium constant critically depending on the free energy change associated to the system upon complex formation. The decrease in free energy is related to the specific and selective interactions between **CD** and guest involved.[34,36,38-40]

1.2 – Chemical modification of cyclodextrins

Chemical derivatization of native **CD**s is an appealing issue, because it can involve a modification of both the physicochemical properties and the binding abilities of the title molecule, and may open the way to new and interesting applications such as catalytic or enzyme-mimetic systems or tailored drug delivery vectors. However, it is often quite a challenge, because of the already highly functionalized nature of the native molecule. The presence of so many hydroxyl groups and their different reaction features do not allow to set up an easy and a priori general synthetic route. The only chance to obtain the desired product is mainly exploiting the different features of the hydroxyl groups[41,42] namely: *i*) the lesser

hindrance of primary -OH groups on C6 position; *ii*) the fair acid character of secondary C2-OH groups; *iii*) the steric hindrance of C3-OH groups.

Regioselective modification of C6-OH groups can be accomplished under neutral conditions, since they are more nucleophilic than the secondary ones. A general synthetic route provides the replacement of the primary -OH groups with better living groups such as *p*-toluensulphonyl group or halogen atoms, which can be afterwards displaced with the desired derivatizing group. Hydroxyl groups on the secondary rim are less reactive due to the rigid nature of this edge, as well as for the presence of the intramolecular hydrogen bond network. Although the nucleophilic character of these -OH may be improved under strongly alkaline conditions, their regioselective modification is unviable (especially for the less reactive C3-OH), owing to the occurrence of large amounts of by-products. In particular, if a leaving groups is present on the C6 positions, strongly alkaline conditions can result in an intramolecular cyclization reaction by alkoxy groups C3 position giving 3,6-anhydro products. Then for the selective modification of the secondary rim it is previously required to protect the primary -OH groups, usually as silylethers. Subsequent reaction with electrophilic species such as acyl chlorides or tosyl-chlorides in stoichiometric amount (1:1 mol:mol) usually involves the more acidic (2)-OH groups. However, it is important to stress that under these conditions complex mixtures of products (mono- and bis- derivatives) are usually obtained, which are often difficult to purify by chromatography. Moreover, the *mono*-2-tosyl **CD** derivatives undergo under alkaline conditions an intramolecular elimination process, affording a *mono*-manno-2,3-epoxide that, after reaction with a nucleophile, ultimately leads to a *mono*-altro-derivative bearing the nucleophilic substituent at the 3-position of the altrose ring (Figure 1.3).

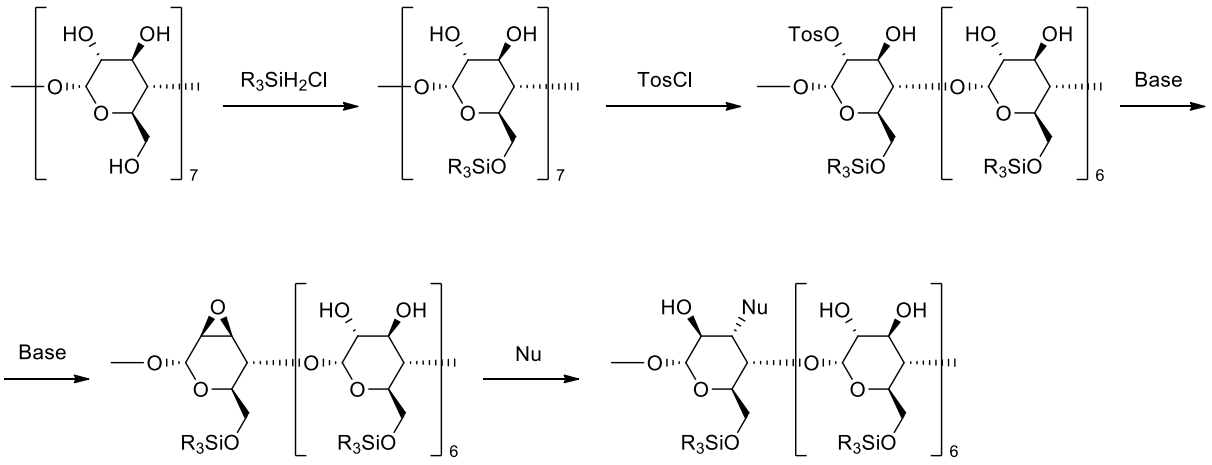

Figure 1.3 – Possible chemical transformations of **CD**s.

Of course, the reaction of the formely protected **CD** with an excess of electrophilic agent, affords the corresponding perfacial derivative. Final deprotection of the primary -OH groups can be accomplished in all cases by reaction with a fluoride ion source such as TBAF.

Considering the reactivity of the hydroxyl groups, it is also necessary to take into account that the derivatizing agent could give rise, depending on its structure and the different cavity volume of the employed **CD**s, to an inclusion complex with **CD**. This may affect the substitution on a specific site, in term of yield and selectivity. Finally, it is also necessary to consider the possible role of the solvent, which can compete for the inclusion in the **CD** cavity, affecting the selectivity of derivatizing process as well.

In term of degree of substitution, the possibility to achieve the mono-, bis-, perfacial or exhaustive derivatization have been explored in detail. Of course, in the first three cases, other than the number of equivalents of the derivatizing agent used, it is necessary to remind that the subsequent introduction of a derivatizing group becomes more and more difficult as the number of groups increases, especially on the crowded secondary rim. However, the exhaustive substitution of all three positions is paradoxically the easiest choice, because it is only necessary to place the **CD** in the presence of a very large excess of derivatizing agent.

As it was mentioned previously, the modification of **CD**s allows to confer them peculiar characteristics, either as physical properties, for example varying their solubility, or using specific derivatizing agent providing **CD**s with suitable chemical properties, allowing them to act as catalysts,[43,44] enzyme-mimetic systems,[45,46] photoreactors[47] etc.[48] In the latter cases the nature and size of the desired derivatizing group plays an important role in determining the better synthetic route. As the derivatizing group structure becomes more and more complex, it is possible to choose between alternative strategies, namely a top-down or a bottom-up approach. The former one consists in the direct insertion of a previously synthetized derivatizing group on the **CD** scaffold, whereas the latter one, provides the progressive construction of the desired derivatizing group on the **CD** scaffold starting from smallest components and following the most suitable series of reactions. The last approach mirrors the rationale behind the synthesis of dendrimers.[49,50] The latter class of macromolecules have become a widespread research topic, due to their almost limitless applications, ranging from the biomedical field (in which they have been used as drug or gene carrier/delivery systems), [51,52] to the material chemistry (sensors, light harvesting agents, confined nano-reactors, capping agents for stabilization of metal nanoparticles).[53]

In the last years attempts have been done in order to join dendritic structures to **CD**s[54] by building up dendritic arms on the **CD** scaffold. Thereby a dendrimer-like structure equipped

with a receptor site could be obtained. In particular, ***polycationic CDs***[55,56] bearing polyamine arms have been prepared by some research groups, basically following a top down strategy. In particular, the syntheses have been accomplished either anchoring an alkinyl polyamine to the *heptakis*-(6-deoxy)-(6-azido)-**βCD** by exploiting the Cu(I)-catalysed azide-alkyne cycloaddition reaction,[57-59] or reacting an isothiocyanate fuctionalized polyamine with the *heptakis*-(6-deoxy)-(6-cysteamyl)-**βCD**.[55] (Figure 1.4)

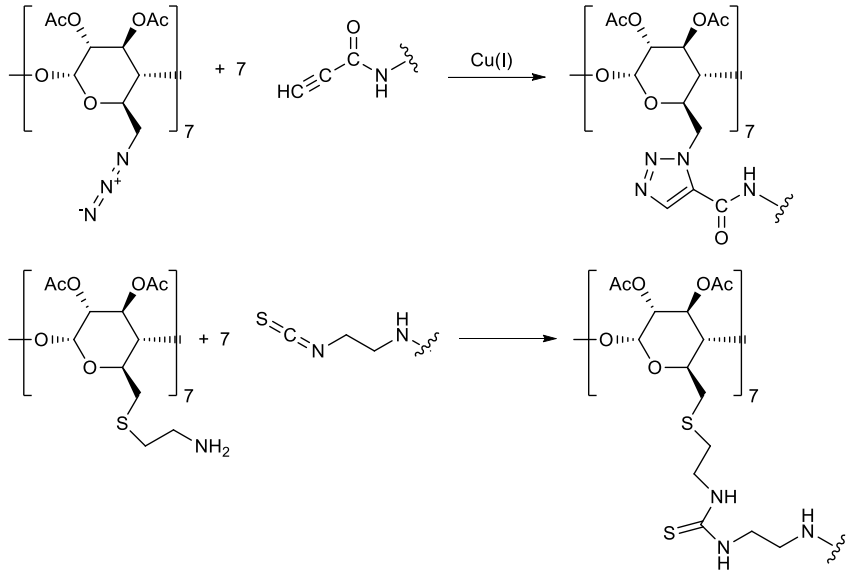

Figure 1.4 – Syntheses of polyaminocyclodextrins.

The obtained **CD** derivatives have been widely studied as gene delivery systems (as will be discussed afterward), but unlike dendrimers their potential ability to work as capping agent for the synthesis and stabilization of metal nanoparticle systems has not been investigated yet, as well as the use of such as catalysts systems towards different class of reactions. On the other hand, native and modified **CD**s have been already used for the stabilization of Rh, Ru, Pd and FePt nanoparticles.[60,61] In particular, *heptakis*-(6-deoxy)-(6-thiol)-β**CD** has been undoubtedly the most important and used modified cyclodextrin for the stabilization of Au,[62] Ag,[63] Pt and Pd[64] nanoparticles.

1.3 - Aim of the work

In the last few years in the research group in which the present PhD project was managed, a new synthetic straightforward protocol to obtain polyaminocyclodextrin (**amCDs**) derivatives has been developed.[65] This protocol relies on the direct nucleophilic displacement reaction between a suitable polyamine and a *heptakis*-(6-deoxy)-(6-halo)-β**CD** derivative. The latter

one, in turn, is easily accessible from a native **βCD** using the Vilsmeier-Haack reaction with Br_2 or I_2 and triphenylphosphine. Noticeably, as shown by NMR and ESI-MS evidences, the resulting products are not pure compounds, but rather non-separable mixtures of **CD** derivatives with a different number of polyamine arms, ranging from 3 to 7, and characterized by the presence of retained hydrohalic acid as well. This is due to the occurrence of poly-substitution reactions by already linked polyamine arms on the **CD** scaffold, towards other halogen atoms present on the nearby glycoside moieties. In any case, a quantitative characterization of the mixture by potentiometric titration allowed defining their average composition. Nevertheless, the **amCD** products obtained in this way have been proven to be good candidates for virtually any application. In particular, preliminary tests showed that they preserve the typical feature of **CD**s to give inclusion complexes with *p*-nitroaniline derivatives, and that they can be used for the stabilization of silver nanoparticles. The latter ones, in turn, were prepared by chemical reduction of the well-known Tollens' reagent (ammoniacal silver nitrate) with formaldehyde in presence of the **amCD**s.

As work for my Chemistry Ms. Thesis, I successfully performed a preliminary study on the possibility to exploit **amCD**-capped silver nanocomposites as catalysts for the reduction of nitroarenes under mild conditions ($NaBH_4$). My results showed the occurrence of a peculiar mixed zero-first-order kinetic course, evidencing the fact that several aspects of the reaction mechanism had not yet been satisfactorily addressed in previous literature, and could not be considered well understood. Starting from this information background and from the aforementioned present state-of-the-art related to polyamine/polycationic **CD**s, this PhD project focused on a surveying investigation of the potential applications of **amCD**s. In particular, the work was articulated as follows.

As a first step, the synthesis of new members of the already exististing small **amCD**s library was explored, according to the previously developed protocol. The new products were subsequently characterized by NMR, ESI-MS and potentiometric titration techniques (Chapter 2). Then the binding abilities of these products were explored, aiming in particular to verify their possible use as bimodal ligands, i.e. able to form supramolecular complexes by exploiting both the **CD** cavity and the polyamine pendant arms. For this purpose, their interaction with some *p*-nitroaniline derivatives and with sodium alginate, as a model polymeric anion, was studied (Chapter 3). This study was preparatory to investigate the possible application of **amCD**s as gene delivery systems. In particular, a plasmidic DNA such as pUC19 was used to study its interaction with **amCD**s; then, the obtained **amCD**-pDNA aggregate was tested in

order to perform gene delivery, and in particular bacterial transformation. For the latter purpose, a Ca-competent *E. coli* cell strain was used (Chapter 4).

As a second step, **amCD**s were used for the synthesis of new adsorbent materials obtained by cross-polymerization with **BrβCD**. This kind of materials can be included in the recently emergent class of ***nanosponges*** (Chapter 5). The materials obtained were characterized by means of FT-IR, DSC, Porosimetry, solid-state NMR and potentiometric titration techniques, in order to define their structures. The pH-tunable absorption/sequestering ability of the nanosponges was then spectrophotometrically assessed towards three different class of guests, namely *p*-nitroaniline derivatives, dyes and nutraceuticals at different pH values.

A further important investigated application of **amCD**s was their ability to stabilize Ag and Pd metal nanoparticles, which were used in turn as catalysts for the nitroarene reduction reaction and for the Suzuki coupling reaction respectively (Chapter 6). In particular, **AgNP** systems were subjected to careful characterization by means of TEM, DLS and ATR-FTIR techniques, in order also to evaluate the modification they may undergo during the catalytic process. Moreover, the nitroarene reaction itself was subjected to a systematic mechanistic investigation, addressing in particular the effects of the electronic and steric features of the organic substrate, as well as the effect of the concentration of the catalysts. Interesting unexpected kinetic effects were observed, which were explained on the grounds of a complex mechanistic scheme. Regarding the Suzuki reaction, the effect of the **amCD** structure on the reaction course was particularly addressed. Moreover, considering the recognized antibacterial properties as well as the photosensitivity of silver salts, attention was paid in investigating the antibacterial properties of **amCD**-capped **AgNP**s prepared by a "*bio-friendly*" synthetic protocol, just exploiting the photoreduction process of Ag^+ (Chapter 7). The Ag^+ photoreduction process was studied in detail, even from a mechanistic point of view, taking into account the different factors which can affect it, namely: *i*) type of light source and wavelength used; *ii*) the structure of the **amCD** used as the capping agent; *iii*) the possible presence of bio-compatible co-reductant species such as citrate, ascorbate or glucose; *iv*) the irradiation source. The antibacterial activity of the **AgNP** composites obtained were then assessed both on Gram-negative (*E. coli*) and Gram-positive (*K. rhizophila*) bacterial strains, with and without the presence of a typical β-lactam antibiotic as ampicillin, in order to evaluate a potential synergistic effect, considering also that the presence of cyclodextrins on **AgNP**s surface could provide a receptor site for the ampicillin.

Finally, the last section of this PhD thesis describes the preliminary results obtained during a stage period in the Prof. Shahgaldian's laboratories at the FHNW University, Basel (Chapter

8). In particular, **CD**-capped gold nanoparticles were synthesized and used to perform thermo-activation of β-Galactosidase anchored on a suitable polymeric support, by means of light-to-heat conversion. Enzyme activity was successfully tested towards a model substrate such as *o*-nitrophenyl-β-galactopyranoside (**ONPG**); kinetic data obtained spectrophotometrically were analysed by means of a classical Michaelis-Menten approach.

- 2 -

SYNTHESIS AND CHARACTERIZATION OF POLYAMINOCYCLODEXTRINS

2.1 - The synthetic protocol

According to the previously reported synthetic protocol,[65] seven **amCD** derivatives were synthesized. Basically, the synthetic protocol provides the previous modification of native **βCD** into the *heptakis*-(6-bromo)-(6-deossi) **βCD** (**BrβCD**)[66,67] and the subsequent replacement of bromine atoms by a S_N2 type reaction with the desired polyamines (see Experimental section). The polyamines used as derivatizing agents are in any case linear diamine or polyamine molecules, characterized by an increase in number of either the aliphatic carbon atoms or the nitrogen atoms present. In particular, 3-(*N*,*N*-dimethylamino)-1-propylamine (**Am1**) for **amCD1,** 3,3'-diamino-*N*-methyl-dipropylamine (**Am2**) for **amCD2**, 1,2-bis(3-amino-propyl-amino)-ethane (**Am3**) for **amCD3**, tetraethylenepentamine (**Am4**) for **amCD4**, pentaethylene-hexamine (**Am5**) for **amCD5**, 1,6 diaminohexane (**Am6**) for **amCD6** and 1,8 diaminooctane (**Am7**) for **amCD7** were used. (Figure 2.1)

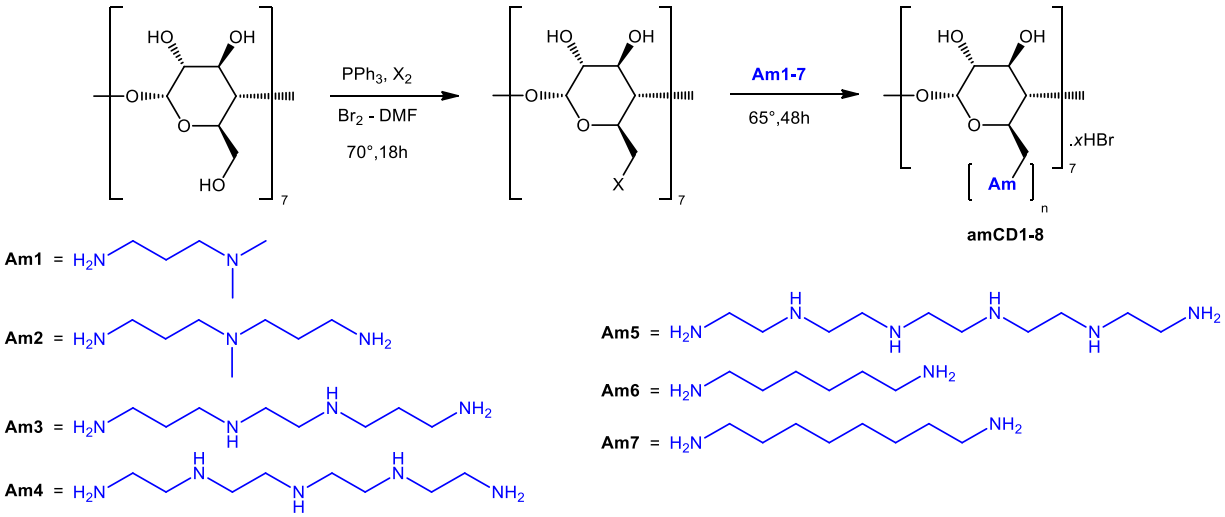

Figure 2.1 – Synthesis and structures of **amCD**s.

It is worth stressing here that the aminolysis reaction is carried out using a 20-fold excess of polyamine equivalents with respect to the **BrβCD** (which correspond to a 140:1 molar ratio), which functions as reaction solvent as well. Such a large amount of polyamine is used in order to ensure the exhaustive substitution of all bromine atoms and statistically maximize the mono-substitution of each polyamine unit towards a single bromine atom, thereby obtaining **amCD**s bearing seven polyamine arms each. Indeed, the excess amine can be recovered during the work-up of the reaction crude.

In each case it was not possible obtain only the *heptakis*-substituted product characterized by a C_7 symmetry, due to the occurrence of poly-substitution phenomena. In fact, a single molecule of polyamine is able to replace more than one bromine atoms present on the same **CD** scaffold leads to the formation of bridge between the glucose moieties of the **CD** (Scheme 2.1).

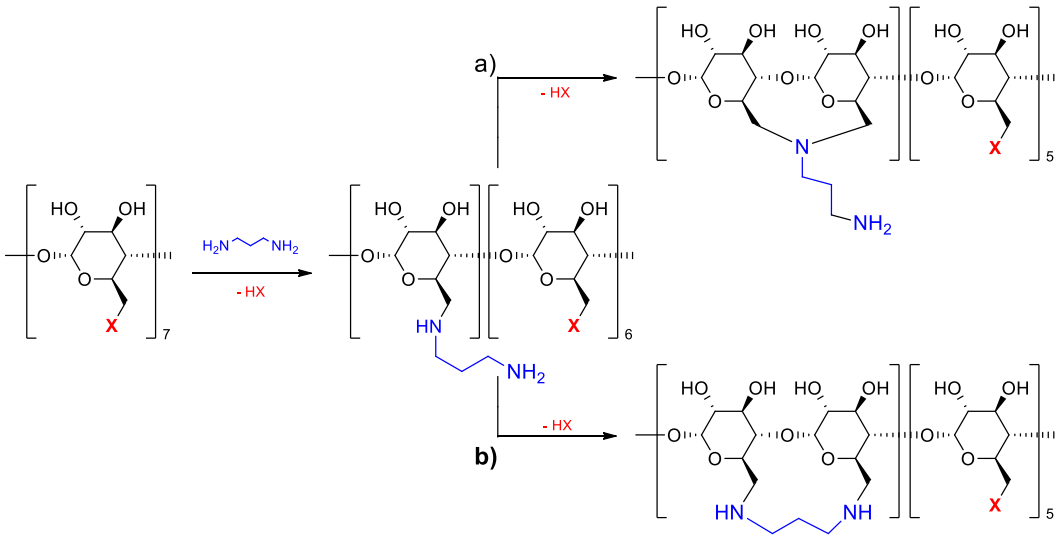

Scheme 2.1

In such a way, although all bromine atoms are actually displaced, not only the *heptakis*-substituted products were obtained, but rather a not separable mixture of products, characterized by a different number of polyamine arms on the **CD** scaffold. This event was also confirmed by NMR and ESI-MS analysis.

2.2 – Characterization of the amCDs

2.2.1 – NMR and ESI-MS characterization

The ^{1}H-NMR spectra of **amCD**s generally present a relatively poor definition of the signal multiplicity and a bad quality of the baseline, probably owing to the concomitant of relatively slow self-inclusion of the polyamine pendant groups; overall resulting in a substantial impossibility to perform a reliable signal integration (Figure 2.2 reports the spectrum of **amCD2**

as a representative example). Nevertheless, some signals are still easily recognizable. In particular, the signal relevant to the anomeric H atoms at ca. 4.9 ppm can be immediately identified. Moreover, in almost all the spectra (except for **amCD4** and **amCD5**) was also possible to distinguish a broad signal centred at ca. 1.6 ppm, corresponding to the methylene H atoms at the 2-position with respect to the N atoms of the polyamine chains.

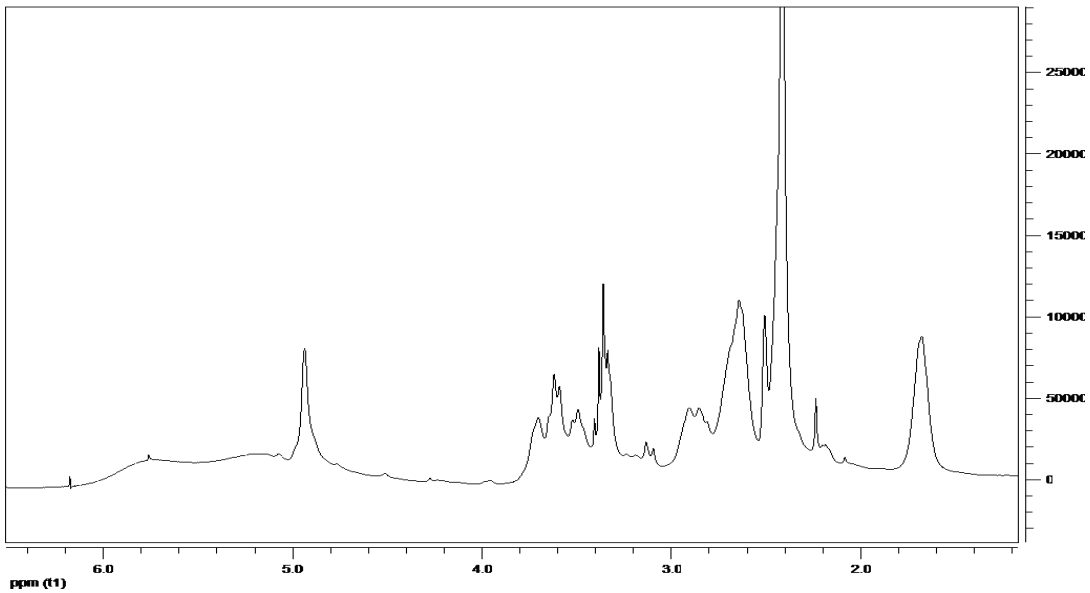

Figure 2.2 – ^{1}H-NMR spectrum (DMSO) of **amCD2**.

The ESI-MS technique is more suitable to analyse product mixtures, owing to the nearly complete absence of fragmentation processes. The resulted ESI-MS spectra show in each case a complex pattern of signals, which can be subdivided in different family peaks according to the ions charge. It is worth noting that spectra usually show from bi- up to hexa-positive ions, whereas mono-positive ions are not detected. Each zone brings in principle the same information, namely the relative amount of each species, characterized by a certain degree of substitution, according to the m/z value of the family peaks (Figure 2.3 shows the ESI-MS spectrum of **amCD2**, as a typical example). It is not possible to have a quantitative estimation of the mixture composition but rather know the different species that compose it. Generally, in each mixture it was observed the presence of product bearing from 3 to 7 polyamine arms, with a substitution degree as closer to the maximum value as the number of nitrogen atoms on polyamine chains decrease. Indeed, at this regard, the ESI-MS spectra of **amCD4** and **amCD5** have shown only the presence of species bearing 2 or 3 polyamine pendants. This peculiar result in comparison for instance with the case of **amCD3** (which presents four N atoms on the polyamine chain), might be related also to the presence of the ethyl linkers between nitrogen atoms. Indeed, the length of this spacer could match with the distance between the glucose C6

position, thereby favouring the poly-substitution phenomena. Then, for this reason, it was ruled out to explore the possible applications of these two derivatives. Moreover, by ESI-MS it was also sees as to the different species in the mixture a certain number of hydrogen bromide (HBr) molecules, are associated. The latter finding indicates that the reaction products obtained have been actually isolated as partial hydrobromides.

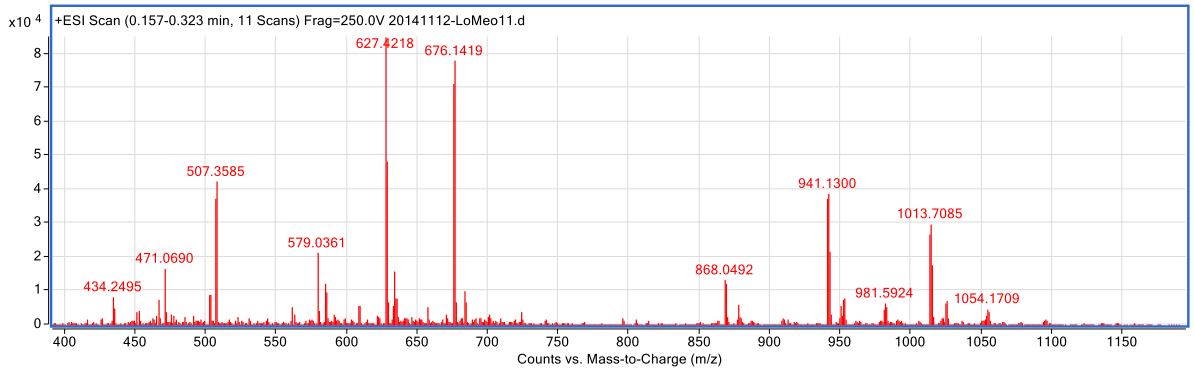

Figure 2.3 – ESI-MS spectrum of **amCD2**.

2.2.2 – Potentiometric tritation

In order to have a quantitative characterization of the **amCD1-3** and **amCD6-7** products, their potentiometric titration was carried out. In particular, a solution obtained dissolving the **amCD** product in the presence of an excess of a strong acid (HCl), was titrated with a standard strong base (NaOH). All the titration curves obtained (a representative example is depicted in Figure 2.4) present a first equivalence point, corresponding to the titration of the excess strong acid, followed by a large smooth region originated by the overlapping of the multiple equivalence points relevant to the different **CD** species in the reaction product.

The experimental titration curves were then subjected to a non-linear regression analysis using a fitting equation obtained considering the analysed systems as a mixture of a certain number of fictitious independent monoprotic weak virtual bases $\mathbf{B}_i$. On performing this kind of analysis, it was found that in the case of **amCD1-3** the experimental curves are satisfactorily described using a four bases fitting model, whereas for **amCD6** and **amCD7** a three weak bases model was considered. (Eq. 2.1)

$$\frac{v_i}{V_o} = \frac{\frac{n_{HCl} + n_{HI}}{V_o} + [OH^-] - [H^+] - N\tilde{n}\sum_{i=1}^{n}\left(\chi_i \frac{[H^+]}{[H^+] + K_{B_iH^+}}\right)}{c_{NaOH} + [H^+] - [OH^-]} \qquad (2.1)$$

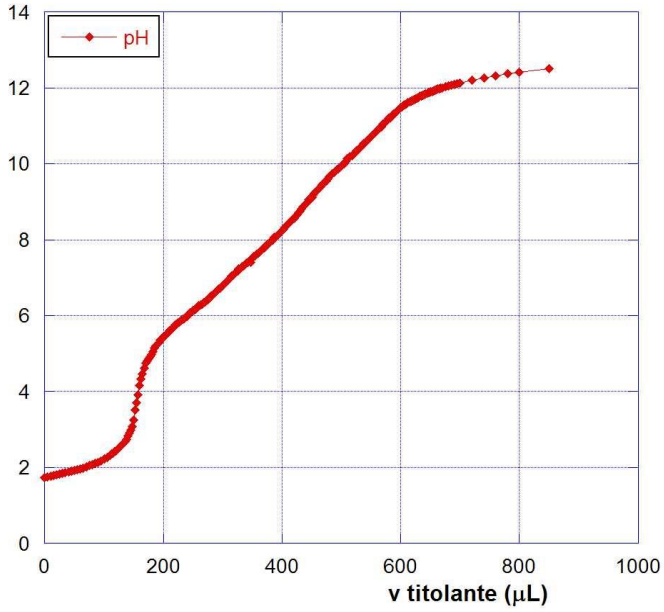

Figure 2.4 – Typical titration curve for **amCD**s.

where V_0 is the initial volume, v_i is the volume of titrant base added, $\boldsymbol{n_{HCl}}$ and $\boldsymbol{n_{HBr}}$ are respectively the moles of HCl and HBr in the sample, $\boldsymbol{N}$ is the number of nitrogen atoms per polyamine unit (i.e. N = 2 for **Am1**, **Am6** and **Am7**; N=3 for **Am2**; N=4 for **Am3**), $\boldsymbol{c_{NaOH}}$ is the concentration of the titrant. Then from the regression data it was possible to calculate the average number of polyamine linkers ($\tilde{\boldsymbol{n}}$) and retained HBr molecules ($\boldsymbol{x}$) per **βCD** unit, together with the apparent mole fractions ($\boldsymbol{\chi_{Bi}}$) and $\boldsymbol{pK_{BiH}}^{+}$, values of the virtual weak bases. These data, were finally used to calculate the corresponding average molecular weight **MW**, as well as the average equivalent weight **EW** for each **amCD** (results are summarized in Table 2.1).

Table 2.1 – Analitical data for **amCD**s

		amCD1	**amCD2**	**amCD3**	**amCD6**	**amCD7**
	$\tilde{\boldsymbol{n}}$	5.9 ± 0.2	5.8 ± 0.3	4.5 ± 0.1	5.5 ± 0.1	7.4 ± 0.2
	$\boldsymbol{x}$	4.0 ± 0.2	5.2 ± 0.4	5.4 ± 0.2	4.4 ± 0.2	4.7 ± 0.1
	$\boldsymbol{n_{(N)}}$	11.8 ± 0.4	17.4 ± 0.9	18.0 ± 0.4	11.0 ± 0.4	14.8± 0.4
	MW	1940 ± 60	2270 ± 70	2230 ± 40	2010 ± 10	2460 ± 30
	EW	164 ± 5	130 ± 4	124 ± 2	182 ± 2	166 ± 2
$\mathbf{B_1}$	χ_{B1}	0.23 ± 0.02	0.30 ± 0.02	0.24 ± 0.01	–	–
	pK_{B1H^+}	5.7 ± 0.1	5.6 ± 0.1	4.8 ± 0.1	–	–
$\mathbf{B_2}$	χ_{B2}	0.26 ± 0.01	0.24 ± 0.01	0.24 ±0.01	0.32 ± 0.01	0.32 ± 0.01
	pK_{B2H^+}	6.7 ± 0.1	7.1 ± 0.1	6.6 ± 0.1	6.8 ± 0.1	6.5 ± 0.1
$\mathbf{B_3}$	χ_{B3}	0.28 ± 0.02	0.20 ± 0.02	0.26 ± 0.01	0.32 ± 0.01	0.34 ± 0.02
	pK_{B3H^+}	8.6 ± 0.1	8.5 ± 0.2	8.5 ± 0.1	8.2 ± 0.1	8.0 ± 0.1
$\mathbf{B_4}$	χ_{B4}	0.23 ± 0.02	0.26 ± 0.01	0.26 ± 0.01	0.36 ± 0.02	0.34 ± 0.02
	pK_{B4H^+}	9.7 ± 0.1	10.1 ± 0.1	10.1 ± 0.1	10.2 ± 0.1	10.2 ± 0.1

From data reported in Table 2.1 it is possible to notice that the average degree of substitution roughly decreases on increasing the structural complexity of the polyamine, while the number of retained HBr molecules per **CD** does not show an apparent rationale, mainly because the amount of HBr actually retained depends also on the number of precipitation/purification steps the product is subjected to (see in the Experimental section). Finally, it is worth noting that in the case of **amCD7** a ***ñ*** value higher to 7 was found. This can be explained considering that the hydrophobic **CD** cavities is able to give a stable inclusion complex with the 1,8 diaminooctane, indeed also after Soxhlet extraction with Et_2O it was not possible to remove this diamine excess.

2.3 - Experimental section

Materials and instrumentation

All commercial materials needed were used as purchased (Aldrich, Fluka) with no further purifications. The non-commercial *heptakis*-(6-deoxy)-(6-boromo)-**βCD** (**BrβCD**) was prepared according to literature.[66] The ^{1}H and ^{13}C NMR spectra (DMSO-*d*6) of **amCD**s were recorded on a Bruker AS 300 MHz instrument; high-resolution ESI-MS mass spectra were acquired in positive mode on an AGILENT Technologies 6540 UHD Accurate Mass Q-TOF LC-MS apparatus (1 kV nozzle voltage, 250 V fragmentor voltage).

*Synthesis of polyaminocyclodextrins **amCD1-amCD7***

The **AmCD**s were prepared according to the procedure illustrated elsewhere.[65] In general, **BrβCD** (315 mg, 0.2 mmoles) was mixed with a 20-fold excess (28 mmoles) of the proper polyamine, namely 3.5 mL (2.86 g) of **Am1**, 4.75 mL (4.08 g) of **Am2**, 5.15 mL (4.90 g) of **Am3**, 3.25 g of **Am6**, 4.04 g of **Am7**,. The mixture was kept in an oil bath at 60 °C under inert atmosphere and stirring for 48 h. Then, 20 mL of methanol were added to the reaction crude, and the resulting solution was added dropwise under vigorous stirring to 250 mL of cold diethyl ether. The system was allowed to settle for a few hours and then decanted, giving a brownish slurry, which was dissolved in 10 mL of methanol and again dropped under stirring into 200 mL of diethyl ether, to afford a second amorphous solid. This dissolution-precipitation procedure was repeated other two or more times, until a pale yellow solid was obtained. The product was finally filtered off and dried under vacuum overnight at 50 °C.

***Poly*-(6-deoxy)-[6-(3-dimethylamino-1-propylamine)]-βCD amCD1**. Yield 94% (365 mg). ^{1}H NMR (DMSO-d_6): δ 1.56 (br s, -CH_2-CH_2-CH_2-); 2.51, 2.60 (two overlapp br s, >N-CH_2-); 2.71 (br m, NH_2-CH_2- and H(6)CD); 3.31 (br s, H(2)CD); 3.40 (br s, H(4)CD); 3.60, 3.66 (two overlap. br m, H(3)CD and H(5)CD); 4.80 (br s, -O*H*, -N*H*-); 4.94 (br s, H(1)CD). ^{13}C NMR:

δ 31.21 (-CH_2-*C*H_2-CH_2-); 38.68 (NH_2-*C*H_2-); 47.41 (>N-*C*H_2-); 49.12-49.86 (cluster, C(6) CD); 70.73 (C(5)CD); 72.71 (C(2)CD); 73.27 (C(3)CD); 83.25-83.90 (cluster, C(4)CD); 102.28-102.97 (cluster C(1)CD). High resolution ESI-MS (*m/z*): 1724.1122 [$C_{77}H_{154}N_{14}O_{28}$ ·H]$^+$ (calcd. 1724.1130); 902.5244 [$C_{77}H_{154}N_{14}O_{28}$·HBr·2H]$^{2+}$ (calcd. 902.5232); 873.5506 [$C_{77}H_{154}N_{14}O_{28}$·Na·H]$^{2+}$ (calcd. 873.5510); 862.5601 [$C_{77}H_{154}N_{14}O_{28}$·2H]$^{2+}$ (calcd. 862.5601); 811.5021 [$C_{72}H_{140}N_{12}O_{28}$·2H]$^{2+}$ (calcd. 811.5023); 760.4445 [$C_{67}H_{126}N_{10}O_{28}$·2H]$^{2+}$ (calcd. 760.4444); 582.7027 [$C_{77}H_{154}N_{14}O_{28}$·Na·2H]$^{3+}$ (calcd. 582.7031); 575.3761 [$C_{77}H_{154}N_{14}O_{28}$ ·3H]$^{3+}$ (calcd. 575.3758).

***Poly*-(6-deoxy)-{6-[(N-methyl-N-(3-aminopropyl)-3-amino)-1-propylamine)]-βCD amCD2**: yield 422 mg (93 %); ^{1}H NMR (DMSO-*d*6) δ (ppm): 1.53, 1.63 (two overlap. br m, -CH_2-*C*H_2-CH_2-); 2.10 (s, >N-CH_3); 2.29, 2.32 (two overlap. br m, >N-CH_2-); 2.50, 2.53 (two overlap. br m, -NH-CH_2- and H(6)CD); 2.78 (br s, NH_2-*C*H_2-); 3.32 (br d, H(2)CD); 3.43 (br s, H(4)CD); 3.61 (br t, H(3)CD); 3.67 (br s, H(5)CD); 4.85 (br s, H(1)CD); 5.12 (br s, -OH, -NH). ^{13}C NMR δ: 27.31 (-CH_2-*C*H_2-CH_2-); 38.47 (NH_2-CH_2-); 41.83 (>N-CH_3); 48.22 (>N-CH_2-); 48.70-49.70 (cluster, C(6)CD); 54.90, 55.76 (>N-CH_2-); 70.89 (C(5)CD); 72.73 (C(2)CD); 73.18 (C(3)CD); 82.64-83.49 (cluster, C(4)CD); 102.25-102.87 (cluster, C(1)CD). High-resolution ESI-MS (*m/z*): 1053.1682 [$C_{91}H_{189}N_{21}O_{28}$·HBr·2H]$^{2+}$ (calcd. 1053.1709); 1024.1977 [$C_{91}H_{189}$ $N_{21}O_{28}$·Na·H]$^{2+}$ (calcd. 1024.1988); 1013.2068 [$C_{91}H_{189}N_{21}O_{28}$ ·2H]$^{2+}$ (calcd. 1013.2078); 980.5897 [$C_{84}H_{170}N_{18}O_{28}$·HBr·2H]$^{2+}$ (calcd. 980.5920); 951.6198 [$C_{84}H_{170}N_{18}O_{28}$·Na·H]$^{2+}$ (calcd. 951.6198); 940.6287 [$C_{84}H_{170}N_{18}O_{28}$·2H]$^{2+}$ (calcd. 940.6289); 877.0572 [$C_{77}H_{151}N_{15}O_{28}$·$H_2O$·2H]$^{2+}$ (calcd. 877.0550); 868.0492 [$C_{77}H_{151}N_{15}O_{28}$·2H]$^{2+}$ (calcd. 868.0495); 683.1345 [$C_{91}H_{189}N_{21}O_{28}$ ·Na·2H]$^{3+}$ (calcd. 608.0790); 675.8076 [$C_{91}H_{189}N_{21}O_{28}$·3H]$^{3+}$ (calcd. 675.8076); 627.4218 [$C_{84}H_{170}N_{18}O_{28}$·3H]$^{3+}$ (calcd. 627.4217); 579.0361 [$C_{77}H_{151}N_{15}O_{28}$·3H]$^{3+}$ (calcd. 579.0357) 507.1080 [$C_{91}H_{189}N_{21}O_{28}$·4H]$^{4+}$ (calcd. 507.1076); 470.8186 [$C_{91}H_{189}N_{21}O_{28}$·4H]$^{4+}$ (calcd. 470.8181).

***Poly*-(6-deoxy)-{6-[3-(2-(3-aminopropylamino)ethylamino)-propylamino]}-βCD amCD3**: yield 410 mg (92 %); ^{1}H NMR (DMSO-*d*6) δ (ppm): 1.59, 1.63 (two overlap. m, -CH_2-*C*H_2-CH_2-), 2.43, 2.55 (two overlap. m, -CH_2-N<), 2.60, 2.63 (two overlap. br m, -CH_2-NH- and H(6)CD), 2.82 (m, -CH_2-NH_2 and H(6)CD), 3.35 (br s, H(2)CD); 3.50 (br s, H(4)CD), 3.66 (br s, H(3)CD), 3.76 (br s, H(5)CD), 4.91 (br s, H(1)CD), 4.95 (br s, -OH, -NH-); ^{13}C NMR δ (ppm) 27.39, 28.32 (-CH_2-*C*H_2-CH_2-), 38.48 (-CH_2-NH_2), 46.61, 47.36, 48.94 (-CH_2-N<), 48.70-49.60 (cluster, C(6)CD), 70.36 (C(5)CD), 72.32 (C(2)CD), 72.80 (C(3)CD), 82.20-85.70 (cluster, C(4)CD), 102.45 (C(1)CD); high-resolution ESI-MS (*m/z*): 1114.8004 [$C_{98}H_{210}N_{28}O_{28}$ ·2H]$^{2+}$ (calcd. 1114.8007); 1038.6996 [$C_{90}H_{188}$N24O_{28}·Na·H]$^{2+}$ (calcd. 1038.6995); 1027.7085

$[C_{90}H_{188}N_{24}O_{28}\cdot 2H]^{2+}$ (calcd. 1027.7085); 951.6077 $[C_{82}H_{166}N_{20}O_{28}\cdot Na\cdot H]^{2+}$ (calcd. 951.6073); 940.6166 $[C_{82}H_{166}N_{20}O_{28}\cdot 2H]^{2+}$ (calcd. 940.6163); 853.5242 $[C_{74}H_{144}N_{16}O_{28}\cdot 2H]^{2+}$ (calcd. 853.5241); 743.5368 $[C_{98}H_{210}N_{28}O_{28}\cdot 3H]^{3+}$ (calcd. 743.5363); 685.4752 $[C_{90}H_{188}N_{24}O_{28}\cdot 3H]^{3+}$ (calcd. 685.4748); 634.4719 $[C_{82}H_{166}N_{20}O_{28}\cdot Na\cdot 2H]^{3+}$ (calcd. 634.4706); 627.4139 $[C_{82}H_{166}N_{20}O_{28}\cdot 3H]^{3+}$ (calcd. 627.4133): 569.3524 $[C_{74}H_{144}N_{16}O_{28}\cdot 3H]^{3+}$ (calcd. 569.3518); 557.9045 $[C_{98}H_{210}N_{28}O_{28}\cdot 4H]^{4+}$ (calcd. 557.9040); 514.3585 $[C_{90}H_{188}N_{24}O_{28}\cdot 4H]^{4+}$ (calcd. 514.3579).

***Poly*-(6-deoxy)-[6-(6-amino-1-hexylamine)]-βCD amCD6**: yield 377 mg (94 %). ^{1}H NMR (DMSO-*d*6) δ (ppm): 1.27, 1.39, 1.52 (3 overlap. br m, -CH_2-*CH_2*-CH_2-); 2.46, 2.55 (two overlap. br m, >N-CH_2-); 2.78-3.06 (two overlap. br m, -NH-CH_2- and H(6)CD); 3.31 (br d, H(2)CD); 3.42 (br s, H(4)CD); 3.61 (br t, H(3)CD); 3.66 (br s, H(5)CD); 4.83 (br s, H(1)CD; overlapped with br s, -OH, -NH-). ^{13}C NMR δ: 25.82, 26.39, 26.88, 27.54, 28.10, 29.82 (-CH_2-*CH_2*-CH_2-); 49.18, 49.59, 49.92 (-NH-CH_2- and C(6)CD); 71.04 (C(5)CD); 72.86 (C(2)CD); 73.26 (C(3)CD); 83.41 (cluster, C(4)CD); 102.52 (C(1)CD). High-resolution ESI-MS (*m/z*): 1822.2168 $[C_{84}H_{168}N_{14}O_{28}\cdot H]^{+}$ (calcd. 1822.2225); 1706.0933 $[C_{78}H_{152}N_{12}O_{28}\cdot H]^{+}$ (calcd. 1706.0912); 1589.9717 $C_{72}H_{136}N_{10}O_{28}\cdot H^{+}$ (calcd. 1589.9598); 922.6055 $[C_{84}H_{168}N_{14}O_{28}\cdot Na\cdot H]^{2+}$ (calcd. 922.6059); 911.6113 $[C_{84}H_{168}N_{14}O_{28}\cdot 2H]^{2+}$ (calcd. 911.6149); 893.5123 $[C_{78}H_{152}N_{12}O_{28}\cdot HBr\cdot 2H]^{2+}$ (calcd. 864.5402); 864.5435 $[C_{78}H_{152}N_{12}O_{28}\cdot Na\cdot H]^{2+}$ (calcd. 864.5402); 853.5489 $[C_{78}H_{152}N_{12}O_{28}\cdot 2H]^{2+}$ (calcd. 853.5492); 795.4899 $[C_{72}H_{136}N_{10}O_{28}\cdot 2H]^{2+}$ (calcd. 795.4836); 608.0762 $[C_{84}H_{168}N_{14}O_{28}\cdot 3H]^{3+}$ (calcd. 608.0790); 569.3711 $[C_{78}H_{152}N_{12}O_{28}\cdot 3H]^{3+}$ (calcd. 569.3686).

***Poly*-(6-deoxy)-[6-(8-amino-1-octylamine)]-βCD amCD7**: yield 451 mg (92 %); ^{1}H NMR (DMSO-*d*6) δ (ppm): 1.23-1.47 (3 overlapped br m, -CH_2-*CH_2*-CH_2-); 2.46, 2.55 (two overlapped br m, -NH-CH_2- and H(6)CD); 2.79 (br m, NH_2-*CH_2*-); 3.28 (br d, H(2)CD); 3.35 (br s, H(4)CD); 3.60 (br t, H(3)CD); 3.67 (br s, H(5)CD); 4.81 (s, H(1)CD; overlapped with a br s, -OH and -NH-). ^{13}C NMR δ: 26.34, 26.71, 27.35, 28.95, 29.26, 30.15 (-CH_2-*CH_2*-CH_2-); 49.67, 50.05, 50.24 (-NH-CH_2- and C(6)CD); 70.99 (C(5)CD); 72.92 (C(2)CD); 73.7 (C(3)CD); 83.50 (cluster, C(4)CD); 102.48 (C(1)CD). High-resolution ESI-MS (*m/z*): 1031.7043 $[C_{98}H_{196}N_{14}O_{28}\cdot 2Na]^{2+}$ (calcd. 1031.7064); 1020.7143 $[C_{98}H_{152}N_{12}O_{28}\cdot Na\cdot H]^{2+}$ (calcd. 1020.7154); 1009.7245 $[C_{98}H_{152}N_{12}O_{28}\cdot 2H]^{2+}$ (calcd. 1009.7245); 948.6373 $[C_{90}H_{176}N_{12}O_{28}\cdot Na\cdot H]^{2+}$ (calcd. 948.6341); 946.6534 $[C_{90}H_{176}N_{12}O_{28}\cdot H_2O\cdot H]^{2+}$ (calcd. 946.6484); 937.6464 $[C_{90}H_{176}N_{12}O_{28}\cdot 2H]^{2+}$ (calcd. 947.6431); 673.4854 $[C_{98}H_{196}N_{14}O_{28}\cdot 3H]^{3+}$ (calcd. 673.4854); 625.4333 $[C_{90}H_{176}N_{12}O_{28}\cdot 3H]^{3+}$ (calcd. 625.4302).

*Titrations of **amCDs***

A carefully weighed amount (ca. 50 mg) of substance was placed in a jacketed vessel thermostated at 25 °C, and dissolved with 10 mL of double-distilled water; then, 5mL of a standard HCl 0.1 M were added, and the resulting solution was degassed by bubbling a fine stream of Ar for 15 min. The solution was titrated with a standard NaOH 1 M solution dispensed by means of a *Chemetron* microsyringe, recording the pH value after each addition of the titrant.

- 3 -

BINDING PROPERTIES OF POLYAMINO-CYCLODEXTRINS TOWARDS ANIONS

3.1 – The binding abilities of polycations

It is well known that polyamine macromolecular materials in general have attracted a widespread interest for their potential applications in different fields. For instance, both linear and branched polyethyleneimine (**PEI**) polymers,[68-73] as well as polypropyleneimine (**PPI**)[74-76] and polyamidoamine (**PAMAM**)[75-84] dendrimers, have been considered as proton sponges,[68,69,74,77,78,82-84] capping agents for the synthesis of noble metal nanoparticles,[70,71,75,76,79-81,85-87] and systems for the complexation and cell transfection of DNA and siRNA.[82-84,88] We already mentioned that complexation and transfection of polynucleotides have also been successfully accomplished by means of polycationic cyclodextrin derivatives,[56,89-92] obtained by anchoring suitable polyammonium or imidazolium pendant groups onto the main cyclodextrin scaffold. Therefore, because of the well-known ability of these macrocycles to form inclusion complexes ("*cavitates*") with suitably sized and shaped organic guest molecules,[4,14,15,93-96] in principle these systems could be exploited for the simultaneous internalization of a polynucleotide (interacting with the polycationic branches) and a further bioactive/drug molecule (included into the host cavity). A main drawback of this approach, of course, is the fact that the syntheses of the tailored cyclodextrin ligands reported so far, as pure chemical individuals, are lengthy and expensive, affording low overall yields. Thus, a cheaper alternative is desirable. Therefore, the **amCD**s described in the previous chapter appear ideal candidates.

Of course, the abilities of our materials as bimodal supramolecular ligands needed a suitable investigation. As a matter of fact, the interaction of the polycationic cyclodextrins[56,89-92] with polynucleotides has been mainly considered by targeting their abilities in inducing gene expression. However, a detailed examination of the relevant stoichiometric or thermodynamic aspects is lacking. So, it could be particularly interesting to verify how the presence of the

polyamine pendant bush located at the primary rim affect the binding abilities of the main cyclodextrin scaffold, on varying its protonation status. Then is the quantitative aspects of a possible interaction with polyanions. Therefore, the interaction of our **amCD**s at different pH values with a set of selected neutral and anionic model *p*-nitroaniline derivatives **1**-**4** (Figure 3.1) was subjected to polarimetric investigation. *p*-Nitroanilines have been proven to constitute an excellent class of probe molecules to test the microscopic behavior of cyclodextrins in general.[35,37,40,97-99] The polarimetric technique[35,100,101] was chosen because of its versatility and informativeness. In fact, it can be profitably exploited with any class of guests, irrespective of their peculiar physicochemical features. Moreover, polarimetry allows collecting and correlating both structural and thermodynamic information. In a subsequent step of this study potential ability of **amCD**s to interact with polyanions in general was tested by studying their behavior towards a model polyanion such as alginate (**Alg**, Figure 3.1) as sodium salt chosen for its stability and easy availability; it is a block copolimer constituted by β-D-mannuronate and β-L-guluronate monomers, linked by β-1,4 glycosidic bridges.

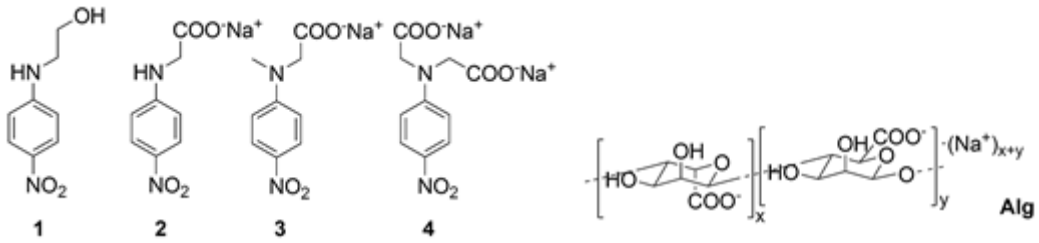

Figure 3.1 – Structures of: *p*-nitroanilines **1**-**4** and Sodium Alginate **Alg**.

3.2 - Results and discussion

*3.2.1 - Polarimetric behavior of **amCD**s*

Owing to the presence of the polyamine pendants linked to the **amCD** scaffold, a preliminary study of the polarimetric behavior of free **amCD1**-**amCD3** materials was a necessary requirement, before addressing their complexation abilities by means of the polarimetric method. Thus, the relevant molar optical activities Θ were measured at different pH values. Results are summarized in Table 3.1 depicted in Fig. 3.2. For the sake of clarity, it is worth stressing here that Θ values were determined in the absence of any buffering or supporting electrolyte, by simply adjusting the pH with small additions of conc. HCl or NaOH. As we can easily notice, on varying the pH value of the solvent medium, and consequently the charge status of the **amCD**s, relevant Θ values show a peculiar M-shaped trend (Figure 3.2a). Starting from ca. pH 12, at which the systems are almost uncharged, Θ values initially increase, then

decrease, then rise again up to a maximum value, and finally undergo a regular decrease till pH 5 and beyond. This behavior appears much sharper for **amCD1** than for the other two materials. Noticeably, **amCD1** shows its minimum and its second maximum located at significantly lower pH values than **amCD2**, which in turn shows its corresponding values at slightly lower pH than **amCD3**. It is worth noting that, if we report Θ values vs. the protonation fraction χ_{H+} of the

Table 3.1 – Molar optical rotations of materials **amCD1-amCD3** as a function of the pH.

amCD1			**amCD2**			**amCD3**		
pH	$<n_{H+}>^a$	Θ (deg dm^{-1} M^{-1})^b	pH	$<n_{H+}>^a$	Θ (deg dm^{-1} M^{-1})^b	pH	$<n_{H+}>^a$	Θ (deg dm^{-1} M^{-1})^b
12.2	0.0	173.2	12.2	0.1	164.8	12.0	0.1	165.5
11.6	0.1	175.2	11.5	0.3	165.7	11.2	0.7	168.1
11.5	0.1	175.4	10.9	1.2	165.6	10.8	1.3	168.5
11.1	0.2	175.9	10.3	2.5	165.3	10.6	1.8	168.2
10.4	1.0	175.7	10.1	3.2	165.0	10.3	2.6	168.1
10.1	1.3	174.8	10.0	3.5	165.3	10.0	3.5	169.3
9.5	2.3	172.2	9.7	4.2	165.8	9.7	4.4	170.8
9.4	2.5	171.6	9.4	4.9	166.5	9.0	6.4	169.2
9.1	3.2	166.5	9.0	6.0	166.7	8.6	7.8	168.5
8.8	3.9	165.2	8.7	6.7	166.7	8.5	8.1	168.2
8.6	4.5	172.0	8.2	8.0	165.7	8.3	8.7	167.9
8.4	4.8	175.3	7.9	8.7	164.7	8.0	9.5	166.8
8.2	5.2	176.2	7.4	10.2	162.7	7.3	11.1	163.5
8.1	5.3	176.5	7.0	11.4	160.9	7.0	11.7	162.8
8.0	5.5	176.7	6.6	12.5	159.1	6.8	12.3	162.0
7.7	5.9	177.3	6.4	13.1	158.6	6.7	12.6	161.8
7.3	6.5	177.8	6.2	13.7	157.9	6.5	13.0	160.6
6.5	8.1	173.2	5.9	14.9	156.5	6.1	14.1	160.2
6.3	8.7	172.1	5.7	15.4	155.6	5.7	14.9	159.6
5.9	9.5	170.8	5.3	16.5	154.8	5.4	15.7	159.2
5.4	10.5	166.4	4.7	17.6	153.0	5.1	16.5	157.9
5.2	10.8	164.8						
5.1	10.9	164.1						
3.8	11.4	157.8						

[a]: Calculated according to analytical data reported on table 2.1, pag 21. [b]: All data are given with a ± 0.5% indetermination.

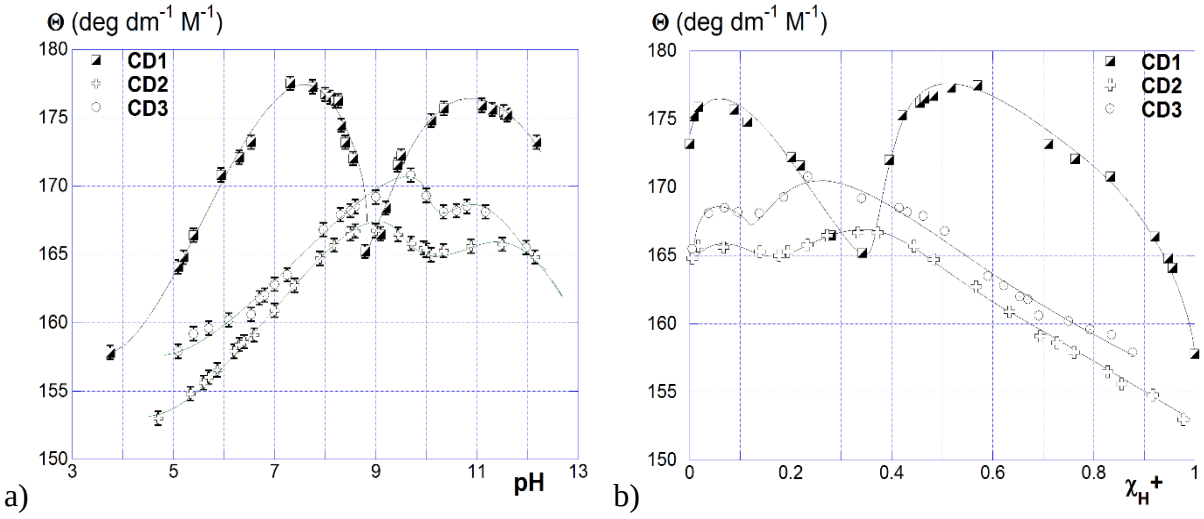

Figure 3.2 – Polarimetric data for **amCD**s.

materials (Fig. 3.2b), the absolute maxima of the three curves occur for χ_{H+} values as large as ca. 0.5, 0.33 and 0.25 for **amCD1**, **amCD2** and **amCD3** respectively.

Keeping into account the number of basic nitrogen atoms of the relevant polyamine branches, i.e. 2 for **A1**, 3 for **A2** and 4 for **A3**, it is immediately apparent that these maxima correspond to the situation in which one H^+ on average has been attached to each polyamine unit. The latter observation is very intriguing, because it was found that in the case of *mono*-[6-(3-dimethylamino)-propylamino]-(6-deoxy)-**βCD** the first protonation step occurs on the farthest N atom with respect to the **CD** cavity.[98] Thus, it is reasonable to expect that the same occurs also with the polyamine branches of our materials, in such a way to minimize Coulomb repulsion between cationic groups. It has been widely shown that the polarimetric response of **CD** derivatives depends at the same time on their intrinsic chirality and on their conformational dynamism. Variations in Θ values upon protonation should reflect either conformational or electron distribution changes. However, we may rule out a significant contribution from the latter effect, because in the case of the *mono*-(6-amino)-(6-deoxy)-β-cyclodextrin it has been found that the free base and the conjugated acid forms present more or less the same Θ value.[102] Consequently, everything considered, data indicate that our **amCD**s experience their most extensive conformational rearrangements as the first protonation step of each polyamine branch occurs. This suggests the occurrence of strong intra-chain interactions, and possibly self-inclusion into the **CD** cavity, before protonation.

*3.2.2 - Binding equilibria of p-nitroaniline derivatives **1-4***

Polarimetric data relevant to the inclusion of guests **1**-**4** into materials **amCD1**-**3** are collected in Tables 3.2 a-c respectively. In particular, the values of the binding constants (*K*) and both the absolute (ΔΘ) and normalized (R_Θ) differential molar optical rotations are reported, as a function of the pH value and the possible presence of a buffer as supporting electrolyte. For the sake of clarity, ΔΘ is the difference between the molar optical rotations of the complex and the host respectively, whereas R_Θ is defined as $100 \cdot \Delta\Theta/\Theta$ (where Θ is the molar optical rotation of the free host under the given conditions). It is worth stressing that ΔΘ values for the different systems studied cannot be directly compared, owing to the intrinsic differences in the absolute molar optical rotations of the different hosts, and for the same host at different pH values.

Therefore, homogeneous comparisons can be rather carried out only on the relative variations as accounted for by the normalized parameter R_Θ.[102] It is also worth recalling that ΔΘ and R_Θ values for *p*-nitroanilines can be correlated with the time averaged tilt angle between the guest

chromophore and the ideal axis of the host cavity. Thus, they can serve as a good probe of the overall conformational rigidity of the complex.[35,100,101,103-106]

Table 3.2a – Polarimetric data for the inclusion of guests **1**-**4** with **amCD1**.

guest	buffer[a]	pH	$<n_{H^+}>$[b]	K (M^{-1})	Θ (deg dm^{-1} M^{-1})[c]	ΔΘ (deg dm^{-1} M^{-1})	R_Θ
1[d]	-	5.1	10.9	280 ± 40	164.1	46.4 ± 2.6	28.3 ± 1.6
	-	6.3	8.7	340 ± 70	172.1	47.3 ± 3.3	27.5 ± 1.9
	-	8.0	5.5	1000 ± 100	176.7	37.6 ± 0.9	21.3 ± 0.5
	-	9.5	2.3	1070 ± 130	172.2	35.3 ± 3.5	20.5 ± 2.0
	-	11.6	0.1	1220 ± 140	175.2	36.6 ± 0.7	20.9 ± 0.4
	P1	6.5	8.1	(<50)	172.9	n.d.	n.d.
	B	8.4	4.8	400 ± 20	173.4	52.2 ± 1.2	30.1 ± 0.7
	Am	9.2	2.9	580 ± 50	171.5	45.1 ± 1.0	26.3 ± 0.6
	P2	11.3	0.2	1200 ± 140	168.0	38.8 ± 1.0	23.1 ± 0.6
2[d]	-	5.4	10.5	1490 ± 160	166.4	50.6 ± 1.2	30.4 ± 0.7
	-	6.5	8.1	1180 ± 250	173.2	54.5 ± 2.0	31.5 ± 1.2
	-	8.1	5.3	1020 ± 190	176.5	57.2 ± 1.6	32.4 ± 0.9
	-	9.5	2.3	960 ± 130	172.2	44.3 ± 1.0	25.7 ± 0.6
	-	11.5	0.1	490 ± 50	175.4	43.9 ± 1.0	25.0 ± 0.6
3	-	5.1	10.9	(<50)	164.1	n.d.	n.d.
	-	7.7	5.9	520 ± 80	177.3	88.6 ± 4.2	50.0 ± 2.4
	-	8.4	4.8	780 ± 160	175.3	64.4 ± 3.1	37.2 ± 1.8
	-	10.1	1.3	1030 ± 30	174.8	47.2 ± 0.3	27.0 ± 0.2
	-	11.5	0.1	1220 ± 140	175.4	36.6 ± 0.7	20.9 ± 0.4
4	-	6.3	8.7	(> 10^4)	172.1	n.d.	n.d.
	-	8.4	4.8	1300 ± 480	175.3	23.9 ± 1.4	13.8 ± 0.8
	-	9.1	3.2	520 ± 70	166.5	22.8 ± 0.5	13.7 ± 0.3
	-	11.1	0.2	67 ± 15	175.9	29.9 ± 2.6	17.0 ± 1.5
	P1	5.9	9.5	(> 10^4)	165.0	(51)	(31)
	B	8.4	4.8	350 ± 30	166.9	21.7 ± 0.4	13.0 ± 0.2
	Am	9.2	2.9	300 ± 40	164.2	22.0 ± 0.6	13.4 ± 0.4
	P2	11.3	0.2	190 ± 20	165.1	24.1 ± 0.6	14.6 ± 0.4

Table 3.2b – Polarimetric data for the inclusion of guests **2** and **4** with **amCD2**.

guest	buffer[a]	pH	$<n_{H^+}>$[b]	K (M^{-1})	Θ (deg dm^{-1} M^{-1})[c]	ΔΘ (deg dm^{-1} M^{-1})	R_Θ
2	-	5.7	15.4	1070 ± 100	155.6	51.0 ± 0.9	32.7 ± 0.6
	-	7.0	11.4	860 ± 40	160.9	54.9 ± 0.6	34.1 ± 0.4
	-	8.7	6.7	790 ± 70	166.7	49.0 ± 1.0	29.4 ± 0.6
	-	10.1	3.2	520 ± 40	165.0	50.8 ± 1.0	30.8 ± 0.6
	Ac	4.7	17.6	430 ± 20	150.0	44.1 ± 0.7	29.4 ± 0.5
	Ac	5.7	15.4	730 ± 100	165.8	45.4 ± 1.4	27.5 ± 0.8
	P1	6.3	13.4	530 ± 70	165.3	50.9 ± 1.4	30.8 ± 0.8
	B	8.6	7.0	490 ± 60	170.1	53.4 ± 1.7	31.4 ± 1.0
	P2	10.8	1.3	540 ± 30	171.2	53.4 ± 0.6	31.2 ± 0.4
4	-	5.7	15.4	(> 10^4)	155.6	n.d.	n.d.
	-	6.6	12.5	4300 ± 600	159.1	32.1 ± 0.6	20.2 ± 0.4
	-	7.9	8.7	1350 ± 140	164.7	26.0 ± 0.3	15.8 ± 0.2
	-	8.7	6.7	1310 ± 90	166.7	25.5 ± 0.5	15.3 ± 0.3
	-	10.0	3.5	610 ± 90	165.3	32.2 ± 1.3	19.5 ± 0.8
	Ac	5.6	15.8	(> 10^4)	168.2	(37)	(22)
	P1	6.2	13.7	4800 ± 500	171.4	32.9 ± 1.9	19.2 ± 1.1
	B	8.5	7.2	320 ± 20	174.1	25.6 ± 0.5	14.7 ± 0.3
	P2	10.9	1.2	200 ± 30	173.7	37.0 ± 1.0	21.3 ± 1.0

[a] Buffers used (I = 0.1 M) are specified as follows: **Ac**, CH_3COOH/CH_3COONa; **Am**, NH_4Cl/NH_3; **B**, $B(OH)_3$/ $NaB(OH)_4$; **P1**, NaH_2PO_4/Na_2HPO_4; **P2**, Na_2HPO_4/Na_3PO_4; "-" indicates no buffer. [b] Calculated according to analytical data from ref. 65. [c] Data given within a ± 0.5 deg dm^{-1} M^{-1} indetermination.

Table 3.2c – Polarimetric data for the inclusion of guests **2** and **4** with **amCD3**.

guest	buffer[a]	pH	$<n_{H^+}>^b$	K (M^{-1})	Θ (deg dm^{-1} M^{-1})[c]	$\Delta\Theta$ (deg dm^{-1} M^{-1})	R_Θ
2	-	5.4	15.7	980 ± 30	159.2	52.0 ± 0.3	32.7 ± 0.2
	-	6.8	12.3	1110 ± 60	162.0	56.2 ± 0.7	34.6 ± 0.4
	-	8.5	8.1	1500 ± 200	168.2	48.4 ± 1.1	28.8 ± 0.7
	-	10.6	1.8	290 ± 30	168.2	57.9 ± 2.3	34.4 ± 1.4
	P1	5.1	16.5	450 ± 30	160.5	43.5 ± 0.7	27.1 ± 0.4
	P1	6.7	12.6	1580 ± 170	172.6	49.2 ± 1.0	28.5 ± 0.6
	B	8.3	8.7	750 ± 90	177.8	47.3 ± 1.3	26.6 ± 0.7
	P2	10.3	2.6	450 ± 30	172.4	48.1 ± 1.7	27.9 ± 0.4
4	-	6.1	14.1	(> 10^4)	160.2	(40)	(25)
	-	7.0	11.7	2700 ± 200	162.8	35.6 ± 0.4	21.9 ± 0.3
	-	8.6	7.8	1170 ± 40	168.5	28.2 ± 0.1	16.7 ± 0.1
	-	10.6	1.8	360 ± 30	168.2	31.4 ± 0.7	18.7 ± 0.4
	P1	5.7	14.9	6000 ± 2000	166.1	31.4 ± 1.6	18.9 ± 1.0
	P1	6.7	12.6	2000 ± 200	172.6	23.5 ± 1.7	13.6 ± 1.0
	B	8.3	8.7	640 ± 50	177.8	23.8 ± 0.4	13.4 ± 0.2
	P2	10.8	1.3	73 ± 7	172.3	35.5 ± 1.0	20.6 ± 0.6

[a] Buffers used (I = 0.1 M) are specified as follows: **Ac**, CH_3COOH/CH_3COONa; **Am**, NH_4Cl/NH_3; **B**, $B(OH)_3/NaB(OH)_4$; **P1**, NaH_2PO_4/Na_2HPO_4; **P2**, Na_2HPO_4/Na_3PO_4; "-" indicates no buffer. [b] Calculated according to analytical data from ref. 65. [c] Data given within a ± 0.5 deg dm^{-1} M^{-1} indetermination.

The behavior of **amCD1** was examined first. It can be immediately noticed that pH variations have large effects on its binding abilities. The neutral guest **1** always forms 1:1 complexes only, as accounted for by the fact that polarimetric data can be perfectly subjected to regression analysis by means of the proper equation[100,101] derived analytically (see Experimental section). The relevant K values regularly decrease on increasing the average charge on the host, in agreement with the behavior already reported in literature for the *mono*-(6amino)-(6-deoxy)-β-cyclodextrin.[102] A buffering electrolyte apparently exerts an unfavorable effect on the inclusion equilibrium. For the anionic guests **2-4**, the situation is more complicated (some trends of the observed optical rotations for the inclusion of **4** are shown in Figure 3.4 as exemplificative examples).

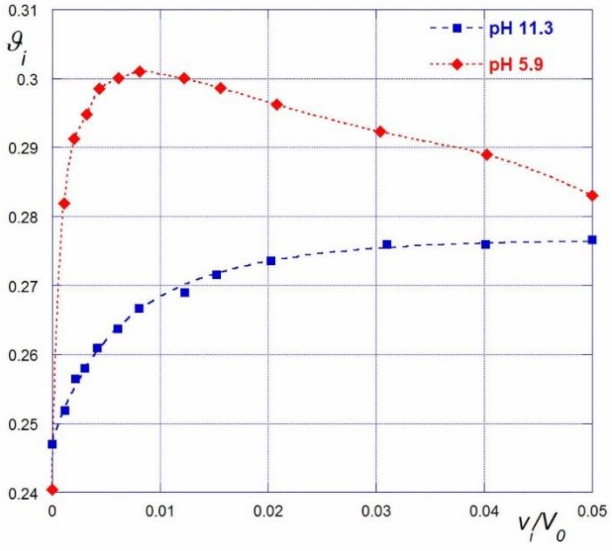

Figure 3.4 – Trends of polarimetric data for the inclusion of guest **4** in **amCD1.**

It is immediately apparent that polarimetric data account for the formation of a simple 1:1 inclusion complex only for the uncharged host at high pH values. By contrast, on decreasing the pH, deviations from the expected trend are systematically shown by the samples prepared at the largest guest concentrations. The same behavior, indeed, is also observed for the inclusion of the same anionic guests in **amCD2** and **amCD3**. This finding indicates the formation of higher-order aggregates, although data did not allow obtaining a reliable evaluation of their stoichiometry or stability, at least within the range of guest concentration considered. We can observe that *K* values for guest **3** decrease on decreasing the pH of the solvent medium, similarly as for neutral guests. By contrast, the opposite behavior is found for **2** and **4**, i.e. a regular increase on increasing the protonation status is observed, which is particularly evident for guest **4**. Finally, regarding the variations in the polarimetric response, we found that R_Θ tend to increase on decreasing the pH value, irrespective of the trend for the relevant *K* values.

On passing to consider the behavior of hosts **amCD2** and **amCD3**, it was decided to restrict the attention on the monoanion **2** and the dianion **4**. The results obtained appear quite peculiar. As a matter of fact, for guest **4** a regular increase in *K* values, similar to the one found with **amCD1**, is observed with the two hosts both in the presence and in the absence of the buffering electrolyte. Even in this case, the presence of the electrolyte disfavors the inclusion process. By contrast, for guest **2** the same simple monotonic trend is observed only with **amCD2** in the absence of a buffer, whereas in the other cases *K* values pass through a maximum. Moreover, in all the cases examined we found that also R_Θ trends appear non-monotonic. It is interesting to notice that the possible presence of a buffering electrolyte significantly affects both Θ and R_Θ values, although general trends cannot be clearly envisaged.

In order to rationalize the whole of these results, a careful consideration of polarimetric responses is particularly useful. According to the regular increase of R_Θ values for the neutral guest **1** with **amCD1** on decreasing the pH, accounts for a decrease of the average tilt of the guest with respect to the ideal host axis. This suggests the idea that the polarized guest molecule penetrates more and more deeply into the cyclodextrin cavity on increasing the positive charge of the host, owing to the occurrence of stronger dipolar interactions. Therefore, the inclusion complex must become stiffer; thus, *K* values decrease because of the consequent entropy unfavorable effects.[102] A further unfavorable contribution, of course, may also be provided by the increasingly difficult desolvation of the electrically charged host. By contrast, for the dianionic guest **4** all these effects appear largely counterbalanced by the concomitant occurrence of very favorable Coulomb interactions. For the monoanionic guest **2**, the occurrence of some non-monotonic trends indicates that such a counterbalance is less effective.

In the case of **amCD1**, the behavior of guest **3** is particularly intriguing, because its *K* trend neatly disagrees with the one for the other anions. This surprising behavior can be explained considering that, owing to the methyl group placed on the amino N atom, the ancillary chain of **3** is unable to give multiple hydrogen bonding with the host cavity.[37] This particular structural feature has been proven to have a significant outcome on the overall thermodynamics of the inclusion process,[35,37] making entropy-unfavorable stiffening effects to act much more severely as compared to double-hydrogen-bond donor guests like **2** and **4**.

Another important piece of information is provided by the fact that a possible supporting electrolyte present in the system systematically affects both Θ and R_Θ values of our systems. Indeed, it is quite reasonable to assume that the polycationc pendant groups of the hosts may interact with the anions of the buffer, by either ion pairing or the formation of multiple hydrogen bonds. Under such circumstances, the mobility of the polyamine chains and, in turn, the conformational dynamics of the entire cyclodextrin scaffold, are heavily affected. These considerations enable us to rationalize the anomalous polarimetric trends mentioned previously for the inclusion of anionic guests. Assuming the possible formation of higher-order aggregates, trivial modelling considerations rule out the possibility that more than one guest molecule might be comfortably accommodated into the host cavity. Therefore, we may reasonably hypothesize the occurrence of a loose ion-pairing external association between the cationic pendant groups of the host and the anionic guest (a possible pictorial representation is shown in Figure 3.4).

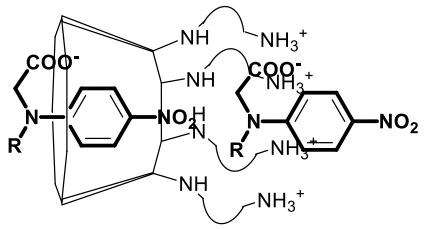

Figure 3.4 – Representation of a possible 1:2 **amCD**-guest aggregate.

3.2.3 - Interaction with the alginate polyanion

Further assessment of the possible interactions between anions and the polycationic pendant "bush" of our materials **amCD1-amCD3** was achieved by studying their behavior towards a suitable model polyanion such as alginate sodium salt. In particular, the main points under investigation were: *i*) the stoichiometry of the possible complex formed; *ii*) the intimate mechanism of the interaction. For these purposes, series of working samples were prepared at given pH values (see Experimental section) by mixing variable micro-amounts of a concentrated solution of the polyanion (25 mN) with fixed aliquots of a solution (1.5 mM) of

each **amCD**. Qualitatively, we could observed three different behaviors. At high pH values, i.e. in the presence of the almost uncharged **amCD**, all samples prepared were clear, irrespective of the amount of polyanion added. On lowering the pH, clear solutions were formed only at the lowest **Alg** concentrations, whereas an intense turbidity developed on increasing the amount of polyanion over a limit value. On further lowering the pH, i.e. as the **amCD** approaches its highest protonation status, the addition of the polyanion in any amount always caused the formation of precipitates. Of course, this suggested that in the latter case the alginate added was completely precipitated off from the solution, due to its interaction with the polycationic **amCD**. This, in turn, implied that a larger and larger amount of **amCD** is subtracted from the solution on increasing the amount of alginate. On the other hand, in the second case the partly charged **amCD** is able to interact with the alginate forming some kind of aggregate, which precipitates off after it reached a saturation level. Noticeably, we verified that alginate alone never forms precipitates under any of the pH conditions examined.

Working samples were subjected to polarimetric analysis (three typical trends are depicted in Figure 3.5).

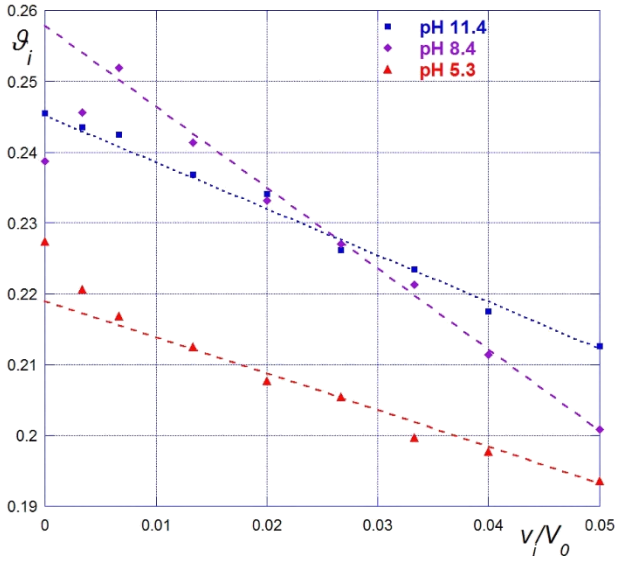

Figure 3.5 – Trends of ϑ_i at different pH values vs v_i/V_0

At large pH values, the optical activity observed was simply the sum of the independent contributions from the **amCD** and the alginate. In particular, we observed a nearly linear decrease of the optical rotation of the samples, owing to the fact that **Alg** is levorotatory. This provides convincing proof that the almost uncharged **amCD** is not able to interact with the polyanion. On the other hand, the samples prepared at the lowest pH values were subjected to centrifugation (see Experimental section), and the optical activities of the supernatant liquor were measured. We observed a regular decrease, accounting for the progressive subtraction of

the **amCD** from the solution. Indicating with n_r the average molar ratio between the **amCD** and the monomer units of alginate in the precipitate formed, by trivial algebraic passages it is possible to derive the expression (Eq. 3.1) for the relationship between of the optical activity of the samples and the amount of polyanion added

$$\vartheta_i = \frac{\vartheta_0 - \frac{v_i}{V_0} \cdot \frac{c_0^{Alg\,Na}}{c_0^{CD}} \cdot \frac{\vartheta_0}{n_r}}{1 + \frac{v_i}{V_0}} \qquad (3.1)$$

where the index *i* applies to the generic *i*-th sample of the series, ϑ_0 is the optical rotation of the relevant sample without **Alg**, v_i and V_0 are the volumes of the **Alg** and **amCD** solutions mixed in the sample respectively, c_0^{AlgNa} and c_0^{CD} the analytical concentrations of the relevant mother solutions. The behavior of the samples prepared at intermediate pH values is more intriguing. Before the formation of the turbidity at low alginate concentrations, either an increase or a decrease in values could be observed, depending on the particular case. On increasing the amount of polyanion, turbid samples were subjected to centrifugation, and the supernatant liquor again showed a regular decrease of the optical activity, according to the equation:

$$\vartheta_i = \frac{\alpha - \frac{v_i}{V_0} \cdot \frac{c_0^{Alg\,Na}}{c_0^{CD}} \cdot \frac{\vartheta_0}{n_r}}{1 + \frac{v_i}{V_0}} \qquad (3.2)$$

which is almost identical to Eq. (3.1), but for the presence of a suitable intercept term α. Thus, in either cases we were able to evaluate the molar ratio n_r. Data obtained, as a function of the **AmCD**, the pH and the possible presence of a buffer electrolyte are collected in Table 3.3 and illustrated in Figure 3.6.

Table 3.3 – n_r values for the **amCD**-**AlgNa** interaction.

amCD1			**amCD1** (with buffer)			**amCD2**			**amCD3**		
pH	$<n_{H^+}>^a$	n_r	pH	$<n_{H^+}>^a$	n_r	pH	$<n_{H^+}>^a$	n_r	pH	$<n_{H^+}>^a$	n_r
11.2	0.1	0	11.4[b]	0.1	0	10.0	3.5	5.9 ± 0.2	9.8	4.2	5.0 ± 0.1
8.4	4.8	4.3 ± 0.3	8.4[c]	4.8	3.5 ± 0.3	9.0	6.0	8.0 ± 0.3	9.0	6.4	7.2 ± 0.3
7.3	6.5	5.0 ± 0.2	6.5[d]	8.1	5.0 ± 0.4	7.8	8.8	10.4 ± 0.3	8.1	9.2	8.2 ± 0.2
6.5	8.1	6.5 ± 0.4	5.3[e]	10.7	9.4 ± 0.6	7.0	11.4	11.5 ± 0.9	7.1	11.5	8.5 ± 0.4
4.6	11.2	6.8 ± 0.5				6.1	13.9	13.2 ± 0.8	5.9	14.5	9.9 ± 0.5

[a] Calculated according to analytical data from ref. 13. [b] Na_2HPO_4/Na_3PO_4 buffer (I = 0.1 M). [c] $B(OH)_3/NaB(OH)_4$ buffer (I = 0.1 M). [d] NaH_2PO_4/Na_2HPO_4 buffer. [e] CH_3COOH/CH_3COONa buffer (I = 0.1 M).

It is interesting to notice that in general n_r values never coincide with the average charge ($<n_{H^+}>$) on the **amCD**. Thus, the precipitate must embed ions coming from the solution. Under this light, it is interesting to consider the behavior of **amCD1** in either the presence or the absence of a buffering electrolyte. In both cases indeed n_r values lower than $<n_{H^+}>$ are found;

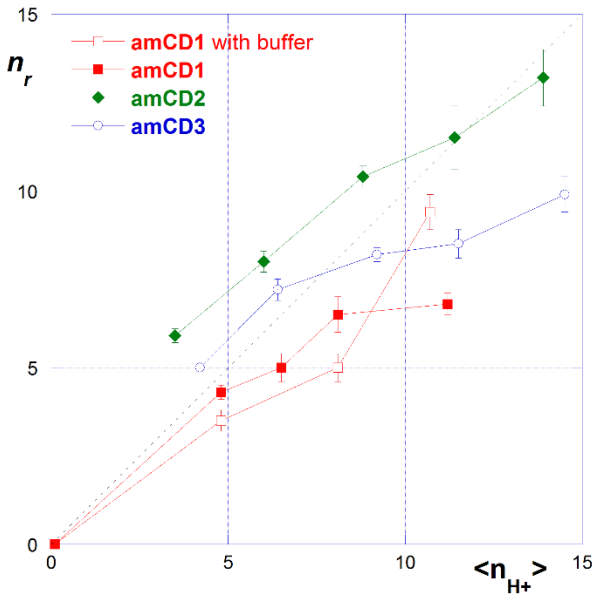

Figure 3.6 – n_r values for the **CD-AlgNa** interaction, as a function of <n_{H+}>.

however, under pH conditions near to neutrality larger n_r values are found in the absence of a buffer. This means that the amount of inorganic anions retained by the precipitate increases on increasing the content of inorganic electrolytes in solution. A close inspection of data reported in Table 2 suggests that the **amCD**s become less effective as precipitating agents on a relative scale, on increasing their protonation status, because n_r values are significantly larger than <n_{H+}> at high pH values, whereas the opposite occurs at low pH. In particular, n_r values for **amCD3** seem to reach nearly a plateau below pH 8. A similar trend is shown also by **amCD1** in the absence of a buffer, whereas data for **amCD2** increase monotonically. A comparison between the three different **amCD**s suggests that **amCD2** is the most effective ligand in interacting with the polyanion, because it shows the largest n_r values at any pH.

In order to rationalize these results, it must be recalled that the three **AmCD**s differ for both the average number of pendant groups (<n_P>) and N atoms on each cyclodextrin scaffold, according to the analytical data reported. As we already mentioned, <n_P> is always less than 7, owing to the possible occurrence of multiple substitution reactions on the same polyamine unit. Analytical data imply that the probability of multiple substitution for polyamines increases in the order **Am2** < **Am1** < **Am3**. This suggest that for **Am3** multiple substitution is likely to occur mainly through different N atoms of the same polyamine chain (path "*b*" of Scheme 2.1, pag. 18), whereas for **Am1** and **Am2** the same N atom is more likely to be involved (path "*a*" of the same Scheme). Under these circumstances, we may reasonably hypothesize that the polyamine "bush" of **amCD2** should experience a larger flexibility and conformational freedom as compared to **amCD3** or **amCD1** (in the latter case because **amCD1** possesses the shortest

chains). As a consequence, **amCD2** results the best ligand towards **Alg** because it is able to achieve the best fitting upon the polyanion chain. Moreover, we also have to consider that protonation of the **amCD** occurs first on the farthest N atoms with respect to the cyclodextrin scaffold, as we mentioned previously. Therefore, at relatively high pH values, charged groups on each **amCD** unit benefit of a larger conformational freedom, in such a way that the ligand can interact with the polyanion in the most effective way. By contrast, at lower pH values, further charges on the **amCD** must allocate themselves in the relatively narrow space around the primary cyclodextrin rim. Therefore, the charge increase cannot improve the binding ability of the ligand, expressed in terms of number of anionic monomers per polycation unit.

3.3 – Experimental section

Sinthesis of N-(4-nitrophenyl)-iminodiacetic acid disodium salt **4**

The synthesis of guest **4** is not described in previous literature; therefore it was prepared according to procedures reported.[35,37,100] Iminodiacetic acid (1.33 g, 10 mmoles) was treated with an equimolar amount of sodium methylate, obtained by dissolving sodium metal (0.46 g, 20 mmoles) in dry methanol (20 mL), and the mixture was distilled in vacuo. The residue was dissolved in DMSO (10 mL); then 4-nitrofluorobenzene (1.41 g, 10 mmoles) and anhydrous Na_2CO_3 (1.06 g, 10 mmoles) were added. The reaction mixture was kept at 70 °C under stirring for 18 hours. Afterwards, the resulting slurry was dissolved in water (200 mL) and the solution was extracted twice with ethyl acetate (ca. 70 mL each); then, the aqueous phase was acidified with HCl 6 M up to pH 2, and the desired product was extracted trice with ethyl acetate (100 ml each). The latter organic extracts were dried (Na_2SO_4) and distilled in vacuo to afford the crude product, which was dissolved in a sodium methylate solution, once again obtained dissolving sodium metal (0.46 g, 20 mmoles) in dry methanol (20 mL). Then, diethyl ether (80 ml) was added to the solution to precipitate the pure product, which was finally filtered off. Yield 60 % (1.79 g). IR (nujol): ν (cm^{-1}) 1597, 1516, 1339. ^{1}H NMR (300 mHz, D_2O): δ 3.95 (s, 4H, -CH_2-), 6.47 and 8.03 (2d, 2H + 2H, J = 9.5 Hz, *p*NO_2-C_6H_4-N<). Elem. anal. C 40.24, H 2.73, N 9.39, Na 15.43 (calcd. for $C_{10}H_8N_2O_6Na_2$: C 40.28, H 2.70, N 9.40, Na 15.42).

Polarimetry

Polarimetric determinations were performed on a JASCO P-1010 polarimeter. In order to obtain molar optical rotations Θ of materials **amCD1**-**amCD3** at different pH values, mother 1.5 mM solutions of the materials in double-distilled water were prepared; then micro-volumes of either standard HCl 1 M or NaOH 1 M were added to aliquots (3 mL each) of the solutions, in order

to adjust the pH to the desired value. From the observed optical rotations of the samples (corrected for the small dilution effect), the relevant Θ values were easily calculated.

Measurements of the binding constants for guests **1-4** were accomplished according to the general procedure described elsewhere.[35,100-102] In brief, stock solutions of the hosts 1.5 mM were prepared, by dissolving the proper amount of substance either in pure water and then adjusting the pH at the desired value by adding small amounts of HCl 1 M or NaOH 1 M, or in an aqueous buffer solution at the desired pH value. Then, sets of sample solutions were prepared, by mixing variable micro-amounts (up to 150 μL) of a concentrated guest solution (usually ca. 0.25 M) to fixed volumes (3 mL) of host solution. Buffer used are specified in the footnote of Table 3). In each case the actual pH value of the solutions was checked with a pH-meter. Polarimetric data were subjected to suitable fitting analysis as described elsewhere,[100] by means of the proper equation derived analytically:

$$\vartheta_i = \frac{\vartheta_0 + \frac{\Delta\Theta}{2}\left(H_0^0 + G_0^0\frac{v_i}{V_0} + \frac{1+v_i/V_0}{K} - \sqrt{\left(H_0^0 + G_0^0\frac{v_i}{V_0} + \frac{1+v_i/V_0}{K}\right)^2 - 4H_0^0G_0^0\frac{v_i}{V_0}}\right)}{1+v_i/V_0} \qquad (3.3)$$

where ϑ_i is the optical rotation measured for the generic *i*-th sample, ϑ_0 the optical rotation of the pure host solution, v_1 is the volume of guest solution added, V_0 is the volume of **amCD** solution, H_0^0 and G_0^0 are the analytical concentrations of the host and guest solutions respectively, $\Delta\Theta$ the differential molar optical activity for the complex, *K* is the binding constant to be determined.

In order to study the interaction between **amCD**s and **Alg**, a stock alginate solution 25 mN was first prepared as follows. The proper amount of substance (99.5 mg) was dissolved in warm water, after cooling to r.t. the volume was adjusted to 20 mL, and finally the solution was filtered through a 0.45 μ Millipore® filter. For the sake of clarity, the concentration was calculated according to the formula weight of the monomeric unit ($C_6H_7O_6Na$). Then, sets of samples were prepared by mixing fixed aliquots (3 ml each) of stock **amCD** solutions at the proper pH value with increasing micro-amounts of **Alg** solution. Each sample was vigorously shaken, allowed to settle overnight and then centrifuged at 5000 rpm for 15 min. The supernatant liquors were carefully pipetted out, and the relevant optical activities were determined. Data were finally subjected to regression analysis according to the Eq.s (3.1) and (3.2).

- 4 -

INTERACTION OF POLYAMINO-CYCLODEXTRINS WITH POLYNUCLEOTIDES

4.1 – Cyclodextrin-based gene delivery systems

In recent decades, gene therapy has experienced a remarkable development, especially since the complete sequence of the human genome was published in 2001.[107,108] This enabled to define the relationship between the misfunction of proteins, involved in certain diseases, and the genes encoding them, as well as to understand the molecular basis of diseases and thus directly act on their causes rather than on their symptoms. To do this, gene therapy[109] exploits the use of genetic material able to alter gene expression in patient's target cells, reducing or correcting the expression of the disease for instance through the endogenous production of functional proteins. It is therefore necessary to introduce genetic material into target cells; however, nature has designed cells in such a way to preserve their genetic information, by hindering the uptake of exogenous nucleic acids. Therefore, the latter process may occur provided that appropriate vectors protect and carry the suitable genetic material (DNA or RNA), leading to its internalization.

The first candidates to carry out these functions have been viruses, which are naturally designed to infect cells and transfer their genetic information. Then, by replacing the viral gene responsible of its replication, with genes of therapeutic interest, it is possible to use a virus as a carrier. Despite the excellent results obtained, several problems arose related to toxicity and immune system, which sees a virus as a danger and therefore tends to fight it.[110,111] For these reasons, the use of viral vectors has been banned from main health surveillance agencies.

Artificial non-viral vectors[91,112-115] have been then developed, which have the advantage to be invisible to the immune system, and can also be constructed in such a way to fit the type and amount of genetic material to be carried. The carriers proposed so far can be divided into two main categories, namely amphiphilic cations (surfactants)[116,117] and cationic polymers,[118,119]

both able to interact electrostatically with nucleic acids and form nanoparticle complexes (called Lipoplex and Poliplex respectively).[120] The latter ones are able to protect the genetic material and facilitate the cell membrane crossing. However, the efficiency and selectivity of these carriers are not yet comparable to viral-based ones, and are not entirely cytotoxicity-free as well.

In order to obtain new carriers with improved abilities, the possible use of cyclodextrins derivatives has been widely investigated.[91,121-125] In fact, they provide better biocompatibility to the systems in which they are implemented by reducing the cytotoxicity of the resulting carrier; and by exploiting their resistance to enzymatic attach because of their non-peptide nature. Moreover, thanks to their ability of complexing some constituent elements of the cell membrane, such as cholesterol,[28] they destabilize the membrane[27] itself increasing the transfection ability of formulations in which they are present.[126-130] There are numerous examples relating to the integration of cyclodextrins in cationic polymers,[131-146] dendrimers[54,147-156] and polyrotaxane.[157-168]

In the last few years, new appealing monodisperse systems based on polycationic cyclodextrins (at physiological pH) have been developed.[56,92,130,169-176] The first design synthetic protocol to obtain this kind of derivatives, rely on the easy regioselective per-modification of the primary hydroxyl groups with aminoalkylamino, guanidinoalkylamino[169,174,175] or oligoethyleneimino groups.[56] (Figure.4.1)

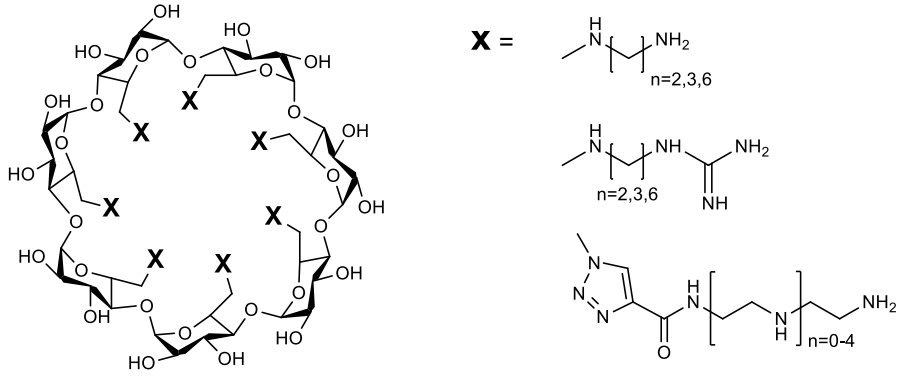

Figure 4.1 – Structures of polyaminocyclodextrin derivatives.

Yannakopoulou et al. have carried out the synthesis of aminoalkylamino and guanidinoalkylamino α-, β- and γ-**CD**s, in order to obtain systems with cell-membrane penetrating features similar to the ones already seen for lisine or arginine-based polypeptides.[177-180] The syntheses were carried out starting in both cases from the *heptakis*-(6-deoxy)-(6-bromo)-**βCD** derivatives; the aminoalkylamino derivatives were then obtained by nucleophilic displacement reaction with the proper diamino alkyl group, whereas the guanidine

derivatives were obtained or by direct guanidilation of the aminoalkylamino derivatives, or by displacement of the bromine atoms with azide groups, the reduction by Staudinger reaction followed by guanidilation of the resulted amino groups.

These systems were found able to bind and protect pDNA and siRNA as demonstrated by its reduced electrophoretic mobility as well by its low interactions with fluorescent ethydium bromide stain, with an efficiency better than the *per*-(6-deoxy)-(6-amino)-**CD**s used as reference systems.[130] This has been attributed to the ability of the aminoalkylamino- e guanidinoalkylamino-**CD**s to condense polynucleotides by forming globular nanoparticle as shown by Atomic Force Microscopy. The assayed derivatives presented an order of efficiency as much higher as the number of substituents on cyclodextrin scaffold increases (resulting in the best activity of γ-**CD**s). The best activity of guanidinoalkylamino-**CD**s is related to the well know guanidine-phosphate specific interaction.[181]

Transfection assays were also carried out on Human embryonic kidney cells (HEK 293T), showing transfection abilities comparable to the commercial available transfecting agent Lipofectamine 2000.[175] Reineke et al. have carried out the synthesis of a library of seven-branched polycationic **βCD**s, bearing linear oligoethyleneimine (OEI) groups characterized by different length and number of protonable sites (Figure 4.1). The syntheses were carried out by anchoring the desired OEI groups, previously modified as acryloyl amide, on *heptakis*-(6-deoxy)-(6-azido)-**βCD**, exploiting the copper (I) catalysed azide-alkyne cycloaddition reaction. All the systems tested have proven to bind pDNA in nanoparticle systems (*Polyplex*), having average diameters ranging from 80 to 130 nm, as shown by DLS and TEM analysis, providing protection to the encapsulate gene materials toward the DNAse degradation. Electrophoretic mobility shift assays have also highlighted that polycationic **CD**s are able to bind pDNA, hindering its electrophoretic migration in a combination ratio, defined N/P (where N is related to the nitrogen atoms on polycationic **CD**s and P is the number of phosphate groups of pDNA), ranging between 1.5 and 2.5 and with an efficiency as higher as the OEI length increase. The same trend was observed probing the transfection abilities of polycationic **CD**s towards human cervix adenocarcinoma (HeLa) and rat cardiomyoblast (H9c2) cells, compare with commercial transfecting agents as cationic polymer Jet-PEI and cationic dendrimer Superfect. In particular, the polycationic **CD**s with OEI chains featured by the presence of 4 and 5 amino groups have revealed the better transfection abilities, with almost the same extent of effectiveness with respect to the reference Jet-Pei and Superfect, but characterized by a lower toxicity towards both the cell lines.[56]

A step forward was accomplished by exploiting the confined and opposite orientated architecture of the **CD** rims, allowing the installation of cationic and hydrophobic defined regions in order to obtain amphiphilic cyclodextrins.[55,90,182-189] This kind of set up took advantage from the *facial amphiphilicity* concept,[91,190,191] relied on the idea that systems featuring opposite positioned cationic and hydrophobic domains, might improve their fusogenic properties toward membrane cell, favouring the internalization process of the particle systems formed upon gene material interaction.

The regioselective insertion of cationic and lipophilic moieties can be carried out on the primary or the secondary rim respectively, giving rise to Skirt-type[55,90,183,184,187,188] designed systems or by a reverse orientation to jellyfish-type systems.[192,193] Both arrangements have been investigated, although the Skirt-type design was the most studied due to its streamlined synthetic pathway and better gene-complexing performances.

At this regard Ortiz-Mellet's group, during the last decade have conceived and developed a wide library of amphiphilic **βCD**s, by anchoring polyamino branches and alkyl tails on the primary and secondary edge respectively.[55,90,184,186-188,193] The insertion of polyamine groups was accomplished by exploiting two different "click" approaches, namely the copper (I) catalysed azide-alkyne cycloaddition reaction between *heptakis*-(6-deoxy)-(6-azido)-**βCD** and alkinyl-polyamines, or the amino isothiocianate coupling reaction between cysteamyl-**βCD** derivatives and polyamino-isothiocianate derivatives (see Figure 1.4), whereas the alkyl chains were linked by ester or ether bond.

All the polycationic amphiphilic cyclodextrin derivaties (**PaCD**s) developed so far, which differ for the architecture of the polyamino groups (length, ramification and number of protonable amino groups), flexibility of the linker (aware that cysteamyl-thioureido moieties is more flexible than tryazole one) and the length of alkyl chain, were tested in order to evaluate their abilities to compact and protect pDNA in nanoparticles systems (CDPlex), as well as favouring its uptake. In any case **PaCD**s have shown by electrophoretic assays the ability to bind pDNA hampering its migration through the agarose gel at an N/P value never exceed 10, protecting the pDNA making it inaccessible to the ethidium bromide intercalating agent, with the resultant disappearance of the electrophoretic line.

In a careful structure-activity relationship study it was concluded that the best **PaCD**s configuration to have the best gene delivery performance is obtained for the aminoethylthioureido pattern joined with hexanoyl tails.[55] In particular, **PaCD**s with a dendritic like structure (Figure 4.2) has reached high level transfection performance towards murine hepatocyte (BNL-CL2) and green monkey epithelial kidney (COS-7) cell lines, with an

efficiency ten-fold higher with respect to the polyethylene imine (considered the referring standard in non-viral gene delivery transfection), but at lower N/P value (5 vs 10) and with a reduced toxic profile.

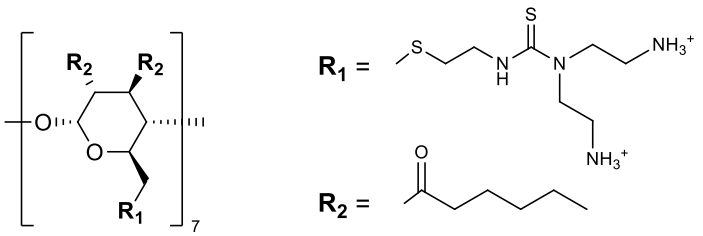

Figure 4.2 – Structures of **PaCD**s

These findings were explained taking into account the dendritic nature of this **PaCD**s, as well as the presence of thioureido moieties which afford the mutual hydrogen bonding and electrostatic interactions, thereby mimicking the reversible recognition abilities of biological receptors towards phosphate groups.[181,194]

Furthermore, this kind of **PaCD**s promote the wrapping of the pDNA in spiral-shaped nanoparticles with an average diameter of 40 nm, constitute by a series of alternating layers of pDNA and **PaCD**s self-assembled each other on the hydrophobic side, as revealed by TEM images. The whole of the results led the authors to consider as an essential feature the presence of lipophilic tails in order to achieve the best complexation performance of pDNA in CDplex and then favour the crossing of membrane cells.[186] In any case, the synthetic methodologies described for the synthesis of **PaCD**s, although affording pure compounds, are characterized by a long series of synthetic steps, or by the need to work in drastic reactive conditions, affecting the overall yield and making the synthetic procedure uneconomical in view of a production on a larger scale.

My work on **amCD** is framed in this context. The **amCD**s, obtained by a more streamlined and cost-effective synthetic process, were tested in order to assess their ability to act as vectors for the protection and transportation of plasmid DNA although present as a mixture of compounds with different degree of substitution. It is noteworthy indeed that these compounds are polycations at physiological pH values, having more than 50% of their basic sites in their protonated form, and therefore it is reasonable to predict that possess, like to the aforementioned **PaCD**s, a comparable ability to interact with the pDNA. In particular, three of the **amCDs** obtained namely **amCD1**, **amCD2** and **amCD3** were assayed for interaction with pUC19 chosen as a suitable target.

4.2 - Results and discussion

4.2.1 – pUC19 complexation EMSA assays

The pUC19 is a plasmid DNA (pDNA) constituted by ca. 2700 bp (base pairs), which is present in three different forms i.e. linear, circular and supercoiled. (Figure 4.3)

pUC19 is characterized by the presence of one ampicillin resistant gene (amp^R). The uptake of this plasmid by a bacterium cell provides it with resistance to ampicillin.

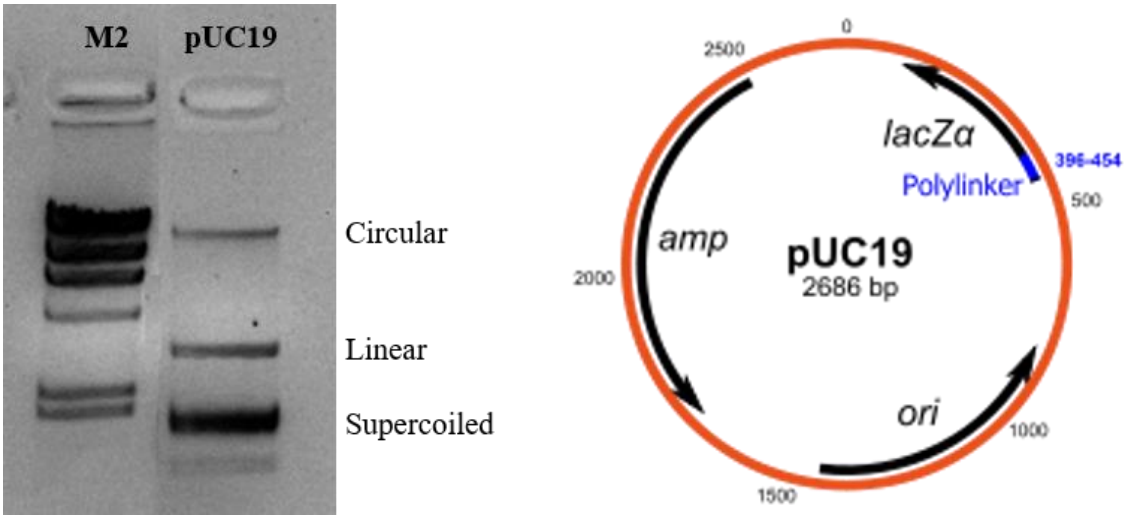

Figure 4.3 – EMSA assay and schematic representation of pUC19.

The pDNA and the proper amount of each **amCD** were mixed in different combination ratios. The latter ones are defined as N/P ratios, i.e. as the ratio between the number of nitrogen atoms on the cyclodextrin core and phosphate groups of pDNA. To do this, as equivalent weight for **amCD**s were used the ones previously reported (see pag. 21), whereas for pDNA an average equivalent weight of 330 was used, which corresponds to the average molecular weight of a nucleotide monophosphate unit.

The first assays were carried out using 200 ng of pDNA, mixed with the appropriate amount of **amCD** in order to obtain the following N/P ratios: *i*) 0.55; *ii*) 2.75; *iii*) 5.5; *iv*) 8.25; *v*) 16.5; *vi*) 27.5 for all the three **amCD**s. After a period of incubation of 20 min at r.t., the complexation of pUC19 by **amCDs** was assessed by means of a gel electrophoresis mobility shift assay, repeating the assay in triplicate for each **amCD** (Figure 4.4).

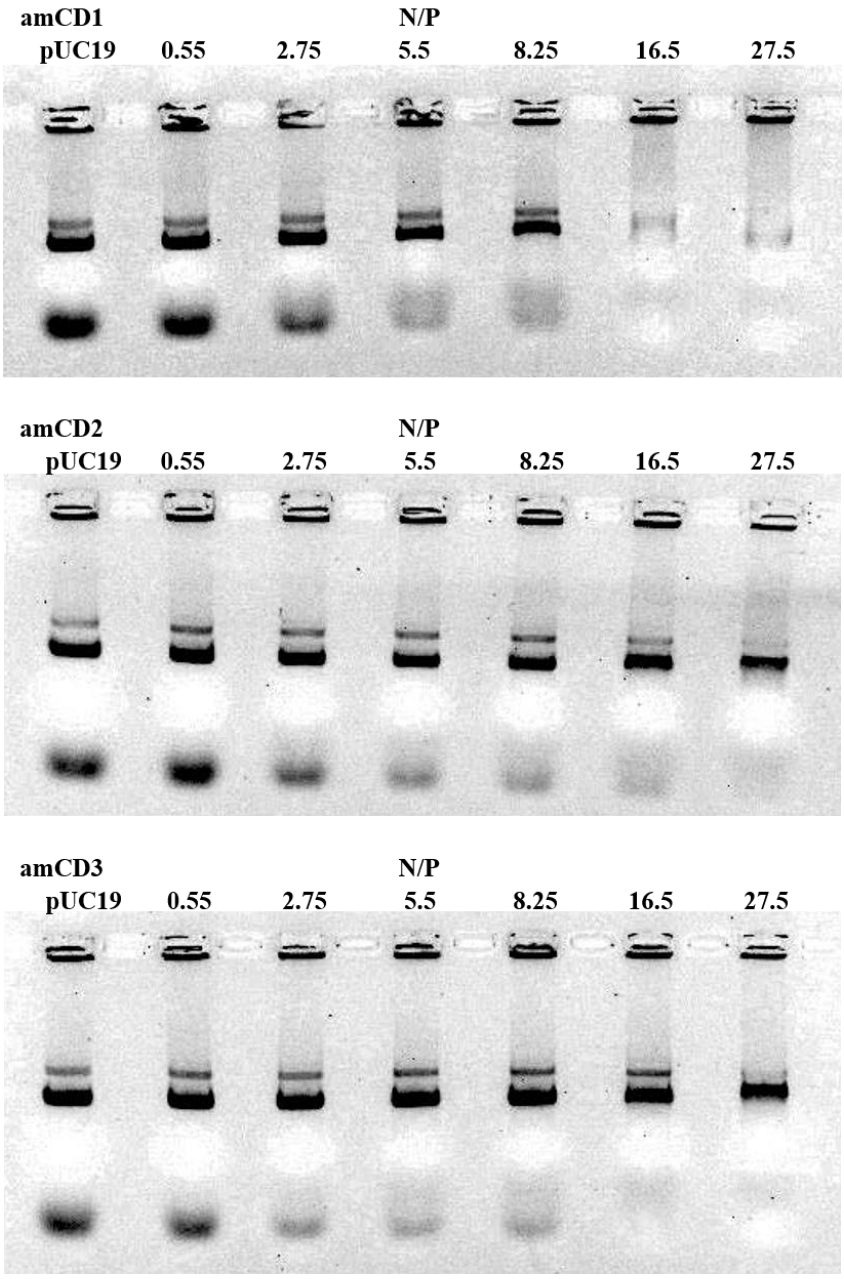

Figure 4.4 – Binding EMSA assays

It is apparent from the photographs related to the EMSA with **amCD1**, **amCD2** and **amCD3** respectively, that **amCD1** has the best binding ability towards pUC19 with respect **amCD2** and **amCD3**. As a matter of fact, **amCD1** binds pUC19 almost completely at N/P as large as 27.5, hindering it to move through the gel; whereas for **amCD2** and **amCD3** there isn't apparently change in the migration ability of pUC19 through the gel, at the different N/P values. For this reasons others EMSA assays were carried out by probing higher N/P values, namely 38.5 49.5 and 60.6. (Fig. 4.5)

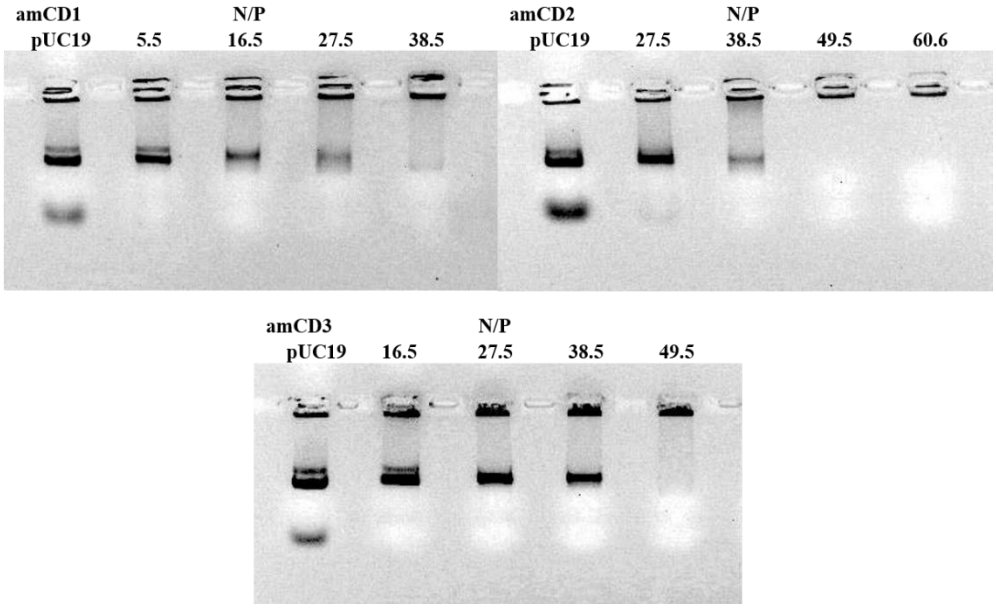

Figure 4.5 – Binding EMSA assays

The photograph shows that in presence of **amCD1**, pUC19 is completely blocked at N/P as large as 38.5, whereas in the case of **amCD2** and **amCD3** it is needed to use a N/P value as large as 49.5. In order to explain the different binding abilities of **amCDs** toward pDNA, it is necessary to keep into account the different factors which could affect their mutual interaction. First of all, by submitting the previous pictures to a more careful analysis it is clear that the binding ability of the **amCDs** is related to the form of pUC19, which is characterized by presence of Circular, Linear and Supercoiled DNA, first second and third line respectively. As a matter of fact, the affinity of **amCD** towards the three different forms of pUC19 follows the order Supercoiled > Circular > Linear. (Table 4.1)

Table 4.1 – Results of binding assays.

	amCD1 (N/P)	**amCD2 (N/P)**	**amCD3 (N/P)**
Supercoiled	5.5	16.5	16.5
Circular	16.5	27.5	27.5
Linear	38.5	49.5	49.5

Obviously the higher affinity for a packed structure such as supercoiled and circular forms could be explained considering that it is easier to compact an already packed structure. On the other hand, as long as the Linear form is concerned, **amCD**s do not seem particularly able in complexing it effectively. Probably the **amCD**s interacting with DNA wrap it longitudinally, in such a way to keep its linear shape, that in conditions of not completely neutralized charge, enables it to migrate through the gel at worse with a reduced steric hindrance.

On passing to consider the effect of the length of the polyamine chains, the best performances of **amCD1** appear in disagreement with the results obtained with alginate. It is worth noting that, under the pH conditions used (i.e. pH 7.5), **amCD1** has a lower average charge (ca. 6.2) as compared to **amCD2** and **amCD3** (ca. 10.4 both). It is reasonable to assume that the presence of the polycation may induce significant conformational changes in the fairly flexible pDNA polyanion, at the cost of inducing a certain amount of strain. Of course, these changes can hardly occur for the much stiffer **Alg** structure. Therefore, **amCD1** may overall appear more effective towards pDNA because, due to its smaller charge, binding involves a larger amount of polycation units, each inducing a relatively small strain along the polyanion chain. By contrast, the most charged **amCD2** or **amCD3** units cause larger strain, overall destabilizing the interaction.

4.2.2 – Bacterial transformation assays

Furthermore, in order to test the gene delivery ability of **amCD**s, some transformation assays were carried out. The interest for this peculiar model relied in the fact that, as it was mentioned in the introduction, polycationic systems such as dendrimers amphiphilic cations and **PaCD**s, are very effective in performing transfection of gene material into eukaryote cells. Therefore, it seemd worth testing the possibility to exploit similar systems also toward prokaryote cells. As a general procedure, *Escherichia coli* DH10B Calcium Competent (CaCO) cells, were subjected to thermal shock in presence of the desired pUC19-**amCD** mix.

Then, the samples obtained were spotted on a petri dish with LB-Agar medium in the presence of ampicillin, used as restriction antibiotic, and incubated at 37 °C O.N. The internalization of pUC19 confers ampicillin resistance to the CaCO *E. coli* cells. Then the transformation ability of **amCD**s can be easily assessed by numbering the resulted bacterial colonies. In particular, taking into account the result obtained by EMSA, the transformations assays were performed using the following N/P ratio i.e 38.5 for **amCD1**; 49.5 for a**mCD2** and **amCD3**; as reference the same amount of free pUC19 was used. The results are summarized in Table 4.2.

Table 4.2 – Results of bacterial transformation assays

	Free pUC19	**amCD1 N/P 38.5**	**amCD2 N/P 49.5**	**amCD3 N/P 49.5**
Bacterial Colonies	1290 ± 10	5.0 ± 1.5	2.0 ± 0.7	140 ± 10

These results show that **amCD**s are ineffective in performing the internalization of pUC19, but rather they hamper it. This could be explained taking into account the peculiar role of Ca^{2+}. The Ca^{2+} ions, indeed, create a positively charged layer on the bacterial surface, attracting in this

way the negatively charged pDNA, which after thermal shock and destabilization of the cell wall is easily internalized. As a consequence of the **amCD** interaction, pDNA can be neutralized or makes positive, thereby do not enabling the electrostatic attraction by Ca^{2+} ions on bacterial surface or worse causing their repulsion.

In comparisons with other literature data concerning polycationic cyclodextrins, it is clear that the results obtained, are very different. In particular, regarding to the electrophoretically assessed ability of **PaCD** to complex pDNA by blocking its migration, N/P values, usually reported range from 1 to as much as 5. Considering the transformation efficiency, the main example reported in literature are related to transfection assays i.e using eukaryote cells as target. Many Authors report transfection efficiencies similar or even better than those obtained using other commercial gene delivery systems (Jet-PEI, Superfect or Lipofectamine), but in almost every case greater with respect the free pDNA.

It is worth mentioning that most of **PaCD** reported in literature, are pure chemical individuals and the polycationic pendant groups present on their primary rim are characterized by a large conformational freedom, which depends on the nature of spacer present between the arms and the **CD** scaffold, as well as by the length of the arms itself. This give to the **PaCD** the possibility to fit upon the pDNA surface in order to maximize their interactions. In the case of **amCD**s a lesser flexibility of the polyamine branches can be assumed. In fact, because of the possibility that the polyamine arms give rise to polysubstitution, a certain amount of them can form bridge on the primary rim of the **CD**. This event as long as causing a decrease in conformational flexibility, also shortens of the effective polyamine length. Obviously, these facts negatively affect ability of **amCD**s to fit themselves to the pDNA. As a consequence, rising the N/P ratio is need for its complexation. This aspect is worsen considering the self-folded tendency of polyamine arms as the number of nitrogen atoms and length become higher, as shown by Ohwada et al. by means of molecular modelling of amphiphilic steroid-polyamine.[195]

Considering the trasformation assays carried out with **amCD**s, cannot be compared to the transfection assays reported in literature using **PaCD**s as gene delivery systems, because deal with different cell strains, with the main difference that the target cells belong to different taxon namely Prokaryota and Eukaryota respectively and then featured by different cell membranes and different permeability towards exogenous materials.

Finally, **PaCD**s reported in literature, as well as it be pure molecules obtained with a long and expensive click chemistry approach, are characterized by the presence of alkyl chains on the secondary rim, which make it amphiphilic. This feature allows them to give rise to self-assembled structures by pDNA interaction, so favouring the protection and delivery of pDNA.

The lack of the alkyl chains in **amCD**s is clearly another explanation to the low ability of them to delivery pDNA into CaCO *E. coli* cells, due to a less affinity of *per*-hydroxy secondary rim of **βCD** with phospholipid membrane, whereas systems with alkyl chain can blend to the cell membrane favouring the transfection process by uptake the **PaCD**-pDNA complex.

4.3 - Experimental section

Plasmid preparation

The plasmid used in this work pUC19, was amplified in *E. coli* culture left to grow under stirring at 37 °C in 1.6 L of *terrific broth* (TB – a high rich culture medium containing bacto triptone, yeast extract, glycerol and a KH_2PO_4 – K_2HPO_4 pH 7.8) in presence of ampicillin as restriction antibiotics. After overnight incubation bacterial cells were collected by centrifugation and subjected to alkaline lysis protocol to recover plasmid DNA. The resulted pellet was resuspended with 90 mL of cold SOL I (50 mM glucose – 25 mM Tris-HCl – 10 mM EDTA) and 10 mL of 10mg/mL Lisozime solution. Then, to the resulting solution 200 mL of SOL II (0.2 M NaOH – 1% SDS) and 10' later, 100 mL of cold SOL III (3M CH_3COOK - 2M CH_3COOH) were added. The resulted solution was stored at 0 °C for 10', then it was centrifuged and filtered. Finally, to the clear solution 240 mL of 2-propanol was added to precipitate pDNA which was finally recovered by centrifugation.

The obtained pDNA, was treated with RNAse and then purified using phenol-chloroform extraction in order to remove the last traces of proteins and RNA. The purified pDNA was suspended in TE buffer (Tris-HCl 10 mM – EDTA 1 mM pH 7.5) and quantified by gel electrophoresis, using a graphical software (*ImageJ*) in order to compare the lines of our pUC19 with lines of λ fragment HindIII Marker used as reference. Moreover, the purity of pDNA was spectrophotometrically assessed considering the absorbance ratios 260/280 and 260/230, which are related to the degree of contamination by RNA and protein respectively. In particular, for pUC19 values of 1.75 and 1.96 were obtained indicating the presence of a quite pure pDNA. The pDNA solution, with a concentration of 200 ng/μL, was aliquoted and stored at -20 °C.

Electrophoretic mobility shift assays

In order to observe the effect of **amCD**s on the electrophoretic mobility of pUC19, different mixtures of **amCD**-pDNA were subjected to electrophoretic assays. In particular, starting from the concentrated solution of pUC19 (200ng/μL) this was diluted 1:3 obtaining a solution 66.7 ng/μL. For the EMSA assays, the composition of each systems characterized by a different N/P ratio (equivalent of nitrogen atoms/equivalent of phosphate groups), was adjusted keeping into

account a constant amount of pDNA (200ng) and a final volume of 20 µL. The proper amount of each **amCDs** was added to the systems starting from stock solutions at a concentration of 33.3 mN for each **amCD**, and performing the due dilutions using in each case TE buffer (Tris-HCl 10 mM – EDTA 1 mM pH 7.5) as the solvent.

Basically, a generic system was composed by 3 µL of pDNA solution 66.7 ng/µL, a variable volume of **amCD** solution and the necessary amount of TE buffer to adjust the final volume to 20 µL. After their preparation the systems were incubate for 20 min at r.t.; then 3 µL of loading buffer (0.25% BFB – 30% Glycerol) were added to each system, which was then loaded on a 0.8% agarose gel (8 mg/mL per 150 mL TBE buffer [Tris 44 mM – boric acid 44 mM – EDTA 1 mM; pH 7.5] stained with 1.5 µL of Ethidium Bromide). Each system was then submitted to 30' electrophoresis under 100 V, using in any case free pDNA as reference.

In vitro transformation assays

Before transformation assays, *E. coli* DH10B CaCO cells were grown in Lauria-Bertani medium (LB - culture medium containing bacto triptone, yeast extract and NaCl) at 37 °C up to an optical density at 650 nm as large as 0.6. Then the culture is stored at 0 °C for 2 hours. Whereupon the cells were subsequently collected by centrifugation, treated with a 70 mM $CaCl_2$ solution, and stored at 0 °C for 1hour. Then cells were again collected by centrifugation, treated with freezing solution (70 Mm $CaCl_2$ – 10% (w/v) glycerol) and finally aliquoted and frozen at -80 °C.

In order to perform the transformation assays, two systems of 20 µL for each **amCD**/pDNA ratio selected (N/P 38.5 for **amCD1** – N/P 49.5 for **amCD2** and **amCD3**), as well as the control systems with free pDNA were prepared, added with 50 µL of *E. coli* DH10B CaCO cells and stored at 0 °C for 30 min; then the systems are warmed up to 42 °C for 45 s and soon after cooled at 0 °C for 2 min. After that 500 µL of LB medium were added to each system afterward left stirring at 37 °C for 1 hour. At this point 50 µL of each starting systems, were spotted on three different Petri discs containing LB-agar medium (10 g/L bacto triptone, 5 g/L yeast extract, 10 g/L NaCl and 12 g/L agar) and 100 µg/mL of ampicillin in such a way to have double triplicate experiment parallelly prepared. The systems were incubated overnight at 37 °C. Afterwards the transformation efficiency was evaluated comparing the number of bacterial colonies formed in presence of **amCD**/pDNA complexes, with respect to those formed with free pDNA.

- 5 -

POLYAMINOCYCLODEXTRIN NANOSPONGES: SYNTHESIS AND pH-TUNABLE SEQUESTRATION ABILITIES

5.1 – The Cyclodextrin-based Nanosponges

Cyclodextrin-based nanosponges (**CD-NS**s) are members of a novel class of hyper-reticulated polymeric materials characterized by a nanoporous 3D-framework. The first reported use of the term nanosponge it dates back to 1998 when Ma et al. have coined this name to label insoluble polymers obtained by cross-linking β-cyclodextrins with organic diisocyanates lynkers.[196] The authors used the so-obtained **CD-NS**s for the removal of organic pollutants as *p*-chlorophenol from waste water.[197]

The rationale behind **CD-NS**s is exploiting and improve the complexation abilities of native **CD**s by cross-linking them with suitable moieties, in such a way to obtain a supramolecular absorbent agent. Noticeably, the presence of linker agents might provide in principle further binding sites to the included molecules both for direct interactions and for the formation of nanochannels in the nanosponge structure, able to function as supplementary host cavities. The most common linker agents used so far are bis-electrophiles[198] as epichlorohydrin; carbonyl compounds (carbonyldiimidazole, diphenylcarbonate, triphosgene); diisocyanates or dianhydrides. In general, for the synthesis of **CD-NS**s two different approaches were exploited namely solvent evaporation approaches and ultrasound-assisted synthesis.[199,200] In the first case the synthesis is carried out by refluxing cyclodextrin with solvent (Ethanol, DMF etc.) in presence of an excess of the desire crosslinker. The second one is a solvent free-method whereby a cyclodextrin-crosslinker blend is left reacting under sonication. In both cases the resulted products are grinded and purified by Soxhlet's extraction using ethanol. Nevertheless, the abovementioned methods are the most used, in literature others strategies as microwave assisted synthesis are reported for the synthesis of **CD-NS**s.[201] It is noteworthy that FTIR-ATR,

solid state NMR and Raman analyses have confirmed that the primary hydroxyl groups are mainly involved in the crosslinking process.[202,203]

The reticulation process gives rise to sub-micrometrical particles featured by a channel-rich structure, like a sponge. [204-207] The nanosponges reported so far in most studies are basically powders constituted by roughly spherical particles with an average diameter of 200-500 nm and a narrow polydispersity. Furthermore, **CD-NS**s with crystalline or paracrystalline structure can be obtained, when ultrasound-assisted synthesis is used. Regarding to the physicochemical properties of nanosponges, a good example is given by the carbonate nanosponges which have showed to be thermally stable up to 300° as well as being autoclave-resistant. Furthermore, the chemical stability of these nanosponges at 60 °C in acidic and basic envoriments was tested as well, showing a limited leakage of cyclodextrin units from the nanosponge structure.

Albeit their hydrophilic nature, accounted for by their high wettability as well as swelling ability in aqueous media, the high degree of reticulation makes water insoluble **CD-NS**s, able to form long lived colloidal suspensions, due to the negative ζ potential ranging from -20 to -40 mV, which is enough large to exert the needed repulsive force to avoid particle coalescence.

In principle, the **CD-NS**s properties might be tuned by acting on the kind of cyclodextrin or linker used, as well as on their ratio. In this way it is possible to affect the reticulation degree and in turn the dimension and accessibility of nanochannels, thereby varying the inclusion abilities.[208] For example, **CD-NS**s obtained using pyromellitic dianhydrides give nanosponges with free carboxylic groups, which although less chemically and thermally stable, are characterized by higher swelling tendency and more negative ζ potential allowing them to include cations, organic molecule and macromolecules.[209] In any case it is necessary to remember that, regardless the type of linker used, nanosponges exhibit many hydroxyl groups, which can be wisely modified changing their properties as well.

The increased inclusion properties of **CD-NS**s with respect the free **CD**s and their controllable ability to catch and release diverse substances, have allowed their application in different fields. The first use of **CD-NS**s was the water purification by different kind of pollutant,[210] as described in a recent review dealing with the environmental use of epichlorohydrin nanosponges.[211] **CD-NS**s have revealed the ability to remove different type of pollutants such as organic molecules or heavy metals with an efficiency higher to the activated carbon, and with the possibility to be easily recovered washing them with a green solvent as ethanol.[212]

In the last decade, thanks to their non-toxic nature, **CD-NS**s have progressively carved a niche in the pharmaceutical field becoming among of the most studied drug delivery systems, [199,204,209] as highlighted in a recent report of EU commission as well.[213]

There are many advantages on the use of **CD-NS**s as drug delivery systems with respect to free **CD**s. First of all, the greater amount of different interaction site, available and their faceted polarities. Indeed, along with the hydrophobic **CD** cavities, there are a lot of hydrophilic site in the nanochannel walls and in the outer **CD** faces, thereby allowing the inclusion of differently polarized molecules.[208,209,214] Second we have to consider that release rates may be regulated by modifying the reticulation degree. Finally, a valuable features is their biodegradable and non-toxic nature (tested both in vitro and in vivo),[215] considering also that the free **βCD** is characterized by low water solubility and cannot be intravenously injected owing to nephrotoxicity issues. Noticeably, drugs characterized by poor water solubility, by dispersion into **CD-NS**s structure can improve their apparent solubility, enhancing their overall bioavalaibility. For instance, Swaminathan et al. showed that water solubility of Itraconazole can be enhanced more than 27 fold using carbonate **CD-NS**s, and up to 55 fold when polyvinyl-pyrrolidone (PVP) is added to the nanosponge.[216]

The inclusion of drugs into **CD-NS**s structure enable to circumvent other drawback namely their possible chemical-, enzymatic- or photo-degradation.[209] For example, the anticancer drug Camptothecin, other its low solubility, is characterized by a low stability, due to the easy hydrolysable lactone ring present in its structure. At this regard Cavalli et al. studied the inclusion of Camptothecin in three carbonate nanosponges differing each other by the linker/**βCD** ratio being 2, 4 and 8 respectively. The interaction of Camptothecin and nanosponges structure was confirmed by FTIR, DSC and XRPD. In any case nanosponges proven their ability to protect Camptothecin by lactone hydrolysis at physiological condition, indeed after 24 h of incubation at 37 °C and pH 7.4, 80% of lactone form was found, with respect to the 20% of the unmixed drug.[217] Furthermore, the nanosponges enable the solubilisation of higher amount of Camphothecin, its slow release over time and an improved activity towards target cells.[218] The last advantage of the use of **CD-NS**s as drug delivery system is their support to the drug release, which can be tuned by acting on the reticulation degree of nanosponges. In fact, it has been seen as the release rate is inversely correlated to the degree of reticulation.[208] Therefore, the possibility to accomplish a controlled release of the drug over the entire dosage period enables the lowering of the drug administration, as it was showed for Flurbiprofen, Nelfinavir mesylate or Acyclovir loaded nanosponges.[209,219,220]

Among other applications, it is worth mentioning the use of **CD-NS**s as support for catalyst, in particular of enzymatic nature, because **CD-NS**s are able to preserve and prolong their activity;[221] the application of **CD-NS**s in agriculture as slow release agent for chemicals;[222] as flame retardant additives for polymers[223], as gas carriers[224] and in enantio-differentiating

photoisomerization processes.[225] The possibility of tuning the absorption and release abilities of **CD-NS**s, in particular the achievement of sensitivity to all conditions, appeared particularly interesting. For this reason, part of the present work was developed to explore the possibility of employing **amCD**s for the construction of new **CD-NS**s.

5.2 - Results and discussion

*5.2.1 – Sinthesis of **ACN** materials*

With the aim to accomplish the syntheses of **amCD**-based nanosponges (**ACN**s), a different approach with respect to previously reported in literature was exploited. Because of the intrinsically nucleophilic nature of the polyamine linkers, it was reasoned that the **βCD** residues could be work as the electrophilic moieties of a nucleophilic displacement reaction. At this regard, the already mentioned **BrβCD** appeared a suitable candidate as the starting material. In a first series of experiments, we tried to react directly **BrβCD** and four polyamines, namely **Am2**, **Am3**, **Am6** and **Am7**. The **BrβCD** and amines were reacted in a 2:7 mol/mol ratio. The carefully blended solvent-free semi-fluid mixture of the reactants was kept at 60 °C for 48 h, in order to ensure that the nucleophilic displacement reaction came to completion. Unfortunately, in this way only intractable, partly water soluble, gummy slurries were obtained. Then, a different approach, was considered, namely the reaction between **amCD2**, **amCD3**, **amCD6** and **amCD7** derivatives with **BrβCD**. In particular, **amCDs** were placed to react with **BrβCD** in a 7:***ñ*** mol/mol combination ratio (**Rt**) which corresponds to a 1:1 equivalent ratio between the two reactants (Figure 5.1). The reaction was performed in the presence of a very small amount of DMSO (ca. 400 mL per g of reactants mixture) just to allow the right homogenization of the reactants. The desired polymers were obtained as amorphous materials which, after repeated washings with methanol and diethyl ether and subsequent drying, could be easily grinded (< 150 μm) to afford the final products as pale brown powders, in very high yields (i.e. 95%, see later).

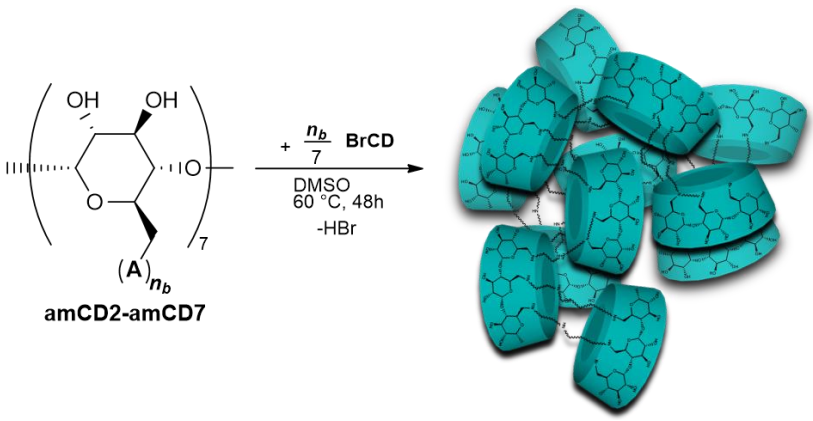

Figure 5.1 – Pictorial representation of **ACN**s.

*5.2.2 - Characterization of the **ACN** materials: solid state NMR*

The resulted polymers, labelled **ACN1**–**ACN4** (according to the **amCD**s order), were firstly characterized by FT-IR and $^{13}C\{^{1}H\}$ CP-MAS NMR spectroscopy. These preliminary spectroscopic characterization, gave information about the polymeric nature of the materials.
FT-IR spectra of **amCD6** and the corresponding material **ACN3** are depicted in Figure 5.2 as representative examples.

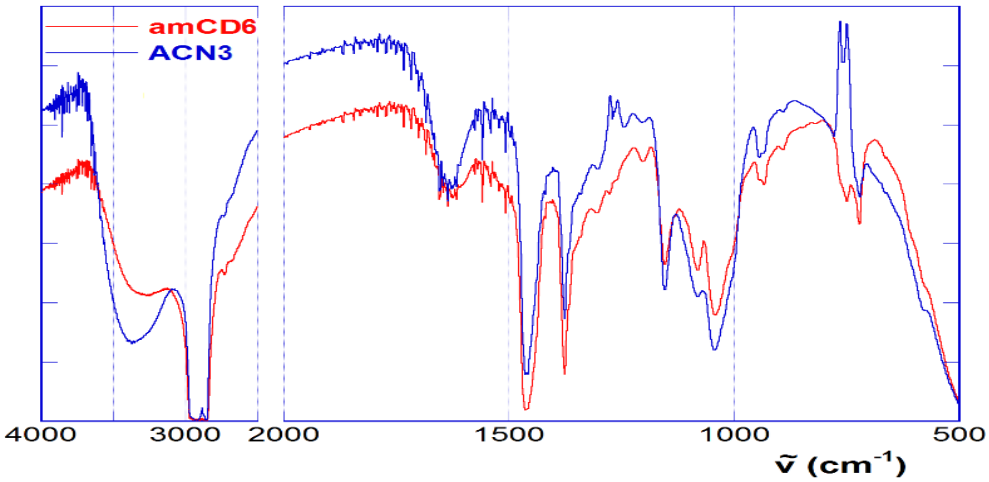

Figure 5.2 – FT-IR spectra of **amCD6** and **ACN1**

As it is possible to see, both spectra show almost the same main features. In particular, we can notice a system of three peaks at 1155, 1084 and 1041 cm^{-1} (together with a minor signal at 946 cm^{-1}) constituting the typical fingerprint of the **CD** scaffold. Spectra also show the large and intense O–H stretching band in the region over 3200 cm^{-1}, which conceals possible N–H stretching bands. Moreover, the presence of residual traces of water is accounted for by the jagged H–O–H bending band centered at ca. 1627 cm^{-1}. The main difference is related to the disappearance of the primary amino group wagging band at 722 cm^{-1} in the **ACN3** spectra, which is a clear evidence of the presence of a polymeric network.
Solid state $^{13}C\{^{1}H\}$ CP-MAS[226] NMR spectra of **ACN** materials are illustrated in Figure 5.3. All spectra show a system of three signals accounting for the **CD** scaffold. In particular, we notice a signal centred at ca. 103 which can be attributed to the anomeric C(1), and two partly overlapped signals at ca. 84 and 73 ppm, the first one attributable to the C(4), the second one cumulatively to the C(2), C(3) and C(5) carbon atoms. The spectra of materials **ACN3** and **ACN4** show two broad signals centred at ca. 50 and 27 ppm, together with a further minor signal at ca. 41 ppm. The signals at ca. 50 and 41 ppm can be reasonably attributed to C atoms directly bound to a nitrogen atom, i.e. the C(6) of the **CD** scaffold and the end-chain C atoms of the diamine linkers **Am6** or **Am7**. The signal at ca. 27 ppm, in turn, can be attributed to the other C atoms of the linker chains.

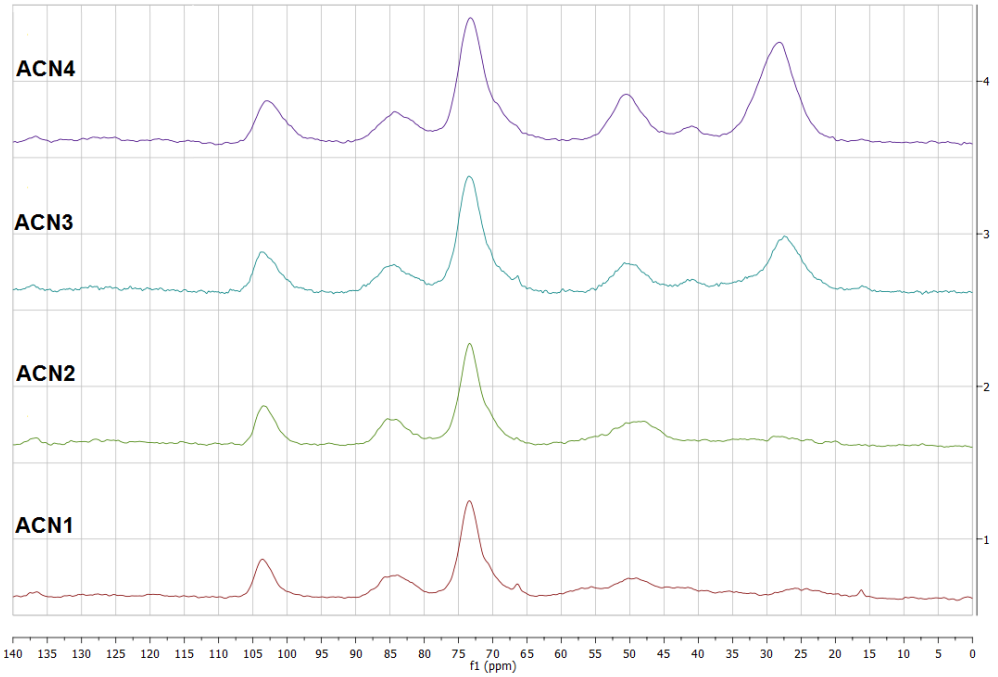

Figure 5.3 – $^{13}C\{^{1}H\}$ CP-MAS solid-state NMR spectra of **ACN**s.

On the other hand, in the spectra of **ACN1** and **ACN2** no signal at 41 ppm is any longer visible, whereas the signal at 27 ppm appears very low in intensity. The latter finding is consistent with the fact that in the relevant linker chains only a minority of carbon atoms is not bound to a nitrogen atom. Along with a qualitative confirmation of the presence of the **βCD** scaffold and the linker chain, the $^{13}C\{^{1}H\}$ CP-MAS NMR technique can afford semi-quantitative information as well. As a matter of fact, under the hypothesis that cross-polarization effects work homogeneously for all the carbon atoms present in the sample, in principle integration analysis of the signals might be performed.[227,228] The peaks integrals for the four spectra, obtained by taking the signal of the anomeric C(1) as the reference standard, are collected in Table 5.1.

Table 5.1 – NMR data for **ACN**s.

		Signal integration			
Attribution	**ppm**	**ACN1**	**ACN2**	**ACN3**	**ACN4**
$C_{CD}(1)$	103	1	1	1	1
$C_{CD}(4)+C_{CD}(2,3,5)$	84, 73	4.14	4.40	4.00	4.17
$C_{CD}(6)+C_{linker,N}$[a]	50, 41	1.30	1.63	2.09	2.00
$C_{linker,c}$[b]	27	2.34	3.85	0.71	0.36

[a]C of the linker chain bound to N atom. [b]C of a linker chain not bound to a N atom

As long as the signals relevant to the **CD** scaffold are cumulative considered, agreement between the expected integral values and the ones found is satisfactory (a 10% deviation is found only for **ACN4)**. Integration of the signals of the linkers afforded more problematic

results. For materials **ACN3** and **ACN4** constituted with the diamine linkers we can cumulate that, if each glucose moiety of a given **βCD** subunit would bind a different linker chain, then integration values of 2.0 and 3.0 respectively, should be expected for the signal at 27 ppm. Experimental values are larger than these upper limits, indicating that for the relevant –CH_2– groups cross-polarization effects work much more effectively as compared to the methine groups of the **βCD**.[229] For materials **ACN1** and **ACN2** a reliable integration of the signal at 27 ppm is made difficult by their low intensity. On the other hand, cumulative integration of the signals at 50 and 41 ppm renders values that are lower than the relevant theoretical upper limits (i.e. 3.5 for **ACN1**, 4 for **ACN2** and 2 for **ACN3** and **ACN4**). This finding suggest that the unfavorable outcome of proximate quadrupolar nuclei such as ^{14}N to the transmission of cross-polarization effects,[230] compensates the peculiar enhancement of –CH_2– groups. Then, by simple algebraic passages, relevant data allowed to estimate an average number of polyamine linkers per **βCD** subunit ($\tilde{n}$) as large as 3.0 ± 0.3 for **ACN1**, 2.3 ± 0.2 for **ACN2**, 2.1 ± 0.2 for **ACN3** and 4.4 ± 0.5 for **ACN4**.

*5.2.3 – Potentiometric titration of **ACN**s*

In order to get an independent quantitative estimation of the average number ($\tilde{n}$) of linkers per **βCD** subunit in the polymers, as well as to evaluate the general abilities of the materials as proton acceptors, potentiometric titration was exploited. This approach is formally analogous to the one used for the characterization of the **amCD** starting materials. A typical titration curve is depicted in Figure 5.4.

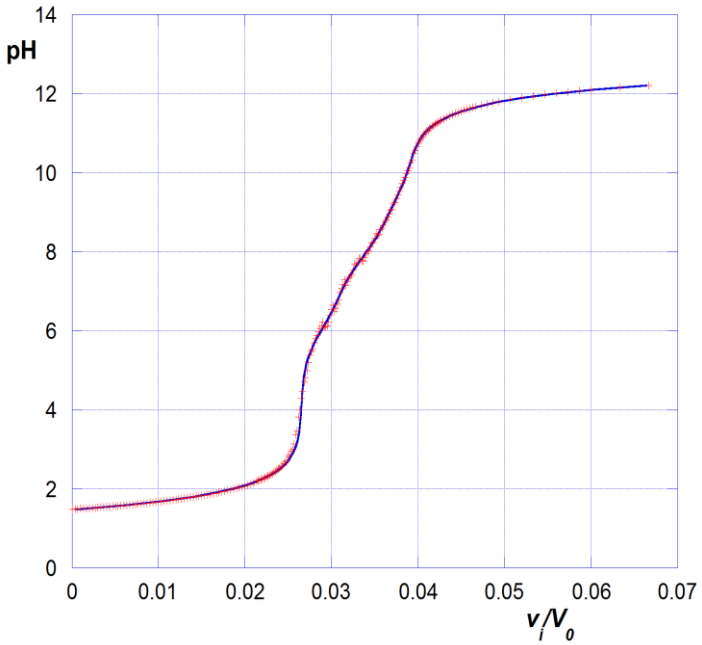

Figure 5.4 – Typical titration curve of **ACN**s.

By analogy with **amCD**s, and confirmed by titration experiment, **ACN** materials are isolated as partial hydrobromides as well. Moreover, even in this case the experimental titration curves obtained resulted comparable to those of **amCD**s, namely a mixture of a certain number of independent virtual weak bases in the presence of an excess strong acid. With a main equivalent point relevant to the neutralization of the excess strong acids, and a region corresponding to the neutralization of the ammonium groups present in the polymer network. Then, data were treated by means of the previously reported fitting equation considering a three weak bases model. The same characterization parameters are summarized in table 5.2

Table 5.2 – Analytical data for **ACN**s.

		ACN1	**ACN2**	**ACN3**	**ACN4**
	$\tilde{n}$	2.6 ± 0.2	2.1 ± 0.2	2.2 ± 0.2	2.8 ± 0.1
	x	3.4 ± 0.3	3.4 ± 0.5	2.6 ± 0.2	3.1 ± 0.2
	FW	1660 ± 40	1650 ± 70	1480 ± 80	1660 ± 30
$\mathbf{B_1}$	χ_{B1}	0.27 ± 0.02	0.25 ± 0.01	0.14 ± 0.01	0.16 ± 0.01
	pK_{B1H^+}	5.6 ± 0.3	5.1 ± 0.2	5.7 ± 0.4	6.1 ± 0.3
$\mathbf{B_2}$	χ_{B2}	0.36 ±0.04	0.27 ± 0.03	0.43 ± 0.03	0.25 ± 0.02
	pK_{B2H^+}	7.5 ± 0.2	7.5 ± 0.3	7.6 ± 0.3	7.5 ± 0.3
$\mathbf{B_3}$	χ_{B3}	0.37 ± 0.04	0.48 ± 0.04	0.43 ± 0.03	0.59 ± 0.03
	pK_{B3H^+}	9.5 ± 0.2	9.5 ± 0.3	9.4 ± 0.5	8.9 ± 0.3
	Rt	1.21	1.46	1.27	0.97
	Rr	0.81 ± 0.08	0.88 ± 0.16	0.67 ± 0.11	0.62 ± 0.05

It is possible to notice that $\tilde{n}$ values obtained from titration curves are consistent with those estimated by NMR (for material **ACN4** the slight disagreement found probably depends on the overestimation of the cumulative integral for the signals at 84 and 73 ppm mentioned previously). Of course, because each linker binds two different **βCD** subunits, the actual average number of polyamine chains linked to a single **βCD** is $2\tilde{n}$. Moreover, by using the data reported in Table 5.2 an average formula weight (**FW**) was calculated, and a real **amCD**/**BrβCD** mol/mol combination ratio (**Rr**) for each material. The latter one, in turn, can be compared with the mol/mol ratio (**Rt**) used in performing the reaction. For all the materials **Rr** values are lower than the corresponding **Rt** values. This implies that a significant fraction of the **amCD** used in the synthesis does not react with the **BrβCD**; therefore, it does not participate in constituting the polymer network and is lost during work-up. The amount of unreacted **amCD** ranges between 33% (**amCD2**) and 47% (**amCD6**). The particularly low **Rr** value found for material **ACN4** is probably due to the fact that the **amCD7** reactant carries a certain amount of unbound diamine, which contributes to the overall reaction. Based on the amount of **BrβCD** used for the synthesis, calculated reaction yields resulted almost quantitative,

being affected by unavoidable losses involved in the isolation procedures. It is also worth stressing that **Rr** values seem to increase on increasing the number of nitrogen atoms per polyamine linker unit, these observations can be rationalized assuming that a single **amCD** unit substitutes more than one bromine atom of the same **BrβCD** unit. It can be reasonably admitted that the hyper-reticulated nature itself of the resulting polymer network restricts the actual number of **BrβCD** units that a given **amCD** can spatially approach to react with. This, of course, favors the occurrence of polysubstitution side-reactions. The observed trend of **Rr** values implies that an increase in the overall number of N atoms on the same **amCD** unit improves its ability to approach different **BrβCD** units at the same time.

*5.2.3 - Differential scanning calorimetry and Porosimetry of **ACN**s*

ACN materials were studied by means of differential scanning calorimetry (DSC) and Porosimetry. The DSC analysis, provides with information regarding the thermal stability of the materials. The DSC curves for **BrβCD**, **amCD3** and the relevant product **ACN2** are depicted in Figure 5.5 as a representative examples. All samples show complete degradation on heating, because the curves are not reversible, and at the end of the experiment carbonized residues are always found.

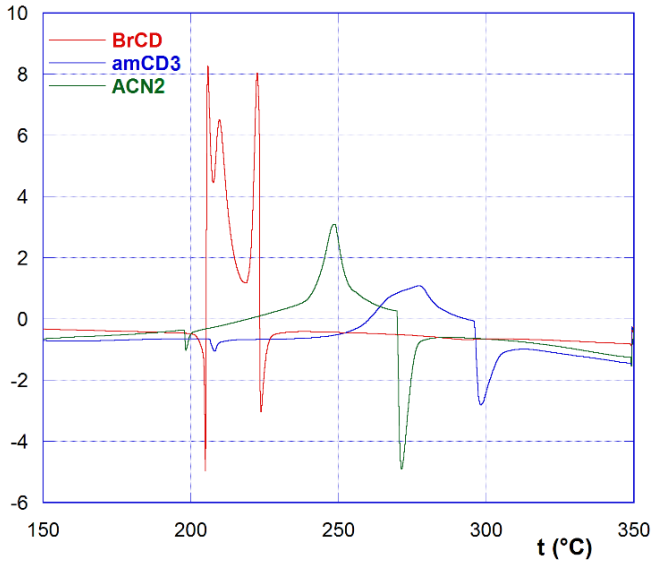

Figure 5.5 – DSC curves for **BrβCD**, **amCD3** and **ACN2**.

The **BrβCD** shows a peculiar trend with three exothermic peaks at 206, 210 and 223 °C, comprised between two endothermic spikes at 205 and 224 °C. On the other hand, free **amCD**s and **ACN**s show very similarly shaped curves, with a first tiny endothermic peak at ca. 200 °C, followed by a large exothermic peak between 240 and 280 °C, and finally a third significant endothermic peak between 250 and 310 °C. Data are summarized in Table 5.3.

Table 5.3 – DSC data for **ACN**s.

	1st peak (°C) endothermic	2nd peak (°C) exothermic	3rd peak (°C) endothermic
amCD2	194	n.d	262
amCD3	208	277	298
amCD6	194	270	287
amCD7	198	280	295
ACN1	199	240	255
ACN2	198	249	271
ACN3	206	234	268
ACN4	nd	244-249	308

According to literature,[231] **BrβCD** decomposes on melting at ca. 220–223 °C. So, the exothermic peaks in its peculiar DSC curve may account for some amorphous–christalline transitions, before thermal decomposition at 224 °C. Data in table 5.3 indicate that, in general, the polymers are less stable as compared to the relevant **amCD**s. The first tiny endothermic peak in the curves might be attributed to a first melting process, although loss of HBr cannot be a priori excluded. Then, the broad exothermic peak could be ascribable to an amorphous–crystalline transition, which is finally followed by thermal degradation. Noticeably, a somehow similar behavior has been observed for composites in which an endothermic melting is followed by an exothermic crystallization and hence by the melting of the new structure.[232] As the mobility of portion of the molecules is increased in the molten state, an imperfect crystallization could occur, as observed in particular for biopolyamides. Higher melting point can account for the occurrence of extensive hydrogen bonding, which affects the order of microchains in the molten state.[233]

On passing to the Porosimetric characterization, it was found out that good quality N_2 adsorption/release isotherms were very difficult to obtain, because of the proximity of obtained values to the lowest limit of instrumental sensitivity. Only in the cases of materials **ACN1** and **ACN4**, it was possible to obtain reasonable results. Average surface areas were determined by applying the standard BET method,[234] whereas by applying the BJH method[235] average pore diameter and the total pore volume were obtained. Relevant data are reported in table 5.4

Table 5.4 – Porosimetric data for **ACN**s.

	Average surface area ($m^2\ g^{-1}$)	Average pore diameter (nm)	Total pore volume ($mm^3\ g^{-1}$)
ACN1	0.70 ± 0.07	3.9 ± 0.4	9.1 ± 0.9
ACN4	0.73 ± 0.07	3.1 ± 0.3	5.3 ± 0.5

These results show that **ACN** materials have a quite compact structure. Considering that the average diameter of the **βCD** subunits is as large as 0.6 nm, pores have on average the size of a small cluster of subunits. However, this compact structure can be easily permeated by an

aqueous solvent because potentiometric titrations were easy to perform and reproducible. Therefore, the materials maintain a hydrophilic character, due to the nature of both the **CD**s scaffold and the polyamine linkers.

*5.2.4 - Adsorption/sequestration abilities of **ACN**s*

In order to investigate the adsorption/sequestration abilities of **ACN**s, at different pH values, a set of diversely structured guests (**1-11**, Figure 5.6) was considered. Noticeably this set comprises some *p*-nitroaniline derivatives[35,37,228] (**1-7**) and some large-sized dyes (**8-9**) and nutraceutic (**10-11**) molecules. The former ones were chosen to compare the results with the binding constants reported in literature for their complexation in native **βCD**; the latter ones were selected because of their size and shape, in order to verify possible drawbacks due to the low porosity of the materials.

In general, a weighed amount of each material was added to a given volume of a stock solution of the guest, buffered at the desired pH value, and the sample was mechanically shaken for 90 min. Then, the suspension was centrifuged and the supernatant analysed spectrophotometrically, to obtain the percent amount of guest sequestered from solution. Experiments were performed at four different pH values, namely 1.0, 4.4, 6.7 and 10.6, to achieve a different protonation status of the **ACN** materials, and consequently a different average charge, according to the titration data (basic sites can be considered unprotonated at pH 10.6, partly protonated at pH 6.7 and 4.4, fully protonated at pH 1.0). The complete adsorption data are collected in table 5.5.

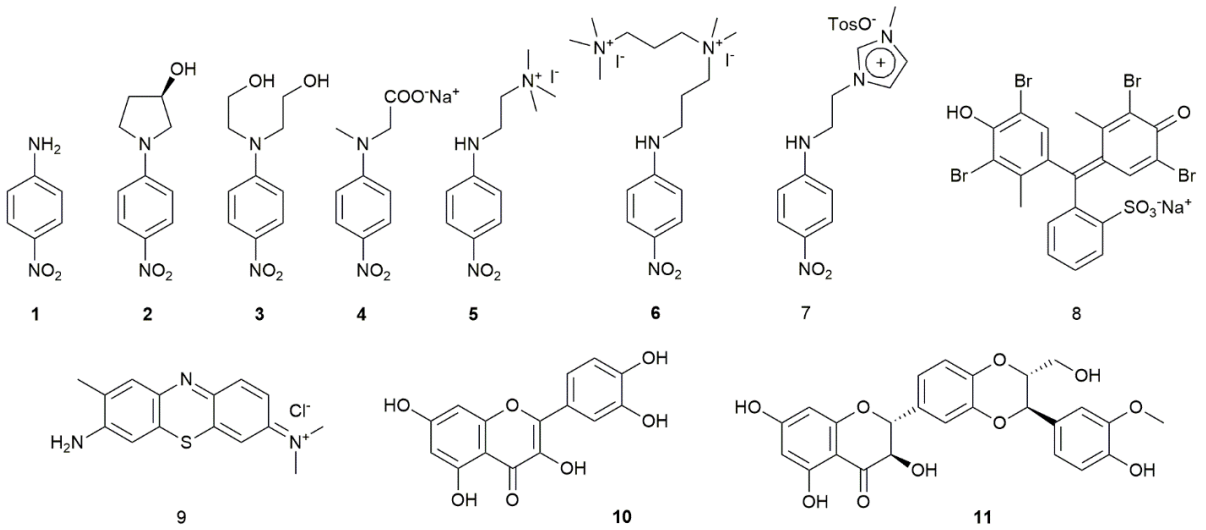

Figure 5.6 – Structures of guests **1-11**.

Table 5.5 – Sequestration data for **ACN**s.

		Guest										
Material	**pH**	**1**	**2**	**3**	**4**	**5**	**6**	**7**	**8**	**9**	**10**	**11**
ACN1	**1.0**	94	15	6	61	0	9	27	99	4	98	91
	4.4	68	21	13	44	2	10	4	98	5	97	94
	6.7	56	30	25	25	8	16	18	77	8	83	89
	10.6	48	23	20	38	22	37	38	52	36	8	30
ACN2	**1.0**	80	9	5	55	0	9	16	56	4	96	93
	4.4	65	22	14	26	0	7	7	98	4	96	92
	6.7	52	25	38	18	8	15	18	53	12	97	87
	10.6	31	39	39	45	29	44	39	37	22	4	29
ACN3	**1.0**	94	22	61	75	6	30	20	78	2	94	88
	4.4	89	30	55	71	0	21	19	81	4	92	93
	6.7	85	45	42	58	19	37	39	91	7	87	91
	10.6	81	51	33	42	30	50	51	35	45	1	18
ACN4	**1.0**	88	12	5	55	0	5	9	93	4	99	94
	4.4	83	18	9	53	0	8	8	94	6	99	99
	6.7	76	26	13	38	6	15	17	98	5	98	97
	10.6	70	34	29	33	20	29	34	37	48	12	8

The sequestration abilities of the polymers show very large variations depending on the nature of guest, on the pH and on the material considered. Comparison between different materials, under homologous conditions, show in general poor correlation. Considered on the whole, the adsorption data confirm that the materials are pH responsive as expected according to the behaviour of **amCD**s described in Chapter 3. Of course, the response of the materials to pH variations changes depending on the particular guest considered. For the cationic guests **5**, **6**, **7** and **9**, for instance, the protonated materials are by far worse adsorbents, whereas the opposite is observed with anionic or ionizable guests **2**, **8**, **10** and **11**. The neutral guest **1** is sequestered quite efficiently in particular by materials **ACN3** and **ACN4**, whose aliphatic linkers are less hydrophilic, whereas less effective adsorption is observed by materials **ACN1** and **ACN2** bearing more hydrophilic polyamine linkers. Moreover, **1** is more favorably adsorbed by the fully protonated materials at pH 1.0, in striking disagreement with the behaviour observed in solution for **amCD**s. Considering the hypothesis that worse inclusion is due to entropically unfavorable stiffening effects, as previously discussed data for **1** suggest; that a similar effect cannot efficiently work in the already stiff hyper-reticulated structure of the polymer. Therefore, absorption in the polymer network is ultimately favored by the occurrence of stronger polar interactions. On passing to the other *p*-nitroaniline derivatives **2**-**7**, worse absorption with respect the parent **1** is observed in most cases, regardless of the size and features of the ancillary chain present on the molecule. The absorption of neutral guests **2** and **3** is generally disfavored on decreasing the pH (with the only exception of **3** with **ACN3**), in agreement with the behaviour of aminocyclodextrins in solution.[35,98] For charged guests, electrostatic interactions seem to play a paramount role. The carboxylic acid derivative **4** shows the best adsorptions at

pH 1.0, and a regular decrease with **ACN3** and **ACN4**, whereas pass through a minimum with **ACN1** and **ACN2**. Probably, in the latter two cases the accommodation of the guest into the **βCD** cavities is disfavored by the occurrence of effective hydrogen bonding and Coulomb interactions between the carboxylate group and the ammonium groups of the polyamine linkers occurring at intermediate pH values. Because these interactions are lost as the polymer becomes completely deprotonated, then sequestration abilities pass through a minimum. The adsorptions of the alkylammonium cations **5** and **6** regularly decrease on decreasing the pH with all the materials. The same trend is found with the imidazolium cation **7** in the presence of **ACN3** and **ACN4**, whereas non-monotonic trends are found with **ACN1** and **ACN2**. The anomalous behaviour of **7** could be due to the presence of tosylate counter-anion, admitting a concomitant strong interaction between the aromatic anion and the polymer at low pH. The behaviour of large guests **8**-**11**, show that sequestration is not affected by molecular size. In particular, if we consider Bromochresol Green **8**, Quercetine **10** and Silibinine **11**, under the various conditions used, these large molecules are sequestered as well as or even much more efficiently than the smallest p-nitroaniline **1** in 35 cases out of 48. More in detail, **8** (which turns from a neutral to a largely delocalized anionic form at around pH 4.8) shows bell-shaped trends. Therefore, the best adsorption conditions occur when the anionic form interacts with the polymer in its cationic form. Nutraceuticals **10** and **11** are almost quantitatively sequestered by all the materials under acidic or nearly neutral pH, whereas a dramatic decrease occur under alkaline conditions, because the molecule becomes a much more hydrophilic anion. Considered on the whole, these data indicate that adsorption/sequestration abilities of **ACN** materials cannot be compared with the binding abilities of **amCD**s in solution. It is worth recalling here that the latter ones are finely regulated by the *induced-fit effect*.[33,35,37,40,100,101] However, because **ACN** have a stiff and poorly solvated structure, induced fit cannot work.

In order to get a deeper understanding of the behaviour of **ACN**s, it seemed interesting to investigate more in detail the possible actual location of a guest inside the polymer lattice. For this purpose, two composites were prepared by adsorbing guests **2** and **10** into material **ACN1**. The composites were easily obtained (see Experimental section) by equilibrating the polymer with a suitable amount of the guests for a sufficiently long time. Loadings were determined by extracting the included guest, and resulted as large as 11% w/w for the **2-ACN1** composite, and 5% w/w for the **10-ACN1** one. On the grounds of trivial stoichiometric calculations, it can be easily shown that loading for **2-ACN1** corresponds to an almost complete occupancy of the cyclodextrin cavities present in the material, whereas for **10-ACN1** occupancy is ca. 30%. The composites obtained were subsequently used to perform solid state 2D (^{1}H-^{13}C) heteronuclear

dipolar correlation NMR experiments, using the frequency-switched Lee-Goldburg homonuclear decoupling sequence (**FSLG**). This technique enables to detect through-space H–C cross-correlations. In this way information comparable to the ROESY spectra in solution can be obtained. The 1D CP-MAS and a low-magnification 2D FSLG spectrum of the composite **2-ACN1** and **10-ACN1** are shown in Figure 5.7.

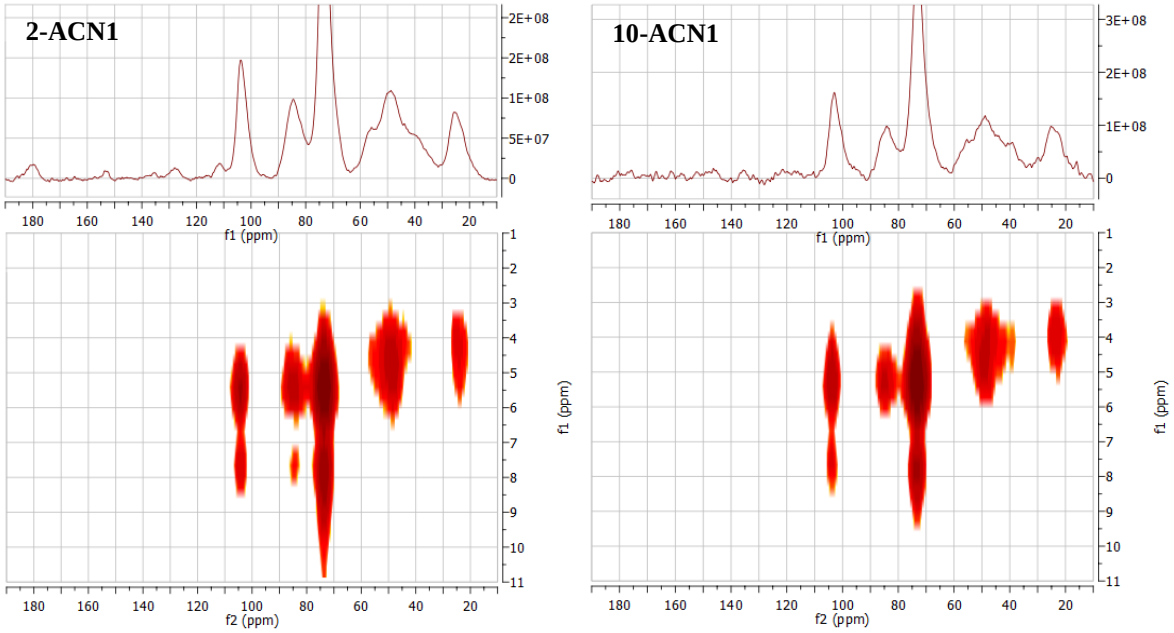

Figure 5.7 – 2D-FSLG spectra of composites **2-ACN1** and **10-ACN1**.

The 1D spectrum of the **2-ACN1** composite clearly shows the presence of low intensity peaks at 111.5, 128.1, 135.7 and 153.5 ppm relevant to aromatic carbon atoms, due to the guest together with significant enhancement of the signals of the high-field aliphatic carbons. The 2D correlation spectrum, shows three cross-peaks at δ_H = 7.82 ppm and δ_C = 73.7 ppm, at δ_H = 7.75 ppm and δ_C = 84.7 and at δ_H = 7.68 ppm and δ_C = 104.2, which account for the spatial proximity, between the aromatic hydrogen atoms of the guest and the **CD** carbons. This finding, together with the simultaneous lack of any intense cross-peak between the same hydrogens and the carbon atoms of the linker units, provides unambiguous evidence that the aromatic moiety of **2** is stably included into the **βCD** subunits, and does not reside in the nanochannels of the polymer. It is worth noting, indeed, that the first cross-peak is by far more intense, in agreement with the fact that the C(3) and C(5) **CD** atoms result closer in the space to the guest, with respect to the C(1) and C(4) atoms. High-magnification of the 2D spectrum even allows to find weak cross-peaks at δ_H = 5.0 ppm and δ_C = 112.2 ppm and at δ_H = 4.9 ppm and δ_C = 127.5 ppm, which can be attributed to the interaction between the aromatic C atoms of the guest and the inner-cavity H(3) of the **CD**. On passing to the composite **10-ACN1**, also in this case the signals

relevant to the guest can be easily recognized in the 1D spectrum, despite the lower loading. In particular, a system of tiny signals between 113 and 126 ppm is relevant to carbons of the pyrocatechine-like moiety. Other signals are constituted by a second cluster between 135 and 145 ppm, and three signals at ca. 158, 162 and 176 ppm, together with a shoulder at ca. 95 ppm. The 2D spectrum shows two correlation peaks at δ_H = 8.1 ppm and δ_C = 73.6 ppm and at δ_H = 7.6 ppm and δ_C = 103.6 ppm, which suggest a spatial proximity between the pirocatechine-like moiety of the guest and the **CD** cavity. This seems confirmed by a weak cross-correlation peak, again apparent only at large magnification, at δ_H = 5.3 ppm and δ_C = 116.9 ppm. Therefore, these findings provide evidence that the guest is only partly included in the **CD** subunits, whereas the chromone-like moiety resides out of the cavity, in the nanochannels region. Noticeably, no interaction seems apparent from the 2D spectrum between this moiety and the linker carbons, indicating a certain degree of mobility. Whole considered, these evidences seem to support the ideas exposed in discussing the sequestration data. Indeed, inclusion of *p*-nitroanilines suffers for the intrinsic rigidity of the **βCD** subunits, because these guests specifically interact with them (Figure 5.8). On the other hand, in the case of large guests, only part of the molecule can get into the host residues, whereas the largest part resides in the nanochannels, interacting only marginally with the linker chains.

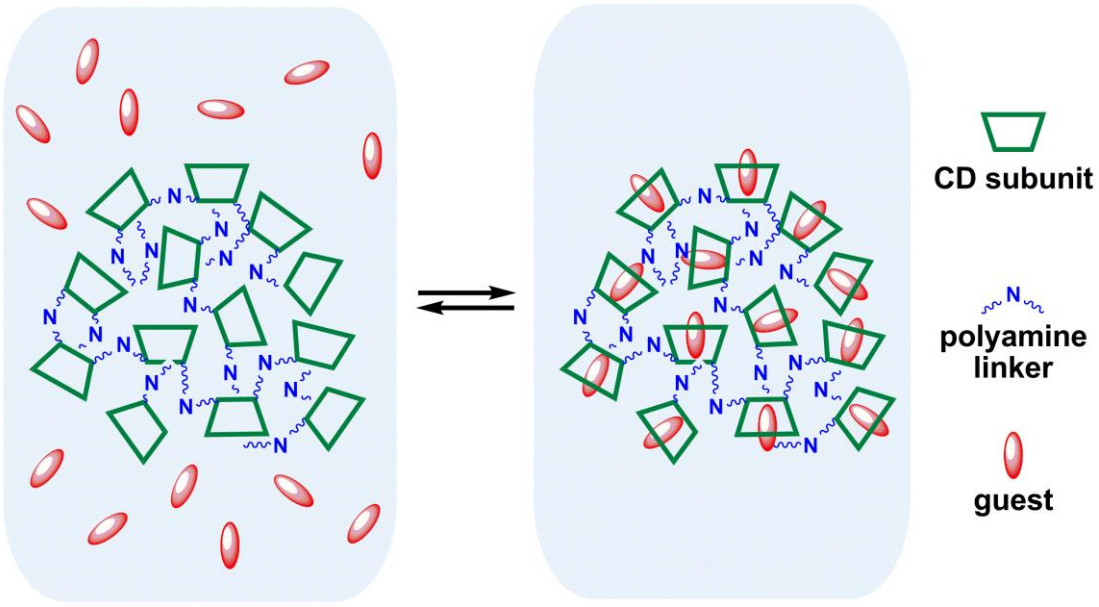

Figure 5.8 – Pictorial representation of the sequestration equilibrium for **ACN**s.

5.3 – Experimental section

*Synthesis of materials **ACN1-ACN4**.*

The **BrβCD** (225.0 mg, 142.8 μmoles) and the proper amounts of **amCD** (see hereinafter) were carefully mixed in a mortar, and the mixture was transferred in a vial. Then, DMSO (250 μL) was added and, after the blend had become homogeneous, the vial was placed in an oil bath at 60 °C for 48 h. The brown gummy product was rapidly kept off, placed in a small beaker with 10 mL of water and mechanically disgregated. The solid was allowed to settle for a few minutes and collected by centrifugation. Then, 10 mL of methanol were added; the system was sonicated for 10 min and centrifugated to collect the solid. The product was subjected to two other similar washings with methanol and a further final washing with diethyl ether. Finally, it was grinded in a mortar, passed through a 150 μm sieve and dried under vacuum overnight at 50 °C. **ACN1**: from 390.5 mg of **amCD2** (172.0 μmoles) were obtained, yield 540.2 mg; **ACN2**: from 495.8 mg of **amCD3** (222.3 μmoles) were obtained, yield 657.0 mg; **ACN3**: from 364.8 mg of **amCD6** (181.5 μmoles) were obtained, yield 320.1 mg; **ACN4**: from 330.8 mg of **amCD7** (134.5 μmoles) were obtained, yield 354.9 mg.

Synthesis of guest 5

The [2-(*p*-nitrophenyl)-aminoethyl]-dimethylamine[40] (1.09 g, 5.2 mmoles) and iodomethane (1.25 mL, 2.84 g, 20 mmoles) were dissolved in acetonitrile (10 mL) and solid K_2CO_3 (2.0 g) was added. The mixture was stirred for 24 h at room temperature. Then the solid crude was filtered off and crystallized from methanol. Yield 1.31 g (62 %). m.f. 206-208 °C. IR (nujol): 3424, 3193, 3173, 1596 cm^{-1}. ^{1}H-NMR (D_2O) δ(ppm): 4.92 (s,1H,-NH-), 5.19, 5.41 (2t, 2H+2H, -CH_2CH_2-, *J* = 6.4 Hz), 6.34 (s, 9 H, -CH_3), 8.30 e 9.68 (2d, 2H+2H, ArH, *J* = 8.6 Hz). High-resolution ESI-MS (*m/z*): 224.1391 $[C_{11}H_{18}N_3O_2]^+$ (calcd. 224.1399).

Synthesis of guest 6

To *p*-nitro-fluorobenzene (1.6 mL, 2.12 g, 15 mmoli) dissolved in DMSO (15 mL) *bis*-*N*,*N*-(3-amino-propyl)-methyl-amine (7.5 mL, 6.1 g, 60 mmoles) was added and the mixture was kept under stirring at r.t. for 3 days. Then the mixture was poured into water (200 mL), acidified with conc. HCl (up to pH ca. 2) and washed with ethyl acetate. The aqueous layer was treated with NaOH (up to pH ca. 12) and repeatedly extracted with ethyl acetate. The collected organic extracts were dried on Na_2SO_4 and distilled under reduced pressure. The collected product was constituted by N^1-(3-aminopropyl)-N^1-methyl-N^3-(*p*-nitro-phenyl)propane-1,3-diamine at a satisfactory degree of purity. Yield 2.76 g (82 %). m.p. 52-54 °C. IR (nujol): 3541, 3239, 3173, 1605, 1466, 1298 cm^{-1}; ^{1}H-NMR (DMSO-*d6*) δ (ppm): 1.54 (m, 2H, -CH_2-CH_2-CH_2-), 1.71 (m,

2H, -CH_2-*CH_2*-CH_2-), 2.10 (s, 3H, -CH_3), 2.30-2.43 (m, 4H, >NCH_2-), 2.56 (t, 2H, >NCH_2-, *J* = 7.2 Hz), 3.15 (t, 2 H, >NCH_2-, *J* = 6.8 Hz), 6.54 e 7.96 (2d, 2H+2H, ArH, *J* = 7.5 Hz). This intermediate product (1.33 g, 5 mmoles) was then dissolved in acetonitrile (10 mL); iodomethane (3 mL, 6.84 g, 48 mmoles) and solid K_2CO_3 (1.5 g) were added, and the mixture was stirred at r.t. for 24 h. The final crude product was filtered off and crystallized from methanol. Yield 2.25 g (78 %). m.p. 207-210 °C. IR (nujol): ν 3421, 3238, 1594 cm^{-1}. ^{1}H-NMR (DMSO-*d6*) δ (ppm): 1.94-2.04 (m, 4H, 2 -CH_2-*CH_2*-CH_2-), 3.08 (s, 9H, $(CH_3)_3)N^+$-, 3.26 (br t, 2H -CH_2-N^+≡), 3.36 (s, 6H, -$(CH_3)_2N^+$-), 3.37-3.43 (m, 6H -CH_2-N^+≡), 6.70 e 8.02 (2d, 2H+2H, ArH, *J* = 7.5 Hz), 7.37 (br s, 1H, -NH-). High-resolution ESI-MS (*m/z*): 162.1259 $[C_{17}H_{32}N_4O_2]^{2+}$ (calcd. 162.1257).

*Characterization of materials **ACN1-ACN4***

*Titrations of **ACN**s*. - A carefully weighed amount (ca. 40 mg) of substance was placed in a jacketed vessel thermostated at 25 °C, wetted with 1 mL of methanol, and then suspended with 10 mL of double-distilled water and 4mL of a standard HCl 0.1 M. The suspension was degassed by bubbling a fine stream of Ar for 15 min and titrated with a standard NaOH 1 M solution as described above.

Porosimetry - For porosimetric determinations, N_2 absorption-desorption isotherms were registered at 77 K using a Quantachrome Nova 2200 Multi-Station High Speed Gas Sorption Analyzer. Samples of the materials were outgassed for 24 h at room temperature in the degas station. Adsorbed nitrogen volumes were normalized to the standard temperature and pressure. The specific surface area (S_{BET}) was calculated according to the standard BET method[110] in the relative absorption pressure (P/P0) range from 0.045 to 0.250. The total pore volume (V_t) was obtained from the nitrogen amount adsorbed in correspondence of P/P_0 = 0.99. The diameter size (d_{BJH}) was calculated by the BJH method.[111]

Differential Scanning Calorimetry - DSC measurements were performed on a DSC Q20 TA Instruments apparatus. For each determination, 0.5 mg of sample were weighed in a small aluminium pan; a heating ramp of 10°/min was used.

Solid-state NMR - CP-MAS (and LFSE as well) NMR spectra were acquired using a Bruker Avance II 400 MHz instrument, equipped with a 15 kHz rotating MAS probe.

Adsorption/sequestration tests

Stock solutions 50 μM of the different guests were prepared in aqueous buffers at the desired pH values. Samples were prepared by mixing 2 mL of guest solution with a carefully weighted

amount (4.00 ± 0.05 mg) of material. The samples were mechanically shaken at room temperature for 60 min, and then centrifuged for 15 min. The supernatant liquor was carefully pipetted and analysed spectrophotometrically to determine the percent amount of guest left in solution at equilibrium.

*Preparation of composites **2-ACN1** and **10-ACN1***

The material **ACN1** (60 mg) was placed in a little beaker, wetted with 1 mL of methanol and suspended with 20 mL of an aqueous acetate buffer solution at pH 4.4. At the same time, the chosen guest (12 mg) was dissolved with 1 mL of a DMSO/methanol mixture 1:1 v/v, and the solution was transferred into a microsyringe. Then, the guest solution was slowly added (at the rate of 5 μL/min) under vigorous stirring into the suspension of the polymer. After the addition was completed, the suspension was further kept under stirring overnight. The solid was then collected by centrifugation, filtered off under vacuum, washed with 3 portions (1 mL each) of cold methanol, and finally dried under vacuum at 50 °C overnight. In order to determine the amount of guest present in the composite, an accurately weighted amount (ca. 2 mg) of composite was placed in a vial, suspended with 1 mL of methanol, and sonicated for 10 min. The vial was then subjected to centrifugation, and the supernatant liquor was carefully pipetted. The procedure was repeated 4 further times, and the collected methanolic extracts were diluted with acetate aqueous buffer (pH 4.4) up to 20 mL. The concentration of the resulting solution was easily determined spectrophotometrically; thus, the amount of guest present in the composite was calculated by few trivial passages, resulting as large as 11 % w/w for **2-ACN1** and 5 % for **10-ACN1**.

- 6 -

POLYAMINOCYCLODEXTRIN-COATED NANOPARTICLES AS CATALYSTS FOR ORGANIC REACTIONS

6.1 – Nanomaterials and Metal Nanoparticles

Nanostructured materials, including nanoparticles, nanomachines, carbon nanoforms, and quantum dots, are the main actors of the most fascinating and appealing field of nanotechnology,[236-241] which has experienced an exponential growth in scientific production during the last decades. The potential applications of nanotechnologies are virtually limitless. During the last half century, since Richard Feynman started the nano-revolution with its prophetic speech *"There's Plenty of Room at the Bottom"*,[242] they have become highly multidisciplinary taking advantage from diverse scientific disciplines, including applied physics, materials science, chemistry, biology, medicine, electronics and engineering. This allowed the application of nanomaterials in contexts such as sensors, optoelectronics, biomedicine, imaging, light-energy conversion, catalysis, and so on.[243-250]

What makes nanomaterials so fascinating is their peculiar characteristic to assume different behaviors depending on their size,[251,252] thus presenting properties that are someway intermediate between those of the bulk material, and the isolated atoms or molecules. This justifies the most widely accepted definition of nanomaterials is that of *"materials whose properties vary according to their size, or the size of their components"*.[253] This is evidenced by the fact that passing from the bulk-phase material to the nanosized one, a considerable increase of the surface-volume ratio occurs. Therefore, the atoms or molecules on the surface represent a significant fraction of the entire mass. Consequently, unexpected new behaviours appear, often of quantum nature, and that in some cases are significantly different as compared to the original material. For instance, in the case of nanoparticles of noble metals such as Au, Ag, Pt, Pd, Cu, it is observed that the redox potentials changes and becomes less positive as

compared with the corresponding bulk metals.[253] Accordingly, the noble metals in the nanoparticle form tend to be oxidized more easily.

Another peculiar feature of metals in nanoparticle form is the appearance of very intense coloration owing to the ability of absorbing radiation in the visible region of the electromagnetic spectrum, a phenomenon known as "Localized Surface Plasmon Resonance" (LSPR).[254-258] This is due to the collective oscillation of the conduction electrons ("surface plasmon"), confined on the surface of the metal nanoparticles, when excited with a suitable electromagnetic radiation. Absorption occurs when the frequency of the incident light is in resonance with the collective oscillation of the conduction electrons, resulting in unique optical properties. Consequently, is necessary that the light possesses a well-defined wavelength; thereby the oscillating electric field of the incident light radiation causes the coherent oscillation of the conduction electrons (Figure 6.1).

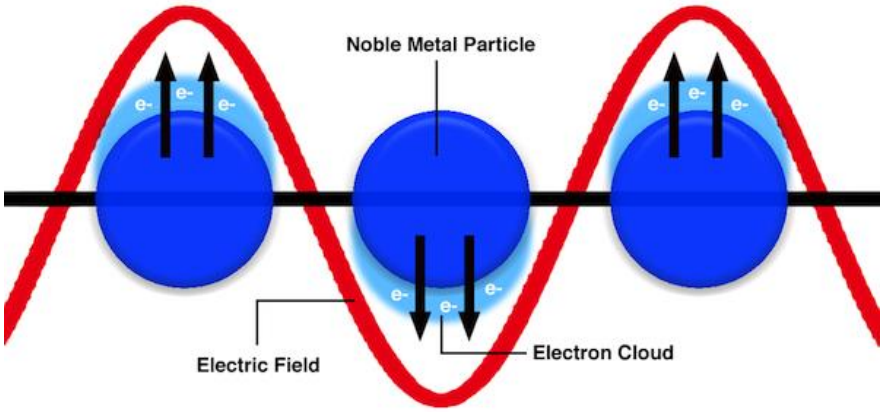

Figure 6.1 – Pictorial representation of LPRS.

The shape of the absorption band, the λ_{max} and the molar extinction coefficient **ε** depend on the type of metal, the dielectric constant of the solvent medium, the electronic interaction of the nanoparticle with the molecular species surrounding it (see later), and finally the size, shape and polydispersity of the nanoparticles[259] as rationalized by Mie.[260] As a general role, the bigger the nanoparticles, the higher its absorption wavelength.[261,262]

The bright color of gold and silver nanoparticle has been widely used throughout history to produce decorative items, such as the famous Lycurgus cup (Figure 6.2), a Roman goblet glass dating from the fourth century A.D. that appears green in reflected light, but red if illuminated from within. The coloration is due to the presence of a mixture of Au-Ag particles of about 70 nm in diameter, embedded in the glass.

Figure 6.2 – The Lycurgus cup.

In addition to decorative purpose and for the production of special optical filters, an important application of the surface plasmon resonance regards the oncology diagnosis and therapy.[263] The excitation of Au and Ag nanoparticles plasmonic surface results in a strong absorption/scattering and in the appearance of a localized electric field around the metal particles.[261] Particles having a marked scattering component of the whole absorption (which generally increases as the size of the nanoparticles increases), are used in the imaging diagnostic. On the other hand, particles that have a high absorption, as the nanoparticles of Au (**AuNP**s), efficiently convert the absorbed light to localized heat. As a matter of fact, the light electric field interacting with **AuNP**s drives the motion of mobile electrons inside **AuNP**s, which in turn convert the energy gained into heat. Then particles can be used for the targeted photothermal destruction of cancer cells.[264]

The study of nanomaterials, and especially the one of nanoparticles (which are undoubtedly the field of nanochemistry most widely studied and characterized) has to cope with the crucial problem, of their synthesis. This is accomplished by two main routes, namely the "top-down" and the "bottom-up" approaches.[265,266] In the first case one starts from the massive material and gradually reduce its size, by physical disintegration, in order to reach the required particle size; in the second case one starts from small atomic or molecular components and tries to assemble them up to the desired size and structure. For example, in the case of metal nanoparticles this can be obtained by reducing a salt of the metal cation in the presence of a stabilizing agent.

The synthesis of nanoparticle systems should satisfy two particular requirements. The first one is obtaining systems with the lowest degree of particle size polydispersity; the second one is obtaining systems stable for long periods of time. Indeed, considering their nature, metals in nanoparticle form, are inherently unstable, since atoms present on the particle surface possess

higher free energy than those present within the particle. This makes the whole system thermodynamically unstable, so that the particles tend to coalesce, forming aggregates of gradually increasing dimensions, finally resulting in a bulk-like material. This processes is known as the "Ostwald ripening".[267] In order to avoid this, it is necessary that the synthesis of the nanoparticles (at least in a bottom-up procedure) occurs in confined spaces, which provide both a dimensional control of the particles during the growing phase, as well as the protection and isolation of these preventing the aggregation. In other words, it is necessary to "dress" the nanoparticles by the use of "coating" or "capping" agents. These agents are suitable molecules capable of stabilizing the nanoparticles, binding them on their surface by means of either covalent or supramolecular interactions, thereby avoiding their mutual contact. In the case of the formation of metallic nanoparticles obtained by reduction of the corresponding salts, commonly used capping agents are donor amphiphilic organic molecules, such as surfactants,[268,269] thiols (widely used for the synthesis of gold nanoparticles),[270-272] amines and polyamines,[273,274] long-chain fat acids,[275] low molecular weight polymers[276] as well as ionic liquids.[277,278]

In the last few years several studies on the use of a new class of molecules, namely dendrimers, have appeared, proving the advantages of the use of these molecules as capping agents. Dendrimers are highly branched polymeric macromolecules built around a central nucleus, from which branch out a number of arms exponentially related to the dendrimer generation.[49,279] Unlike polymers, they are characterized by a high degree of monodispersity. This feature, together with the ability to assume a globular structure over a number of generations and then behave like "molecular boxes",[280] makes them suitable capping agents for the synthesis of metal nanoparticles. This is particularly true in the case of dendrimers which contain heteroatoms as in PAMAM (polyamidoamine) or PPI (polypropyleneimine) derivatives[76,85,281,282] (Figure 6.3).

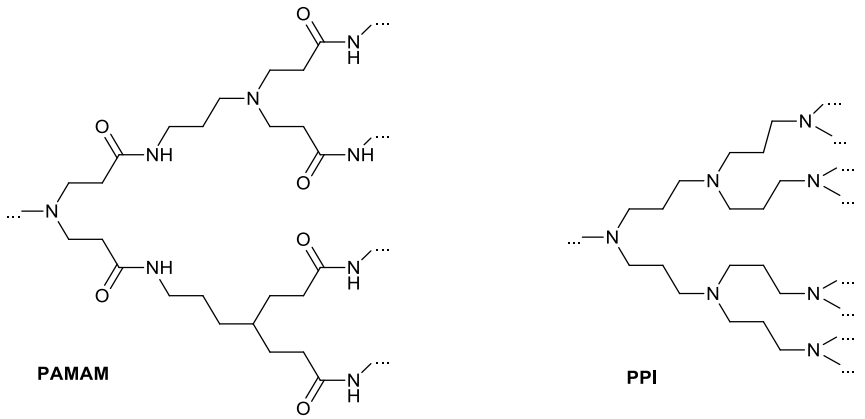

Figure 6.3 – Structures of PAMAM and PPI dendrimers.

The synthesis of metal nanoparticles, by chemical reduction of the corresponding salt in presence of these kind dendrimers relies on the prior complexation on the metal ions on the donor sites present in the dendrimer structure. Then after reduction, has occurred, the same donor groups provide suitable protection of the nanosized metal.[87] (Figure 6.4).

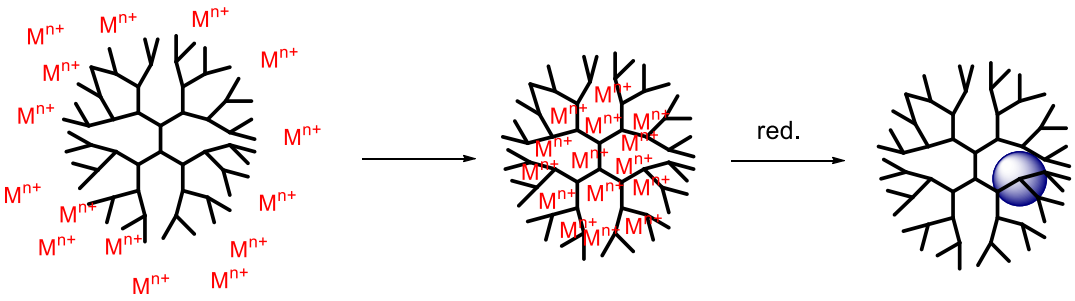

Figure 6.4 – Mechanism of nanoparticle formation with dendrimers.

Indeed, it is possible define such systems as "nano-reactors",[283] because they offer an effective dimensional control on the average size of the nanoparticles (which can be modulated by using appropriate dendrimer generations), and also allow the uniformity of the size particle as a reflection of the low degree of polydispersity of dendrimers. Taking advantage from the progress in the synthesis and stabilization of metal nanoparticles, in particular if obtained in the presence of dendrimeric materials, it was made possible their use in the strategical sector of catalysis.[85,284]

6.2 - Metal Nanoparticles in Catalysis

6.2.1 – Generalities

Many chemical processes, both for the production of *commodities* and *fine chemicals*, require catalytic stages, which can be heterogeneous[285] or homogeneous[286] depending on the particular circumstances. The two types of catalysis possess their own advantages and disadvantages. In the case of heterogeneous catalysis the main advantage is the easy removal of the catalyst from the reaction mixture, as well as the possibility to work at high temperatures provided that the catalyst has a high thermal stability (metal or metal oxide) in bulk phase. Between the main disadvantages, there are the lack of selectivity and a low efficiency in comparison with the relevant counterpart in homogeneous phase. Regarding homogeneous catalysis, the situation is in principle reversed: it benefits from high efficiency (owing to a reactivity ratio 1:1) and selectivity, but has the drawback of an uneasy removal of the catalyst from the reaction mixture, and of limited thermal stability of the catalyst itself. Nanoparticle systems used as catalysts, are matter of factly placed on the border region heterogeneous and homogeneous catalysis. Indeed,

on one side they maintain the features of heterogeneous catalysts, because the reaction occurs on the surface of the particles. Moreover, because to the nanoscale size of the particles, the catalysis is closer to that in homogeneous phase, thus being characterized by greater efficiency and selectivity. Of course, according to the conditions under which the nanoparticles are used, it is possible to head towards one or the other kind of catalysis. If the nanoparticles are dispersed in a solvent, compatibly with the nature of the capping agent, we will have a homogeneous catalysis. Differently if the nanoparticles are fixed onto inert solid supports (silica, alumina, zeolite, graphite), then act as heterogeneous catalysts. For these reasons, when nanoparticle systems are used this is sometimes referred to as semi-heterogeneous catalysis.[287,288]

An example of the use of metallic nanoparticles as heterogeneous catalysts is given by the so-called trivalent catalytic converter (the "catalytic muffler"). This device is able of converting hydrocarbons, CO and nitrogen oxides into CO_2, H_2O and N_2, using the Pt, Pd, Rh and Ir nanoparticles dispersed in a high surface area ceramic matrix (cerium oxide, alumina or silica). Furthermore, a recent example of heterogeneous catalysis is the use of metal oxides nanoparticles to create systems able to mimic the photosynthesis process.[289,290]

Regarding to the application of metal nanoparticles as homogeneous/semi-heterogeneous catalysts the use of Pd nanoparticle as an effective catalyst for Heck, Stille, Suzuki, Sonogashira and Negishi C-C coupling type reactions,[288,291-294] as well as for the hydrogenation reactions[283,295] and reduction of aromatic nitro compounds has been widely investigated. The latter reaction can be profitably accomplished also with diversely capped Ag, Au and Pt nanocomposites. On the ground of the experience gained during my Master Thesis in Chemistry, it seemed appropriate to investigate in detail the possibility to exploit **amCD**-capped metal nanoparticles as catalyst for organic reactions. In particular, I focused my attention on the Ag-catalyzed reduction of nitroarenes with borohydride and on the Pd-catalyzed Suzuky C-C bond formation reaction.

6.2.2 – The reduction of aromatic nitrocompounds

Nitroarenes, are a class of important reaction intermediates in organic synthesis, especially from on industrial point of view, because of the easy introduction of nitro group on the aromatic system, and the subsequent possibility to convert it upon reduction into different products, depending on the reaction conditions and the reducing agent used (Scheme 6.1).[296] The nitrobenzene reduction products are valuable synthetic intermediates for the synthesis of other chemicals, particularly anilines, which constitute the starting materials for the synthesis of diazonium and isocyanates, used in the production of dyes, additives for rubbers,

pharmaceuticals, herbicides and so on. As shown in the figure reported above, there are basically three main ways to obtain the corresponding aniline from nitrobenzene, namely: *i*) reduction with metals in highly acidic environment; *ii*) by catalytic hydrogenation; *iii*) with strong hydride donors such as $LiAlH_4$. The first two are the main methods used at the industrial level, being characterized by high efficiency and low costs. Nevertheless, they have some drawbacks: in the first case operating under drastic acidic conditions unsuitable in the presence of hydrolysable groups, in the other one requirement of special equipment and operating conditions. Finally, in all the three cases there is a low selectivity, which can result in the reduction of other groups present on the molecule. For instance, catalytic hydrogenation cannot be performed on substrates containing alkene or alkyne groups.

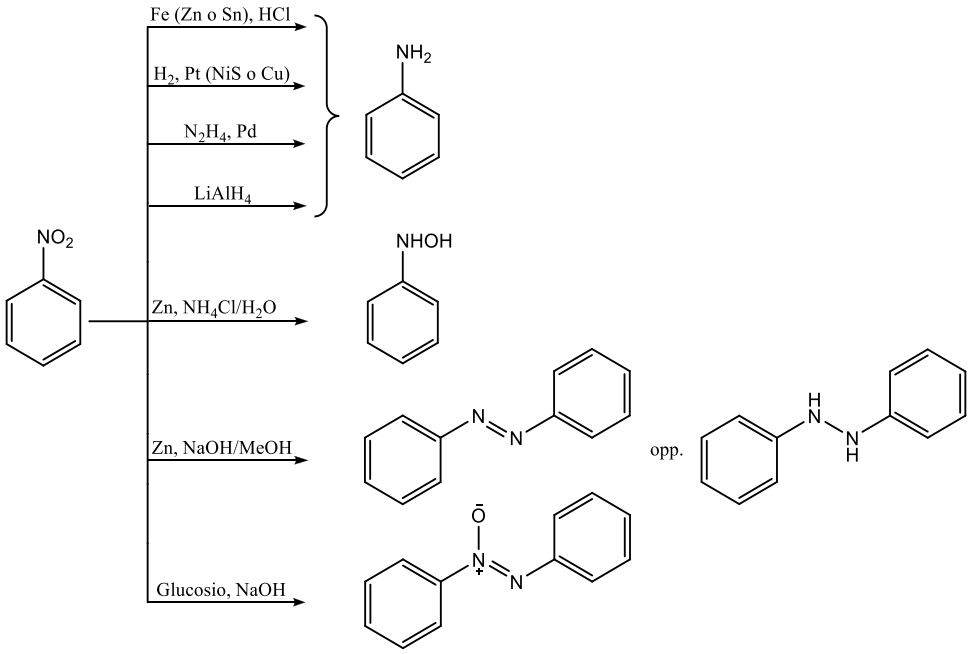

Scheme 6.1

Returning to the use of $LiAlH_4$, it should be noted that hydride-complexes with a low redox potential such as $NaBH_4$ are completely ineffective in conducting the reduction of nitro compounds. However, it was observed that metals such as Pd, Pt, Au and Ag in nanoparticle form, in the presence of suitable stabilizing agents, are capable of catalyse the reduction of nitro compounds such as *p*-nitrophenol[70,75,76,297-302] or *p*-nitroaniline[303,304] using just the $NaBH_4$ as a reducing agent, according to the reaction:

$$4\ ArNO_2 + 3\ BH_4^- + 4\ H_2O \rightarrow 4\ ArNH_2 + 3\ B(OH)_4^-$$

Noticeably, several aspects of the reaction mechanism, in particular the actual kinetics, the actual role of the catalytic surface and of the hydride donor species and the possible presence of an induction period, are still unclear and partly contradictory reports can be found in literature.

6.2.3 – The Suzuki reaction

The palladium-catalyzed C-C bond formation reactions, such Heck, Sonogashira, Suzuki-Miyaura reactions and similar, assume a paramount interest in modern organic synthesis, as accounted for by the enormous amount of literature devoted to the topic.[291,292] In particular, the use of catalysts based on suitably capped Pd nanoparticles (**PdNP**s) - either free or implemented on materials such as polymers, zeolites, supported ionic liquids, carbon nanoforms and so on - has some undoubted advantages with respect to the "classical" homogeneous-phase versions with soluble Pd(0) complexes, showing improved performances in terms of activity, recoverability and reusability of the catalyst.[305-309]

Among Pd-catalyzed processes, Suzuki reaction involves the formation of a new C-C bond starting from an aryl-boronic acid and an aryl halide in the presence of a base.[310-312] A general mechanistic scheme is depicted in Scheme 6.2.

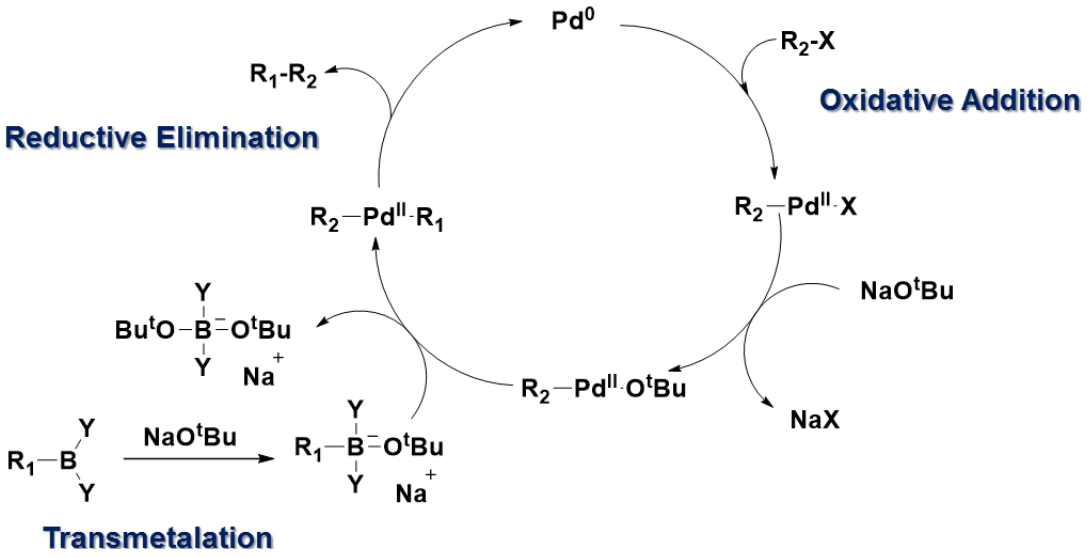

Scheme 6.2

The key steps of the catalytic cycle are: *i*) the oxidative coupling between a Pd(0) species and the aryl halide; *ii*) the subsequent addition of the boronate species by a ligand exchange process (transmetallation); *iii*) the reductive elimination of the product molecule after formation of the new C-C bond in the coordination sphere of the metal.[313-315] As a general role, the reactivity of aryl halides decreases in the order Ar-I > Ar-Br >> Ar-Cl (chlorides are very poorly reactive). Of course, the outcome of the reaction depends largely on the conditions and, in the case of **PdNP**s as catalysts, on the nature of the capping agent. However, it has been observed that the reaction may require exceptionally small amounts of catalysts (0.1% mole/mole or even less), in such a way that the expression "homeopathic catalysis" has been occasionally used.[316]

6.3 - Results and discussion

*6.3.1 – Synthesis and characterization of the **AgNP** catalysts for nitroarene reduction*

On the grounds of the results acquired in previous works about the ability of **amCD** to allow the synthesis and stabilization of **AgNP**s synthesis, it was decided to select some of these systems and investigate their catalytic properties. In particular, as reaction model it was considered the reduction of aromatic nitrocompounds, selecting at this regard 8 different *para*-substituted derivatives characterized by different steric and electronic properties (Figure 6.5)

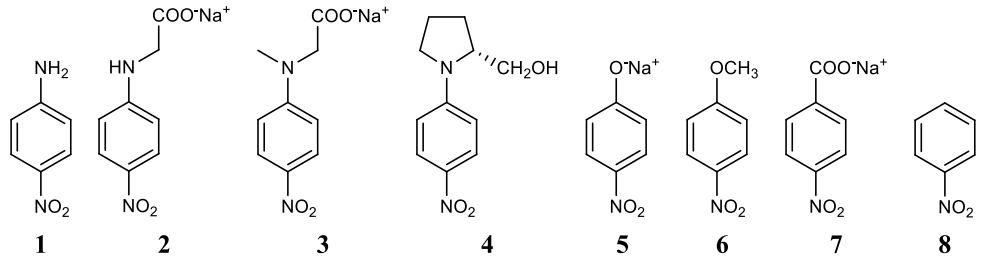

Figure 6.5 – Model nitroarenes.

First of all, in order to prepare the **amCD** capped **AgNP**s it was chosen **amCD1** as capping agent. Generally the synthesis can be performed by reacting in the dark a solution of the $[Ag(NH_3)_2]^+$ complex in the presence of a suitable amount of the auxiliary **amCD1**, with an excess of formaldehyde at 40 °C for 90 min. The formation of the **AgNP**s is evident by the appearance of the typical reddish color due to the characteristic surface plasmon resonance (SPR) absorption band. In a series of preliminary experiments it was investigated the effect on the NP formation process from changing the concentrations of the reactants and their molar ratio, in particular: *i*) by fixing the $[Ag(NH_3)_2]^+$ concentration (1.0 mM) and varying the **amCD1** (0.4–10.0 mN; the normality of the **amCD1** solution is defined according to the average number of nitrogen atoms per CD unit); *ii*) by fixing the **amCD1** (2 mN) and varying the $[Ag(NH_3)_2]^+$ 0.2–5.0 mM); *iii*) by simultaneously varying both the reactants, while keeping constant their equivalent ratio (1:2 eq/eq). The obtained systems were preliminarily characterized by UV–vis spectroscopy (results are summarized in Table 6.1). The outcome of the NP formation process strictly depends on the $[Ag(NH_3)_2]^+$/**amCD1** equivalent ratio used. Nearly no reaction occurred with ratios larger than 4:1. In the other cases the systems showed an absorption band centered at 401 ± 2 nm, the intensity of which regularly increases on decreasing the equivalent ratio. Moreover, the same ratio heavily affects the stability of the system. Samples obtained with a 1:2 ratio are stable for several weeks, if kept in the dark at room temperature. By contrast, systems with a 1:0.4 ratio or prepared with the largest $[Ag(NH_3)_2]^+$ concentrations, appear cloudy or turbid and form reddish-brown precipitates

within few days. Data suggest that NP formation is hampered at the highest $[Ag(NH_3)_2]^+$/**amCD** ratios, is partial for the ideal 1:2 value, and becomes almost complete at the lowest ratios. Therefore, it seems reasonable to hypothesize that NPs prepared with a 1:2 ratio are constituted by a metal core, surrounded by a shell of **amCD** units complexing a certain amount of Ag^+ ions by means of their amine donor groups. The presence of a significant positive charge on the NP surface ensures the time stability of the system. On the other hand, in systems prepared at 1:0.4 ratio the NPs formed bear nearly no charge on their surface, and consequently can aggregate or coalesce. In order to confirm these hypotheses, the systems were thoroughly investigated and chosen as representative NP systems, to be afterwards used as the catalysts for studying the nitroarene reduction reaction. These systems, labelled henceforth as Catalysts **I** and **II**, were prepared at a 1 mM $[Ag(NH_3)_2]^+$ concentration, and **amCD** concentrations of 0.4 mN and 2 mN, which correspond to **amCD**/Ag^+ mole/mole ratios (**ρ**) as large as 0.035 and 0.175 respectively. Moreover, as it will be illustrated more in detail in Section 6.3.2, in order to perform the nitroarene reduction reaction Catalysts **I** and **II** are subjected to dilution (up to 1:750 v/v., i.e. 1.33 μM) and subsequent interaction with $NaBH_4$. This causes modifications in the structure of the nanocomposite, as it can be evidenced by simple observations. After dilution 1:1 or 1:9 v/v of the preformed Catalyst **II** with water, a significant enlargement and decrease in intensity of the SPR band centered at 401 nm, and the appearance of a new band at 567 nm can be noticed in the normalized UV–vis spectra (Figure 6.6). The corresponding color change is apparent even at naked eye.

Table 6.1. ε values for the **AgNP** systems at the relevant λ_{max}.

		Ag^+ (mM)				
		0.2	0.5	1.0	2.0	5.0
amCD (mN)	0.4	No reaction		12420		
	1.0		4670	10020		
	2.0	No reaction	No reaction	5540	9240	Turbid
	4.0			440	5060	
	10.0			No reaction		Turbid

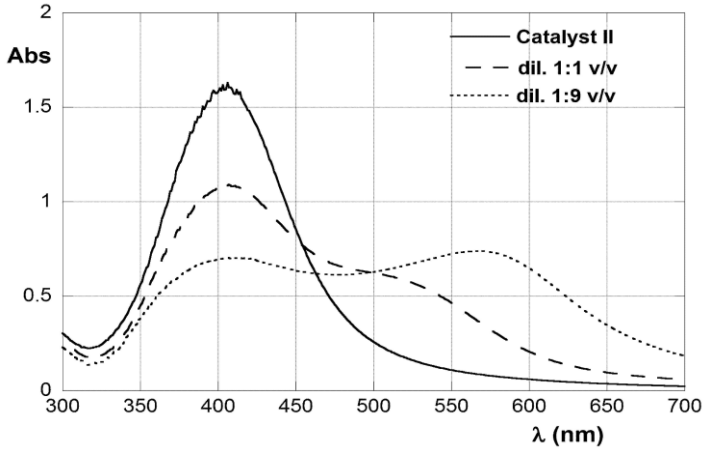

Figure 6.6 – UV-vis spectra of Catalyst **II** before and after dilution.

The observed behavior accounts for a concomitant change in the polar character and the local refractive index of the coordination shell immediately surrounding the metal core.[258] It is worth stressing that polarity or refractive index variation may in turn be the result of a ligand exchange at the NP surface. For example, it has been recently shown that the position of the SPR is significantly shifted in presence of halide ions.[317,318]

The residual Ag^+ possibly present at the NP surface (in particular in the case of Catalyst **II**) can be easily reduced to Ag^0 by borohydride ion. As a matter of fact, addition of $NaBH_4$ to a solution containing $[Ag(NH_3)_2]^+$ and **amCD** (at the same concentrations as in Catalyst **II**) instantaneously causes the formation of a turbid brown suspension, which precipitates down in few minutes.

For these reasons, together with "as-prepared" Catalysts **I** and **II**, we subjected to further investigation three control systems, namely two dilutions1:1 and 1:9 v/v of Catalyst **II** with water (indicated as **IIdilA** and **IIdilB** respectively), and a mixture 1:1 v/v between Catalyst **II** and a freshly prepared $NaBH_4$ 48.0 mM solution (indicated as **IIred**). In particular, size and morphology of the systems were studied by means of transmission electron microscopy (TEM), Dynamic Light Scattering (DLS) techniques. For our, it is worth noting that TEM and DLS provide with complementary information, because the former one focuses on the metal core alone, whereas the latter looks at the entire nanocomposite, including its coating and hydration shell, and analyses a more statistically representative sample. TEM micrographs for Catalysts **I**, **II** and for control systems **IIdilB** and **IIred** are shown in Figure 6.7. The pristine Catalysts **I** and **II** show well defined, quite spherical, individual metal cores with a relatively low polydispersity and scarce tendency to aggregation. The **AgNP**s show also a quite crystalline structure with the occasional presence of decahedral-shaped objects. Statistical analysis of TEM images indicates unimodal diameter distributions centered at ca. 27 and 19 nm respectively, indicating that in the presence of a lesser amount of **amCD** larger NPs are formed. Therefore, trivial calculation suggest that the particles, can be constituted on average by $6 \cdot 10^5$ or $2 \cdot 10^5$ atoms respectively, and have average surface areas of 2300 and 1100 nm^2 respectively. Dilution seems to cause a fair tendency to aggregation, together with the appearance of a new population of small faint objects having an average diameter of ca. 3.6 nm. By contrast, significant modifications occur after treatment with $NaBH_4$. TEM images show, along with tendency to aggregation, a modification in both the size and the morphology of the pristine metal cores together with the formation of new small sized cores. Statistical analysis of images reveals a completely different diameter distribution, with a maximum frequency centered at ca. 9.7 nm.

Catalyst **I**

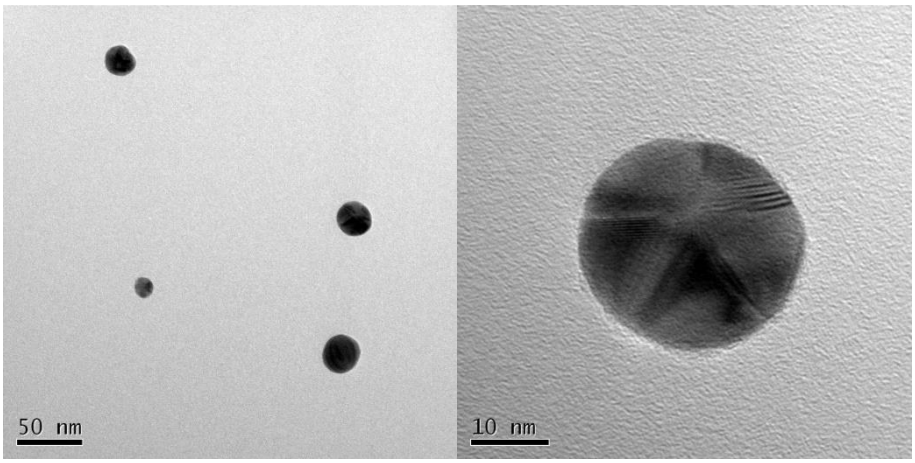

Catalyst **II**

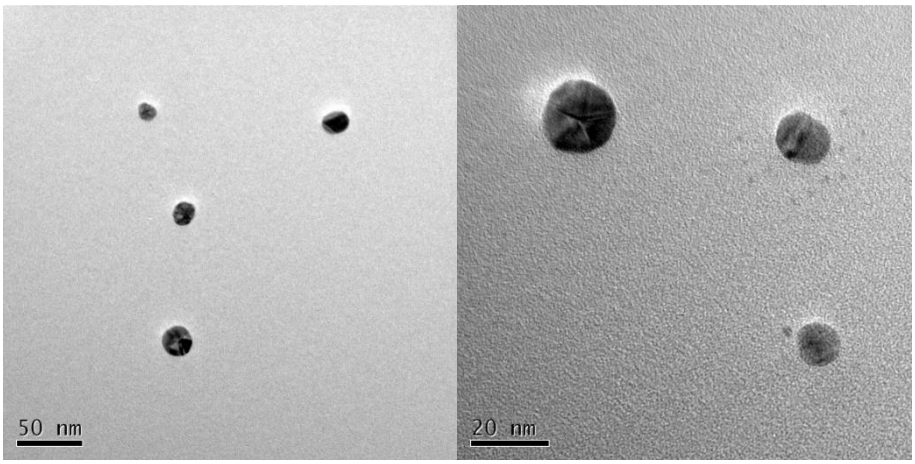

Catalyst **IIdilB**

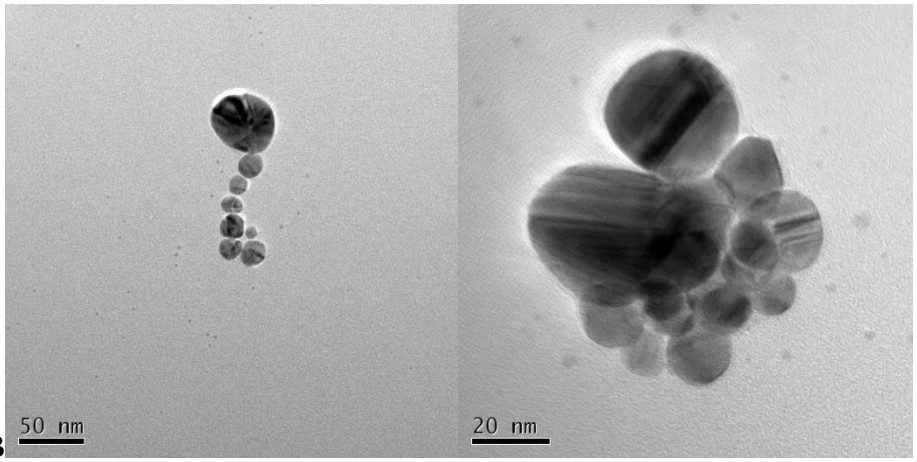

Catalyst **IIred**

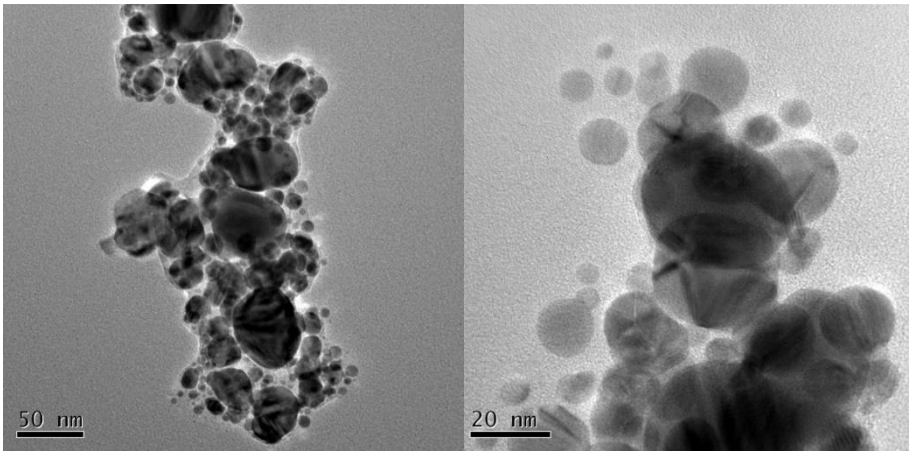

Figure 6.7 – TEM images of **AgNP** catalysts.

On passing to DLS, data for the system "as-prepared" indicate the presence of smaller aggregates with Catalyst **I** than with Catalyst **II**, having average diameters as large as 86 and 149 nm respectively (evaluated by applying the CONTIN method see Experimental section), with unimodal distributions. For the control systems **IIdilA** and **IIdilB** average diameters of 149 and 59 nm respectively are found, indicating that dilution (namely 1:9 v/v) causes a large size decrease. By contrast, after Catalyst **II** has been treated with $NaBH_4$, for the system **IIred** the aggregates in suspension grow dramatically in size, with an average value of the diameter of 464 nm, and show high polydispersity in agreement with TEM evidence.

On the ground of simple molecular models, one could estimate that a single **amCD** unit might cover on the NP surface an area approximately comprised between 3 and 7 nm^2. (The latter estimation is based on the fact that the **βCD** torus alone has an average diameter of 1.54 nm, and that the length of a stretched diamine pendant chain can be estimated (MM2) as c.a. 0.8 nm). Keeping into account the actual composition of the systems, in particular the values of the aforementioned **amCD**/Ag^+ mole ratios **ρ**, TEM evidences implies that only a minor fraction (less than 5%) of the **amCD** present might actually come in direct contact with the metal core. Consequently, DLS results may be interpreted that pristine metal cores, formed upon the reduction of silver ions with formaldehyde, are surrounded by a thick layer-structured coating, constituted by shells of **amCD** units held together by weak interactions, including the mutual inclusion of the polyamine tails into the **CD** cavities, and by the complexation of residual unreacted Ag^+ ions with the polyamines. This coating offers both a steric and an electrostatic barrier against the aggregation/coalescence of the NPs and, of course, is thicker for Catalyst **II**, prepared with the largest amount of **amCD**. Dilution of the catalyst progressively dissolving these shells and favors formation of new Ag^+-**amCD** microaggregates (the faint objects observed in **IIdilB**), which act as seeds for the formation of new small Ag cores after treatment with $NaBH_4$. The latter process may also results in the aggregation of further metal ions on the pristine cores, and this modifies their size and shape (as observed in **IIred**). The concomitant exhaustive reduction of Ag^+ removes at the same time the electrostatic barrier, and so aggregation occurs (Scheme 6.3).

Confirmation of the composite nature of **amCD**-**AgNP** systems was achieved by means of FT-IR evidence. By subjecting a large amount of Catalyst **I** to centrifugation, a sample of **AgNP**s was isolated and its IR spectrum (KBr) was recorded (Figure 6.8).

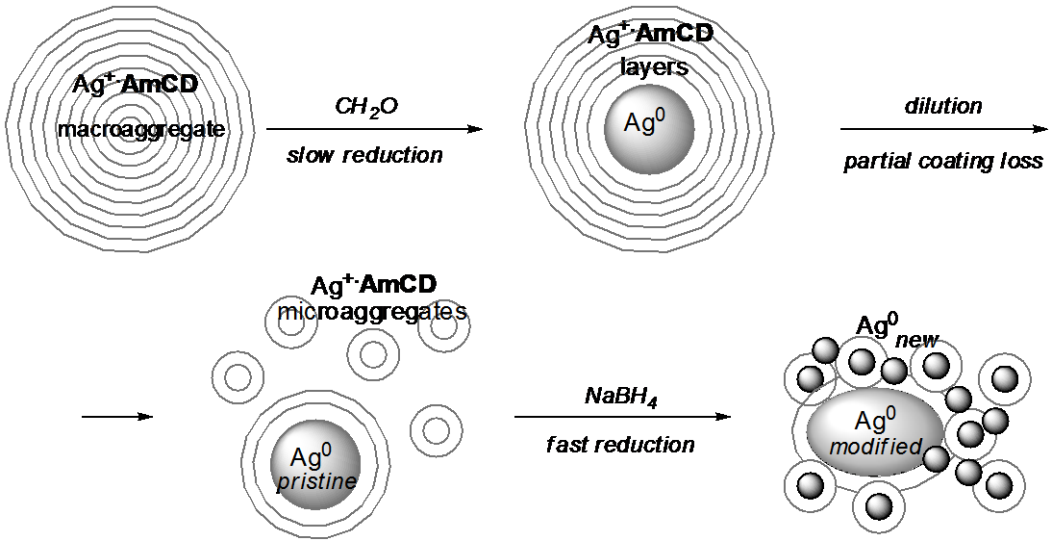

Scheme 6.3

Comparison with the spectrum of free **amCD**, reveals the presence in the composite of the signals expected for the organic capping agent. The original **amCD** band at 3310 cm^{-1}, originated by the superimposition of the OH and NH groups stretching, splits in two bands centered at 3470 and 3136 cm^{-1} respectively. This indicates a neat discrimination between the two different groups, reasonably owing to the occurrence of the N-Ag interactions at the NP surface. Furthermore, together with the **amCD** fingerprints at 1153, 1086, 1041 (C-O stretching) and 943 cm^{-1} (OH bending), a new signal appears at 839 cm^{-1}, whereas **amCD** band at 756 cm^{-1}, which can be attributed to N-H wagging disappears. This confirms the occurrence of strong N-Ag interactions at the primary **CD** rim. Finally, the spectrum of the composite shows two strong bands at 1456 and 1385 cm^{-1} due to carbonate ion (superimposed to the expected C-H bending bands of the **amCD** at 1466 and 1368 cm^{-1}), which can be easily explained as due to CO_2 uptake by the quite alkaline NP solution.

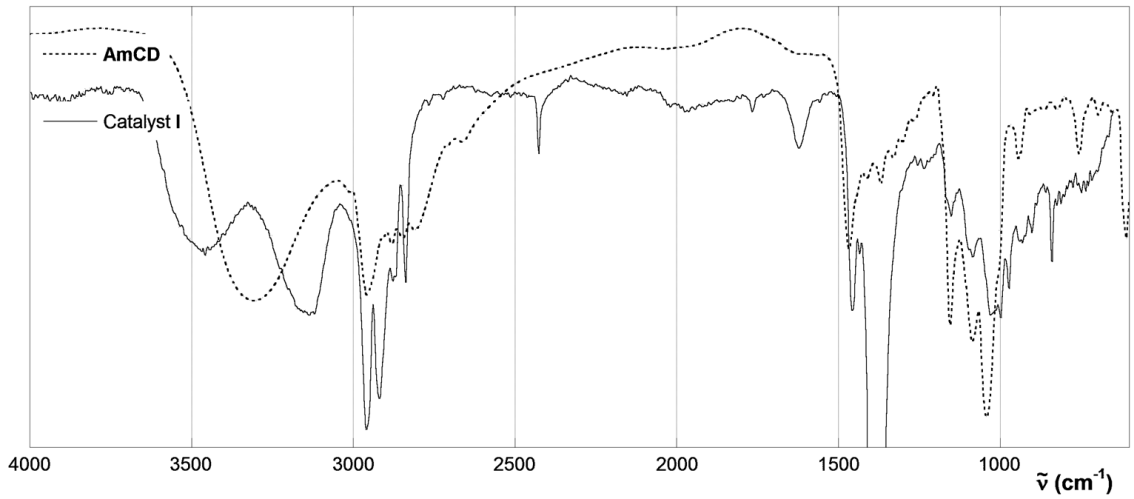

Figure 6.8 – IR spectra of **amCD1** and catalyst **I.**

6.3.2 - Kinetic study of the nitroarene reduction

In order to study the kinetics of the reduction reaction of nitroarenes **1**-**8** mediated by **AgNP**s, sample systems were prepared in such a way to have initial concentrations of the substrate and $NaBH_4$ of 0.1 mM and 4.0 mM respectively, and a catalyst concentration ranging between 1.33 and 83.3 μM. For the sake of clarity the latter one is the equivalent concentration of silver ion (C_{Ag}) needed in order to obtain the actual amount of NPs introduced in the sample. The reducing agent, which is the last component introduced in the system immediately before starting the registration of the kinetic experiment, is always used in large excess with respect to the nitroarene substrate. Kinetics were followed at 40 °C, monitoring by UV–vis spectrophotometry the disappearance of the absorption band of the substrate, at its λ_{max} value. A typical trace is shown in Figure 6.9. In agreement with literature,[302,319-322] a preliminary induction period is present. Subsequent data points monotonically decrease, till a plateau is almost abruptly reached.

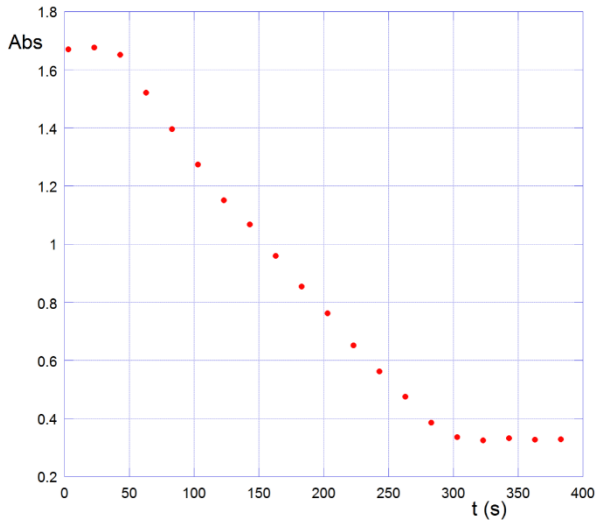

Figure 6.9 – Typical kinetic trace for nitroarene reduction.

In striking contrast with previous literature, the decreasing branch of the kinetic trace cannot be satisfactorily fitted neither as a first order exponential decay, nor as a zeroth-order straight line process. Rather, experimental points appear tentatively adaptable at a first approximation by a parabolic trend. In a preliminary set of control experiments performed with 4-nitroaniline 1, the amount of catalyst was fixed (50 μM) and suitably varied the borohydride concentration in the range 1.0 – 8.0 mM. Then, by means of the initial rate method, the reaction resulted first-order in the borohydride reducing reactant. According to literature,[70,297] a curvilinear dependence of the initial rate vs. borohydride concentration would have been expected at much larger concentrations (>10 mM).

The kinetics of NPs catalyzed reactions is generally approached by means of the Langmuir-Hinshelwood model,[322-328] considering the reversible association of the reactants on different sites of the catalyst surface. The curvilinear dependence of the initial reaction rate, can be rationalized admitting a fast association pre-equilibrium between the catalyst and the BH_4^- ion. The **AgNP** catalyst surface is considered as divided in effective area cells **α**, each as large as the average surface covered by a single **amCD** unit. Then, the reaction product is formed in a rate-limiting step from a surface-substrate-borohydride ternary complex, deriving from a series of fast pre-equilibria (Scheme 6.4).

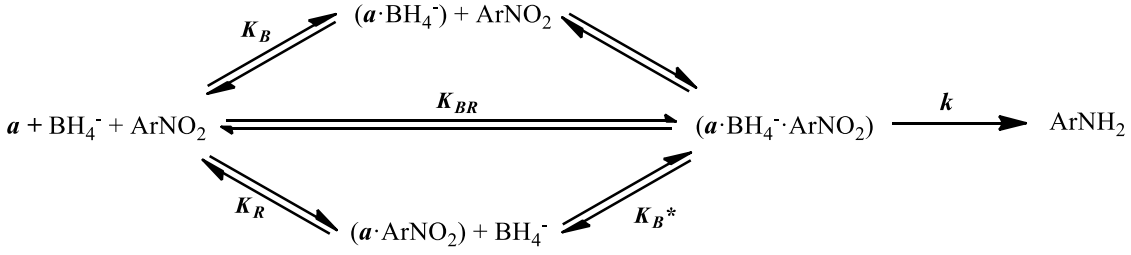

Scheme 6.4

It can be assumed that **α** cells have a formal concentration (C_a) proportional to C_{Ag} according to the relationship $C_a = \sigma \cdot C_{Ag}$, where σ is the ratio between the total surface for the NPs generated by one mole of silver ion, and the average surface which can be covered by one mole of **amCD** units. From Scheme 6.3 the following differential kinetic expression can be obtained:

$$v = -\frac{d[ArNO_2]}{dt} = k[\alpha \cdot BH_4^- \cdot ArNO_2] = \frac{kK_{BR}C_\alpha[BH_4^-][ArNO_2]}{1 + K_B[BH_4^-] + K_R[ArNO_2] + K_{BR}[BH_4^-][ArNO_2]} \quad (6.1)$$

where K_B, K_R and K_{BR} are the stability constants for the binary complex (**α**·$ArNO_2$) and (**α**·BH_4^-) and the overall stability constant for the reactive ternary complex (**α**·BH_4^-·$ArNO_2$) respectively; *k* is the kinetic constant for the rate determining step. Eq. (6.1) can be simplified by considering that the observed linear dependence of the reaction rate on $[BH_4^-]$ implies the algebraic condition: $1+K_R[ArNO_2] \gg K_B[BH_4^-]+K_{BR}[BH_4^-][ArNO_2]$, then:

$$v = -\frac{d[ArNO_2]}{dt} = \frac{kK_{BR}C_\alpha[BH_4^-][ArNO_2]}{1 + K_R[ArNO_2]} = \frac{kK_{BR}\sigma C_{Ag}[BH_4^-][ArNO_2]}{1 + K_R[ArNO_2]} \quad (6.2)$$

This expression reduces to either a first order or a zeroth order expression, by imposing the conditions $1 \gg K_R[ArNO_2]$ or $1 \ll K_R[ArNO_2]$ respectively. However, it can be integrated as:

$$t = t_i + (1/k_{obs})([ArNO_2]_i - [ArNO_2]) + (1/k_{obs}K_R)\ln([ArNO_2]_i/[ArNO_2]) \quad (6.3)$$

where t_i is the length of the induction period, and $k_{obs} = k(K_{BR}/K_R)\sigma C_{Ag}[BH_4^-]$. The latter condition may be also written as $k_{obs} = kK_{B*}\sigma C_{Ag}[BH_4^-]$,where K_{B*} is the equilibrium constant for the association between the preformed (**α**·$ArNO_2$) binary complex and BH_4^-. The integrated Eq. (6.3) comprises both a zeroth-order (linear) and a first-order (logarithmic) term in the substrate. So, it can be suitably used to perform the regression analysis of the experimental kinetic traces. The expression for k_{obs} predicts a linear dependence of the reaction rate on both the concentrations of the reducing agent and the catalyst as well.[323,329,330] Surprisingly, however, experimental results showed for k_{obs} a non-linear dependence on C_{Ag} (Figure 6.10, the complete data collection is reported in the Experimental Section, Tables 6.7-12).

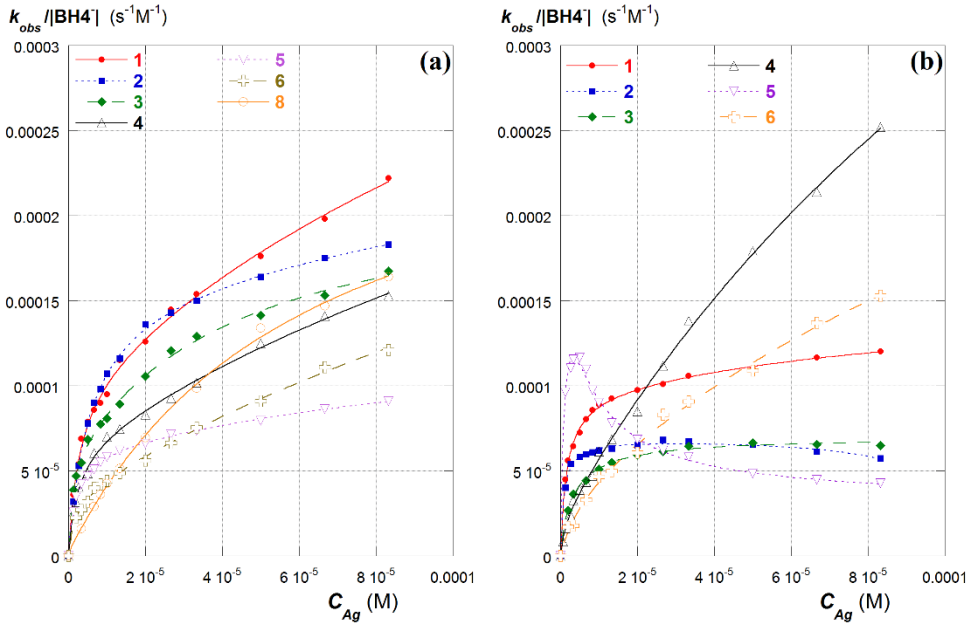

Figure 6.10 – Trends of k_{obs} vs C_{Ag} for different substrates: (a) Catalyst **I**; (b) Catalyst **II**.

In some cases, namely with Catalyst **II** and anionic substrates **2** (sodium N-4-nitrophenyl-glicinate), **3** (sodium N-methyl-N-4-nitrophenyl-glicinate) and **5** (sodium 4-nitrophenate), non-monotonical trends were found. No reaction could be observed for substrate **7** (sodium 4-nitrobenzoate) with both catalysts, and for **8** (nitrobenzene) with Catalyst **II**. In order to explain the latter results it is reasonable to admit that the catalytic NP surface may have a different efficiency depending on how many **amCD** layers cover it (Figure 6.11). Considering that **amCD** layers are lost on dilution, probably uncovered or singly-covered portions of the surface have a good efficiency, whereas double- or multiply-covered portion are not effective, simply because the reactants are shifted far from the surface. The latter hypothesis was verified in a set of control experiments performed with *p*-nitroaniline **1** and Catalyst **I** (50 μM), by adding increasing amounts of **amCD**: a progressive decrease in the reaction rate is observed, until

substantial inhibition is achieved for **amCD** concentrations larger than 1.0 mM. Therefore, a more complex mechanistic scheme was considered (Scheme 6.5).

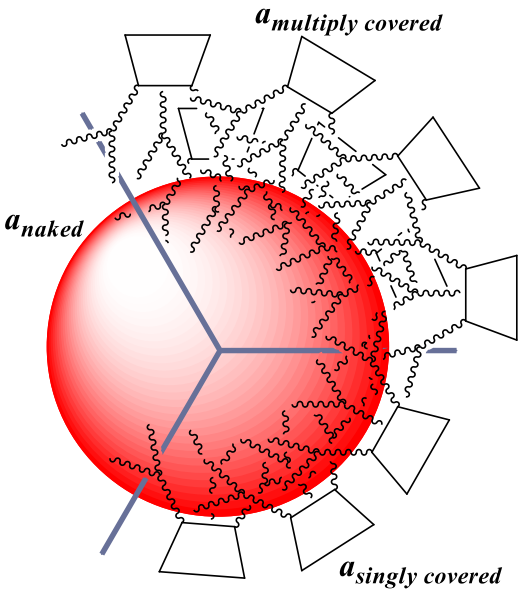

Figure 6.11 – Representation of the differently covered surface elements of the catalysts.

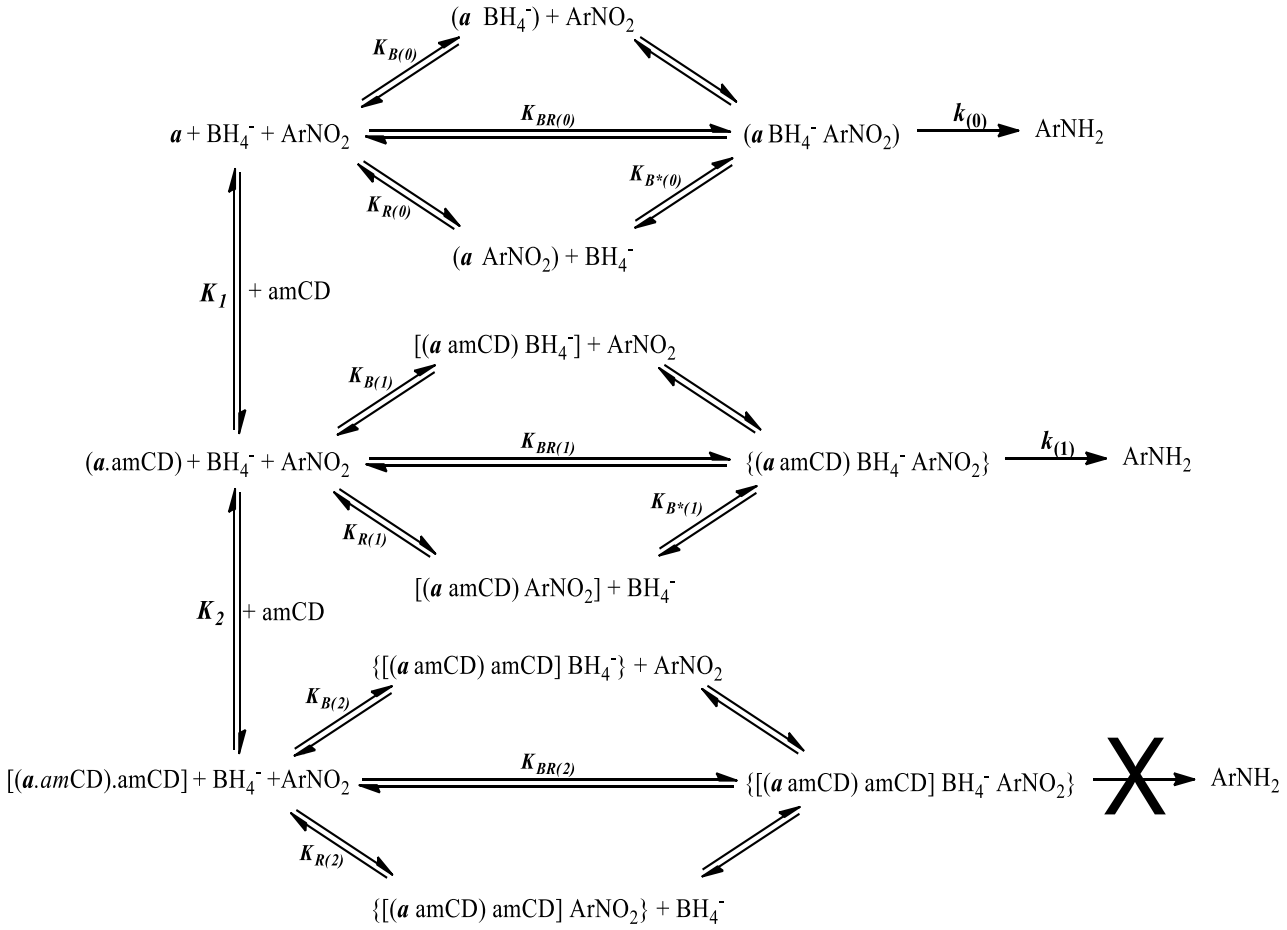

Scheme 6.5

In principle, the reaction rate should depend on the concentrations of the possible active catalyst-substrate-borohydride ternary complexes, according to the expression:

$$v = k_{(0)}[\alpha\cdot ArNO_2\cdot BH_4^-] + k_{(1)}[(\alpha\cdot amCD)\cdot ArNO2\cdot BH_4^-] =$$

$$= k_{(0)}K_{R(0)}K_{B*(0)}[\alpha][amCD][ArNO_2][BH_4^-] + k_{(1)}K_{(1)}K_{R(1)}K_{B*(1)}[\alpha][ArNO_2][BH_4^-] \quad (6.4)$$

From Scheme 6.5, considering the mass balance on the surface cells and the equilibrium conditions, and applying few useful simplifications, the following kinetic equation was obtained:

$$v = -\frac{d[ArNO_2]}{dt} = k_{(0)}[\alpha\cdot BH_4^-\cdot ArNO_2] + k_{(1)}[(\alpha\cdot amCD)\cdot BH_4^-\cdot ArNO_2] =$$
$$= \frac{\{(k_{(0)}K_{R(0)}K_{B*(0)} + k_{(1)}K_{R(1)}K_{B*(1)}[amCD])\cdot\sigma C_{Ag}[BH_4^-]\}[ArNO_2]}{(1+K_1[amCD]+K_1K_2[amCD]^2)+(K_{R(0)}+K_1K_{R(1)}[amCD]+K_1K_2K_{R(2)}[amCD]^2)[ArNO_2]} \quad (6.5)$$

In Eq. (6.5) the concentration of free **amCD** is accounted. The total amount of **amCD** in the system (C_{CD}) is bound to C_{Ag} by the relationship: $C_{CD} = \rho\cdot C_{Ag}$, where ρ is the **amCD**/Ag^+ mole ratio defined above. However, at a first approximation it can be assumed [a**mCD**] ≈ $\rho\cdot C_{Ag}$, i.e. the concentrations of the various complexes may be considered negligible with respect to free **amCD**. (The latter statement relies on the fact that, considering the binding constant of inclusion complex between guest **1-8** and native **βCD** used as reference, the resulted concentration of **amCD**·$ArNO_2$ complexes is actually negligible with respect to free **amCD**). Then, the following final kinetic expression can be obtained:

$$v = -\frac{d[ArNO_2]}{dt} = \frac{(k_{(0)}K_{R(0)}K_{B*(0)} + k_{(1)}K_1K_{R(1)}K_{B*(1)}\rho C_{Ag})\cdot\sigma C_{Ag}[BH_4^-][ArNO_2]}{(1+K_1\rho C_{Ag}+K_1K_2\rho^2C_{Ag}^2)+(K_{R(0)}+K_1K_{R(1)}\rho C_{Ag}+K_1K_2K_{R(2)}\rho^2C_{Ag}^2)[ArNO_2]} \quad (6.6)$$

Although the disheartening form assumed by the Eq.(6.6), it can be reduced to the same expression of the Eq.(6.2) and then it can be integrated in the same way to afford the similar final expression:

$$t = t_i + (1/k_{obs})([ArNO_2]_i-[ArNO_2]) + (1/k_{obs}K_{App})\ln([ArNO_2]_i-[ArNO_2]) \quad (6.7)$$

where:

$$k_{obs} = C_{Ag}[BH_4^-]\frac{[\sigma k_{(0)}K_{B*(0)}]+[\sigma k_{(1)}K_1(K_{R(1)}/K_{R(0)})K_{B*(1)}]\rho C_{Ag}}{1+K_1(K_{R(1)}/K_{R(0)})\rho C_{Ag}+K_1K_2(K_{R(2)}/K_{R(0)})\rho^2C_{Ag}^2} \quad (6.8)$$

and

$$K_{app} = \frac{K_{R(0)}+K_1K_{R(1)}\rho C_{Ag}+K_1K_2K_{R(2)}\rho^2C_{Ag}^2}{1+K_1\rho C_{Ag}+K_1K_2\rho^2C_{Ag}^2} \quad (6.9)$$

Considering again Eq.(6.8) this can be also written as:

$$\frac{k_{obs}}{|BH_4^-|} = \frac{k_{obs,0}C_{Ag} + k_{obs,1}K_{app,1}\rho C_{Ag}^2}{1 + K_{app,1}\rho C_{Ag} + K_{app,1}K_{app,2}\rho^2 C_{Ag}^2} \quad (6.10)$$

Where $k_{obs,0} = \sigma\, k_0 K_{B^*,(0)}$, $k_{obs,1} = \sigma\, k_1 K_{B^*,(1)}$, $K_{app,1} = K_1(K_{R(1)}/K_{R(0)})$ and $K_{app,2} = K_2(K_{R(2)}/K_{R(0)})$. Noticeably, $k_{obs,0}$ and $k_{obs,1}$ provide a quantitative estimation of the catalytic efficiency of the naked and the singly-covered NP surface respectively. The catalytic efficiency depends, in turn, on the morphological characteristics of the NPs (according to σ), on the ability of the NP-substrate pre-complex to bind the reducing agent (according to $K_{B^*(0)}$ or $K_{B^*(1)}$) and on the intrinsic reactivity of the substrate onto the particular catalyst cell (according to k_0 or k_1); $K_{app,1}$ and $K_{app,2}$ represent the conditional binding constants between the NP surface and the **amCD** layers in the presence of the different substrates. Eq. (6.10) can adequately describe the non-monotonical k_{obs} vs. C_{Ag} trends observed with Catalyst **II** and anionic substrates. However, as long as data relevant to Catalyst **I** are considered, the use of Eq. (6.10) leads to unreliable $K_{app,2}$ values, characterized by large uncertainty. On the other hand, considering the term $K_{app,1}K_{app,2}\rho^2 C_{Ag}^2$ negligible with respect to $1+K_{app,1}\rho C_{Ag}$, a simplified form of Eq. (6.10) can be more suitably used:

$$\frac{k_{obs}}{|BH_4^-|} = \frac{k_{obs,0}C_{Ag} + k_{obs,1}K_{app,1}\rho C_{Ag}^2}{1 + K_{app,1}\rho C_{Ag}} \quad (6.11)$$

The results obtained by analyzing the apparent kinetic constants k_{obs} for substrates **1-8** with either Eq. (6.10) or (6.11) are summarized in Table 6.2. Noticeably $k_{obs,0}$ values spun over a much larger range for Catalyst **II** than for Catalyst **I**, indicating larger variations in reactivity between the various substrates, and therefore a larger selectivity for the catalyst. Moreover, larger $K_{app,1}$ values are generally observed with Catalyst **I** than for Catalyst **II**. These differences among the two catalysts may be ascribed to the different amount of unreduced Ag^+ ion present on the catalyst, which is likely to interact with the nitroarene substrate before the addition of borohydride. Then, after BH_4^- is introduced to start the reaction, the residual Ag^+ is reduced. Thus, the consequent modifications in the morphology of the catalyst may be affected by the possible occurrence of significant Ag^+-substrate interactions. This seems particularly evident in the case of anionic substrates, for which non-monotonical trends in k_{obs} values vs. C_{Ag} are observed.

Table 6.2 – Kinetic constants for the nitroarenes reduction.

Sub	Catalyst I				
	Eq.	$k_{obs,0}$ **($s^{-1} M^{-1}$)**	$k_{obs,1}$**($s^{-1} M^{-1}$)**	$k_{app,1}$**($10^{-6} M^{-1}$)**	$k_{app,2}$ **($10^{-6} M^{-1}$)**
1	11	36.2 ± 1.4	1.30 ± 0.07	8.4 ± 0.8	n.d.
2	11	29.0 ± 0.4	0.40 ± 0.03	5.1 ± 0.2	n.d.
3	11	36.0 ± 2.0	0.88 ± 0.09	10.0 ± 1.8	n.d.
4	11	26.7 ± 1.1	1.00 ± 0.05	9.8 ± 1.2	n.d.
5	11	32.0 ± 0.6	0.33 ± 0.02	13.7 ± 0.7	n.d.
6	11	16.9 ± 0.7	0.93 ± 0.03	10.0 ± 1.2	n.d.
7	-	n.d.	n.d.	n.d.	n.d.
8	11	5.2 ± 0.3	0.67 ± 0.07	0.84 ± 0.07	n.d.
Sub	**Catalyst II**				
	Eq.	$k_{obs,0}$ **($s^{-1} M^{-1}$)**	$k_{obs,1}$**($s^{-1} M^{-1}$)**	$k_{app,1}$**($10^{-6} M^{-1}$)**	$k_{app,2}$ **($10^{-6} M^{-1}$)**
1	10	62 ± 3	2.0 ± 1.0	3.9 ± 0.4	0.8 ± 0.4
2	10	65 ± 2	(<0.2)	5.2 ± 0.2	(<0.4)
3	10	23 ± 2	0.6 ± 0.4	2.0 ± 0.2	0.5 ± 0.3
4	11	11 ± 2	2.4 ± 0.1	0.8 ± 0.2	n.d.
5	10	131 ± 2	6.3 ± 2.0	3.2 ± 0.8	1.2 ± 0.3
6	11	7 ± 1	1.1 ± 0.1	0.44 ± 0.10	n.d.
7	-	n.d.	n.d.	n.d.	n.d.
8	-	n.d.	n.d.	n.d.	n.d.

Analysis of data reported in Table 6.2 indicates that the presence of a strong electrondonating substituent at the para position with respect to the reacting nitro group, is an important requirement for the reaction to occur. On passing to consider the $k_{obs,0}$ values related to, nitroanilines **1**-**4** and nitrophenate **5** appear significantly more reactive than nitroanisole **6** and nitrobenzene **8**, whereas nitrobenzoate **7** is not reactive at all. This result might appear quite surprising, because the reduction reaction should imply either an electron transfer process[298,331] or the nucleophilic attack of a hydride species to the nitro group. The latter type of process is consistent with the hypothesis reported in literature that BH_4^- transfers a hydride ion onto the NP surface.[322,326,332] In both cases the reaction should be unfavorably affected by electrondonating substituents. By contrast, the behavior observed indicates that the mechanistic course of the process relies on the interaction of the nitroarene with an electrophilic species, which must be identified with the catalyst surface. Nitroanilines **1**-**4** give further insights on the role of the para substituent group. N-substituted derivatives **2**-**4** do not appear more reactive than parent nitroaniline **1**, despite alkyl substituents on the N atom should enhance the overall electrondonating character of the group. Therefore, the presence of a negative charge on the ancillary chain bound to the N atom (substrates **2** and **3**), or the occurrence of significant steric hindrances (substrate **4**), play an unfavorable role. This probably reflects a more difficult approach of the anionic reducing agent to the nitroarene-catalyst pre-complex, and a lower stability of the reactive ternary complex. The reactivity of nitrophenate **5** with Catalyst **II** appears exceptionally high. This is probably due to peculiar modifications in the NP surface

morphology, occurring as a consequence of particular Ag^+-substrate interactions, as discussed previously. On passing to analyze $k_{obs,1}$ values, it is possible to notice that the singly-covered surface cells appear by far less catalytically active than uncovered ones. More in detail, $k_{obs,0}/k_{obs,1}$ ratios range from 4.6 (substrate **4** with Catalyst **II**) up to 97 (substrate **5** with Catalyst **I**). A lesser activity for singly-covered cells, indicates that inclusion into the **CD** cavity does not lead the nitroarene to approach more easily the catalytic surface. This, however, is in contrast with the fact that the organic molecule is correctly included with the nitro group directed towards the primary **CD** rim.[35,37,40,98,101-106] By considering data for Catalyst **I**, the lowest $k_{obs,1}$ values are observed for substrates **2** (sodium N-(4-nitrophenyl)-glicinate) and **5** (sodium 4-nitrophenate). The former one is known to form a very stiff inclusion complex with native **βCD**,[37] due to the occurrence of multiple hydrogen bonding with the secondary host rim. The same effect likely blocks this substrate quite rigidly within the **amCD** cavity. By contrast, other substrates unable to undergo multiple hydrogen bonding form more flexible complexes,[37] and consequently are able to slip down more easily onto the NP surface after inclusion. It is interesting to notice that even the parent nitrobenzene **8** appears relatively reactive onto the singly-covered catalyst. Finally, the scarce reactivity of **5** may be likely attributed to the occurrence of a strong hydrogen bond interaction of the anionic centre with the secondary host rim, thereby keeping it far from the NP surface. Keeping into account the apparent binding constants K_{app} present in Eq. (6.7) and (6.9) and the conditional binding constants $K_{app,1}$ and $K_{app,2}$ present in Eq. (6.10) and (6.11), K_{app} reflects the actual contribution from the first order term to the overall reaction kinetics. This contribution increases in importance as K_{app} decreases; consequently, larger deviations are observed in the kinetic trace with respect to the ideal linear trend expected for a purely zeroth order process. Unlike a true binding constant, K_{app} depends on the concentration of the catalyst according to Eq. (6.9). Observed values usually range between $4 \cdot 10^4$ up to $4 \cdot 10^5$ M^{-1}. However, they are affected by very large uncertainty (up to 40 %), so that a detailed analysis cannot be performed. On passing to $K_{app,1}$ and $K_{app,2}$, their values depend on both the intrinsic affinity of the **amCD** towards the naked or singly covered NP surface (irrespective of the substrate, as accounted for by K_1 and K_2 respectively), and on the different abilities of the naked, singly- or doubly-covered cells to bind the nitroarene (as accounted for by the ratios (K_{R1}/K_{R0}) and (K_{R2}/K_{R1})).Therefore, large differences in $K_{app,1}$ or $K_{app,2}$ between different substrates have to reflect similar differences in the latter ratios. For instance, nitrobenzene **8** shows with Catalyst **I** a much smaller $K_{app,1}$ value as compared to the other substrates. This reflects its much lesser affinity for the host cavity, consequent to the smaller value of its binding constant with native **βCD**[97] as compared with

nitroanilines. The same argumentation can be applied to nitroanisole **6** with Catalyst **II**. However, it should be reminded that $K_{app,1}$ values for Catalyst **II** are influenced by the deep modifications of the catalyst upon introduction of the reducing agent, as discussed previously. The outcome of the possible substrate-Ag^+ interactions on such modifications is not easily predictable. Regarding to $K_{app,2}$, its estimation was possible only in few cases, but values appear quite lower as compared to $K_{app,1}$. It is worth stressing that $K_{app,2}$ accounts for the interaction between superimposed layers of **amCD**, which probably involves the inclusion of the diamine pendants of the outer layer into the cavities of the inner one. Therefore, data suggest that the latter interaction is significantly less effective. Finally, regarding induction times t_i, for each substrate-catalyst combination examined it was observed as values increase on decreasing the concentration of the catalyst (data for substrate 1with Catalyst **I** are shown in Figure 6.12).

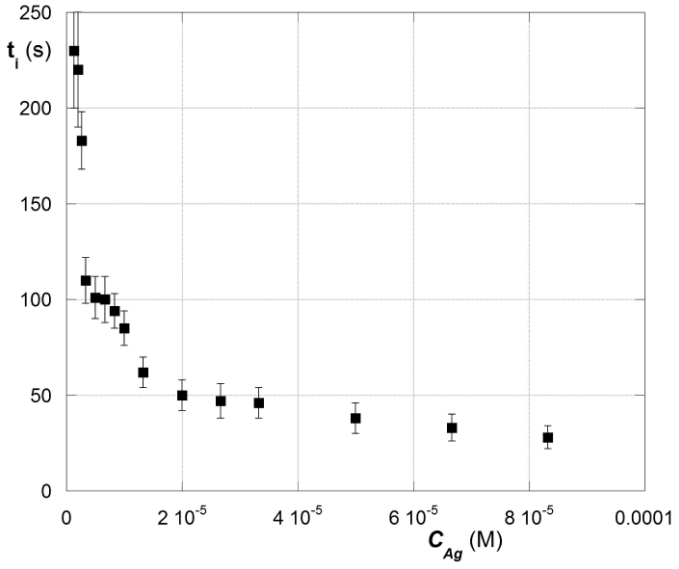

Figure 6.12 – Trend of the t_i values vs $C_{Ag.}$

Induction times vary with both the substrate and the catalyst. Nitroanilines **1**-**4** show smaller values than nitrophenate **5** and nitroanisole **6**, whereas nitrobenzene shows the largest values. At the largest NP concentrations, slightly shorter induction times are observed with Catalyst **I**, with the exception of nitrophenate **5**. The occurrence of an induction period has been justified in different ways. It was formerly admitted that the catalytic process can start only after a tiny layer of silver oxide possibly present on the NP surface had been reduced by BH_4^-.[321] It has been alternatively proposed that induction times (viewed as the inverse of a sort of kinetic constant[322]) might be related to the diffusion of the reacting species onto the catalyst surface,[302] or to the reconstruction of the NP surface.[322] The obtained results, however, seem to rule out these interpretations, because they cannot explain neither the observed dependence on the concentration of the catalyst and on the structure of the substrate as well, nor the fact that

induction occurs also with Catalyst **II**, having a significant amount of Ag^+ instantly reduced in situ by borohydride. On the other hand, it is well known that induction is typical for mechanisms involving free-radical species. Therefore, it might be tentatively interpreted as an indication that the nitroarene substrate undergoes single electrontransfer processes leading to short-lived radical species, which are scavenged by the molecular O_2 present in solution. There is also a literature evidence that induction times for *p*-nitrophenol reduction are suppressed by exclusion of O_2 from the reaction system.[319] As a consequence, the target reaction cannot properly start unless all the O_2 has been consumed by reaction with the excess borohydride. The latter process will be catalyzed by NPs and, as a consequence, its duration will depend on the concentration of the catalyst. On the other hand, it can be expected that the NP-substrate interaction will favor this process, with an increasing effect on increasing the electrondonating character of the substrate itself.

*6.3.3 - **PdNP**s as catalysts for the Suzuki reaction*

After having verified the abilities of **amCD**s to function as capping agents for the synthesis of **AgNP**s, as a proceeding of this work the possibility to exploit the same products for the synthesis and stabilization of Pd nanoparticles was considered. The synthesis of the nanocomposite can be accomplished in a perfectly analogous way as the one reported when dendrimers are used as the capping agent, by reduction of the aqueous complex anion $PdCl_4^{2-}$ (prepared in situ from $PdCl_2$ and NaCl) with $NaBH_4$ in the presence of the proper amount of **amCD**, according to the reaction:

$$4\ [Pd(Cl)_4]^{2-} + BH_4^- + 8\ OH^- \rightarrow 4\ Pd + B(OH)_4^- + 16\ Cl^- + 4\ H_2O$$

Noticeably, in order to accomplish the reaction, $PdCl_4^{2-}$ and **amCD** must be allowed to react under stirring for at least 90 min, in order to ensure that the displacement of chloride ions by the polyamine comes to completion. Then addition of the borohydride reducing agent causes the rapid formation of the Pd nanoparticles, as evidenced by the fact that the solution immediately turns from a pale amber color to grey. More in detail, in a first series of experiments a set of assay samples were prepared, having a fixed concentration of Pd salt 1 mM, and varying **amCD** and $NaBH_4$ concentrations according to the grid reported in Table 6.3.

Table 6.3 – Working grid for the **PdNP**s preparation.

		[**amCD**] (mN)			
		0.25	0.50	1.0	2.5
[BH_4^-] (mM)	0.04	**Ia**	**Ib**	**Ic**	**Id**
	0.20	**IIa**	**IIb**	**IIc**	**IId**
	1.0	**IIIa**	**IIIb**	**IIIc**	**IIId**

Analysis of the UV-vis spectra of the samples reveals that the grey color is due to an extremely large absorption band, with no apparent maximum in the region between 300 and 800 nm. Therefore, it seemed convenient to quantify the extent of the reduction process by monitoring the absorbance of the pseudo-solution at 500 nm, at which the absorbance of the solution before reduction is nearly null. The absorbances of the sample systems (expressed as the corresponding ε values) after reduction with borohydride are summarized in Table 6.4.

Table 6.4 – ε values at 500 nm of the Pd/**amCD** nanoparticles.

sample	[BH_4^-] (mM)	Pd/**amCD** eq/eq	**amCD1**	**amCD2**	**amCD3**
Ia	0.04	1:1	1380	1290	1170
Ib	0.04	1:2	820	1020	870
Ic	0.04	1:4	650	670	280
Id	0.04	1:10	390	360	250
IIa	0.20	1:1	1920	1760	1770
IIb	0.20	1:2	1760	1690	1960
IIc	0.20	1:4	1610	1490	1910
IId	0.20	1:10	1360	1350	1980
IIIa	1.0	1:1	2100	1810	2210
IIIb	1.0	1:2	2100	1890	2280
IIIc	1.0	1:4	2100	1810	2270
IIId	1.0	1:10	2100	1810	2190

Analysis of these results easily shows that on increasing the amount of **amCD** the absorbance of the samples decreases, indicating a protective effect of the capping agent towards the metal ion, which strictly resembles the one observed in the case of **AgNP**s. Moreover, reduction results complete only at the highest concentration of borohydride, and therefore only with the presence of a large excess of reducing agent. These systems were also subjected to DLS analyses (unfortunately, TEM characterization was not possible because of lack of instrumental facilities). Data indicated that before the reduction with borohydride quite large and fairly polydispersed aggregates are formed, with average diameters ranging between 185 and 560 nm; average diameters increase on increasing the amount of **amCD**, irrespective of the particular **amCD** used. After the reduction has occurred, DLS analyses show the presence in the samples of at least two very polydispersed populations of objects. The first ones have average diameters more or less similar to those found before reduction; the second one is constituted by very large

objects, up to 1000 nm or even more. Noticeably, all these systems appear quite less stable than the **AgNP**s described previously, and tend to precipitate within hours or few days at the best; precipitation is faster for the systems prepared with the largest amount of borohydride.

Most literature reports of TEM analyses on Pd nanoparticles, agree in describing them as very small objects, usually having average diameters around 5 nm or so. Therefore, everything considered, DLS results suggest that, similarly as for Ag, the interaction between the Pd(II) ions and the polyamine arms of the **amCD** units forms very large aggregates, which function as nests for the subsequent formation of the metal particles after the reducing agent is added. Probably, the actual nanoparticles are as small as those described in literature, and are covered by a thick layer of **amCD** units complexing unreduced Pd ions. However, the large tendency to aggregate, in particular whenever the reduction process is almost complete (large excess of borohydride) indicate that these layers cannot ensure an effective electrostatic barrier to coalescence.

On the grounds of these preliminary semi-quantitative results, it was decided to test some representative **PdNP** systems for their possible catalytic efficiency towards the Suzuki coupling reaction, chosen as a suitable probe reaction.

As a particular probe reaction, phenyl-boronic acids and *p*-bromo-acetophenone were chosen as substrates, in the presence of potassium carbonate as the base and ethanol as the solvent (Figure 6.13):

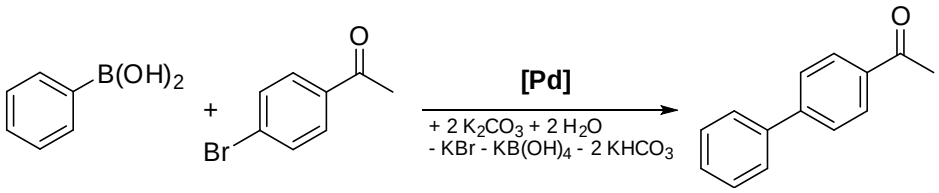

Figure 6.13 – Scheme of the Suzuki reaction used as probe.

For each **amCD** only the **Ic**-type ant the **IIIc**-type catalysts were considered, i.e. those prepared with Pd 0.25 mM, **amCD** 1.0 mN, BH_4^- 0.04 mM (**Ic**) or 1.0 mM (**IIIc**). Sample systems were prepared by dissolving into 3 mL of the chosen catalyst 1.0 mmoles of bromoacetophenone, 1.1 mmoles of phenylboronic acid and 1.2 mmoles of K_2CO_3. The samples were reacted for 19 h at either 25 °C or 50°C. Then, the reaction mixtures were poured in water and extracted with dichlorometane. Distillation in vacuo of the organic extracts afforded a crude, which was weighed and analyzed by NMR. In fact, the ^1H NMR spectrum of the mixture (a representative example is shown in Figure 6.13) shows two neat singlets at 2.52 and 2.59 ppm, which can be attributed to the methyl groups of the bromoacetophenone and the product methyl-biphenylyl-ketone respectively. Integration of the latter signals enables to calculate the mole fractions of

the two substances in the mixture; then, by few trivial passages conversion and yields can be easily calculated. The results are summarized in Table 6.5

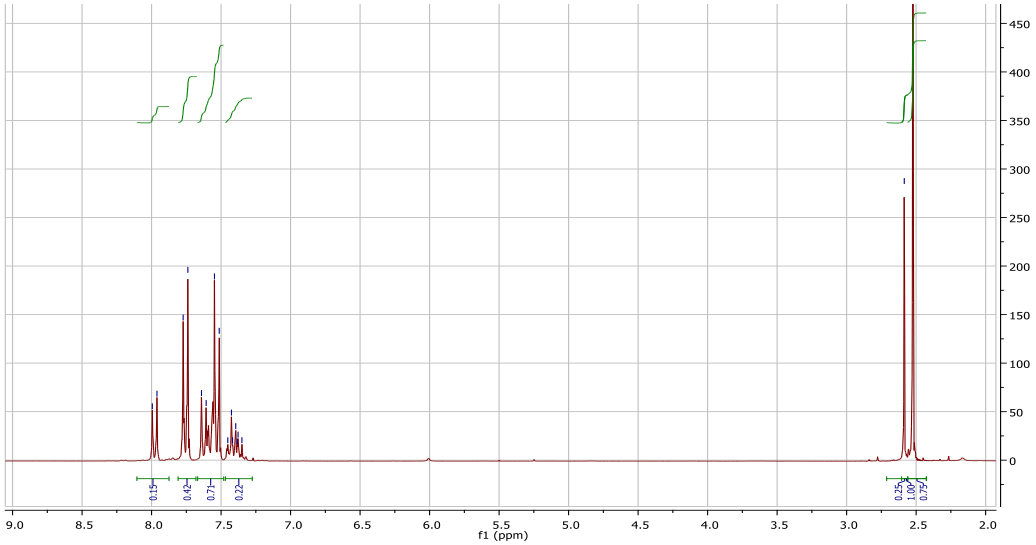

Figure 6.13 – ^{1}H-NMR spectra of the reaction crude.

Table 6.5 – Yields and conversions of the reaction using different catalytic systems and conditions.

entry	amCD	system	Rection time (h)	T (°C)	X_P	recover (mg)	conv. (%)	yield (%)	Yield on conv. (%)
1	**CD1**	**IIIc**	19	25	0.258	200	34	23	68
2	**CD1**	**Ic**	19	25	0.757	209	77	71	92
3	**CD1**	**IIIc**	19	50	0.607	185	67	50	75
4	**CD1**	**Ic**	19	50	0.871	167.8	90	66	73
5	**CD2**	**IIIc**	19	25	0	207	8	0	0
6	**CD2**	**Ic**	19	25	0	192	15	0	0
7	**CD2**	**IIIc**	19	50	< 0.01	192.5	14	tracce	
8	**CD2**	**Ic**	19	50	< 0.01	197.5	12	tracce	
9	**CD3**	**IIIc**	19	25	0	203	10	0	0
10	**CD3**	**Ic**	19	25	0	198	12	0	0
11	**CD3**	**IIIc**	19	50	0	252.9	0	0	0
12	**CD3**	**Ic**	19	50	0	211	6	0	0

It can be easily seen that **PdNP**s capped with the **amCD2** and the **amCD3** are ineffective in catalyzing the reaction. Even more interestingly, the **Ic**-type catalyst prepared with **amCD1** appears much more effective than the corresponding **IIIc**-type one. This indicates that the reaction course takes advantage from the presence of the Pd^{++} ion in the reaction system. In order to clarify the role of the **amCD1** lingand and of the Pd^{++} ion, further reaction samples were prepared (Table 6.6), namely: *i*) preparing the "**c**"-type catalysts without borohydride (entries 13-16); *ii*) substituting the **amCD** with the corresponding free polyamine, without adding the borohydride (entries 17-19); *iii*) adding a competitive guest (entries 20-21). It can

be easily seen that the Pd^{++} only, is able to catalyze the reaction, improving conversions and yields, at least in presence of **amCD1**. This, confirming the importance of Pd^{++} in the whole mechanistic course of the Suzuki reaction.

Table 6.6 – Yields and conversion of the reaction using different Pd^{++} systems.

entry	amCD	system	Rection time (h)	T (°C)	X_P	recover (mg)	conv. (%)	yield (%)	Yield on conv. (%)
13	**CD1**	[Pd^{++}]	19	25	0.820	184.1	85	68	80
14	**CD1**	[Pd^{++}]	19	50	0.938	147.3	96	62	65
15	**CD2**	[Pd^{++}]	19	25	< 0.01	191.1	15	traces	
16	**CD3**	[Pd^{++}]	19	25	0	253.7	0	0	0
17	**(A1)**	[Pd^{++}]	19	25	0.146	197.4	25	13	52
18	**(A2)**	[Pd^{++}]	19	25	0	206.2	8	0	0
19	**(A3)**	[Pd^{++}]	19	25	0	287.2	0	0	0
20	**CD1** + $AdaO^-$	[Pd^{++}]	19	25	0.218	189.2	37	21	57
21	**CD1** + AcO^-	[Pd^{++}]	19	25	0.832	185.1	86	69	81

Furthermore, it is very interesting to notice that substitution of the **amCD** with an equivalent amount of polyamine causes a dramatic decrease in the catalytic efficiency. The very favorable effect of the **amCD** might be explained in principle both with its ability to form large aggregates of the catalytic nanoparticles, and with the possibility that the formation of supramolecular complexes between the aromatic reactants and the **amCD** cavity favors the approach of the reactants on the **PdNP** surface. Thus, in order to verify the latter hypothesis, the reaction was performed in the presence of potassium adamantate. Indeed, adamantyl derivatives are known to form very stable complexes with **βCD**s, because their size perfectly fits into the **βCD** cavity. A significant decrease in the catalytic activity was observed (entry 20), which cannot be attributed to the mere addition of a generic carboxylate salt, because no effect occurs if potassium adamantate is substituted with an equivalent amount of potassium acetate (entry 21). These observations positively assess the possible favorable contribution to the reaction course due to the inclusion of the reactants into the **amCD** cavity.

As a final remark, it is worth stressing that the amount of catalyst in the sample systems is very little, i.e. 0.075 %mol than the aryl bromide limiting reactant. This indicates that **amCD**-capped **PdNP**s present catalytic performances in line with the bests catalytic systems reported in recent literature.[306,307]

6.4 – Experimental section

Instrumentations

UV-vis spectra were recorded on a Beckmann DU 800 spectrophotometer, equipped with a Peltier thermostatic apparatus, which was used also to perform the kinetic experiments.

TEM micrographs were acquired using a JEM-2100 (JEOL, Japan) electron microscope operating at 200 kV accelerating voltage. A drop of each suspension was put onto a 3 mm Cu grid "lacey carbon" for analysis and let the solvent to complete evaporation.

DLS measurements have been carried out by using a 90 Plus Particle Size Analyzer (Brookhaven Instrument Corp., Holtsville, NY, USA) equipped with a BI-9000AT Digital Autocorrelator. The source was a He-Ne 632.8 nm laser and the detector was a photomultiplier tube, both mounted on a turntable; measurements were performed at 90°. By using the software supplied by Brookhaven Corp, data were obtained directly as electric field self-correlation function, $G(\tau)$, versus decay time, τ. In order to check data reproducibility and the stability of the suspension, measurements have been repeated in triplicate on different freshly prepared samples. Electric field self-correlation functions have been analyzed to obtain diffusion coefficients, D. The scattering particle diameters, d, have been evaluated by means of the Stokes-Einstein equation: $D = K_B T/3\pi\eta d$ once provided the absolute temperature T, and the viscosity of the solution η. Owing to the low concentration of the systems, the latter can be assumed coincident with the one of the pure solvent, within the limits of experimental errors. The self-correlation function computed by using the Cumulant analysis,[333] did not satisfactorily reproduce the experimental data, thus suggesting that the particles in suspension were polydisperse. Therefore, a more appropriate analysis was performed by means of the CONTIN method.[334,335]

*Synthesis of **AgNPs***

Mother solutions of $[Ag(NH_3)_2]^+$ 15 mM and **amCD** 6 mN were prepared in double-distilled water, previously degassed with a fine stream of Ar for 15 minutes. Then, samples were prepared by mixing in a dark vial the proper amounts of water, $[Ag(NH_3)_2]^+$ and **amCD** solutions up to 14 mL. The samples, kept under Ar atmosphere, were placed in an oil bath thermostated at 40 °C, inoculated with 1 mL of formaldehyde solution 33.4 mM, and allowed to react for 90 minutes. UV-vis spectra of the samples were recorded immediately after the reaction time. Catalysts **I** and **II** were carefully kept and stored in the dark before use.

Kinetics of nitroarene reduction.

Kinetic experiments were performed at 313 K, according to the following procedure. In a quartz cuvette the proper amount of a stock solution of catalyst (1.0 mM) was diluted in the proper amount of freshly double-distilled water (degassed with a fine stream of Ar for 15 minutes), in such a way to have 2.65 mL of solution; then, 100 μL of a stock solution 3.0 mM of the substrate were added, and the mixture was thermostated. A 48.0 mM solution of $NaBH_4$ was prepared just before use by dissolving a weighed amount in a volumetric flask; then 250 μL were rapidly introduced in the cuvette, and the registration of the kinetic trace immediately started, following by UV-vis spectrophotometry the disappearance of the nitroarene substrate.

Table 6.7 - [k_{obs}/|BH_4^-|] values ($10^5 s^{-1}M^{-1}$) for the reduction of substrates **1-6** and **8** with Catalyst **I**.

C_{Ag}(μM)	**1**	**2**	**3**	**4**	**5**	**6**	**8**
83.3	22.2±0.6	18.3±0.5	16.7±0.5	15.3±0.4	9.1±0.3	12.1±0.3	16.4±0.4
66.7	19.8±0.6	17.5±0.5	15.3±0.5	14.1±0.4	8.6±0.3	10.6±0.3	14.7±0.4
50.0	17.6±0.5	16.4±0.5	14.1±0.4	12.5±0.4	7.9±0.3	9.1±0.3	12.4±0.4
33.3	15.4±0.5	15.0±0.5	12.9±0.4	10.2±0.4	7.3±0.3	7.5±0.3	9.8±0.4
26.7	14.5±0.5	14.3±0.5	12.1±0.4	9.3±0.3	7.1±0.3	6.6±0.3	
20.0	12.6±0.4	13.6±0.5	10.6±0.4	8.3±0.3	6.6±0.3	5.6±0.2	6.9±0.4
13.3	11.5±0.5	11.6±0.5	8.9±0.4	7.5±0.3	6.2±0.3	4.9±0.2	5.1±0.3
10.0	9.5±0.4	10.7±0.4	8.1±0.4	7.0±0.3	5.8±0.2	4.4±0.2	4.2±0.3
8.33	9.0±0.4	9.8±0.4	7.7±0.4		5.5±0.2	4.2±0.2	3.6±0.3
6.67	8.6±0.4	9.0±0.4		6.0±0.3	5.1±0.2	4.0±0.2	2.9±0.2
5.00	7.9±0.4	7.8±0.4	6.8±0.4	4.8±0.3	4.7±0.2	3.2±0.2	
3.33	6.9±0.3		5.5±0.4		4.2±0.2	2.7±0.2	1.6±0.2
2.67	5.4±0.3	5.3±0.3		4.0±0.2			
2.00	4.7±0.3		4.7±0.3	3.2±0.2	3.4±0.2	2.2±0.2	
1.33	3.6±0.3	3.2±0.3	3.9±0.3	2.6±0.2	2.6±0.2		

Table 6.8 - K_{app} values ($10^{-5}M^{-1}$) for the reduction of substrates **1-6** and **8** with Catalyst **I**.

C_{Ag}(μM)	**1**	**2**	**3**	**4**	**5**	**6**	**8**
83.3	1.0±0.4	1.0±0.3	1.2±0.2	3.2±0.5	1.1±0.2	1.4±0.2	1.4±0.4
66.7	1.5±0.4	0.9±0.3	1.2±0.2	3.4±0.5	1.4±0.2	1.8±0.2	1.2±0.3
50.0	1.8±0.3	0.8±0.2	1.2±0.2	3.6±0.6	1.9±0.2	2.8±0.3	1.2±0.4
33.3	2.4±0.3	0.8±0.2	1.0±0.3	3.7±0.6	2.2±0.3	3.4±0.3	1.3±0.3
26.7	2.4±0.4	0.8±0.2	0.8±0.2	3.1±0.5	2.1±0.3	3.9±0.5	
20.0	2.6±0.4	0.7±0.2	0.9±0.2	3.0±0.5	2.2±0.3	4.0±0.9	1.4±0.3
13.3	2.0±0.3	0.8±0.2	0.9±0.2	3.1±0.5	2.1±0.2	3.9±0.8	1.7±0.4
10.0	2.0±0.4	0.9±0.2	1.0±0.2	2.7±0.5	2.0±0.3	3.6±0.7	1.8±0.2
8.33	1.7±0.4	0.9±0.2	1.1±0.3		1.7±0.2	3.4±0.8	1.0±0.3
6.67	2.1±0.4	1.0±0.2		2.6±0.5	1.4±0.2	3.3±0.4	0.9±0.3
5.00	2.2±0.5	1.1±0.2	1.1±0.2	2.2±0.4	1.0±0.2	3.4±0.5	
3.33	2.1±0.3		1.0±0.2		0.7±0.2	3.3±0.3	0.6±0.3
2.67	1.6±0.4	1.4±0.3		1.7±0.4			
2.00	0.9±0.4		1.5±0.3	1.6±0.3	0.4±0.1	2.5±0.4	
1.33	1.0±0.4	1.2±0.3	1.8±0.4	1.5±0.3	0.3±0.1		

Table 6.9 - t_i values (s) for the reduction of substrates **1-6** and **8** with Catalyst **I.**

C_{Ag}(μM)	**1**	**2**	**3**	**4**	**5**	**6**	**8**
83.3	28±6	36±6	30±5	31±6	47±8	37±6	65±8
66.7	33±7	44±6	32±6	35±5	55±8	48±8	96±10
50.0	38±8	56±8	37±5	51±6	67±9	49±8	114±9
33.3	46±8	65±7	42±7	65±7	94±9	62±8	127±12
26.7	47±9	59±9	58±9	87±7	104±7	64±7	
20.0	50±8	75±8	69±8	109±9	133±15	87±9	200±20
13.3	62±8	87±9	79±10	114±8	170±20	95±12	350±30
10.0	85±9	85±10	82±10	136±10	210±20	110±15	350±40
8.33	94±9	96±12	90±12		230±30	119±16	620±70
6.67	100±12	103±10		150±12	250±40	137±19	710±90
5.00	101±11	143±17	94±15	146±13	280±60	150±20	
3.33	110±12		102±16		250±30	150±30	1090±90
2.67	183±15	230±30		176±17			
2.00	220±30		130±20	185±15	270±40	170±30	
1.33	230±30	290±40	150±30	200±20	330±50		

Table 6.10 - [k_{obs}/|BH_4^-|] values ($10^5 s^{-1}M^{-1}$) for the reduction of substrates **1-6** with Catalyst **II**.

C_{Ag}(μM)	**1**	**2**	**3**	**4**	**5**	**6**
83.3	12.0±0.6	5.7±0.4	6.5±0.3	25.2±1.0	4.3±0.4	15.3±0.4
66.7	11.7±0.6	6.1±0.4	6.6±0.4	21.4±1.2	4.5±0.3	13.7±0.4
50.0	11.2±0.6	6.5±0.3	6.6±0.4	17.9±0.9	4.8±0.4	11.3±0.3
33.3	10.6±0.5	6.7±0.4	6.4±0.3	13.5±0.6	5.8±0.4	9.1±0.4
26.7	10.2±0.5	6.7±0.4	6.1±0.5	11.2±0.7	6.2±0.4	8.3±0.4
20.0	9.7±0.5	6.6±0.3	5.9±0.4	8.8±0.6	6.8±0.6	6.4±0.4
13.3	9.3±0.6	6.3±0.3	5.5±0.4	6.9±0.5	7.9±0.5	5.0±0.3
10.0	8.9±0.5	6.2±0.3	5.1±0.3	6.1±0.5	9.0±0.7	4.6±0.3
8.33	8.6±0.5	6.1±0.4		4.9±0.4	9.8±0.8	
6.67	8.0±0.4	6.0±0.3	4.4±0.3	4.3±0.3	10.9±0.7	3.3±0.2
5.00	7.2±0.4	5.8±0.3		3.9±0.4	11.4±0.8	
3.33	6.4±0.4		3.6±0.3	3.3±0.3	11.1±0.8	1.8±0.2
2.67		5.1±0.3		2.4±0.3	10.3±0.7	
2.00	5.6±0.3		2.7±0.3			1.6±0.2
1.33	4.5±0.3	3.9±0.3		1.6±0.2	9.4±0.7	

Table 6.11 - K_{app} values ($10^{-5}M^{-1}$) for the reduction of substrates **1-6** with Catalyst **II**.

C_{Ag}(μM)	**1**	**2**	**3**	**4**	**5**	**6**
83.3	0.7±0.1	1.1±0.2	0.9±0.2	1.5±0.2	2.1±0.2	1.1±0.2
66.7	0.9±0.2	1.0±0.3	0.9±0.3	1.6±0.3	2.2±0.3	1.1±0.3
50.0	1.1±0.2	0.9±0.3	0.8±0.2	1.7±0.4	2.1±0.2	1.3±0.3
33.3	1.2±0.3	0.8±0.2	0.8±0.2	2.2±0.5	1.6±0.2	1.1±0.3
26.7	1.2±0.3	0.7±0.2	0.8±0.3	2.5±0.4	1.4±0.2	1.2±0.2
20.0	1.1±0.3	0.7±0.1	0.7±0.2	2.9±0.6	1.1±0.2	0.9±0.2
13.3	0.9±0.2	0.7±0.2	0.7±0.1	3.4±0.7	0.8±0.2	0.7±0.2
10.0	0.7±0.2	0.7±0.2	0.7±0.2	3.2±0.7	0.7±0.2	0.6±0.1
8.33	0.7±0.1	0.7±0.1	0.7±0.2	3.1±0.6	0.5±0.1	
6.67	0.6±0.1	0.6±0.1	0.7±0.2	2.8±0.5	0.4±0.1	0.5±0.1
5.00	0.6±0.1	0.6±0.2		2.7±0.6	0.4±0.1	
3.33	0.6±0.2		0.5±0.2	2.4±0.5	0.3±0.1	0.6±0.2
2.67		0.5±0.1		1.2±0.3	0.26±0.08	
2.00	0.6±0.1		0.3±0.1			0.5±0.2
1.33	0.5±0.1	0.24±0.08		0.9±0.2	0.20±0.07	

Table 6.12 - t_i values (s) for the reduction of substrates **1-6** with Catalyst **II**.

C_{Ag}(μM)	**1**	**2**	**3**	**4**	**5**	**6**
83.3	58±12	53±13	52±10	37±9	37±8	40±10
66.7	68±11	57±11	63±11	42±9	44±7	46±12
50.0	70±13	61±14	70±12	44±10	56±8	54±13
33.3	80±13	78±15	98±15	45±9	68±9	57±15
26.7	84±12	90±14	101±15	79±12	92±10	62±17
20.0	92±14	101±16	116±16	87±14	103±12	64±18
13.3	99±16	104±18	111±18	95±15	117±11	90±20
10.0	103±16	109±17	130±20	103±16	127±15	124±18
8.33	104±15	115±20		170±20	134±12	
6.67	106±18	130±20	150±30	170±30	136±13	150±30
5.00	120±20	140±30		240±40	140±20	
3.33	130±20		200±40	250±50	150±20	170±40
2.67		180±40		260±80	160±30	
2.00	140±20		250±50			200±50
1.33	160±30	240±40		440±90	170±30	

*Synthesis of **PdNP**s*

A mother solution of the $PdCl_4^{2-}$ complex was obtained by dissolving 26.6 mg of $PdCl_2$ and 178 mg of NaCl in 50 mL of water; mother solutions of the **amCD**s 10 mN were also prepared. The proper amounts of the $PdCl_4^{2-}$ solution, **amCD** solution and ethanol were mixed and allowed to stir at r.t. for 90 min, giving a pale brown solution; then the proper amount of a freshly prepared $NaBH_4$ 10 mM solution was added. It is important to stress that the amount of ethanol added to each sample was adjusted in order to have a final volume of 3 mL. After addition of the reducing agent the solution immediately turned to grey, and was used as such for both physicochemical analyses and catalysis experiments.

Catalysis of Suzuki reaction

Samples were prepared by mixing 226 mg (1 mmole) of *p*-bromo-acetophenone, 137 mg (1.13 mmoles) of phenylboronic acid and 167 mg of anhydrous potassium carbonate (1.2 mmoles). To each sample the solution of the **PdNP** catalyst (prepared as described above) was added, and the solution was allowed to stir at 25 or 50 °C for 19 h (as specified in Tables 6.4 and 6.5). Then, 20 mL of dichloromethane are added and the solution is washed trice with brine (20 mL each). The organic phase is carefully distilled in vacuo up to constant weight, and the residue is dissolved in $CDCl_3$ for NMR analysis.

- 7 -

PHOTOCHEMICAL SYNTHESIS OF POLYAMINOCYCLODEXTRIN-CAPPED SILVER NANOPARTICLES AS POTENTIAL BIOCIDES

7.1 – Photochemical synthesis of AgNPs

The synthesis of silver-based nanoparticle systems (**AgNP**s) is an extensively studied research topic owing to the many properties and consequent uses of **AgNP**s, which have found applications in various fields spanning from optics to biosensors, diagnostics[336] and catalysis[337] (as it has been shown in the previous chapter). Moreover, **AgNP**s find biomedical applications[338] because of the well-known antibacterial properties of silver (as will be showed afterwards). Several applications, take advantage of the peculiar optical properties of silver nanoparticles, due to the characteristic LSPR absorption band, which makes these systems active substrates for SERS investigations (Surface Enhanced Raman Scattering).[339] The wavelength, the intensity and the FWHM (Full With at Half Maximum) of the LSPR band is related to the shape, size and **AgNP**s chemical environment,[258] whereby using a synthetic procedure which allows to modulate these characteristics, it is possible to obtain nanoparticle systems with tailored optical properties, in such a way to adapt them to a specific use.[340]

As previously reported, the synthesis of metal nanoparticles can be carried out in different ways; among them the use of light to promote it has become a further and widely investigated field, in particular for the synthesis of **AgNP**s.[341] The light-assisted preparation of metal nanoparticles[342] can be based on photophysical (top-down approach) or photochemical (bottom-up approach) process. (Figure.7.1) The first one consist in the ablation of bulk metal by the use of laser light, which is a general procedure for the synthesis of nanoparticles of several metal.[343] On the other hand, the photochemical approach, which relies on the photoreduction of the corresponding metal cation, it has assumed great importance in the synthesis of **AgNP**s. Since in the 18th century Johnann Schulze discovered that silver salt darken

upon light exposure, the photoreduction of silver was widely exploited in photography, but only during the last decades was developed for the synthesis of **AgNP**s as well.

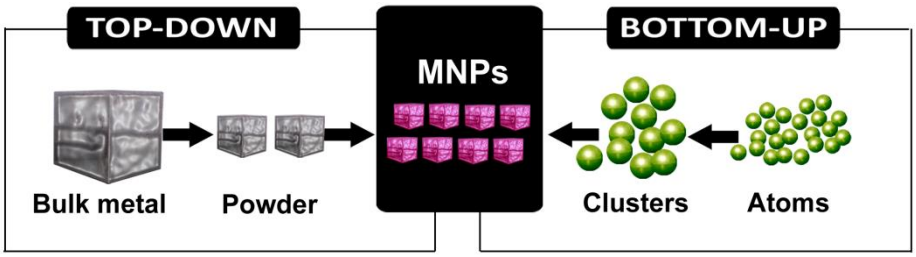

Figure 7.1 – Top down vs Bottom up photochemical synthesis of metal nanoparticles.

In particular, following the photochemical methods, the photoreduction of silver cations can be in turn, either a direct or indirect process. The direct photoreduction of a silver salt for the **AgNP**s synthesis, has the advantage to require no presence of a reducing agent, thereby allowing their formation in several environments such as polymer or gel matrix, zeolite, clays, glasses, cells, etc.[342]

The first mechanism for the photochemical synthesis of **AgNP**s by direct irradiation of Ag^+ ions in solution was proposed by Hada et al. studying the UV-irradiation of $Ag(ClO_4)$ in aqueous and alcoholic solution, they have proposed that upon photo-excitation of Ag^+ an electron transfer process is promoted from a solvent molecule to the excited Ag^+ giving Ag^0, which aggregations affording the **AgNP**s.

$$Ag^+ + H_2O \xrightarrow{hv} Ag^0 + H^+ + HO^\bullet$$

They also highlighted that, when the solvent is an alcohol, this process is more efficient and characterized by a larger quantum yield. As a matter of fact, after the first formal hydrogen removal, the resulted radical is able to further reduce Ag^+, boosting the Ag^0 formation, together with the synthesis of aldehyde specie in turn a chemical reducing agent.

$$Ag^+ + RCH_2OH \xrightarrow{hv} Ag^0 + H^+ + R\dot{C}HOH$$

$$Ag^+ + R\dot{C}HOH \xrightarrow{hv} Ag^0 + H^+ + RCHO$$

$$nAg^0 \xrightarrow{hv} AgNP$$

Finally, they also found out this process is heavily favoured in presence of a secondary alcohol, thanks to the easier hydrogen removal from the α-position.[344]

In order to obtain long lived **AgNP**s by direct photoreduction, the synthesis is commonly carried out in the presence of a reducing/stabilizing agent, as reported by Huang et al. and by Guang-nian, which synthesised PVP-coated **AgNP**s by UV-irradiation (254 nm) of aqueous solution

of $AgNO_3$ and $[Ag(NH_3)_2]^+$ respectively. In both cases they synthesised spherical **AgNP**s. The light absorption intensity at the maximum wavelength (and to a lesser extent the λ_{max} itself) which reflect the AgNPs concentration, is strictly related to the PVP concentration, as well as to the irradiation time.[345,346] For the sake of clarity, it is important to specify that the photoreduction of Ag^+ in presence of PVP could not be completely classified as a direct photoreduction process. As a matter of fact, as conceived by Huang et al. the photoexcitation of carbonyls moieties of PVP can produce ketyl radicals which in turn can reduce the Ag^+.

As it was mentioned above an alternative photochemical route for **AgNP**s synthesis, is the indirect photoreduction by means of photosensitizer molecules.[347] This can overcome the main problem of the direct photoreduction, that is the use of the UV irradiation needed for the excitation of most metal cations. As a matter of fact, the UV irradiation have the main drawback to be absorbed by most of the stabilizing agent and solvent as well, reducing the quantum yield of the photoreduction and then amplify the irradiation time, as well as being an expensive light source. The photosensitizer molecules, such as aromatic ketones or dyes, upon irradiation give radical species able to reduce the metal cation. Because photosensitizers have the advantage to absorb between 300 – 700 nm, the use of visible light for photoreduction becomes viable.

The fate of the photosensitizer after irradiation can be basically divided in two different paths namely: *i*) formation of excited state organic molecules, which upon hydrogen abstraction from a donor solvent molecule, give rise to radical species; *ii*) direct generation of organic radicals by homolytic bond cleavage. In the first case ketone derivative molecules are commonly used, because upon irradiation between 300 and 360 nm these are excited to a singlet state which rapidly decays to triplet excited state by intersystem crossing. This species, due to a n-π^* transition, has the ability to abstract a hydrogen from a donor molecule, generally an alcohol used as solvent in these type of process, giving a ketyl and an alcoholic radical both able to reduce Ag^+ to Ag^0 and regenerate the ketone,[342] together with aldehyde derivative from alcoholic radical (as depicted in previous equation) (Scheme 7.1).

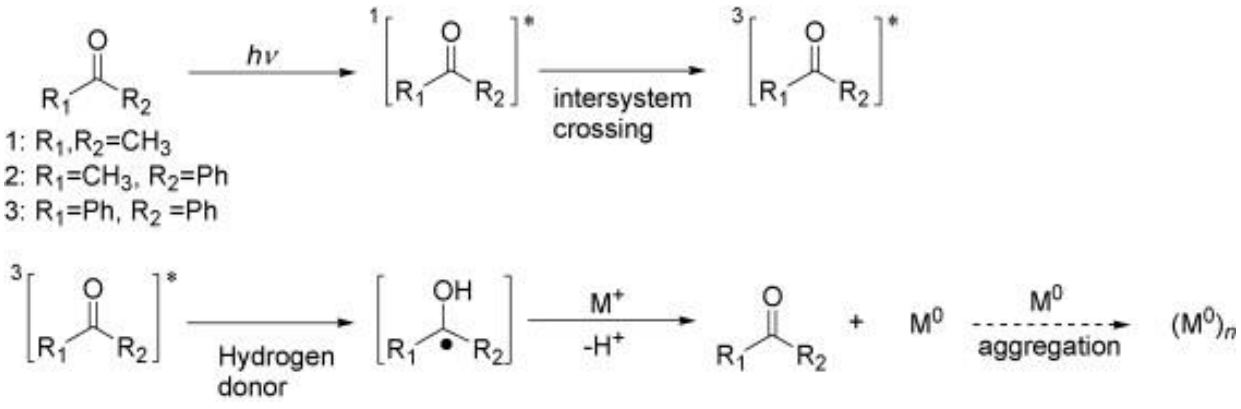

Scheme 7.1

On the other hand, the direct light-promoted bond cleavage, to give radical species (irradiating in the same previous mentioned spectral window), is usually accomplished by the use of benzoin derivatives or other α-hydroxyl ketones. This class of molecules is commonly represented by 2-hydroxy-4'-(2-hydroxy-ethoxy)-2-methyl-propiophenone, a widely used photosensitizer it is known as well with the commercial name of Irgacure-2959®. This molecule upon irradiation at 320 nm give rise to benzoyl and ketyl radicals by Norrish I type reaction.[342,348] (Scheme 7.2)

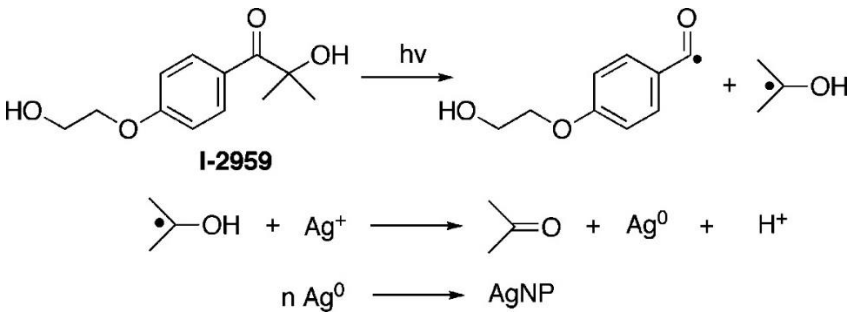

Scheme 7.2

Scaiano et al. have extensively investigated the photosensitizer processes for the Ag photoreduction in particular using I-2959 in different solvent media with and without citrate as stabilizing agent, as well as in presence of amines. The latter ones have been used as buffer agent considering that the reduction of Ag^+ by ketyl radical give protons as byproduct.[341]
Besides, they have established also that the destiny of benzoyl radical is the formation of the corresponding carboxylic acid 4-(2-hydroxyethoxy) benzoic acid (HEBA) which give a certain contribute to the stabilization of forming **AgNP**s.[341] Finally, it is worth noting that their studies have highlighted as the first step of the **AgNP**s is the formation of the Ag_2 dimer, followed by even numbers coupling of dimers during the growing process.[349]
Coming back to the use of visible light to promote **AgNP**s synthesis, during the last few decades several papers dealing with the shape photoconversion of **AgNP**s were appeared in literature.
In particular, visible light (400 – 700 nm) promotes the photoconversion of silver seeds is solution (**AgNP**s < 5 nm), usually obtained via chemical reduction of $AgNO_3$ with $NaBH_4$ in the presence of citrate or PVP as stabilizing agents, in order to obtain NPs of desired morphology hence featured by specific optical properties.[318,350-355] The irradiation is commonly carried out using either laser or LED type light source, although sunlight or halogen lamp are becoming fairly common as well. As a matter of fact, depending on the specific wavelength used, it is possible to obtain differently shaped anisotropic **AgNP**s, i.e. nanoplates, nanodiscs, nanoprisms, nanotetrahedra, nanodecahedra or nanorods. (Figure 7.2)

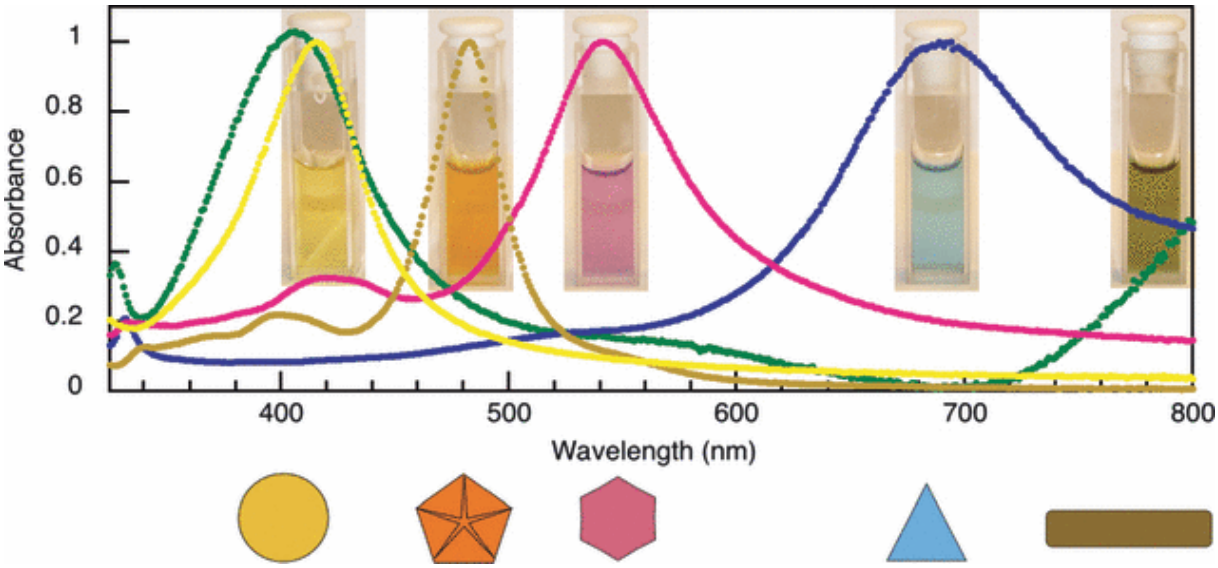

Figure 7.2 – Characteristic SPR band of anisotropic **AgNP**s.

Of course the shape of the restructured **AgNP**s can be monitored by TEM micrography: nevertheless, even the colour change of the solution, related in turn to the variation in the LSPR absorption maximum, give naked eye evidence of the ongoing morphological change.

Finally, the use of light to carry out the formation of **AgNP**s, as well as being an alternative synthetic route (not only a simple style exercise), is a promising green process considering the virtual absence of chemical reducing agents, which could be addressed to the synthesis of biologically useful **AgNP**s.

7.2 - Antibacterial properties of Silver

Since antiquity, Silver has been one of the most used noble metals by mankind. Besides the production of decorative object, coins and cutlery, due to its corrosion resistant properties, it has been widely exploited also for its early discovered antibacterial activity first time mentioned by Herodot.[356]

There are a lot of historical witnessess regarding the use of metallic silver by Egyptians, Persian, Romans and Greeks, for storage of water or food.[356] Since the middle age as *lunar caustic* (or *lapis infernalis*), basically a stick of silver nitrate added with hydrochloric acid and potassium nitrate, has found medical applications as antiseptic topical agent for the treatment of burnt skin, wounds and ulcers to hamper infections.[357] Silver nitrate as aqueous solution has been also used to prevent infection by oral assumption or for the preparation of eyewash used to avoid Gonorrhea type infections in newborn babies from infected mothers.[338]

The use of silver and its compounds as broad-spectrum antibacterial agents has been a common practice till the half of 20th century, when antibiotics were discovered. Then the use of silver

became negligible, but during the last decades it has gained an increasing interest again, due to the growing resistance of some bacterial strains towards the most common antibiotics.[358,359]

For this reason, the antibacterial action mechanism of silver has been deeply investigated considering also different silver containing compounds.[360] In particular, **AgNP**s have received attentions in the last few years by researchers. Studies carried out up to date have revealed that **AgNP**s possess an antibacterial broad range activity toward both Gram-negative and Gram-positive bacterial strain.[361] In general, **AgNP**s of smaller size possess greater antibacterial action. This finding might be rationalized considering that smaller particles possess an overall larger surface, and therefore are able to release Ag^+ ions to a larger extent, or alternatively to interact more effectively with the cell wall. In any case, **AgNP**s can be considered in fact as "Trojan horses" for Ag^+ release into cell itself.[338,362]

Despite the efforts by researchers, antibacterial mechanism of action of Ag^+ and **AgNP**s, has not been fully understood yet. In any case three different kind of interactions of silver compound with bacterial cells[363] were claimed, namely: *i*) interaction with cell wall; *ii*) interaction with proteins, enzymes and DNA; *iii*) silver promoted formation of reactive oxygen species (ROS). These possible interactions are depicted in Figure 7.3.

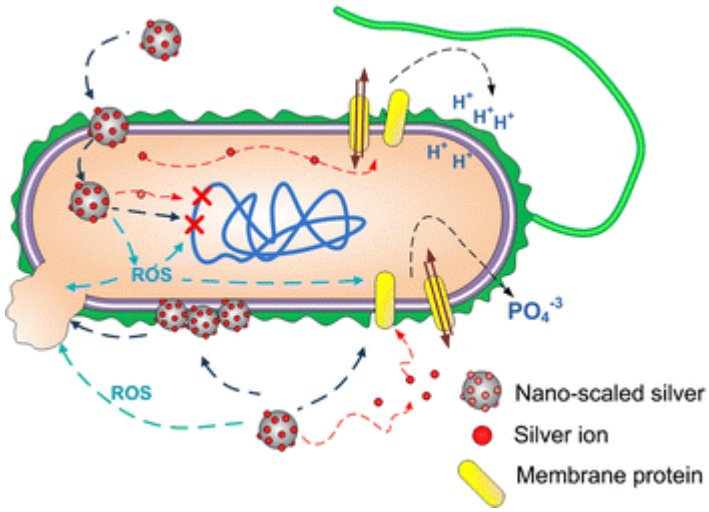

Figure 7.3 – Antibacterial mechanisms of action of Ag^+ and **AgNP**s.

In order to discuss the interaction between silver and cell membrane, it is important to depict the differences in the cell wall structures between the two main categories bacteria, i.e. Gram-positive and Gram-negative bacteria. The main constituent of cell wall is the peptidoglycan layer, surrounding plasm membrane, which is constituted by different polymeric sheets of *N*-acetylglucosamine and *N*-acetylmuramic acid, linked each other by peptide bridges in such a way to form a net-like structure.

The peptidoglycan layer is common to both type of bacteria, with the difference that in the case of Gram-positive bacteria it is thicker (15-80 nm) and is also characterized by the presence of teichoic acids, which confer a negative charge to the cell wall of Gram-positive bacteria. Differently, in the case of Gram-negative bacteria the peptidoglycan layer is thinner (~2 nm), and it is covered by a further external membrane of phospholipid and lipopolysaccharides.

It has been shown that Ag^+ is able to provoke the lysis of both Gram-negative as *Escherichia Coli* and Gram-positive as *Staphylococcus aureus* bacteria. It was possible evaluate by TEM analysis that Ag^+ destabilize the cell wall, with consequent detachment from plasm membrane and spillage of plasma components leading to cell death. In the case of Gram-negative bacteria, this effect was resulted greater than for Gram-positive ones.[364,365] Almost the same effect was observed in the case of **AgNP**s towards Gram-negative and Gram-positive bacteria, although the mechanism of action of **AgNP**s is till today debated.[366,367]

Indeed, at this regard it is necessary to keep in mind some aspects affecting the **AgNP**s activity, such as ζ Potential. As a matter of fact, the right interaction of **AgNP**s and Gram-positive or Gram-negative bacteria is governed by the counterbalance of their respective charges. A clear example was reported by Tolaymat et al. which have studied the antibacterial activity of citrate and branched-polyethyleneimine capped **AgNP**s towards Gram-positive *bacillus* strains featured by a negatively charged surface. Their findings have revealed as the branched polyethyleneimine-**AgNP**s with a net positive charge on their surface have a greater toxicity on *bacillus* cell thanks to the favoured electrostatic interaction established.[368]

It is necessary to highlight that in some cases **AgNP**s cause the cell death without bringing to cell lysis, hence in order to explain this eventuality other action mechanisms were conceived. One of these has been proposed by Mirzajani et al., which supposed that **AgNP**s are able to create holes in the cell wall, of both Gram-positive and Gram-negative bacteria, by removal of *N*-acetylglucosamine and *N*-acetylmuramic acid building blocks from the peptidoglycane layer, allowing the entry of **AgNP**s or Ag^+ inside the cell and their interaction with intracellular components.[369]

Nevertheless, as already mentioned the release of Ag^+ from **AgNP**s is the mainly accepted reason to explain the antibacterial activity of **AgNP**s.[370-375] The Ag^+ release was considered as an oxygen-mediated oxidative process either by a direct four electron transfer:

$$4\,Ag + O_2 + 2\,H_2O \rightarrow 4\,Ag^+ + 4\,OH^-$$

Or by a peroxide mediated reduction of oxygen to water:

$$2\,Ag + H_2O_2 + 2\,H^+ \rightarrow 2\,Ag^+ + 2\,H_2O$$

Once crossed the plasm membrane, silver can interact with many components as DNA, enzymes and membrane proteins. The interaction of silver with DNA was easily assessed by means of TEM images in which it has been possible sees as the DNA is closely packed when bacterial cells are treated both with Ag^+ and **AgNP**s, hindering its replication ability and gene expression.[364,376]

Silver ion is able to give silver-amino acids complexes and then interact with enzymes and proteins affecting their structures and in the case of enzymes can replace other possibly cations present in the enzyme receptor site. Regarding to silver-amino acids complex is necessary to consider that, albeit cysteine is commonly accepted as the best site for silver protein interaction, due to the soft-soft interaction between silver and sulphur, this is not confirmed by theoretical calculation which consider lysine, arginine and histidine the best ligands for Ag^+.[377]

Nevertheless, it has been shown that the interaction of Ag^+ with the NADH dehydrogenase take place at level of the thiol groups of cysteine residues hindering the bacterial respiratory chain.[378]

A study of the effect of Ag^+ on *Vibrio Cholera* has indeed revealed as micromolar concentrations of Ag^+ lead to the downfall of the proton motive force across the plasm membrane, with the leakage of proton across the plasm membrane and consequent cell death.[379]

A similar effect it was also reported for *Escherichia Coli* and *Staphylococcus aureus* treated with **AgNP**s.[376,380]

Another result of the interactions of silver with NADH dehydrogenase is the enhancement formation of Reactive Oxygen Species (ROS), free radical species produced by every aerobic organism as by-product of the respiratory chain, able to harm essential cell components as DNA, RNA, lipids and proteins. In a study on the antibacterial activity of Ag^+ on Gram-negative and Gram-positive strains under aerobic and anaerobic conditions, Park et al. highlighted as the antibacterial activity increase in aerobic conditions and that the level on activation of SoxR and OxyR (sensing protein activated by the presence of superoxide radical anion and hydrogen peroxide respectively), show an enhanced formation of superoxide radical anion.[381] Gordon et al.[196] supposed also that Ag^+ mediated demolition of the Fe-S cluster cofactor (present in the NADH dehydrogenase of respiratory chain), give rise to hydroxyl radicals by Fenton reaction.[382]

Considering the contribution of **AgNP**s some researchers have proved by EPR analysis the direct formation of silver radical directly from **AgNP**s;[383] whereas on the other hand some authors have attributed the increased antibacterial activity of **AgNP**s in aerobic conditions, only to the higher release of Ag^+ by oxidation of **AgNP**s surface.[374]

Undoubtedly the antibacterial activity of silver has a faceted nature with many contributions which can affect it, such as the particular bacterial strains, the form in which silver is present, the availability of Ag^+; the latter one can be in turn affected by the counter anion causing its precipitation. Moreover, working with **AgNP**s other factor become important as dimension of nanoparticles, coating agents present on their surface and shape as well, as recently showed by the higher activity of triangular shaped nanoparticles with respect to spherical one.[384]

In conclusion as a final remark, is necessary mention a rising trend in the last few years related to the antibacterial activity of **AgNP**s joined with common broad-spectrum antibiotics. The studies so far carried out have showed as the resultant antibacterial effect is affected by the bacterial strains, as well as the antibiotic class used. In any case the obtained findings are very promising showing often a synergistic effect[385] (higher to the sum of the part) among **AgNP**s and antibiotics with a consequent reduction of MIC (minimum inhibitory concentration), hence leading to a possible reduction of the administered antibiotics.[361]

7.3 - Results and discussion

*7.3.1 – Photochemical synthesis of **AgNP**s systems*

As it was illustrated in the previous chapter, **amCD**s are good capping agents for the synthesis and stabilization of silver nanoparticles. This reaction was carried out by chemical reduction with formaldehyde of a silver nitrate ammonia solution. Even though long lived **AgNP**s colloidal solution were obtained, very useful as catalyst, these systems cannot be used for biological applications in particular in order to test their antibacterial properties. This is due to the presence of species such as formaldehyde and nitrate ions, which could have toxic effects on the bacterial cells. This in turn could concealing the real antibacterial properties of **AgNP**s, investigation of which is part of the work. Therefore, it was necessary to design a different synthesis in order to obtain more biocompatible **AgNP**s. For this reason, it was decided to use CH_3COOAg as silver salt, in such a way to eliminate the nitrate ions. The silver reduction one could carried out in principle by a chemical route, using biocompatible reducing agents, as extensively reported in literature, such as glucose, citrate or other natural extracts; alternatively, the photoreduction properties of Ag could be exploited.

The first possibility was investigated by preliminary assays, using systems with the same composition of those used in the previous chapter (1 mM Ag^+, 0.4-2.0 mN **amCD**), and different reducing agents, in particular glucose, sodium ascorbate and citrate, each one at a 2 mM concentration. In all cases the reactions, performed in the dark at 40 °C for 90 min, gave unsatisfactory results. More in detail, systems with citrate and glucose did not show the typical

reddish color of **AgNP**s systems, even after a further warming up to 60 °C for 30 min (in the presence of glucose only a pale red color appears). By contrast, systems with ascorbate immediately gave rise to brown-greyish precipitates at r.t.

Then, it was seemed appropriate to accomplish a systematic investigation of a possible photoreduction approach to **AgNP**s sysnthesis. Keeping into account the possible photoreduction mechanisms mentioned previously, is necessary the presence of a sacrificial reducing agent, which must oxidize itself, providing the electron to reduce Ag^+. In our case amino groups on **amCD** would assume this role, as well as that of capping agent.

For this purpose, in order to find the best reaction conditions to carry out Ag^+ photoreduction in presence of **amCDs,** different operational variables, were taken into account, namely: *i*) the type of irradiation source; *ii*) the irradiation power (W/m^2); *iii*) the features of the **amCD** used; *iv*) the Ag/**amCD** equivalent ratio; *v*) the possible presence of a further sacrificial reducing agent; *vi*) the irradiation time.

First, it was necessary to establish which light source could be the best candidate in term of effectiveness and convenience, to perform the process. In particular, three different light source were compared, i.e. a solar simulator (SUNTEST XLS+ set in "indoor configuration") with an irradiation power of 30 W/m^2; a Rayonet apparatus equipped with 16 lamps each one with a power of 8 W and characterized by a sharp emission at 365 nm; a commercially available halogen lamp with a power of 50 W placed at a distance of 12 cm from the irradiated systems by means of a home-made reactor (which will be described in the experimental section). The effectiveness of each light source was assessed by irradiation of the usual two Ag^+/**amCD** combination systems (1:0.4 – 1:2.0) prepared using silver acetate and three different type of **amCD** namely **amCD1**, **amCD2** and **amCD3**. After irradiation for 10 min, each system (regardless of the light source used) showed the characteristic red-amber coloration, sign of the **AgNP**s formation. Then to have a more careful characterization of the **AgNP**s systems, their UV-vis spectra were recorded and it was also take notes of the stability over time (colour variation, precipitate formation), of the systems prepared with the different light source, over a week. The resulted UV-vis spectra, show two main differences with respect to those obtained by the chemical protocol discussed in the previous chapter. The first one is the intensity of the SPR band (related to the amount of reduced Ag present). The relevant **ε** value is in any case lower than the one obtained for the reduction performed with formaldehyde (**ε** = 5500), implying that a significant amount of Ag^+ ion remains unreduced in the process.

The second one is that the obtained spectra are characterized by a shoulder or a side band in the region between 480 and 530 nm (as exemplified by the spectra in Figure 7.3).

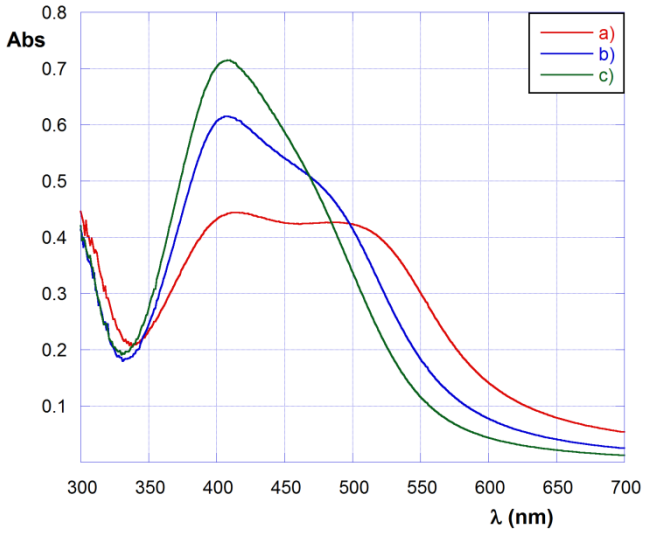

Figure7.3 – Spectra of Ag/**amCD** 1:2 systems after 10 min halogen lamp irradiation; a) **amCD1**; b) **amCD2**; c) **amCD3**.

A similar effect was previously observed on dilution of the **AgNP**s obtained by the chemical protocol, and was attributed to the modification of the chemical micro-environment around **AgNP**s. Therefore, this modification could be reasonably attributed to a partial degradation of the coating agent.

In order to have a semi-quantitative index to evaluate such a possible degradation, it was decided to use the ratio $\boldsymbol{R_\varepsilon}$ of the absorbances at 400 and 500 nm ($\boldsymbol{R_\varepsilon} = \varepsilon_{500}/\varepsilon_{400}$). Data obtained are collected in Table 7.1, together with an indication of the stability of the systems.

Table 7.1 – ε values and stability of the Ag/**amCD** systems irradiated with different sources.

amCD	Light source	Ag/amCD	ε_{400}	ε_{500}	R_ε	Stability
amCD1	Solar sim.	1:2	2850	2450	0.860	<1h
		1:0.4	3900	3150	0.808	<1h
	Halo L.	1:2	2400	1450	0.604	1d
		1:0.4	720	745	1.035	1d
	Rayonet	1:2	3350	2600	0.776	1d
		1:0.4	3400	2750	0.809	1d
amCD2	Solar sim.	1:2	1835	1775	0.967	<1h
		1:0.4	3990	3460	0.867	<1h
	Halo L.	1:2	2630	2480	0.943	3d
		1:0.4	1900	1405	0.739	3d
	Rayonet	1:2	2525	2305	0.913	2d
		1:0.4	4030	2490	0.618	1d
amCD3	Solar sim.	1:2	4240	3170	0.748	<1h
		1:0.4	2210	2150	0.973	<1h
	Halo L.	1:2	3800	2900	0.763	7d
		1:0.4	2490	1420	0.570	7d
	Rayonet	1:2	3590	1725	0.481	2d
		1:0.4	3660	2015	0.551	1d

Considering the time stability, it is clear that the use of the solar simulator affords in all cases unsatisfactory systems, whereas for the halogen lamp or the Rayonet apparatus, the time stability depends on the nature of the **amCD** used, with a stability order **amCD3** > **amCD2** > **amCD1**. This trend indicates an enhancement in stability related to the increase of the length of the polyamine pendants.

On passing to consider the absorbance values, as a general trend the systems prepared using **amCD3** and **amCD1** show the highest and lowest values respectively, but taking into account the Ag/**amCD** ratio the values show the opposite trend. Indeed, in the case of solar simulator systems with 1:0.4 ratio present the highest absorbances, whereas for the halogen lamp the same finding is observed for systems with 1:2 ratios. For the systems irradiated using the Rayonet there is no particular difference in the absorbance according to the ratio.

The trends for the R_ε, seem fairly complicated to rationalize. Nevertheless, lower R_ε values in the case of **amCD3** with respect other **amCD**s were obtained, confirming again the important role that the number of nitrogen atoms and the length of the polyamino pendants exert in determining the features of a photochemical synthesised **AgNP**s systems. Under this viewpoint, the resemblance to the chemically obtained **AgNP**s systems was considered as the reference standard in term of time stability, and similarity of the UV-vis absorption profile as well.

Then taking into account the obtained results, and in particular those related to the time stability, it was decided to carry on the photochemical investigation by the use of the halogen lamp, which both seemed to provide the best results, and has the advantage to be by far the cheapest irradiation apparatus as compared to the other ones.

Then, it was possible to carefully investigate the outcome of other experimental parameters. The first set of assays was carried out using a wide range of Ag/**amCD** ratios; the relevant results are collected in Table 7.2 and illustrated in Figures 7.4

Table 7.2 – Effect of the amount of **amCD** on the ε values of the Ag/**amCD** systems.

amCD	Ag/amCD	ε_{400}	ε_{500}	R_ε
amCD1	1:0.4	720	745	1.035
	1:1	2450	2200	0.898
	1:2	2400	2000	0.833
	1:5	1400	1200	0.857
	1:10	1300	1000	0.769
amCD2	1:0.4	1900	1400	0.737
	1:1	3690	2930	0.794
	1:2	2830	2480	0.876
	1:5	2630	1830	0.696
	1:10	2290	1680	0.734
amCD3	1:0.4	2490	1420	0.570
	1:1	3800	2500	0.658
	1:2	3800	2900	0.763
	1:5	3080	1700	0.552
	1:10	2600	1130	0.435

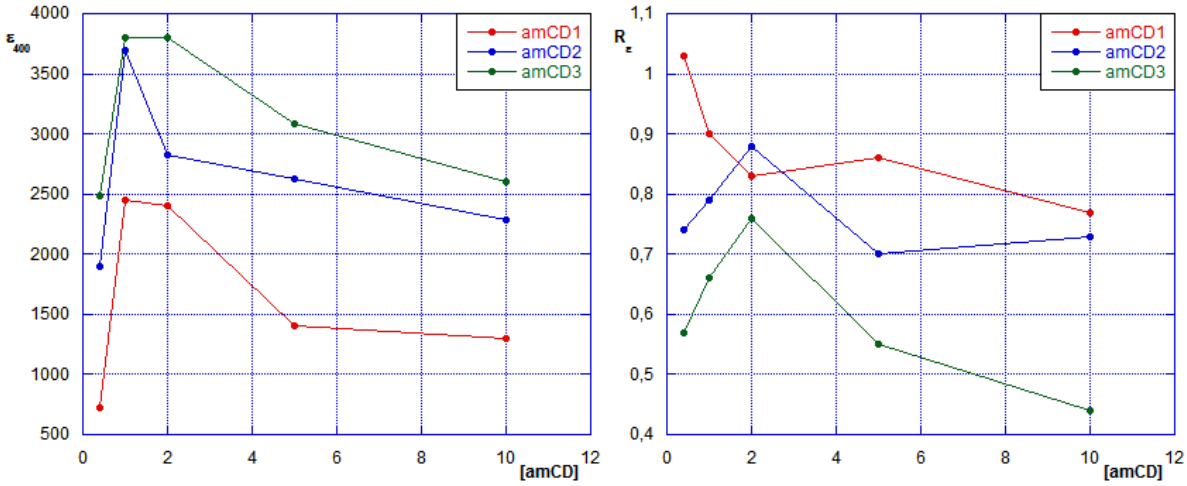

Figure 7.4 – Trend of ε_{400} (left) and R_ε (right) vs [**amCD**].

Data for ε_{400} show a bell-shaped trend, with a maximum occurring for a **amCD** concentration between 1 and 2 mM. This indicates the existence of an optimum Ag/**amCD** ratio, that maximizes the amount of reduced silver.

A similar trend was observed for $\boldsymbol{R_\varepsilon}$, in the cases of **amCD2** and **amCD3**, with the highest values, occurring for nearly the same concentration of **amCD** at which the maximum absorbance was obtained. This means that the best Ag/**amCD** ratio, at which the highest degree of reduction is reached, is also the same that provide **AgNP**s characterized by the largest degradation of the coating agent on their surface. A more complicated trend was observed in the case of **amCD1**.

On passing to consider the irradiation time, some systems were selected to test its effect on the photoreduction process. In particular, systems prepared using **amCD2** and **amCD3** both with 1:2 and 1:0.4 ratio, systems prepared using **amCD1** with 1:0.4 in presence of 2 and 20 mM glucose and system 1:2 in presence of glucose 20 mM were chosen (the razio of these three systems will be hereafter explained). Each system was then irradiated for different times, up to 15 min, after which the UV-vis spectrum was recorded. The resulted data are summarized in Table 7.3

In general, by plotting the data obtained, it is possible to observe that absorbances increase roughly according a first order trend. However, absorbances at 400 nm increase faster than those at 500 nm, with a consequent increase of $\boldsymbol{R\varepsilon}$ values (Figure 7.5). This implies that the appearance of a shoulder, or a possible side band, in the UV-vis spectra is a consequence of the prolonged irradiation.

Table 7.3 – Effect of the irradiation time on ε values and their ratio.

amCD	Ag/amCD		t (min)	ε_{400}	ε_{500}	R_ε
amCD2	1:0.4		3	510	415	0.814
			6	1120	760	0.679
			10	1900	1405	0.739
	1:2		3	1795	1205	0.671
			6	2600	1975	0.760
			10	2630	2480	0.943
amCD3	1:0.4		3	700	320	0.457
			6	1455	745	0.512
			10	2490	1420	0.570
			15	2750	1850	0.673
	1:2		3	1900	850	0.447
			6	3285	1700	0.517
			10	3800	2900	0.763
			15	4000	3500	0.875
amCD1	1:0.4	+ glu 2 mM	3	900	650	0.722
			6	1450	1300	0.897
			10	1500	1500	1.000
	1:0.4	+ glu 20 mM	3	1420	1220	0.857
			6	2150	1680	0.785
			10	2150	1685	0.784
	1:2	+ glu 20 mM	3	1200	720	0.600
			6	1700	1550	0.912
			10	1950	1685	0.864

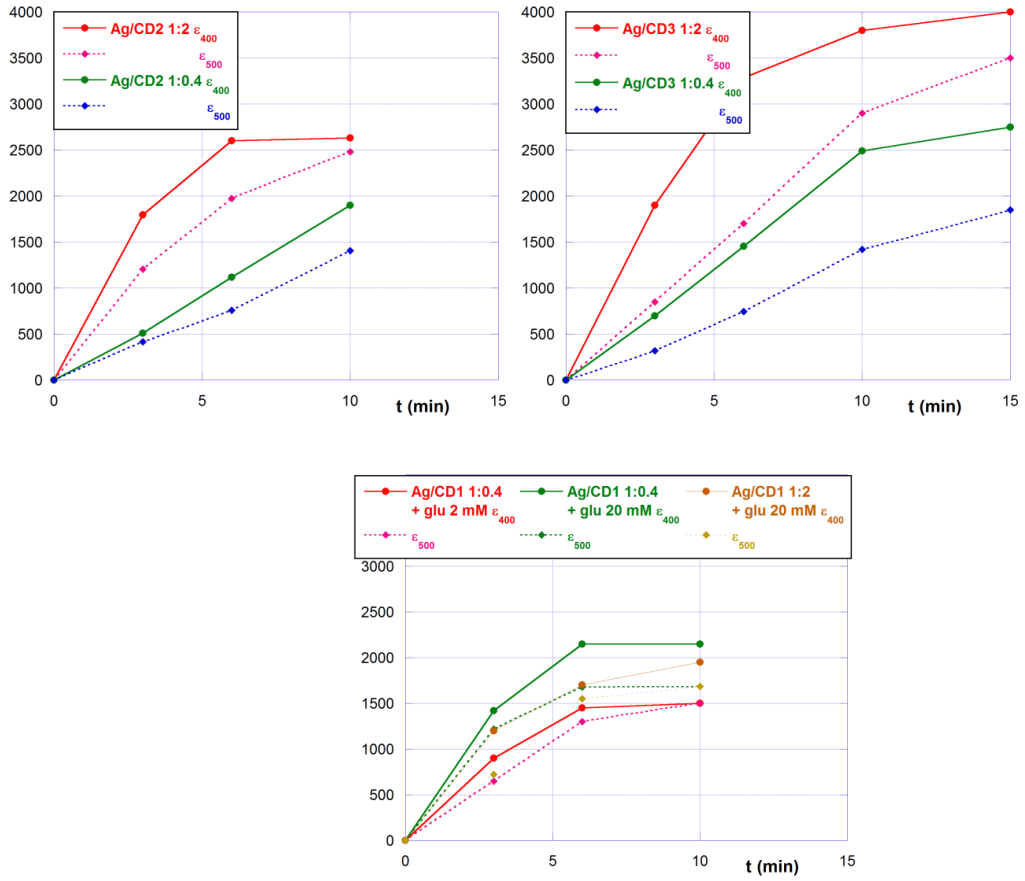

Figure 7.5 – Rising trend of the ε values, faster in the case of ε_{400}.

In the case of systems prepared with **amCD1** in presence of glucose as a sacrificial co-reductant, it is interesting to note that as the amount of glucose increases, a decrease and stabilization over time of the R_ε values can be observed. This means that large amounts of glucose can effectively contribute to the silver reduction. In order to explain the whole of these results, it should be preliminarily considered that, on the grounds of the mechanistic hypotheses reported so far in literature, a ligand-to-metal photo-induced single electron transfer (s.e.t.) process must occur. This implies that in fact the ligand functions as sacrificial reducing agent. Therefore, an increase in the efficiency of photoreduction should be expected on increasing the amount of **amCD** present in the reaction system. This conclusion is contradicted by the experimental result of a bell-shaped trend for the absorbance at 400 nm. It is worth recalling here that chemical reduction of Ag^+ by formaldehyde in the presence of **amCD** is hampered by a large excess of the capping agent. Moreover, the s.e.t. process should form from the **amCD** some radical-cation species, which in turn might function as reductant themselves. Thus everything considered, it is possible put forward the following mechanistic hypothesis. (Scheme 7.3)

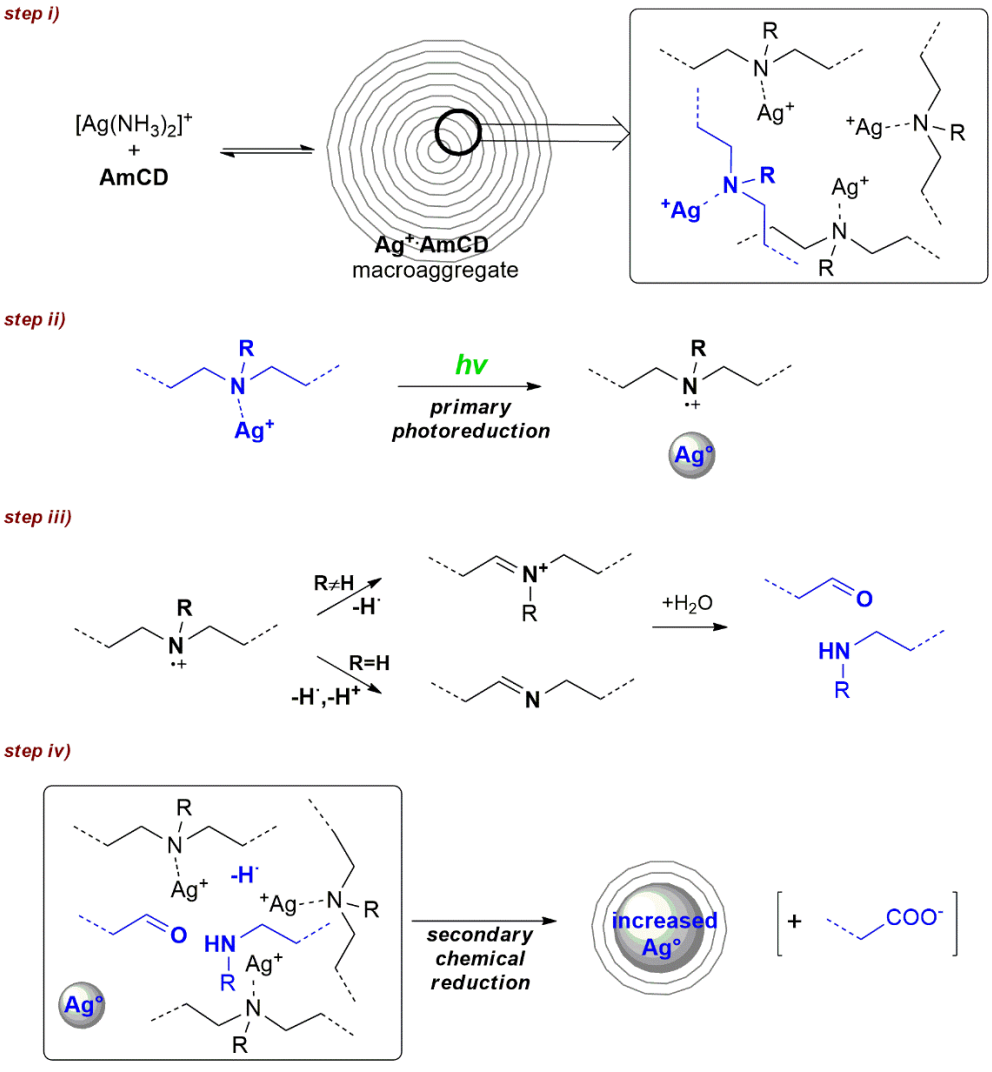

Scheme 7.3

The first step (step *i*) is obviously the complexation of Ag^+ by the polyamino pendants of **amCD**s which afford large aggregates (between 100 and 1000 nm according to DLS evidences). Then (step *ii*) this complex undergoes a photoinduced s.e.t. process from the ligand to the Ag^+ giving rise to Ag^0 and an unstable nitrogen radical cation species. It is reasonable to assume that Ag^0 forms small NP nucleation seeds able to further growing. On the other hand, the nitrogen radical-cation species of the polyamine branches may undergo different fates (step *iii*), depending on their peculiar nature. From secondary or primary amine groups, the loss of $H^{\cdot}$ leads to imines which can be easily hydrolized to aldehyde. From tertiary amine groups, loss of H^+ leads to iminium ions that once again may undergo hydrolysis to aldehydes. In any case, $H^{\cdot}$ radical, imines and aldehyde derivatives are reducing agent, which can subsequently reduce a further amount of Ag^+ as well (step *iv*), causing further growing of the former **AgNP**s nuclei. This mechanism results in part similar to that one reported by Sukhishvili et al. for the Ag^+ photoreduction in presence of branched polyethyleneimine, in particular regarding the aldehyde derivatives formation. In that case, however, there is the fundamental difference that the process was mediated by UV irradiation of oxygenated solution, whereas in the present case visible irradiation and degassed solution were used.[386]

Of course, the effectiveness of the secondary chemical reduction process, carried out by the side products of the photoreduction, is related to the concentration of the **amCD** according to the same inverse relationship observed for the chemical reduction with formaldehyde. Therefore, an increase in the amount of **amCD** must necessarily hamper the interaction of the reducing agent with Ag^+. This mechanistic hypothesis adequately explains the different kinetic trends observed for the absorbances at 400 and 500 nm. As a matter of fact, the second one accounts for the occurrence of the deterioration of the coating consequent to the secondary reduction process, which takes place after the actual formation of the **AgNP**s.

On the grounds of the experimental data, the performance of **amCD**s follows the order **amCD3** > **amCD2** >> **amCD1**. Considering this, it seemed interesting to verify if the Ag photoreduction in presence of **amCD** could be improved by the addition of a further sacrificial co-reducing agent. Taking into account the possibility of further biological application of the **AgNP**s systems prepared, it was decided to use the biocompatible glucose. In order to carry out this set of experiment two different Ag/**amCD1** ratios, namely 1:2 and 1:0.4, were used. Then, a series of irradiation tests were performed in presence of an increasing concentration of glucose in the range 2 - 20 mM. The results, collected in Table 7.4, show as in the case of the Ag/**amCD1** 1:2 ratio, the addition of glucose does not appear to have a marked effect on the final amount of reduced Ag^+, while there is an increase of $\boldsymbol{R_\varepsilon}$ ratio. In the case of the Ag/**amCD1** 1:0.4 ratio,

glucose addition actually seems to have a positive effect both on the amount of reduced Ag^+, and on spectrum quality. For the sake of completeness, two further control tests with the **amCD2** and the **amCD3** adding glucose in a concentration of 2 mM were done, but in both cases the observed effect was substantially negligible.

Table 7.4 – Effect of glucose concentration on the ε values and their ratio.

[Glucose] (mM)	**Ag/amCD1 1:2**			**Ag/amCD1 1:0.4**		
	ε_{400}	ε_{500}	R_ε	ε_{400}	ε_{500}	R_ε
1	1900	1250	0.658	1500	1500	1.000
2	1800	1430	0.794	1400	1300	0.929
5	1830	1640	0.896	1830	1750	0.956
10	1950	1685	0.864	2150	1685	0.784

Once acquired the information related to best conditions to carry out the **AgNP**s synthesis, the role of the irradiation source used was re-considered. In particular, some collateral effects related to the "halogen lamp system", were taken into account in order to understand if they could affect the photoreduction process in some way. The first aspect considered was the irradiation power of the "halogen lamp system" which supplies 276 W/m^2 (at 12 cm), with the drawback of warming up the reaction system to a rate of 3.5 ± 0.1 °C/min (estimated by a linear regression of T vs t). Then, a set of assays were performed to investigate the effect of power irradiation and the warming up. First, by placing the halogen lamp at a distance of 18 cm the irradiation power of the system was reduced of 2,24 fold (123 W/m^2) as also confirmed by the same extent reduction of the recorded warming up rate i.e. 1.5 ± 0.1 °C/min.

The photoreduction of two model systems, Ag/**amCD2** 1:2 and 1:0.4, was then repeated under this condition, observing a slowdown in the reaction rate proportional to the power reduction. As a matter of fact, the absorbance at 400 nm of the systems, after 10 min, was ca. less than half compared to that of the experiment conducted with the lamp placed at 12 cm, while using a 20 min reaction time, the spectrum of the system was substantially comparable to that obtained after 10 minutes with the lamp at 12 cm. Moreover, in order to test the effect of the warming up, a system, covered with aluminium foil, was exposed to the heat provided by the light irradiation, but albeit the reached temperature (ca. 55 °C) no reaction was observed. In any case it was decided to modify the home made system by the addition of two fans in order to allow a constant flux of fresh air and keep the temperature almost stable (warming rate 0.2 ± 0.1 °C/min). Nevertheless, also in this case no variation was observed in the behaviour of the system previously irradiated without fans, confirming a negligible effect of the temperature.

In order to better understand the difference, and then the advantages, of the home-made "halogen lamp system" with respect to Solar simulator and Rayonet, it was decided to record their emission profiles, depicted in the Figure 7.6

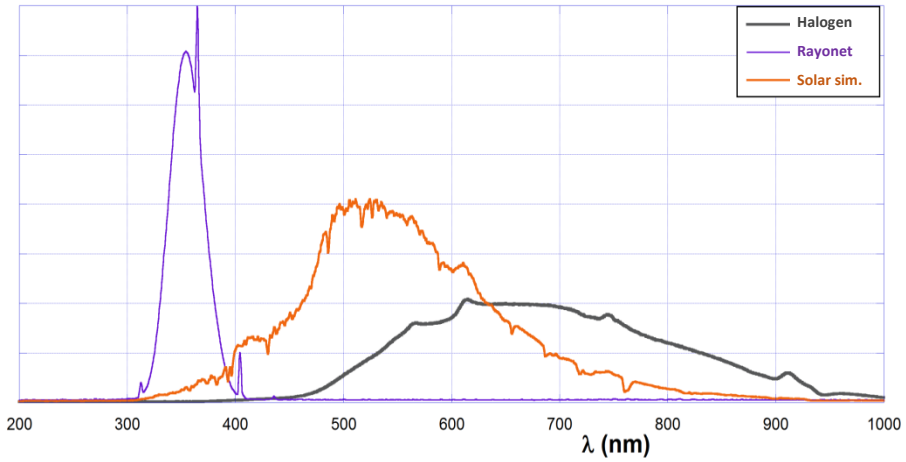

Figure 7.6 – Emission spectra of irradiation sources.

As it is possible to see, the Rayonet is characterized by a narrow emissions range between 300 and 400 nm. On the contrary, the solar simulator and halogen lamp emit largely beyond 400 nm. Furthermore, unlike to the solar simulator, the halogen lamp has a significant emission component in the NIR (Near-InfraRed) region. To verify the influence of this component to the photoreduction process, the halogen lamp was replaced with a commercially available infrared lamp (Philips, 250 W) and tested on system Ag/**amCD3** 1:2. Owing to the higher irradiation power of this lamp (ca. 1375 W/m^2 at 12 cm) it leads to a strong heating (14.8 ± 0.3 °C/min) also with the fans, in order to circumvent in part this drawback, it was decided to irradiate the system for period of 2,5 min each cooling the system to r.t. after each irradiation step. After the fourth irradiation, (10 min of irradiation) the UV-vis spectra of the system was recorded. The spectra, compared to that one resulted by halogen lamp irradiation is reported in Figure 7.7.

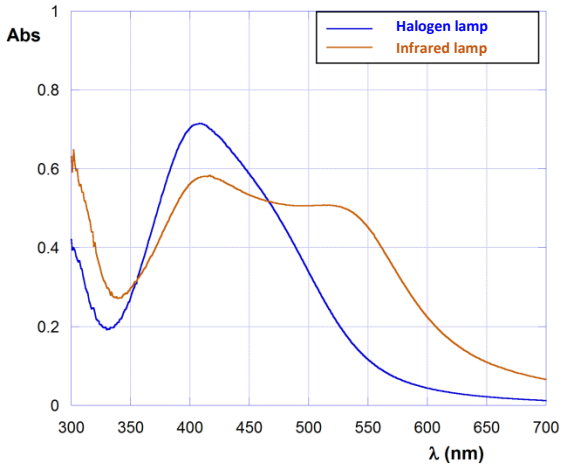

Figure 7.7 – Spectra related to the Ag/**amCD3** 1:2 systems irradiated with halogen lamp and IR lamp.

Surprisingly, it was found that the photoreduction carried out with the "infrared" lamp is by far less effective than the halogen lamp, and the resulted spectrum features a significant absorption band at 530 nm can accounting for a large occurrence of the degradation processes of the capping agent. This, in turn, suggest that the irradiation source used to perform the silver photoreduction, has to possess also a visible component. For this reason, a series of test using Ag/**amCD3** 1:2 and 1:0.4 systems irradiated with four different coloured filament lamps (red, yellow, blue and green light) were carried out. The emission spectra of the various lamps were recorded in Figure 7.8. In this case the distance of the lamps was shifted again to ca.13 cm in order to compensate the slight increase of their power i.e. 60 W. The irradiation time was always set at 10 minutes, after which the spectra of the resulting systems were recorded (Figure 7.9), and the corresponding absorbance values at 400 and 500 nm, as well as their ratio R_ε are reported in Table 7.5.

All coloured lamps have a NIR component as well. The emission maximum for blue, green, yellow, red and infrared lamps are respectively 500, 530, 610, 650 and 656 nm. The spectra of the obtained nanoparticles clearly show as green light is far the best light source for the silver photoreduction, while with the others light the extent of formation of the nanoparticles is very small or even absent.

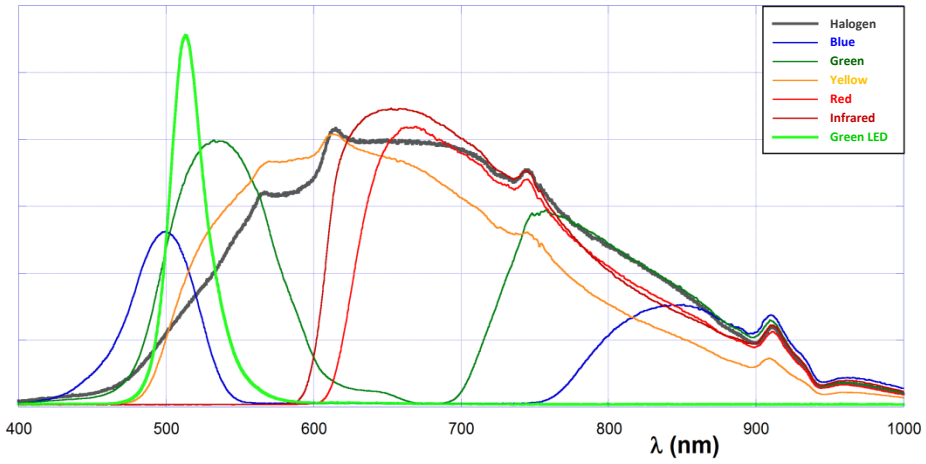

Figure 7.8 – Emission spectra of coloured irradiation sources.

Table 7.5 – Effects of the coloured irradiation source on the ε values of the irradiated systems.

Lamp	Ag/amCD3 1:2			Ag/amCD3 1:0.4		
	ε_{400}	ε_{500}	R_ε	ε_{400}	ε_{500}	R_ε
Solar. sim	1835	1775	0.967	3990	3460	0.867
halogen	3800	2500	0.658	3850	2725	0.708
Rayonet	3500	2830	0.809	3590	1725	0.481
infrared	2815	2530	0.899	1140	1070	0.939
RED	585	335	0.573		n.r.	
YELLOW	1425	635	0.446	545	360	0.661
GREEN	4125	1455	0.353	2295	1525	0.664
BLUE	670	315	0.470		n.r.	
Green LED	3910	1640	0.420	2245	1255	0.559

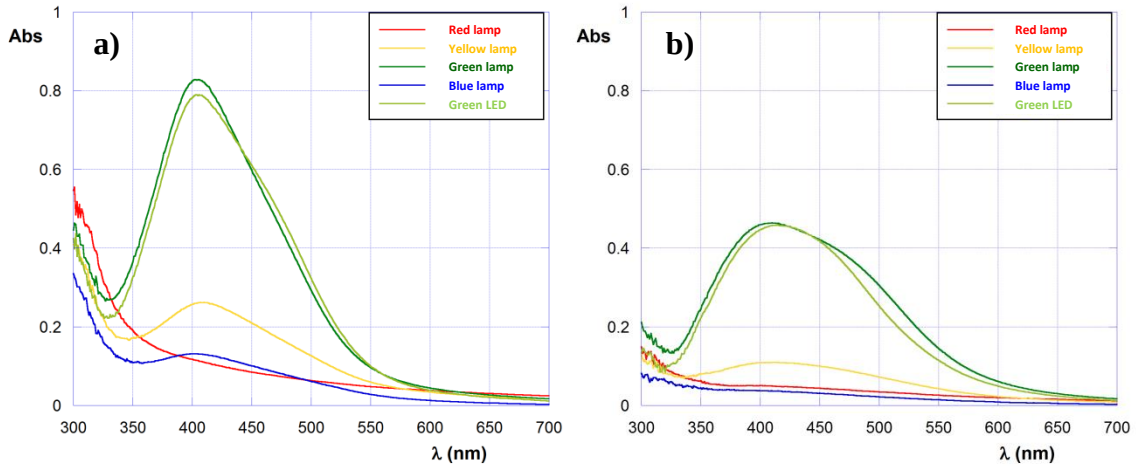

Figure 7.9 – UV-vis spectra of Ag/**amCD3** [**a)**1:2; **b)**1:0.4] systems irradiated for 10 min with different coloured lamp.

Considering this, NIR component was eliminated by irradiating the systems with a green source LED, whose emission spectrum consists of a single narrow band centered at 513 nm (FWHM 28 nm). In this case considering the power of the LED source (5W) the distance of irradiation was set to ca 3,5 cm. The resulted spectra of the systems are very similar to those obtained with the green filament lamp. Blue or yellow LED source afforded no photoreduction.

A careful analysis of the data (Table 7.5), in particular the comparison between the results for the halogen, infrared, green filament lamps and green LED, suggests that the main effect of the NIR component seems to increase the contribution relevant to the absorbance at 500 nm in the spectrum of the nanocomposite. According to what previously discussed, this indicates that the NIR component could increases the effectiveness of the secondary reduction process of Ag. Indeed, considering the well-known ability of metal nanoparticles to absorb IR light, and convert it to localized heat[387] (see the last chapter), this could provide the need energy to support the further Ag^+ photoreduction by the reducing species deriving from the first photochemical process. The latter one, in turn, should be attributed to the visible component of the green emission source. It is also very interesting to note that for systems Ag/**amCD3** 1:2 the use of two green source would seem to give slightly better results in terms of intensity of the absorption at 400 nm; whereas, in the 1:0.4 systems the behaviour is reversed, and the green source give spectra with an intensity around 60% with respect to those obtained with halogen lamp. This indicates that the presence of the visible and NIR components is necessary, because they act synergistically in promoting the overall reduction of silver, and then the process of formation of the **AgNP**s. Obviously the price to be paid, is a more extensive degradation of the capping agent, as evidenced by the R_e values.

Finally, it is worth stressing that the irradiation power could be also contribute to the degradation of the coating agent. Indeed, if in the case of coloured lamps and LED source it

was possible to keep constant the irradiation power to which one of the halogen lamp system, in the case of solar simulator, Rayonet and infrared lamps it was not possible owing to configuration limits of these systems. In fact, in the case of solar simulator the set irradiation power (30 W/m^2) is related to the emission between 300 and 400 nm (used by the instrument as reference), while considering the power of the lamp and the distance of irradiation (1700 W, 38 cm) the effective irradiation power is 940 W/m^2. On passing to Rayonet the effective irradiation power is 600 W/m^2 (128 W at a distance of 13 cm). As a matter of fact, the systems expose to solar simulator and infrared lamp, namely the source with the strongest irradiation power, was characterized by the lower stability, thereby confirming a not negligible role provided by irradiation power to the photodegradation of the coating agent.

*7.3.2 - Morphological characterization of **AgNP**s systems*

Once individuated the best conditions to perform the **AgNP**s photoreduction in the presence of **amCD**, it was decided to carry out a thorough structural characterization. First, in order to demonstrate that the **amCDs** stably reside, as a covered layer on **AgNP**s surface giving rise to a nanocomposites, FT-IR spectra of some sample were recorded. For this purpose the tendency of the system to give precipitates over time was exploited, and speeded up by subjecting the systems to centrifugation. Indeed, all the systems, when subjected to centrifugation at 13000 rpm for 20 min, resulted in a completely colorless supernatant and the formation of a red-brownish pellet. It is worth stressing at this regard that the precipitate obtained can be re-suspended in pure water by sonication, to afford again a quite stable pseudo-solution. The possibility to isolate and subsequently re-suspend an NP composite might be interesting, in view of possible applications. In this case the pellet was afterward used to the FT-IR measurements. Noticeably, upon addition of conc. HCl to the supernatant liquor, no precipitate or turbidity was qualitatively observed. Therefore, the presence of residual Ag^+ in the liquor can be ruled out.

In particular, the FT-IR spectra of four representative systems were recorded. These were prepared using in each case an 1:2 ratio and irradiated for 10 min with halongen lamp system namely Ag/**amCD1** (sample **A**), Ag/**amCD1** – Glucose 2 mM (sample **B**), Ag/**amCD2** (sample **C**) and Ag/**amCD3** (sample **D**). The spectrum of the Ag/**amCD1** 1:2 system obtained by reduction with formaldehyde (Sample **E**) was recorded too, for suitable comparison. Moreover, the spectra of the three **amCDs** were recorded as well and used as reference systems. The spectra of the **amCD1**, and sample **E**, **A** and **D** are reported in Figure 7.10.

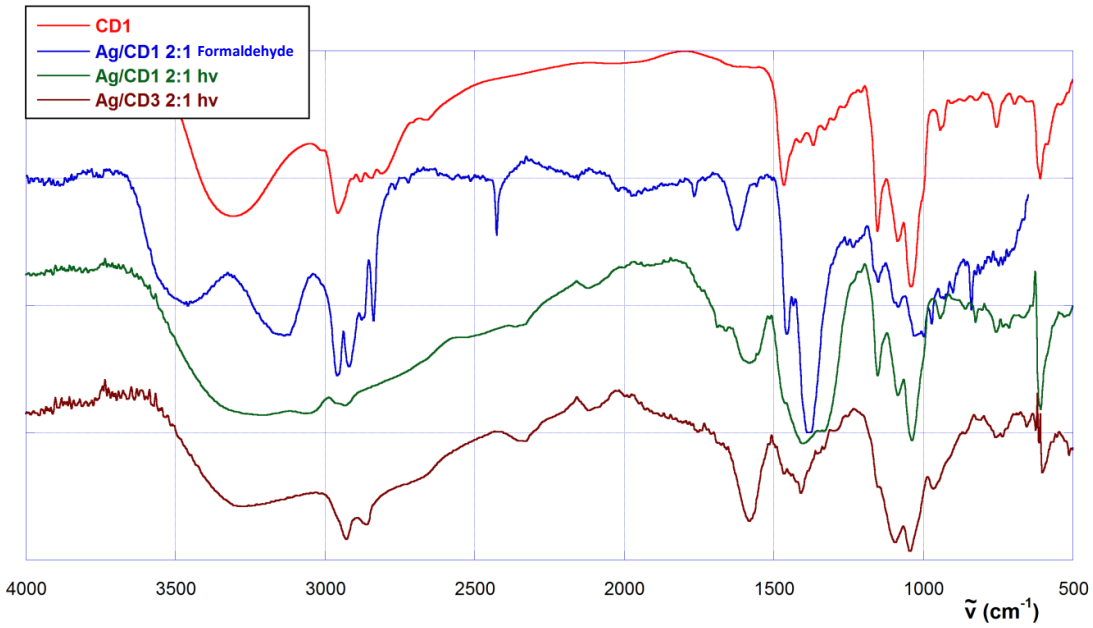

Figure 7.10 – FTIR spectra of **amCD1** (red line); Ag/**amCD1** chemically reduced (blue line); Ag/**amCD1** irradiated (green line); Ag/**amCD3** irradiated (brown line).

First of all, the spectra of the three **amCDs** are very similar. In each one it is possible to assign the broadband at ca. 3300 cm^{-1} of the hydroxyl groups, the system bands around 3000~2800 cm^{-1} related to the stretching of -CH_2- groups of the polyamine chains, and the characteristic fingerprint system of **CD** between 1500 and 1000 cm^{-1}. In the **E** sample, obtained by chemical reduction, it is easy to observe the presence of the stretching of -CH_2- groups and the fingerprints of **amCD1**, on which, an intense band at ca. 1400 cm^{-1} is overlapped. The latter was attributed to the CO_3^{2-} stretching, in turn, probably due to the ability of the basic-nature system to absorb CO_2. On passing to the sample **A**, some different features can be noticed. The hydroxyl stretching band gets wides and the signals of the -CH_2- stretching nearly disappear. Moreover, there is the presence of an intense band at 1585 cm^{-1}, which can be attributed to the asymmetric stretching of a carboxylate group. The corresponding symmetrical stretching band is not well distinguishable, because it is overlapped with the signal of CO_3^{2-} in the area around 1400 cm^{-1}. Furthermore, the band at 1585 cm^{-1}, is characterized by the presence of a shoulder at 1660 cm^{-1}, which can be attributed to the >C=N- stretching of an imine group. Finally, the three bands of the cyclodextrin fingerprint between 1200 and 1000 cm-1 are perfectly visible. The spectrum of the sample **B** (not shown) shows the same characteristics. These observations provide a convincing evidence of the fact that the diamine chains **amCD1** undergo an extensive oxidative degradation process, with the final formation of carboxyl groups, through the supposed sequence of reactions in the Scheme 7.3 (imine → aldehyde → carboxylic acid). On passing to the sample **D**, it is possible to notice that the stretching of -CH_2- groups are not

completely suppressed, the band of the carboxylate at 1585 cm^{-1} does not show a shoulder and the corresponding symmetric stretching 1405 cm^{-1} is well detectable. These findings confirm that the longest polyamine chains have a better resistance to the oxidative degradation, ensuring a more efficient coating of the **AgNP**s.

Furthermore, a further characterization on a carefully selected set on **AgNP**s systems was accomplished. In particular, TEM micrographs (Figure 7.11) of systems **A**, **B**, **C** and **D** were acquired. The morphological features and the aggregation/coalescence tendency of the obtained **AgNP**s change according to the **amCD** used. The NPs of sample **A**, are characterized by a higher degree of polydispersity, with the presence of amorphous and irregular particles, immersed in a sort of gluey matrix. This, together with the fact that the UV-vis spectra of the systems prepared with **amCD1** have usually highest R_{ε} values, is a further confirmation of the more extensive degradation undergone by **amCD1** during the photoreduction process, with respect to other **amCDs**. The features of the NPs significantly improve when glucose is added to the system (sample **B**). In the case of the system prepared with the **amCD2** (sample **C**) a certain aggregation tendency is still observed, but the metal cores are more regular shaped, less polydispersed, and more crystalline. The system prepared with the **amCD3** (sample **D**), shows little aggregation, a lower degree of polydispersity, and even more crystalline NPs. By the use of all the obtained micrographs, it was possible to carry out a statistical analysis of the NPs diameters distribution (Figure 7.12, Table 7.6).

Sample **A** has the maximum polydispersity degree, apparently with a bimodal distribution. For the sample **B** is clear as the addition of glucose make the distribution almost symmetric and centred at about 28 nm. The symmetry of the distribution remember which one found in the case of the "chemistry" reduction with formaldehyde, and then confirms the idea that in the case of systems prepared with the addition of glucose, this one contribute to the further reduction of Ag^{+}. The use of **amCD2** (sample **C**) allows to obtain a skewed single-mode distribution of the diameters, and a lower polydispersity than that obtained with **amCD1**. Finally, with **amCD3**, the lowest degree of polydispersity is obtained, joined with an even less skewed distribution and the presence of the smallest NPs.

Regarding to the degree of crystallinity of **AgNP**s, this one was best established for **C** and **D** samples by recording **SAED** (**S**elected **A**rea **E**lectron **D**iffraction) images (Figure 7.13).

Sample A

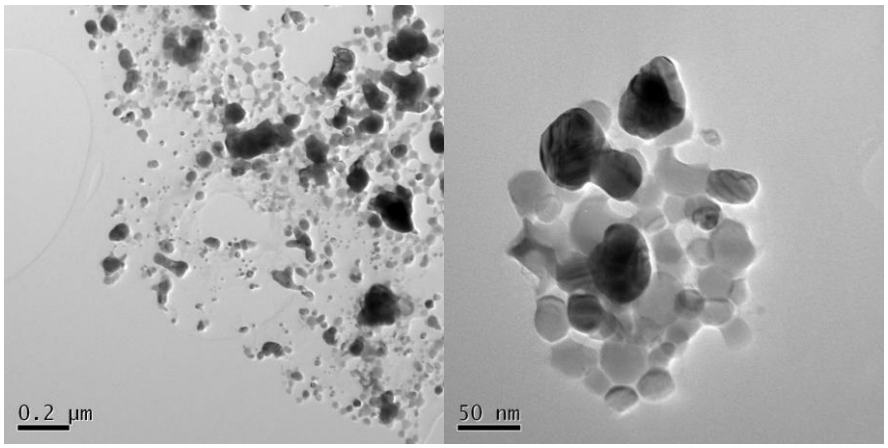

Sample B

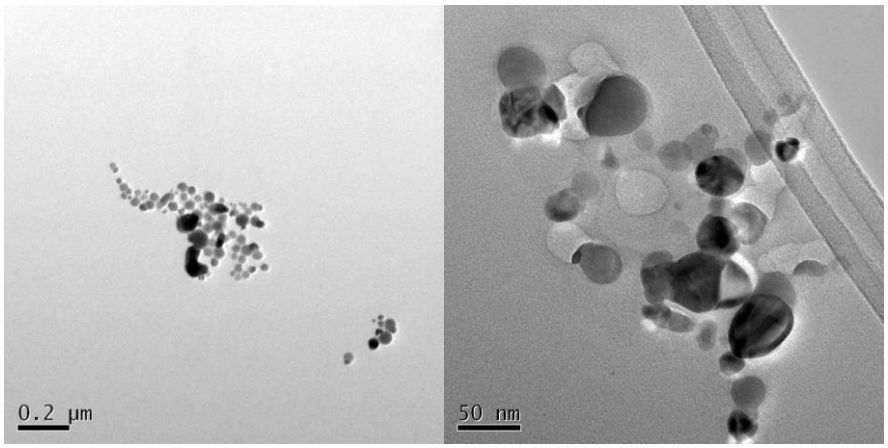

Sample C

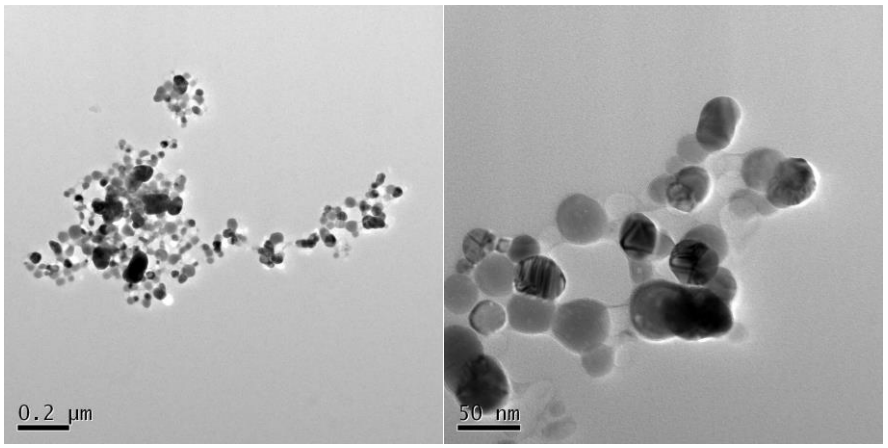

Sample D

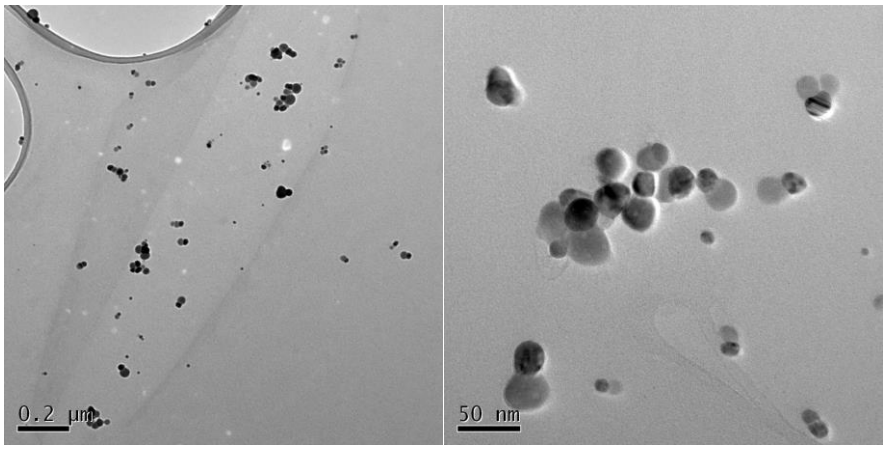

Figure 7.11 – TEM micrographies of the relevant samples.

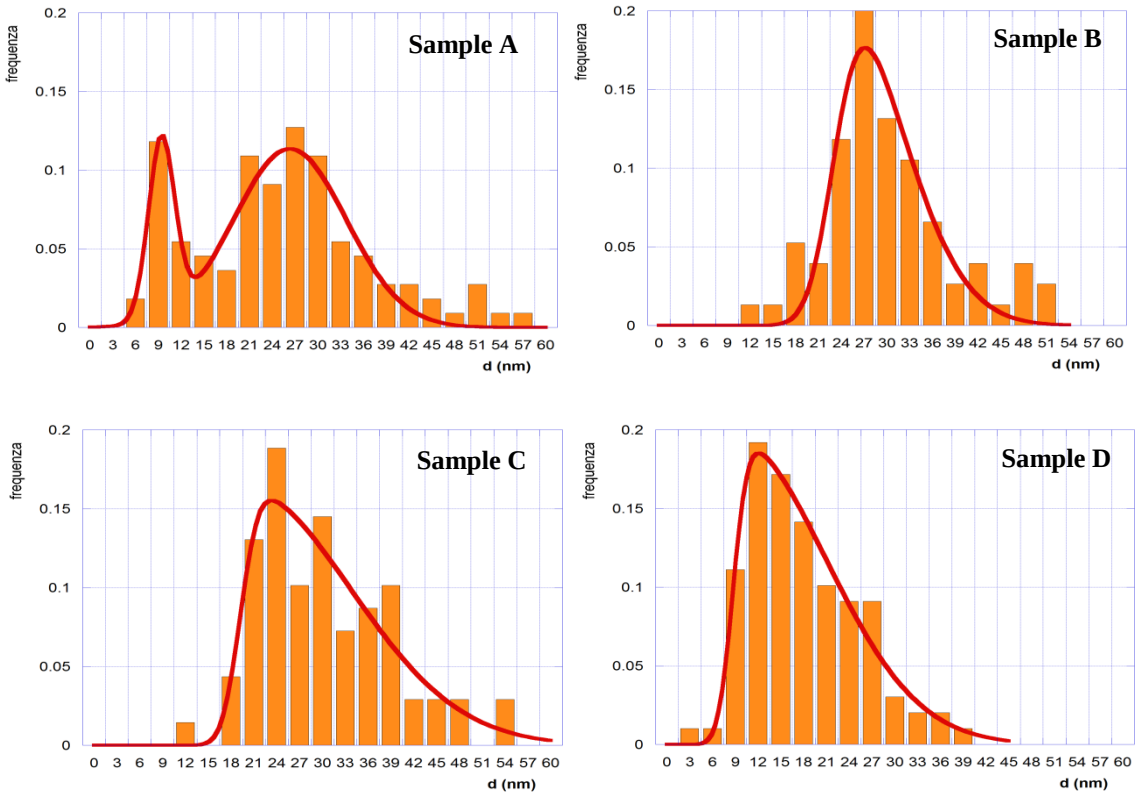

Figure 7.12 – Size distribution of the relevant samples.

Table 7.6. Statistical distribution of particles size.

Sample	Mode	Mean	σ	Skewness (Pearson index)
A	(9 nm, 27 nm)	28.9 nm	14.7 nm	-
B	27.9 nm	36.0 nm	15.6 nm	0.52
C	22.8 nm	31.9 nm	8.9 nm	1.02
D	14.7 nm	19.9 nm	7.1 nm	0.70

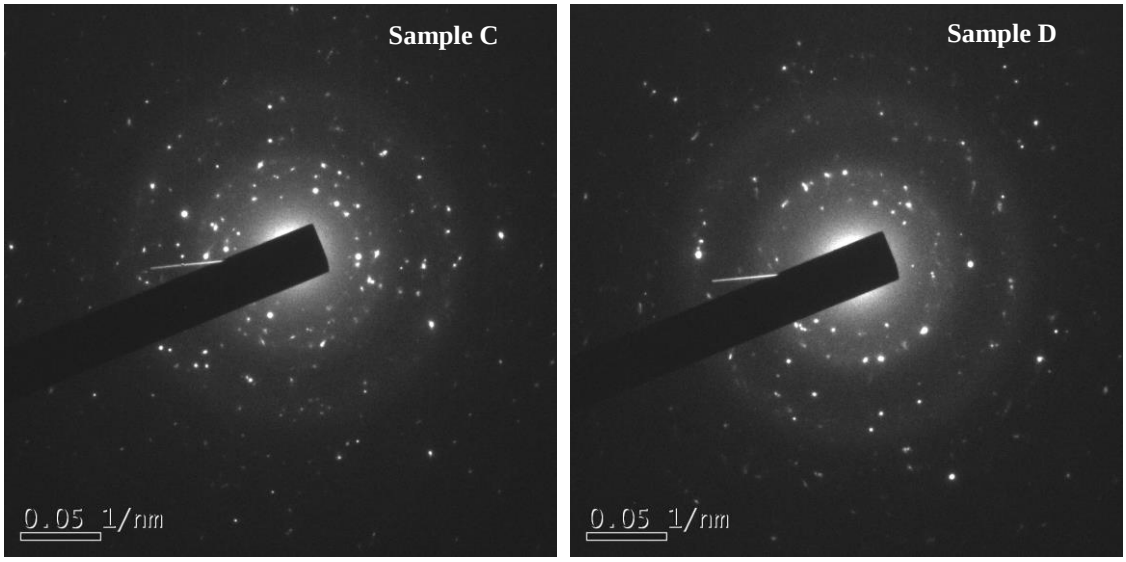

Figure 7.13 – SAED images of systems Ag/**amCD2** (sample **C**) and Ag/**amCD3** (sample **D**).

SAED analysis is a diffraction technique similar to the X-ray diffraction, but with the main difference to use high energy electron; it has the advantage to allow the selected diffraction analysis of surface in the order of hundreds nanometer. Basically, the atom disposition inside a solid act as a diffraction grating for the high energy electron (owing to the comparable dimension on the interatomic distance and the electron's wavelength). Then when an electron hit an atom, it will be scattered of a certain angle, according to the peculiar crystalline structure of the sample, giving rise to a light spot. As a matter of fact, bright and regularly-radial distributed light spot give proof to a high degree of crystallinity of the system; conversely the presence of high number of seamless radial distributed light spot take into account amorphous material. As it is possible to see in the picture both systems present a radial positioning of the light spot, consistent with the d-spacing of the *fcc* phase of Ag indexed as 111, 200, 220 and 311 reflections from the centre of the SAED pattern and then confirming a good degree of crystallinity, higher for **amCD3**.

7.3.3 - Antimicrobial activity

As previously mentioned many reports describe the antimicrobial activity of biologically or chemically synthesized **AgNP**s. In particular, Andrade et al. successfully tested the antimicrobial efficacy of **βCD**-coated pseudo-spherical **AgNP**s (28 nm average diameter), revealing bactericidal effect at the concentration of 10 µg/mL against the Gram-negative *E. coli* used as tester strain.[362] Therefore, testing the antibacterial properties of the photochemically synthesised Ag/**amCD** nanocomposites, seemed an obvious proceeding of the work.

In order to assess the antimicrobial activity of the Ag/**amCD** nanocomposites, micro-biological assays were performed using the Gram-negative *E. coli* and the Gram-positive *Kocuria rhizophila* strains as suitable testers. At this regard, it was decided to use the systems Ag/**amCD3** 1:2 obtained upon 10 min of irradiation by halogen lamp. Preliminary agar diffusion tests were performed by spotting on bacterial overlays aliquots of suspensions containing different amounts (corresponding to 1, 0.1, 0.01 and 0.001 µg of total Ag respectively) of both the "as prepared" Ag/**amCD3** system (**AP** Ag/**amCD3)** and also a forcedly precipitated and resuspended Ag/**amCD3** system (**FPR** Ag/**amCD3)**. The latter, in particular, was chosen to test the viability of the centrifugation/resuspension protocol reported in literature.[388] Moreover, other systems as free **amCD**, ammoniacal silver acetate, the Ag^{+}-**amCD3** complex prior to irradiation and the mother liquors from the forced precipitation of the composite were used as suitable controls. These preliminary tests revealed no or negligible inhibition of bacterial growth for the free **amCD3** and for the mother liquors respectively,

whereas the other tested silver sources showed significant antimicrobial activity against both the tester strains, due to the easier available Ag^+ ions present. In particular, for the tested composites 0.01 and 0.1 µg of Ag were sufficient to afford growth inhibition of *K. rhizophila* and *E. coli* respectively. It is worth noting that the antibacterial efficacy measured as the area of bacterial growth inhibition halos, revealed that both **AP** and **FPR** Ag/**amCD**3 composites possess a similar activity, with the second one showing only a fair decrease in efficacy against both testers (Figure 7.14).

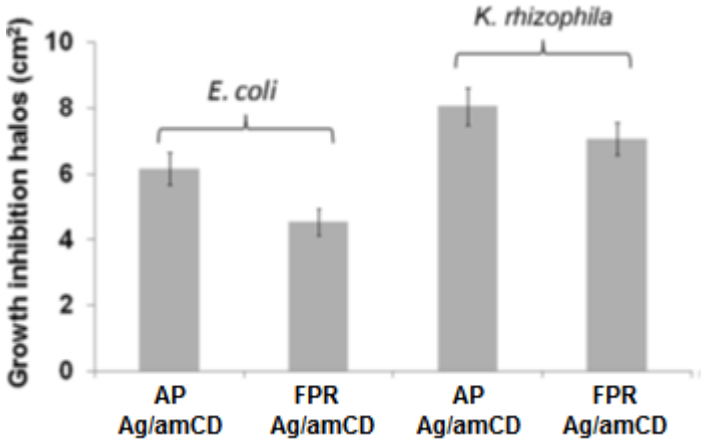

Figure 7.14 – Area of bacterial growth inhibition halos produced by AP and FPR Ag/**amCD** systems.

Nevertheless, considered that differences in activity were in fact modest, the capability of being separated from aqueous phase by centrifugation is undoubtedly a valuable characteristic for our nanocomposites. Therefore, everything considered, further investigations were carried out on the **FPR** Ag/**amCD3** system only. As a final observation, lack of activity for the mother liquors indicates that unreduced Ag^+ ions possibly present in the **AP** Ag/**amCD3** pseudo-solution co-precipitate within the nanocomposite during centrifugation. In order to achieve quantitative evaluation of the antibacterial efficacy of the **FPR** Ag/**amCD3** system, **MIC_{90}** and **MBC** tests were performed (relevant results are summarized in Table 7.7). In particular, we found values of 5 mg/mL for both **MIC_{90}** and **MBC** against *E. coli* and 1 and 5 µg/mL for **MIC_{90}** and **MBC** against *K. rhizophila*, respectively.

Table 7.7 – MIC_{90} and MBCvalues of Ag composites against *E. coli* and *K. rhizophila*.

	E. coli		***K. rhizophila***	
Ag source	**MIC_{90} (µg/ml)**	**MBC (µg/ml)**	**MIC_{90} (µg/ml)**	**MBC (µg/ml)**
Ag acetate	5	5	0.5	0.5
Ag^+-**amCD3**	5	5	1	1
FPR Ag/**amCD3**	5	5	1	5

The quantitative data of **MIC$_{90}$** and **MBC** values obtained for **FPR** Ag/**amCD3** towards *E. coli* strain were identical to those measured for the control silver acetate or the Ag^+-**amCD3** not irradiated pre-complex. In the case of *K. rhizophila*, a slightly higher activity for Ag acetate and Ag^+-**amCD3** not irradiated pre-complex was observed with respect to **FPR** Ag/**amCD3.** This evidence could be explained considering the different composition of the cell wall of Gram positive and negative bacteria. Indeed, the higher amount of Ag^+ ions present in the Ag acetate and Ag^+-**amCD3** systems, it could statistically favoured the Ag^+ diffusion through the thicker peptidoglycane layer of the Gram positive bacteria. Then for the same reason the internalization of Ag/**amCD3** nanocomposites could be a little bit disfavoured.

It was already mentioned that the mechanism of bactericidal actions of **AgNP**s has been extensively studied and different mechanisms of toxicity have been proposed.[361,363,364,380] These include bacterial cell membrane disruption, inhibition of respiratory enzymes, inhibition of cell-wall biosynthesis, interaction with bacterial DNA and the ability to produce Reactive Oxygen Species (ROS). In all these events the capability of silver nanocomposite to release Ag^+ by the **AgNP**s oxidation is fundamental to exert biological activity.[362,367,370-372,375]

In any case the obtained results suggest a considerable capability of Ag^+ production from the **FPR** Ag/**amCD3**. It is worth stressing that **MIC** values for **FPR** Ag/**amCD3** are similar or lower than those reported in other works against the same bacterial strains, ranging from 0.25 to 100 μg/mL, in dependence of the capping agent and the **AgNP** size.[359,361,383,389,390]

In particular, for **AgNP**s having a size similar to that of **FPR** Ag/**amCD3**, **MICs** against *E. coli* ranging from 10 to 75 mg/mL have been reported. On passing to *K. rhizophila* strain instead, the lowest **AgNP MIC** ever reported is as large as 4 mg/mL.[391]

The possible combination of antimicrobial activity of **AgNP**s and antibiotic molecules has been explored giving interesting results whenever the combined system showed improved efficacy.[385,392,393] Then taking into account the peculiar structure of Ag/**amCD3**, which can function as a potential supramolecular carrier, it was decided to test its possible interaction with ampicillin (amp). In particular, amp was chosen due to its already observed synergistic effect when combined with **AgNP**s against *E. coli* strains. The ability of **amCD3** to bind amp was positively assessed by means of polarimetric measurements (see Experimental section for details), which allowed to estimate for the **amCD3-amp** complex a stability constant as large as 650 ± 100 M^{-1} (Figure 7.15).

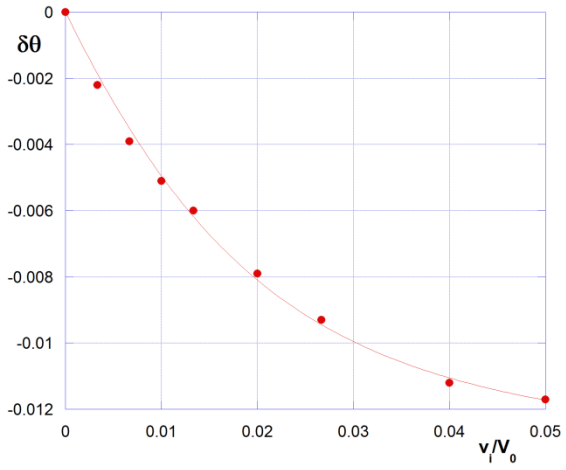

Figure 7.15 – Trend of δϑ vs v_i/V_0 for the inclusion of **amp**.

Then, considering the resulted value, a quite stable inclusion complex is formed between **amCD3** and **amp**. Thus, amp was added to both the Ag^+-**amCD3** pre-complex and the **FPR** Ag/**amCD3** composite in a 1:1 weight ratio, and the resulting complexes were subjected to tests to evaluate its antibacterial activity (Table 7.8).

Table 7.8 – MIC_{90} and MBC values of Ag - amp composites against *E. coli* and amp^R *E. coli*.

	Ag source	**MIC_{90} (µg/ml)**	**MBC (µg/ml)**
E. coli	**Ag^+-amCD3 + amp**	1	1
	FPR Ag/amCD3 + amp	1	1
amp^R *E. coli*	**Ag acetate**	5	5
	Ag^+-amCD3	5	5
	FPR Ag/amCD3	5	5
	Ag^+-amCD3 + amp	10	10
	FPR Ag/amCD3 + amp	5	5

The antimicrobial assays performed on *E. coli* revealed a 5-fold improvement of bacterial-growth inhibitory and bactericidal activity for the both systems. This result is particularly interesting, because the amount of amp used is significantly smaller as compared with other works,[394] and is at least one order of magnitude lower than the **MIC** and **MBC** values against *E. coli* strain calculated in this study (i.e. 10 and 25 µg/mL, respectively). In particular, the **MIC** value is in agreement with the one reported in literature for the same strain.[395,396] Further control tests (using also the others Ag source as comparison) were performed with an *E. coli* strain which expresses a β-lactamase gene *bla*, contained in a high-copy number DNA vector plasmid and conferring high level of amp resistance (more than 100 µg/mL). In particular, **FPR** Ag/**amCD3** + **amp** **MIC_{90}** and **MBC** values against the **amp^R** *E. coli* strain resulted comparable to the ones found for the **FPR** Ag/**amCD3** alone. The latter result indicates that the improvement of antimicrobial activity is specifically due to synergistic action of the composite and **amp**. Noticeably, the **FPR** Ag/**amCD3** + **amp** system showed increased activity as compared to **FPR** Ag/**amCD3** even if sub-lethal amounts of **amp** were bound on the Ag

nanocomposite, suggesting that the antimicrobial activity of this system still resides in the activity of **AgNP** whereas the **amp** molecule can increase the affinity of **AgNP**s surface for the bacterial cell wall, as already proposed by Fayaz et al.[392] Therefore, based on these considerations, the **FPR** Ag/**amCD3** system exerts a powerful antibacterial efficacy and may have an applicability in those fields where antimicrobial capability is a desired feature.

7.4 – Experimental section

Instrumentation

UV-vis spectra were recorded on a Beckmann DU 800 spectrophotometer. FT-IR spectra (2% in KBr) were acquired on a Bruker VERTEX 70 apparatus. TEM micrographs were acquired using a JEM-2100 (JEOL, Japan) electron microscope operating at 200 kV accelerating voltage. A drop of each suspension was put onto a 3 mm Cu grid "lacey carbon" for analysis and let the solvent to complete evaporation. Polarimetric measurements were performed on a JASCO P-1010 polarimeter.

*Preparation of the Ag-**amCD** composites.*

A stock solution of ammoniacal Ag acetate 15 mM was prepared as follows: 250.3 mg of salt (0.15 mmoles) were dissolved in distilled water (ca. 50 mL); then a slight excess of NH_3 1 M was added dropwise until the solution turned perfectly clear, and the volume was finally adjusted to 100 mL with distilled water. The solution can be stored indefinitely in the dark. In parallel, a stock solution of **amCD** 6 mN was prepared by dissolving the proper amount of each **amCD** in 20 mL of distilled water.

In order to prepare the **AP** Ag-**amCD** nanocomposite, 1.8 mL of water, 200 μL of ammoniacal Ag acetate 15 mM solution and 1.0 mL of **amCD** 6 mN solution were rapidly mixed in a screw-cap vial. The carefully closed vial containing the solution was accommodated in a box having the inner walls covered in tinfoil, and exposed for 10 min to the light of a common 50 W halogen lamp placed at a distance of 12 cm. The resulting amber red solution was immediately stored in the dark. The **C** Ag-**amCD** precipitated composite was obtained by subjecting a freshly prepared sample of **AP** Ag-**amCD** to centrifugation at 14000 rpm for 30 min. Then, the clear, almost colourless supernatant liquor was carefully decanted and the brown residue was lyophilized overnight.

The **FPR** Ag-**amCD** system was prepared by subjecting 1 mL of freshly prepared **AP** Ag-**amCD** pseudo-solution to centrifugation at 14000 rpm for 30 min in an Eppendorf vial. The

mother liquors were carefully pipetted, and replaced with 1 mL of fresh water. The system was then subjected to sonication using a Sonics and Material inc. Vibra cell sonicator for 10 s.

*Polarimetric determination of the **amCD3-amp** binding constant.*

According to the standard procedure reported in literature,[100,101] stock solutions of **amCD** (2.5 mM) and **amp** (150 mM) were prepared by dissolving the proper amounts of substance in pure water. Samples were prepared by adding different micro-amounts (from 0 up to 150 μL) of the guest **amp** solution to 3 mL of the host **amCD** solution. Then, the optical activities of the samples were measured. Because the chiral guest **amp** possesses a non-null optical activity, regression analysis of polarimetric data was accomplished by means of the proper equation derived analytically (which is a generalization of the Eq. (3.3), pag. 38):

$$\delta\vartheta_i = \left[\vartheta_i (1 + v_i / V_0) - \vartheta_0 - G_0^0 \frac{v_i}{V_0} \Theta_G \right] = \\ = \frac{\Delta\Theta}{2} \left(H_0^0 + G_0^0 \frac{v_i}{V_0} + \frac{1 + v_i / V_0}{K} - \sqrt{\left(H_0^0 + G_0^0 \frac{v_i}{V_0} + \frac{1 + v_i / V_0}{K} \right)^2 - 4 H_0^0 G_0^0 \frac{v_i}{V_0}} \right) \quad (7.1)$$

where, for the generic *i*-th sample, ϑ_i and ϑ_0 are the optical rotations measured for the sample and the pure host solution respectively, v_i is the volume of **amp** added, V_0 is the volume of **amCD** solution, Θ_G is the molar optical rotation of the guest, H_0^0 and G_0^0 are the analytical concentrations of the host and guest solutions respectively, $\Delta\Theta$ the differential molar optical activity for the complex, *K* is the binding constant to be determined.

Microbiological assays.

Microbiological assays were performed using *E. coli* K12 DH10B and *K. rhizophila* ATCC 9341 as Gram-negative and Gram-positive tester strains, respectively. The **amp** resistant strain was obtained by transformation of chemically-competent *E. coli* K12 DH10B cells by using the high-copy number plasmid pUC19 (Invitrogen), which carries the *bla* gene encoding a β-lactamase, according to supplier instructions.

Agar diffusion tests were performed using 5 mL of soft-agar - i.e. 7.5% (w/v) bactoagar in Luria Bertani (LB) broth - containing 10^8-10^9 bacteria cells (colony forming units or CFU) of tester strain. A range of concentrations (corresponding to 1, 0.1, 0.01 and 0.001 μg of total Ag) of the **AgNP** composites were directly spotted on an overlay of bacteria on agar plate. Growth inhibition halos from at least three independent replicas were observed after overnight incubation at 37 °C.

In order to gain a quantitative assessment of the antimicrobial activity, MIC and MBC values were calculated. In particular, different suspensions of 1 mL LB broth containing each tester strain at the concentration of 10^6 CFU mL^{-1} were incubated in sterile 24-well plates (37°C, 200 r.p.m. in orbital shaker) with different amounts of total Ag (0.1, 0.5, 1, 5, 10, 20, 50 and 100 μg mL^{-1}). Untreated bacterial cultivations were used as reference control condition. Each cultivation was performed in parallel triplicates. After 24 h of incubation, the MIC and MBC values were evaluated. The MIC was determined spectrophotometrically as the lowest concentration that inhibited the 90% of bacterial growth (MIC_{90}) in the respect of untreated cultivation in terms of OD measured at 600 nm. The MBC, defined as the lowest concentration causing a 99.9% decrease of the starting CFU, was determined by plating and incubating 100 μL from serial dilutions of cultures on LB-agar plates overnight at 37°C for CFU counting. Statistical test (one way ANOVA) was performed to asses significance ($p < 0.05$ or $p < 0.01$) of spectrophotometric measurements (OD values) and viable cell count (CFU values) by using XLSTAT software (Addinsoft). Each measurement was obtained by three biological and technical replicates.

- 8 -

GOLD NANOPARTICLE-MEDIATED ACTIVATION OF β-GALACTOSIDASE BY PHOTOTHERMAL CONVERSION

8.1 - Light to heat conversion properties of AuNPs

Gold nanoparticles (**AuNP**s) are one of the most representative members of metal nanoparticles class, owing to their peculiar physico-chemical properties. The most remarkable properties of Gold Nanoparticles are their surface plasmon-derived optical characteristic, the strong affinity for sulphur-containing capping agent (which enabling their easy surface functionalization) and their biocompatibility. All these characteristics have allowed the use of **AuNP**s in diverse application fields.[397] In particular, the biomedical field has been one of the most affected by **AuNP**s based nanotechnology. For instance, **AuNP**s have been widely used as drug/biological material delivery systems, for bioimaging or photothermal therapy.[264,398] The latter use, in particular, takes advantage from the peculiar characteristic of nano gold to absorb and efficiently convert light into localized heat, which in turn is used for the release of drug/biological molecules or for the thermal destruction of cancer cells. The ability of Metal NPs and in particular **AuNP**s, to convert light to heat, relies on their characteristic low optical quantum yield, namely the inability to work as light emitters. Hence, almost the whole amount of absorbed light is converted into heat.[387] As a result, the dissipation of generate heat outside the **AuNP**s structures leads to a temperature increase of the surrounding medium. This effect acquires more importance as the wavelength of the interacting light is near to the surface plasmon band of nanoparticles used, namely the resonance frequency leading to the simultaneous motion of a higher amount of electrons. Consequently, the right frequency to match the SPR band and then obtain a higher amount of heat, is related to the dimension and shape of **AuNP**s.[399,400] In particular, spherical nanoparticles of rising dimension or moving

toward different shaped **AuNP**s as nanorods (**AuNR**s), it has been observed a progressive bathocromic shift of the SPR band. For example, many papers report the use of **AuNR**s to carry out photothermal treatment, due to the capability of them to absorb in the *near-infrared* (NIR) region (690-900 nm) also known as "water window". The great advantage to work in this region is related to the transparency of biological systems to NIR radiation, enabling a deeper penetration of the radiation into the biological tissues and the entire conversion of light to heat without interferences.[401,402]

Although heat formation is characterized by a straightforward mechanism, the determination of temperature variations at nanometric level is not so easy. Indeed, these have been usually evaluated by indirect ways, for example by following the phase transformation of a surrounding matrix around **AuNP**s, as ice or polymer matrixes.[403,404] However, by theoretical calculations and experimental determinations it has been seen than the amount of generated heat is related to the light intensity used which in turn is related to the surface area of **AuNP**s exposed to light. Therefore, it has also been established that the temperature increase is proportional to the radius squared of NP. Moreover, the amount of generated heat, and the consequent increase of the temperature, is directly correlated to the overall number of NPs.[387]

The heat generated by **AuNP**s could be in principle used for the thermal activation of biochemical reaction, with the advantage to have a remote control on the process by the use of light.[398,405,406] As a matter of fact, the use of a proper light source enable turning on or off the process, using an external stimulus. This could be of great importance in all the biotechnological process involving enzymes, which work at different range temperature (related to the type of enzymes), in order to achieve the highest activity. The association between **AuNP**s and an enzyme would enable it to activate the enzymatic reaction providing the need heat at molecular level by simply using a selected light radiation which can be tuned using properly shaped AuNPs, in order to match their SPR absorption with the desired light radiation. In such a way it is not necessary the warming up of the whole reaction mixture, with the advantages to save energy and to avoid thermal deterioration of substances, a crucial point in the enzymatic process of the food industry.

Albeit the presence of a lot of work dealing with the interaction of **AuNP**s with enzymes to modulate their activity, only few example exist related to the use of light to heat conversion ability of **AuNP**s to activate enzyme conjugated to them.[407]

In the present work it has been investigated the thermal activation of β-Galactosidase conjugated by supramolecular interaction with *heptakis*-(6-deoxy)-(6-thiol)-**βCD** - capped **AuNP**s, performing the irradiation of the systems by a laser light with a wavelength near to

SPR absorption of **AuNP**s. The activity of β-Galactosidase (βGal) was assessed spectrophotometrically following the formation of o-nitrophenate (**ONP**) derived from the hydrolysis of o-nitrophenyl-β-Galactopiranoside (**ONPG**), used as artificial substrate.

8.2 - Results and Discussion

The first step of the work was the synthesis of water soluble **AuNP**s capped with *heptakis*-(6-deoxy)-(6-thiol)-**βCD** (**βCD(SH)$_7$**) following the protocol previously reported by Kaifer et al.[62] (Scheme 8.1).

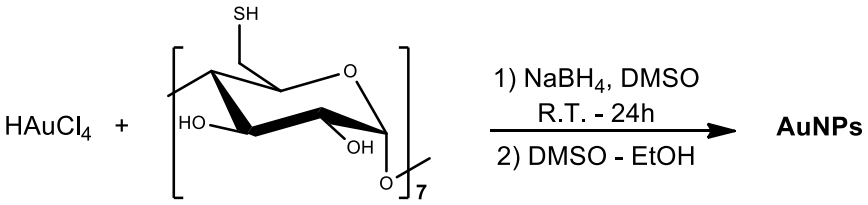

Scheme 8.1

In particular, the synthesis of **βCD(SH)$_7$**-capped **AuNP**s was carried out in a one pot process by direct reduction of a $HAuCl_4$ DMSO solution with $NaBH_4$ in presence of **βCD(SH)$_7$**. The formation of **AuNP**s is clearly highlighted by the intense colour variation of the reaction mixture, which turn from yellow to dark upon $NaBH_4$ addition. The synthesis of **AuNP**s was carried out using two different Au^{3+}/**βCD(SH)$_7$** equivalent ratios, namely 1:1 for **A** systems and 1:0.4 for **B** systems. After purification the resulted **AuNP**s were spectrophotometrically characterized recording the UV-vis spectra of a 1mg/mL solution of each system. (Figure 8.1).

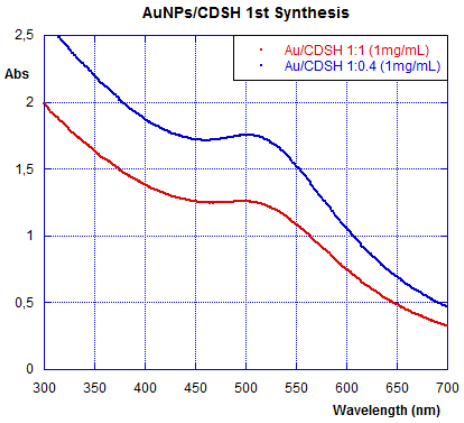

Figure 8.1 – UV-vis spectra of **βCD(SH)$_7$**-capped **AuNP**s.

The resulted λ_{max} for **A** and **B** systems are 497 and 502 nm respectively, accounting for the presence of **AuNP**s with an average diameter around 3 nm for each system, in agreement with those reported in literature. Obviously the **AuNP**s of **B** system are slightly bigger with respect to those of **A** system.

In order to evaluate the ability of these nanoparticles to activate an enzymatic process, under light irradiation, as target enzyme β-Galactosidase was chosen. β-Galactosidase (βGal) is a tetrameric hydrolase which catalyses the hydrolysis of β-galactosides, by cleavage of the β-glycosidic bond.

For the best exploitation of the heat generated by **AuNP**s is necessary to conjugate in an easy and stable way the enzyme on the **AuNP**s surface in order to reduce the distance and then the heat dissipation. To do this, a supramolecular interaction between **AuNP**s and polymer modified βGal (PM-βGal) was established. More in detail, βGal was modified by linking to it an acrylamide based polymer, prepared in a previous work[408] and constituted by three different monomers namely acrylamide, adamantyl acrylamide and acryloyl-6-aminocaproic acid. The polymer is characterized by an average molecular weight of 11600, a polydispersity index of 2.2 and the presence of 8.1 adamantyl moieties on average per polymer chain. The presence of acryloyl-6-aminocaproic acid affords the anchoring site to link the polymer with the βGal by an amide forming reaction using 1-ethyl-3-(3-dimethylaminopropyl)-carbodiimide (**EDC**) and *N*-hydroxysulfosuccinimide (**NHS**) to activate the carboxylic group which becoming more electrophiles undergo the attack of the amino groups of lysine residues present on the enzyme surface (Scheme 8.2).

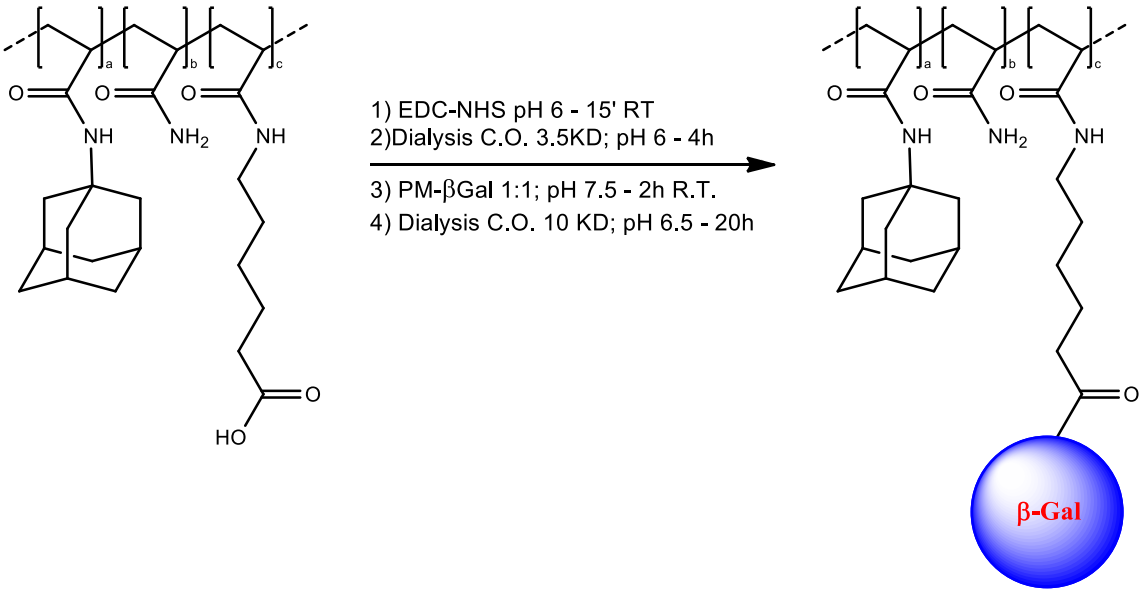

Scheme 8.2

On the other hand, the presence of adamantyl moieties enable to conjugate the PM-βGal with the **βCD(SH)**$_7$-capped **AuNP**s by exploiting the formation of a supramolecular complex between adamantly groups and **CD** cavities on **AuNP**s. At this regard in necessary to remember that the adamantly group is one of the best guest know able to fit the **βCD** cavity giving very stable inclusion complex characterized by the greatest binding constant.

Prior to perform the conjugation with **AuNP**s, the βGal activity was assessed both before and after it had been grafted to the acrylamide-based polymer, in order to verify if the presence of the polymer could affect its activity. The latter one expressed as U/mg, estimates the capability of 1 mg of enzyme to produce 1 µmol of product per minute (U). In this case, the activity tests were carried out checking the quantity of **ONP** (recording its absorption at 420 nm) produced by a certain amount of βGal from the hydrolysis of **ONPG** performed at 40 °C per 5 min (Scheme 8.3).

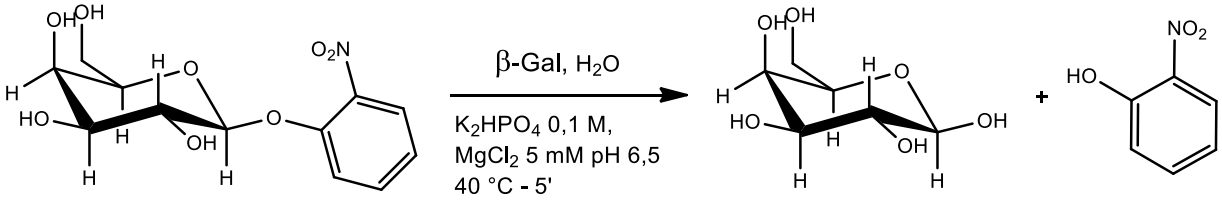

Scheme 8.3

For pristine βGal and PM-βGal were found values of 274 ± 7 and 264 ± 5 U/mg respectively, then only a minor reduction in activity was undergo after βGal polymer modification.
At this point, the conjugation (Figure 8.2) between **AuNP**s and PM-βGal was carried out using such amount of **AuNP**s and PM-βGal in order to have a final concentration of 100µg/mL and 1µg/mL respectively. In particular, it was decided to use the **A** system of **AuNP**s due to the higher presence of **βCD(SH)$_7$** which can afford more interacting site between **AuNP**s and PM-βGal. The conjugation was then performed simply placing together the components and stirring the resulted system for 1 h at 25 °C.

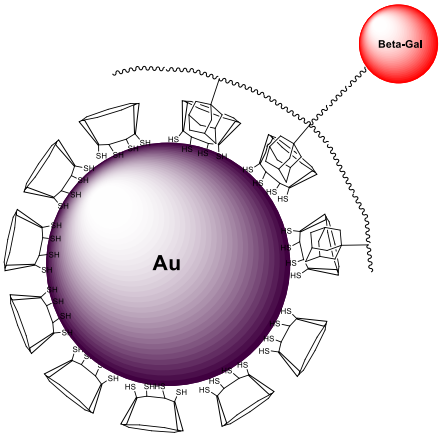

Figure 8.2 – Coniugated system **AuNP**s/PM-βGal.

At this point in order to define if the light irradiation actually promotes the enzyme activation by means of **AuNP**s photothermal conversion, systems **AuNP**s/PM-βGal in presence of **ONPG**

were irradiated at different wavelengths ranging from 400 to 800 nm, using systems without **AuNP**s as reference. In particular, each system was conceived in order to have a βGal concentration of 0.5 µg/mL and a **ONPG** concentration of 20 mM. After its preparation on eppendorf tube, each system was cooled in an ice bath and placed at a distance of 3.5 cm from the light source namely a laser with a power of 500 mW.

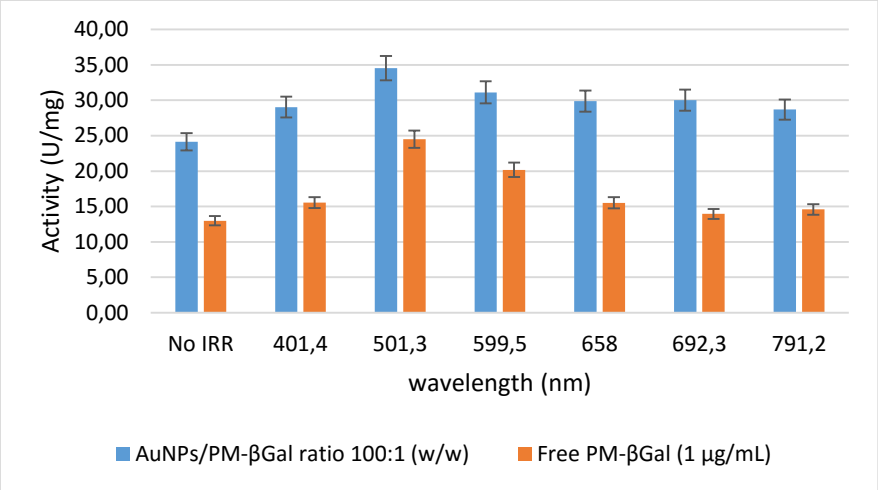

Figure 8.3 – Irradiation (30 min) at different wavelength of system with and without **AuNP**s.

As it is apparent from the result depicted in Figure 8.3, these assays provided with evidence of the thermal activation on the enzymes by means of **AuNP**s, upon light irradiation. The activity of the systems in presence of **AuNP**s is higher at all the wavelength used, although the best activity was obtained by irradiation at 501.3 nm i.e the one matching to the SPR absorption of the **AuNP**s used. It is worth mentioning that in any case the activity is lower rather than that one observed by thermal activation of PM-βGal. This can be clearly understood considering that the low temperature of the bulk medium reduces the mobility of enzyme and **ONPG** (also due of an increased solvent viscosity), and then their effective collisions, with the result of a drops in activity.

Another curious finding was the increase in activity in presence of **AuNP**s also without irradiation, this has given some doubt about the effective role of **AuNP**s, which other to locally warming up the conjugated enzyme, could be promote the **ONPG** hydrolysis, or maybe **ONPG** itself could be easily hydrolysed upon irradiation.

In order to verify this hypothesis, the same systems previously used, but without enzyme were irradiated in the same conditions.

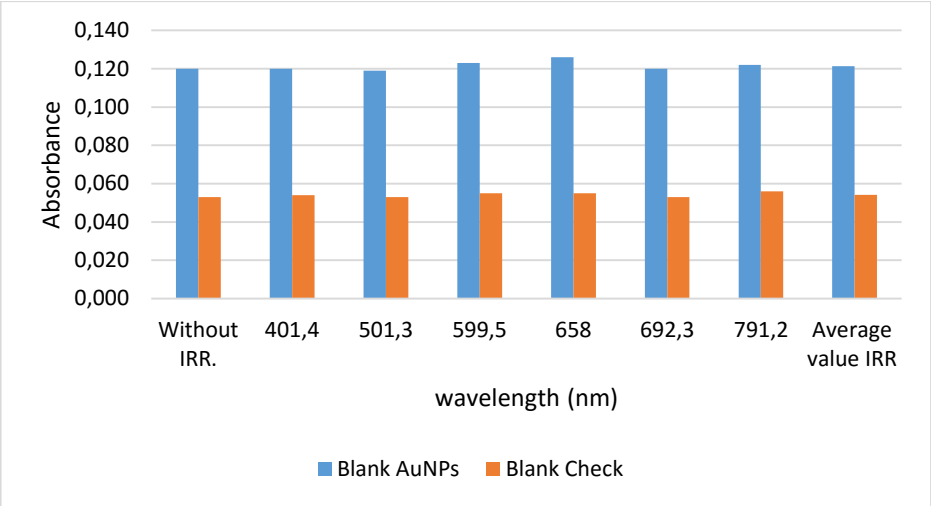

Figure 8.4 – Irradiation of the systems without enzyme.

As it is clearly depicted in Figure 8.4, no difference in absorbance can be found between the irradiate systems and those not irradiated; thus no contribution of gold or light mediated **ONPG** hydrolysis occurs. Moreover, the differences in absorbance between systems with and without **AuNP**s is due to their proper absorbance, which was considered and subtracted in the previous determination.

Curiously, this behavior was also observed during routine activity assays performed by common thermal test to check the time stability of PM-βGal, with and without presence of **AuNP**s, and to have a reference of the highest activity achievable of the systems before of each set of proves.

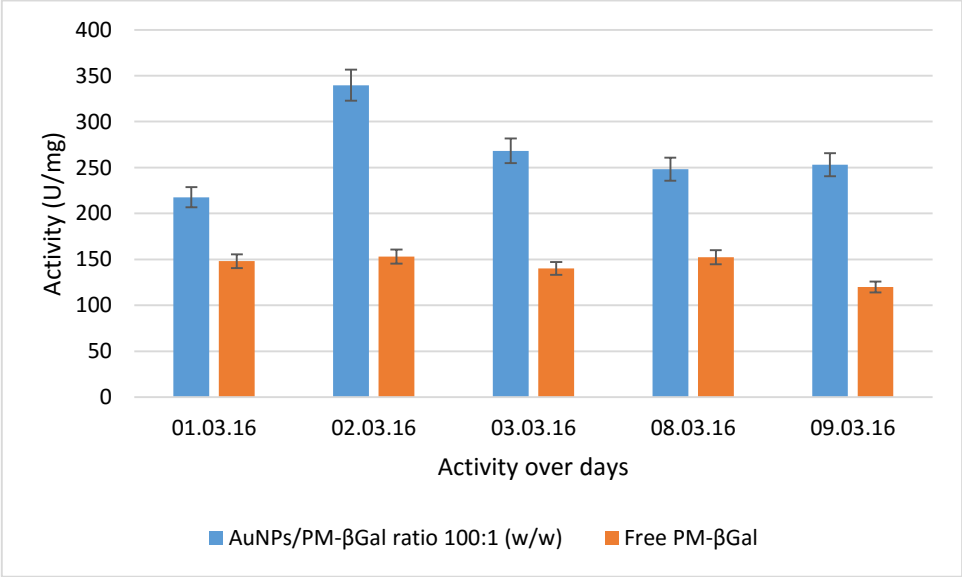

Figure 8.5 - Activity of systems over different days, performed by heating at 40 °C.

As a matter of fact, even by conventional heating at 40 °C the activity of PM-βGal in presence of **AuNP**s was higher in every case with respect free PM-βGal (Figure 8.5). Then, proceeding with other irradiation experiments, it seemed interesting to investigate this phenomenon.

In order to evaluate if the rise in activity is due to a real effect of **AuNP**s on βGal, such to improve their ability to hydrolysed **ONPG**, it was necessary to verify if **AuNP**s could in some way distort the real activity by secondary effects not involving βGal. After the elimination of a possible contribution given from irradiation, it was considered the possibility that an interaction of formed **ONP** or the **ONPG** itself with **AuNP**s could cause an hyperchromic effect on the recorded absorbance resulting in an overestimation of the real activity. The first test was to record the absorption spectra of systems prepared using the same amount of **AuNP**s and different **ONP** concentration (in presence of K_2CO_3 used to stop the enzymatic reaction and keep the **ONP** in its deprotonated form) (Figure 8.6).

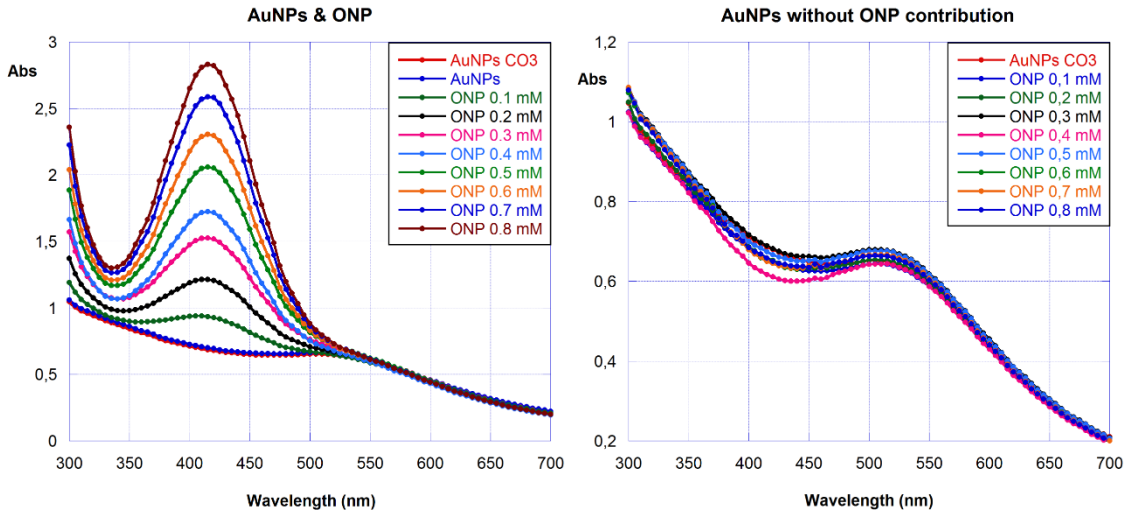

Figure 8.6 – UV-vis spectra of **AuNP**s in presence of different [**ONP**] (left); UV-vis spectra of **AuNP**s by subtracting **ONP** contribution (right).

By subtracting the contribution given by **ONP** to the absorption spectra of **AuNP**s it was possible to see as there is no influence between **AuNP**s and **ONP**, and the same thing was found in the case of **ONPG**.

Another considered possibility it was the change in the absorption spectra on **AuNP**s upon supramolecular interaction with PM-βGal, but also in this case no particular change was observed (Figure 8.7). This has given also an experimental prove of the supramolecular interaction between **βCD(SH)$_7$** capped **AuNP**s and PM-βGal, indeed on the other hand recording the absorption spectra of citrate capped **AuNP**s, in presence of PM-βGal was observed a strong variation on the colour of the solution and then in its spectra.

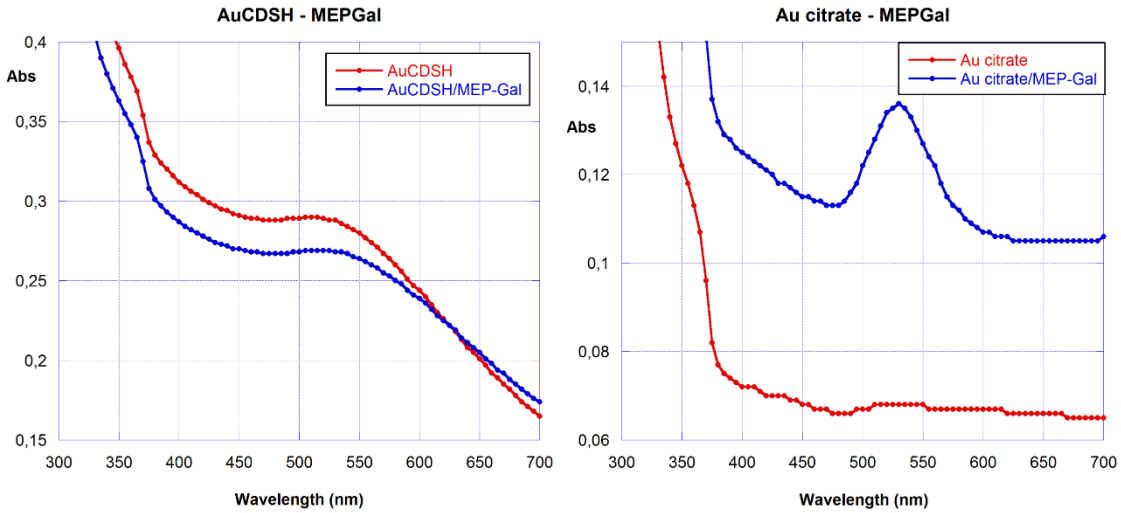

Figure 8.7 – UV-vis spectra of **βCD(SH)$_7$**–**AuNP**s/PM-βGal (left); UV-vis spectra of citrate capped **AuNP**s in presence of PM-βGal (right).

This is due to the replacing of citrate capping agent on **AuNP**s surface, by the thiol groups present on the cysteine residues present on the enzyme structure, which could cause also a structural modification affecting its activity. Actually a signifier reduction of the activity of PM-βGal in the presence of citrate-**AuNP**s was observed with respect to the free PM-βGal.This provide a confirmation that the higher activity of PM-βGal in presence of **βCD(SH)$_7$** – **AuNP**s has to be found in the structure on these particles.

All these results enabled to formulate a possible hypothesis in order to explain the higher activity on the enzyme in presence of **AuNP**s. This relies on the idea that the presence of **CDs** on the **AuNP**s surface can partially complex **ONPG**, by including its nitrophenyl groups. Moreover, the nitrogroup can directly interact with the **AuNP**s surface. In both cases this ability of the **AuNP**s to intercept **ONPG** molecules, it could allow them to act as a reservoir of substrate for the enzymes present on their surface. The labile interaction between **ONPG** and the **CD** cavity, or the gold surface, provides to the enzyme with a large availability of easy accessible substrate, the concentration of which is virtually enhanced. Therefore, the favoured diffusion of the substrate toward the enzyme results in an increased activity.

In order to obtain a partial and indirect prove of this hypothesis, activity assays were repeated using a different substrate namely lactose. Lactose should not be included by cyclodextrin cavities, owing to its hydrophilic character and do not interact with gold surface as well. The enzymatic ability of βGal to hydrolyse lactose was assessed monitoring the reaction by the use of an electronic device commonly used to check the glucose blood concentration. Unfortunately, this device is not able to check the glucose concentration in aqueous media. Therefore, it was not possible to use an aqueous lactose solution. The problem was

circumvented using milk as medium containing lactose, in order to have a qualitative estimation of the different activity of PM-βGal with and without **AuNP**s. In particular, the assays were carried out using the same systems of PM-βGal with and without **AuNP**s, but replacing the **ONPG** with the same volume of milk. The resulting systems were left under stirring at 40 °C (following the glucose formation checking its concentration each 5 min) (Figure 8.8).

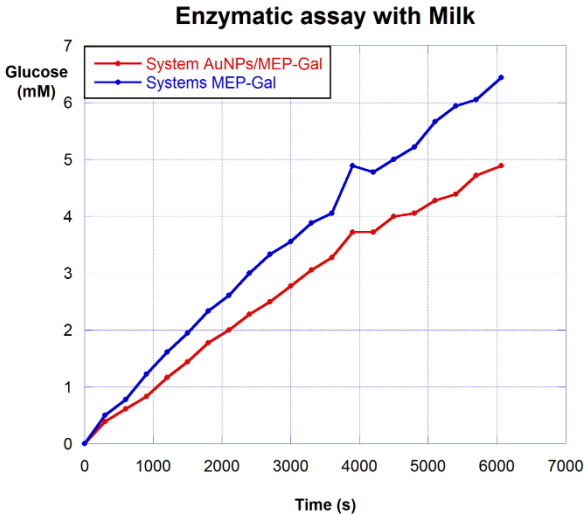

Figure 8.8 – Activity of PM-βGal with (red line) and without gold (blue line) using milk as substrate.

In this case the glucose formation and then the lactose hydrolysis is higher for the free PM-βGal. Then in this case the presence of PM-βGal on **AuNPs** can reduce its activity owing competition of spatially close enzyme, which cannot take advantage by the substrate supply by the **AuNP**s surface as supposed in **ONPG** case.

The contribution of the irradiation to the enzymatic process, was carefully investigated, by determining the kinetics parameters commonly used to characterize the catalytic ability of an enzyme. Its mechanism of action can be described by a Michelis-Menten type kinetic, namely its V_{max} and K_m under given conditions. V_{max} is the highest speed at which an enzyme can work and is reached when all the enzyme molecules are complexed with substrate molecules and the concentration of free enzyme is negligible. K_m or *Michaelis constant* corresponds to the substrate concentration at which half of V_{max} is reached or, as the substrate concentration at which half of the enzyme active sites are filled with substrate molecules. Indeed, it is also considered as a measure of the dissociation constant enzyme-substrate, because to a higher K_m value correspond a weaker enzyme-substrate complex.

The kinetic assays were performed at ca. 0 °C, using systems with increasing concentrations of **ONPG** (from 1mM to 20 mM), following the kinetic for 1 h, by the absorption at 420 nm, of an aliquot of the system picked up each 5 min. In particular, four different kinetics for each **ONPG** concentration were carried out,

The couple of systems labelled **A** and **B** are related to systems with and without **AuNP**s respectively, subjected to laser irradiation; whereas those labelled **C** and **D** refer to the same former systems, but which kinetics is carried out in the dark without irradiation. In such a way it was possible to have a double reference system, taking into account the effect due to irradiation with and without presence of **AuNP**s.

From the trend obtained by the kinetics at different **ONPG** concentrations, the variation of V_i were calculated considering the first linear portion of each kinetic, in which the substrate concentration is highest and all enzyme molecule can be considered complexed and then work at the maximum speed.

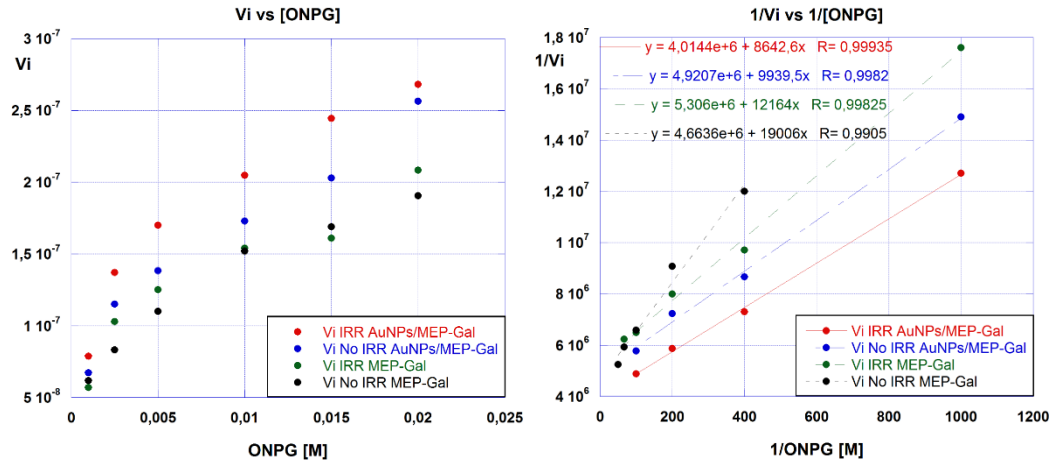

Figure 8.9 – Trend of V_i vs [**ONPG**] (left); trend of $1/V_i$ vs 1/[**ONPG**] (right)

After that as shown in the Figure 8.9, using the method of the *double-reciprocal* by plotting $1/V_i$ vs 1/[**ONPG**] it was possible to obtain K_m and V_{max} from the slope and intercept of the resulted linear trend, which results are summarized in the Table 8.1.

Table 8.1 – Michelis-Menten parameters of the kinetics

[ONPG] M	System (A)	System (B)	System (C)	System (D)
K_m/V_{max}	8642.6	12164	9939.5	19006
$1/V_{max}$	$4.01 \cdot 10^{6}$	$5.31 \cdot 10^{6}$	$4.92 \cdot 10^{6}$	$4.66 \cdot 10^{6}$
$1/K_m$	$4.64 \cdot 10^{2}$	$4.36 \cdot 10^{2}$	$4.95 \cdot 10^{2}$	$2.45 \cdot 10^{2}$
V_{max} (M*s^{-1})	$2.49 \pm 0.13 \cdot 10^{-7}$	$1.88 \pm 0.09 \cdot 10^{-7}$	$2.03 \pm 0.11 \cdot 10^{-7}$	$2.14 \pm 0.11 \cdot 10^{-7}$
K_m (M)	$2.15 \pm 0.11 \cdot 10^{-3}$	$2.29 \pm 0.12 \cdot 10^{-3}$	$2.02 \pm 0.11 \cdot 10^{-3}$	$4.08 \pm 0.21 \cdot 10^{-3}$

The analysis of the trend related to V_i vs the **ONPG** concentration, and also the slightly higher V_{max} value of system **A** with respect to the **B** system, give a first prove of concept of the **AuNP**s-mediated thermal activation of βGal at low temperature under light irradiation. However, the data do not show strong enhancement in activity and often are not so easy to rationalized as for example in the case of V_{max} related to **C** and **D** systems, namely not irradiated systems, which

are closer to the V_{max} of system A. On passing to the K_m values the data related to **A** and **C** systems, namely those in presence of **AuNP**s, have a slightly lower values with respect to the others, suggesting a more stable interaction between enzyme and substrate in presence of **AuNP**s, which could be interpreted as a partial confirmation of the supposed **ONPG - AuNP**s surface interaction. Nevertheless, also in this case the observed differences are fairly low and then, variation due to random fluctuation cannot be excluded a priori. As matter of fact, the absence of marked variation could be due to several factor, which might affect the kinetic process, and can be divided from one side in the nature of the component of systems used and in the other side on the setup used to carry out the kinetics.

Regarding to the first aspect the use on **AuNP**s with a diameter of few nanometers can reduce their ability to convert light in localized heat, which as stated before, increase with the second power of **AuNP**s radius. Moreover, the use of βGal as target enzyme, which possesses a certain extent of activity at low temperature as well, could cause a progressive increase in activity upon little increase of temperature, due to the **AuNP**s hiding its real enhancement effect. In the case of thermophilic enzymes indeed, the presence of a threshold temperature which enable its activation, highlights the thermal contribution of **AuNP**s boosting the enzyme activity as it was recently shown by Wong et al., which have studied the **AuNP**s-mediated light activation of *Aeropyrum pernix glucokinase* as model thermophilic enzyme.[407]

On passing to the set up used to performing the kinetics, the main aspect that can be considered are the irradiation power and the temperature of the bulk medium. Indeed, the irradiation power used, around 16 W/cm^2, it could not be enough to establish the necessary thermal gradient to activate the βGal on the **AuNP**s surface or, keeping in mind the low temperature of the bulk medium, a rapid dissipation of the formed heat could occur joined with the reduction of **ONPG** diffusion as previously depicted. Finally, another important aspect to take into account is that would be necessary to perform the kinetics for a longer period of time, indeed as it is possible to see in Figure 8.9 the curves of V_i vs **ONPG** do not never reach a plateau, indicating that the enzyme is not working at the highest velocity.

8.3 - Experimental section

*Synthesis of **βCD(SH)$_7$** capped **AuNP**s*

The **βCD(SH)$_7$** was prepared and purified according to literature.[409] **AuNP**s capped with **βCD(SH)$_7$** were synthesized following the one pot process reported by Kaifer et al.[62] In particular two systems **A** and **B** with a different Au/**βCD(SH)$_7$** equivalent ratio, namely 1:1 and 1:0.4 were prepared. In a round bottom flask of 100 mL, 60 mg ($1.52 \cdot 10^{-4}$ mol) of

$HAuCl_4 \cdot 3H_2O$ were solubilized with 20 mL of DMSO. To the resulted yellow solution, 20 mL of soon before prepared DMSO solution containing the proper amount of **βCD(SH)$_7$** and 75.5 g ($2 \cdot 10^{-3}$mol) were quickly added. The solution turns instantaneously to a dark brown-purple pseudo-solution, which was left stirring at r.t.

After 24 hours, the solution was centrifuged for 5 min at 4000 rpm and the resulted pellet of **AuNP**s was washed twice with 30 ml of DMSO/CH_3CN 1:1 and 30 ml of EtOH, then **AuNP**s were collected by centrifugation for 15 min at 4000 rpm and dried under vacuum at 60 °C overnight. At the end for system **A** and **B**, 66 mg and 51 mg of a dark powder were obtained.

β-Galactosidase purification

β-Galactosidase was obtained by dialysis of Aldrich Lactozyme solution. In particular, 10.5 mL of this solution was dialyzed at 4 °C using a 10 kDa CO membrane in 2 L of K_2HPO_4 0.1 M, NaCl 0.1 M, $MgCl_2$ 5 mM buffer pH 6,5 for 21 h, changing the buffer after 15 h. At the end of dialysis 16.07 mL of βGal solution were collected, which concentration (4.1 ± 0.14 mg/mL) was assessed by Bradford method using BSA as reference.

Acrylamide based polymer (AP) - βGal conjugation (PM-βGal)

In a 100 mL round bottom flask, 20.2 mg ($1{,}74 \cdot 10^{-6}$ mol) of AP was solubilized using 20 mL of MES buffer (2-(*N*-morpholino)-ethanesulfonic acid, 5mM, pH 6.1), then to the clear solution obtained, 8.2 mg ($4.2 \cdot 10^{-5}$mol) of EDC and 21.8 mg ($1 \cdot 10^{-4}$mol) of NHS were added under stirring. The solution was left stirring at r.t. for 15 min. After that the recovered solution (19.9 mL) was dialyzed at 4 °C using a 3.5 kDa CO membrane in 2L of MES buffer pH 6 for 4 h, changing the buffer after 90 min. After dialysis 20.7 mL of activated AP were recovered. It's necessary to use the activated MEP as soon as possible after dialysis to reduce hydrolysis process.

To 207 µL of this solution were added 2 mL of a βGal solution 4.1 mg/mL then the same total volume of phosphate buffer 0.1 M, pH 7.5 was added. The resulting solution (that should have a pH near 7) was left stirring for 2 h at r.t. Whereupon the solution was dialyzed at 4 °C using a 10 kDa CO membrane in 2 L of K_2HPO_4 0.1 M, $MgCl_2$ 5 mM buffer pH 7 for 20 h.

After 13 h buffer was change and dialysis was continued for others 6 h; at the end 4.1 mL of PM-βGal solution were collected, and considering the starting amount (4.4 mL) it was assumed that haven't been any volume variation after dialysis and the difference is only due to little loss of solution during transfer. Then, the resulted PM-βGal solution should have a concentration of 1.86 mg/mL.

β-Galactosidase activity assays

The activity assays were carried out using systems with a final volume of 200 µL constituted by 100 µL of βGal solution and 100 µL of **ONPG** solution, both with the desired concentration. After the separate pre-warming at 40 °C for 2 min, the components were mixed and stirred at 650 rpm for 5 min at the same temperature. At this point the reaction was stopped by adding 200 µL of 1M Na_2CO_3 solution, and absorbance was measured at 420 nm, using a BioTeck Instruments Synergy H1 hybrid multi-mode Microplate reader. Then starting from the **ONP** concentration, calculated using an **ONP** standard curve as reference, and considering the amount of βGal used and the reaction time its activity was calculated. The same protocol was followed in the case on irradiated systems, with the difference that the systems, dive in ice, were irradiated for 30' before to stop the reaction, with a green laser (equipment of an Accurion Ellipsometer Nanofilm_ep3, λ: 501,3 nm, distance of 3,5 cm), which considering the 2 mm diameters of the green spot above the surface of the sample have an irradiation of 16 W/cm^2.

Kinetics experiments

The systems used for the kinetic assays, were designed in order to have a final volume of 1.4 mL, in such a way to have enough sample volume to pick up an aliquot of 100 µL every 5 min for 1h to follow the [**ONP**] variation after addition of 100 µL of Na_2CO_3 1M and measuring absorbance at 420 nm. Each pair of systems with the same composition (**A**-**C** and **B**-**D**), which differ between them only for the exposition to irradiation, were prepared starting from the same stock solution, freshly prepared before each pair of kinetics. In particular, for the systems with **AuNP**s the stock solution was prepared by mixing 150 µL of **AuNP**s solution (type **A**; C: 1mg/mL), 150 µL of PM-βGal (C: 10 µg/mL) and 1.2 mL of activity buffer (K_2HPO_4 0.1 M; $MgCl_2$ 5 mM; pH 6.5), in order to have **AuNP**s/PM-βGal 100/1(w/w) ratio. This system was then split to give two identical systems constituted by 700 µL of the stock system and 700 µL of **ONPG** solution at the desired concentration, in such a way to have a final PM-βGal concentration of 0.5 µg/mL. The kinetics of the two systems was carried out simultaneously (but with certain delay in order to avoid overlapping) with and without irradiation respectively. On passing to **B** and **D** systems, these were prepared following the same protocol with the difference that in this case the stock solution was prepared by mixing 150 µL of PM-βGal (C: 10 µg/mL) and 1.35 mL of activity buffer. Obviously for each type of sample the corresponding blank, (constituted by **AuNP**s, activity buffer and **ONPG** for **A** and **C** systems, and by activity buffer and **ONPG** for **B** and **D**), were used.

- 9 -

CONCLUSIONS

Polyaminocyclodextrins (**amCD**s) were synthesized following a straightforward protocol, relying on the nucleophilic displacement of bromine atoms on the cyclodextrin scaffold by the desired polyamine. The NMR and ESI-MS characterizations confirmed that each product is a mixture of differently substituted derivatives. Nevertheless, potentiometric titration enabled to determine the average composition on each mixture. Moreover, this particular feature was not at all an obstacle for the further use and application of **amCD**s derivatives.

At this regard, it was first investigated how the polyamino pendants on the cyclodextrin scaffold could affect its ability to give host-guest complex both as free species and as structural constituents of hyper-reticulated polymers, i.e. nanosponge materials. In both cases, a set of diversely structurated guests was used. As long as the free **amCD**s are concerned, it was observed by polarimetric measurements that the inclusion process is affected by both the pH and the possible presence of electrolytes, and it is regulated by a balancing between the charges of the polyamine pendants and the guest as well. Then, in order to explain the observed trends it is necessary to consider the occurring Coulomb interactions and the conformational restraints.

On passing to the **amCD**-based nanosponges, these systems were easily obtained by solvent-free polymerization of **amCD**s with **BrβCD**, and were characterized by solid-state NMR, FTIR, DSC, porosimetry and potentiometric titration as well, in order to confirm their polymeric and compact structure. Even in this case, the absorption/sequestration properties are strongly pH-dependent, indicating that Coulomb interactions related to the charge status of the polymer lattice and the guest as well mainly affect the absorption equilibrium. By contrast, data suggest that, because the cyclodextrin scaffold is quite stiffly blocked within the polymer lattice, sequestration properties do not benefit of the typical *induced fit effect* operating for free **CD**s. Indeed, it is worth noting that the sequestering of guest molecules tested occur exclusively at level of the cyclodextrin caviteis, as confirmed by solid state NMR of two guest-**amCD** composites.

The presence of the polyamine pendants obviously allows increasing the potential applications of these materials. The "external" binding abilities were preliminarily assessed towards a polyanion model molecule (alginate) and then towards a low molecular weight polynucleotide (pUC19). In particular, **amCD**s revealed a lesser binding ability for pDNA (as accounted for by the N/P values) if compared to the comparable policationic cyclodextrins in literature. Moreover, transformation assays performed on calcium competent (CaCO) *E. coli* cells showed that the presence of **amCD**s seems to hinder the uptake process rather than favouring it. Although the resulted data seem discouraging, it is necessary to highlight that the conformation of the pDNA can itself affect the interaction with **amCD**s, whereas in the case of the transformation assays the presence of Ca^{2+} in the *E. coli* competent cells can interfere with the **amCD**-pDNA complex.

Another important feature of **amCD**s is their ability to act as capping agents for the stabilization of metal nanoparticles. Here this ability was exploited to prepare Ag/**amCD** and Pd/**amCD** nanocomposite systems, by following different synthetic protocols. First, two different Ag/**amCD1** systems were prepared by chemical reduction of Ag^{+} using formaldehyde. Afterward these systems were used as catalysts for the $NaBH_4$ mediated reduction of aromatic nitrocompounds, and a thorough kinetic study of this process was performed. The kinetic trends undoubtedly showed the presence of mixed kinetic order. This was rationalized considering the surface of the catalysts covered by several **amCD** layers, which can be partially removed from the catalyst surface upon reaction condition, as confirmed by UV-vis and TEM evidences. This event gives rise to differently covered region of the catalyst surface, which provide a different catalytic contribution. Experimental results were then rationalized conceiving a mechanistic scheme based on a modified Langmuir-Hinshelwood-type model. Moreover, the non-linear trends of the apparent k_{obs} vs catalyst concentration were also rationalized taking into account the possible interaction between the nitrocompounds and both the **amCD** cavity and the **AgNP** surface. The obtained results show that the presence of a *para* electron-donating group on the organic substrate is necessary to carry out the reduction of nitro group, indicating that **AgNP** surface is indeed electrophilic in nature. Second, Pd/**amCD** systems were prepared and used as particularly effective catalysts for a model Suzuki reaction. Experimental results undoubtedly outline how the preorganization effect provided by the **amCD** has a highly positive outcome on the reaction course. Moreover, it is important to stress that the catalytic systems used provide an effective "homeopathic" catalysis to the process.

Moreover, it was investigated the ability of **amCD**s to support the photochemical synthesis of **AgNP**s, in order to develop a more biocompatible synthetic protocol. The investigation

performed using different light sources, irradiation times and Ag/**amCD** ratios, showed that **amCD**s has a double role, namely acting both as capping agent and sacrificial reducing agent. In fact, together with a primary *s.e.t.* photoreduction process, also a secondary chemical reduction process is involved. This relied on the aldehyde species occurring upon **amCD** photodegradation, which provides a further reduction of Ag^+ ions and allows the growth of the former metal nuclei. The best photoreduction efficiency was obtained for the Ag/**amCD3** 1:2 systems upon 10 min irradiation using common halogen lamp. This type of light source, has revealed as the simultaneous presence of a green and NIR irradiation are necessary in order to support the first and second irradiation process respectively. The more biocompatible **AgNP**s obtained (due also to the use of silver acetate rather than the nitrate salt), were then exploited to investigate their antibacterial properties towards model Gram negative (*E. coli*) and Gram-positive (*K. rhizophila*) strains. The resulted data have shown that the Ag/**amCD3** system has antibacterial properties comparable to the free Ag^+, which can be improved by the presence of ampicillin. Indeed, in the latter case a cooperative effect was observed.

As a final remark, it is worth stressing that the **amCD**s investigated in this work, albeit not pure chemical individuals, have indeed shown almost limitless potential applicabilities. In perspective, it is possible to suppose that in a near future they might find further implementation both in the field of nanosized platforms for catalysis and biomedicine, as well as in the emerging area of nanosponges for both environmental remediation and drug delivery.

Bibliography

1. Villiers, A. *Bull. Soc. Chim. Paris* **1891**, *45*.
2. Atwood, J. L.; Lehn, J. M. *Comprehensive Supramolecular Chemistry: Cyclodextrins*; Pergamon, **1996**.
3. Rees, D. A. *J. Chem. Soc. B* **1970**, 877.
4. Szejtli, J. *Chem. Rev.* **1998**, *98*, 1743.
5. Schardinger, F. *Wien. Klin. Wochenschr.* **1904**, *17*.
6. Gotsev, M. G.; Ivanov, P. M. *Int. J. Quantum Chem* **2007**, *107*, 1657.
7. Ivanov, P. *J. Mol. Struct.* **2012**, *1009*, 3.
8. Saenger, W.; Jacob, J.; Gessler, K.; Steiner, T.; Hoffmann, D.; Sanbe, H.; Koizumi, K.; Smith, S. M.; Takaha, T. *Chem. Rev.* **1998**, *98*, 1787.
9. Nakagawa, T.; Ueno, K.; Kashiwa, M.; Watanabe, J. *Tetrahedron Lett.* **1994**, *35*, 1921.
10. Lipkowitz, K. B. *Chem. Rev.* **1998**, *98*, 1829.
11. Lichtenthaler, F. W.; Immel, S. *Liebigs Annalen* **1996**, *1996*, 27.
12. Sakurai, M.; Kitagawa, M.; Hoshi, H.; Inoue, Y.; Chûjô, R. *Carbohydr. Res.* **1990**, *198*, 181.
13. Szente, L.; Szejtli, J. *Adv. Drug. Del. Rev.* **1999**, *36*, 17.
14. Connors, K. A. *Chem. Rev.* **1997**, *97*, 1325.
15. Rekharsky, M. V.; Inoue, Y. *Chem. Rev.* **1998**, *98*, 1875.
16. Tabushi, I.; Kiyosuke, Y.; Sugimoto, T.; Yamamura, K. *J. Am. Chem. Soc.* **1978**, *100*, 916.
17. Loftsson, T.; Duchêne, D. *Int. J. Pharm.* **2007**, *329*, 1.
18. Uekama, K.; Hirayama, F.; Irie, T. *Chem. Rev.* **1998**, *98*, 2045.
19. Malton, P. J.; Holland, L. A. M.; Rizzi, G.; Heltovics, G.; Google Patents: **2000**.
20. Foley, P. R.; Kaiser, C. E.; Sadler, J. D.; Burckhardt, E. E.; Liu, Z.; Google Patents: **2001**.
21. Astray, G.; Gonzalez-Barreiro, C.; Mejuto, J. C.; Rial-Otero, R.; Simal-Gándara, J. *Food Hydrocolloids* **2009**, *23*, 1631.
22. Li, S.; Purdy, W. C. *Chem. Rev.* **1992**, *92*, 1457.
23. Hedges, A. R. *Chem. Rev.* **1998**, *98*, 2035.
24. Del Valle, E. M. M. *Process Biochem.* **2004**, *39*, 1033.
25. Puglisi, G.; Fresta, M.; Ventura, C. A. *J. Colloid Interf. Sci.* **1996**, *180*, 542.
26. Nakanishi, K.; Nadai, T.; Masada, M.; Miyajima, K. *Chem. Pharm. Bull.* **1992**, *40*, 1252.
27. Zidovetzki, R.; Levitan, I. *Biochim. Biophys. Acta* **2007**, *1768*, 1311.
28. Rodal, S. K.; Skretting, G.; Garred, Ø.; Vilhardt, F.; van Deurs, B.; Sandvig, K. *Mol. Biol. Cell* **1999**, *10*, 961.
29. Szejtli, J.; Cserháti, T.; Szögyi, M. *Carbohydr. Polym.* **1986**, *6*, 35.
30. Tabushi, I.; Mizutani, T. *Tetrahedron* **1987**, *43*, 1439.
31. Liu, L.; Guo, Q.-X. *J. Incl. Phenom. Macrocycl. Chem.* **2002**, *42*, 1.
32. Saenger, W.; Noltemeyer, M.; Manor, P. C.; Hingerty, B.; Klar, B. *Bioorg. Chem.* **1976**, *5*, 187.
33. Rekharsky, M. V.; Yamamura, H.; Kawai, M.; Inoue, Y. *J. Org. Chem.* **2003**, *68*, 5228.
34. Rekharsky, M. V.; Inoue, Y. *J. Am. Chem. Soc.* **2002**, *124*, 813.
35. Lo Meo, P.; D'Anna, F.; Riela, S.; Gruttadauria, M.; Noto, R. *Tetrahedron* **2009**, *65*, 2037.
36. Rekharsky, M.; Inoue, Y. *J. Am. Chem. Soc.* **2000**, *122*, 4418.
37. Lo Meo, P.; D'Anna, F.; Gruttadauria, M.; Riela, S.; Noto, R. *Tetrahedron* **2004**, *60*, 9099.
38. Rekharsky, M. V.; Mayhew, M. P.; Goldberg, R. N.; Ross, P. D.; Yamashoji, Y.; Inoue, Y. *J. Phys. Chem. B* **1997**, *101*, 87.
39. Wedig, M.; Laug, S.; Christians, T.; Thunhorst, M.; Holzgrabe, U. *J. Pharm. Biomed. Anal.* **2002**, *27*, 531.
40. Lo Meo, P.; D'Anna, F.; Riela, S.; Gruttadauria, M.; Noto, R. *Org. Biomol. Chem.* **2003**, *1*, 1584.
41. Khan, A. R.; Forgo, P.; Stine, K. J.; D'Souza, V. T. *Chem. Rev.* **1998**, *98*, 1977.
42. Jicsinsky, L. F., E.; Hashimoto, H.; Ueno, A. In *Comprehensive Supramolecular Chemistry*; Oxford, P., Ed. **1996**; Vol. 3.
43. Takahashi, K. *Chem. Rev.* **1998**, *98*, 2013.
44. Bricout, H.; Hapiot, F.; Ponchel, A.; Tilloy, S.; Monflier, E. *Sustainability* **2009**, *1*, 924.
45. Breslow, R.; Dong, S. D. *Chem. Rev.* **1998**, *98*, 1997.
46. Singh, M.; Sharma, R.; Banerjee, U. C. *Biotechnol. Adv.* **2002**, *20*, 341.
47. Jullien, L.; Canceill, J.; Valeur, B.; Bardez, E.; Lefèvre, J.-P.; Lehn, J.-M.; Marchi-Artzner, V.; Pansu, R. *J. Am. Chem. Soc.* **1996**, *118*, 5432.
48. Lipkowitz, K. B.; Coner, R.; Peterson, M. A.; Morreale, A.; Shackelford, J. *J. Org. Chem.* **1998**, *63*, 732.
49. Tomalia, D. A.; Baker, H.; Dewald, J.; Hall, M.; Kallos, G.; Martin, S.; Roeck, J.; Ryder, J.; Smith, P. *Polym. J.* **1985**, *17*, 117.
50. Abbasi, E.; Aval, S. F.; Akbarzadeh, A.; Milani, M.; Nasrabadi, H. T.; Joo, S. W.; Hanifehpour, Y.; Nejati-Koshki, K.; Pashaei-Asl, R. *Nanoscale Res. Lett.* **2014**, *9*, 247.
51. Kesharwani, P.; Jain, K.; Jain, N. K. *Prog. Polym. Sci.* **2014**, *39*, 268.

52. Hsu, H.-J.; Bugno, J.; Lee, S.-r.; Hong, S. *Wiley Interdisciplinary Reviews: Nanomedicine and Nanobiotechnology* **2016**, n/a.
53. Astruc, D.; Boisselier, E.; Ornelas, C. *Chem. Rev.* **2010**, *110*, 1857.
54. Arima, H.; Motoyama, K.; Higashi, T. *Pharmaceutics* **2012**, *4*, 130.
55. Díaz-Moscoso, A.; Le Gourriérec, L.; Gómez-García, M.; Benito, J. M.; Balbuena, P.; Ortega-Caballero, F.; Guilloteau, N.; Di Giorgio, C.; Vierling, P.; Defaye, J.; Ortiz Mellet, C.; García Fernández, J. M. *Chem. Eur. J.* **2009**, *15*, 12871.
56. Srinivasachari, S.; Fichter, K. M.; Reineke, T. M. *J. Am. Chem. Soc.* **2008**, *130*, 4618.
57. Meldal, M.; Tornøe, C. W. *Chem. Rev.* **2008**, *108*, 2952.
58. Lallana, E.; Sousa-Herves, A.; Fernandez-Trillo, F.; Riguera, R.; Fernandez-Megia, E. *Pharm. Res.* **2012**, *29*, 1.
59. Faugeras, P.-A.; Boëns, B.; Elchinger, P.-H.; Brouillette, F.; Montplaisir, D.; Zerrouki, R.; Lucas, R. *Eur. J. Org. Chem.* **2012**, *2012*, 4087.
60. Denicourt-Nowicki, A.; Roucoux, A. *Curr. Org. Chem.* **2010**, *14*, 1266.
61. Noël, S.; Léger, B.; Ponchel, A.; Philippot, K.; Denicourt-Nowicki, A.; Roucoux, A.; Monflier, E. *Catal. Today* **2014**, *235*, 20.
62. Liu, J.; Ong, W.; Román, E.; Lynn, M. J.; Kaifer, A. E. *Langmuir* **2000**, *16*, 3000.
63. Liu, J.; Ong, W.; Kaifer, A. E.; Peinador, C. *Langmuir* **2002**, *18*, 5981.
64. Alvarez, J.; Liu, J.; Roman, E.; Kaifer, A. E. *Chem. Commun.* **2000**, 1151.
65. Lo Meo, P.; D'Anna, F.; Gruttadauria, M.; Riela, S.; Noto, R. *Carbohydr. Res.* **2012**, *347*, 32.
66. Gorin, B. I.; Riopelle, R. J.; Thatcher, G. R. J. *Tetrahedron Lett.* **1996**, *37*, 4647.
67. Gadelle, A.; Defaye, J. *Angew. Chem. Int. Ed. Eng.* **1991**, *30*, 78.
68. Jager, M.; Schubert, S.; Ochrimenko, S.; Fischer, D.; Schubert, U. S. *Chem. Soc. Rev.* **2012**, *41*, 4755.
69. Sabín, J.; Vázquez-Vázquez, C.; Prieto, G.; Bordi, F.; Sarmiento, F. *Langmuir* **2012**, *28*, 10534.
70. Signori, A. M.; Santos, K. d. O.; Eising, R.; Albuquerque, B. L.; Giacomelli, F. C.; Domingos, J. B. *Langmuir* **2010**, *26*, 17772.
71. Santos, K. d. O.; Elias, W. C.; Signori, A. M.; Giacomelli, F. C.; Yang, H.; Domingos, J. B. *J. Phys. Chem. C* **2012**, *116*, 4594.
72. Fröhlich, T.; Edinger, D.; Kläger, R.; Troiber, C.; Salcher, E.; Badgujar, N.; Martin, I.; Schaffert, D.; Cengizeroglu, A.; Hadwiger, P.; Vornlocher, H.-P.; Wagner, E. *J. Controlled Release* **2012**, *160*, 532.
73. Yue, Y.; Jin, F.; Deng, R.; Cai, J.; Dai, Z.; Lin, M. C. M.; Kung, H.-F.; Mattebjerg, M. A.; Andresen, T. L.; Wu, C. *J. Controlled Release* **2011**, *152*, 143.
74. Daniel, M.-C.; Grow, M. E.; Pan, H.; Bednarek, M.; Ghann, W. E.; Zabetakis, K.; Cornish, J. *New J. Chem.* **2011**, *35*, 2366.
75. Hayakawa, K.; Yoshimura, T.; Esumi, K. *Langmuir* **2003**, *19*, 5517.
76. Esumi, K.; Isono, R.; Yoshimura, T. *Langmuir* **2004**, *20*, 237.
77. Fernandez, L.; Gonzalez, M.; Cerecetto, H.; Santo, M.; Silber, J. J. *Supramol. Chem.* **2006**, *18*, 633.
78. Takahashi, T.; Hirose, J.; Kojima, C.; Harada, A.; Kono, K. *Bioconjugate Chem.* **2007**, *18*, 1163.
79. Endo, T.; Yoshimura, T.; Esumi, K. *J. Colloid Interf. Sci.* **2005**, *286*, 602.
80. Gittins, P. J.; Twyman, L. J. *Supramol. Chem.* **2003**, *15*, 5.
81. Liu, Z.; Wang, X.; Wu, H.; Li, C. *J. Colloid Interf. Sci.* **2005**, *287*, 604.
82. Ouyang, D.; Zhang, H.; Parekh, H. S.; Smith, S. C. *Biophys. Chem.* **2011**, *158*, 126.
83. Patil, M. L.; Zhang, M.; Minko, T. *ACS Nano* **2011**, *5*, 1877.
84. Patil, M. L.; Zhang, M.; Taratula, O.; Garbuzenko, O. B.; He, H.; Minko, T. *Biomacromolecules* **2009**, *10*, 258.
85. Crooks, R. M.; Zhao, M.; Sun, L.; Chechik, V.; Yeung, L. K. *Acc. Chem. Res.* **2001**, *34*, 181.
86. Esumi, K.; Hosoya, T.; Suzuki, A.; Torigoe, K. *J. Colloid Interf. Sci.* **2000**, *226*, 346.
87. Scott, R. W. J.; Wilson, O. M.; Crooks, R. M. *J. Phys. Chem. B* **2005**, *109*, 692.
88. Pavan, G. M.; Posocco, P.; Tagliabue, A.; Maly, M.; Malek, A.; Danani, A.; Ragg, E.; Catapano, C. V.; Pricl, S. *Chem. Eur. J.* **2010**, *16*, 7781.
89. Decroocq, C.; Rodríguez-Lucena, D.; Russo, V.; Mena Barragán, T.; Ortiz Mellet, C.; Compain, P. *Chem. Eur. J.* **2011**, *17*, 13825.
90. Mendez-Ardoy, A.; Gomez-Garcia, M.; Mellet, C. O.; Sevillano, N.; Dolores Giron, M.; Salto, R.; Santoyo-Gonzalez, F.; Garcia Fernandez, J. M. *Org. Biomol. Chem.* **2009**, *7*, 2681.
91. Ortiz Mellet, C.; Benito, J. M.; García Fernández, J. M. *Chem. Eur. J.* **2010**, *16*, 6728.
92. Deng, J.; Li, N.; Mai, K.; Yang, C.; Yan, L.; Zhang, L.-M. *J. Mater. Chem.* **2011**, *21*, 5273.
93. Nijenhuis, W. F.; Buitenhuis, E. G.; De Jong, F.; Sudholter, E. J. R.; Reinhoudt, D. N. *J. Am. Chem. Soc.* **1991**, *113*, 7963.
94. Schneider, H.-J. *Angew. Chem. Int. Ed.* **2009**, *48*, 3924.
95. Liu, Y.; Li, C.-J.; Guo, D.-S.; Pan, Z.-H.; Li, Z. *Supramol. Chem.* **2007**, *19*, 517.
96. Danil de Namor, A. F.; Cleverley, R. M.; Zapata-Ormachea, M. L. *Chem. Rev.* **1998**, *98*, 2495.
97. D'Anna, F.; Meo, P. L.; Riela, S.; Gruttadauria, M.; Noto, R. *Tetrahedron* **2001**, *57*, 6823.
98. Lo Meo, P.; D'Anna, F.; Riela, S.; Gruttadauria, M.; Noto, R. *Tetrahedron* **2002**, *58*, 6039.

99. Meo, P. L.; D'Anna, F.; Riela, S.; Gruttadauria, M.; Noto, R. *J. Incl. Phenom. Macrocycl. Chem.* **2011**, *71*, 121.
100. Lo Meo, P.; D'Anna, F.; Riela, S.; Gruttadauria, M.; Noto, R. *Tetrahedron Lett.* **2006**, *47*, 9099.
101. Lo Meo, P.; D'Anna, F.; Riela, S.; Gruttadauria, M.; Noto, R. *Tetrahedron* **2007**, *63*, 9163.
102. Lo Meo, P.; D'Anna, F.; Gruttadauria, M.; Riela, S.; Noto, R. *Tetrahedron* **2009**, *65*, 10413.
103. Bonora, G. M.; Fornasier, R.; Scrimin, P.; Tonellato, U. *J. Chem. Soc. Perkin Trans. 2* **1985**, 367.
104. Lu, T.-X.; Zhand, D.-B.; Dong, S.-J. *J. Chem. Soc. Faraday Trans. 2* **1989**, *85*, 1439.
105. Schneider, H.-J.; Hacket, F.; Rüdiger, V.; Ikeda, H. *Chem. Rev.* **1998**, *98*, 1755.
106. Tee, O. S.; Mazza, C.; Du, X. X. *J. Org. Chem.* **1990**, *55*, 3603.
107. Lander, E. S.; et al. *Nature* **2001**, *409*, 860.
108. Venter, J. C.; et al. *Science* **2001**, *291*, 1304.
109. Friedmann, T.; Roblin, R. *Science* **1972**, *175*, 949.
110. Sheridan, C. *Nat Biotech* **2011**, *29*, 121.
111. Fischer, A.; Hacein-Bey-Abina, S.; Cavazzana-Calvo, M. *Nat Immunol* **2010**, *11*, 457.
112. Mintzer, M. A.; Simanek, E. E. *Chem. Rev.* **2009**, *109*, 259.
113. Jafari, M.; Soltani, M.; Naahidi, S.; Karunaratne, D. N.; Chen, P. *Curr. Med. Chem.* **2012**, *19*, 197.
114. Mastrobattista, E.; Bravo, S. A.; van der Aa, M.; Crommelin, D. J. A. *Drug Discovery Today: Technologies* **2005**, *2*, 103.
115. Guo, X.; Huang, L. *Acc. Chem. Res.* **2012**, *45*, 971.
116. Srinivas, R.; Samanta, S.; Chaudhuri, A. *Chem. Soc. Rev.* **2009**, *38*, 3326.
117. Bhattacharya, S.; Bajaj, A. *Chem. Commun.* **2009**, 4632.
118. Nimesh, S.; Gupta, N.; Chandra, R. *J. Biomed. Nanotechnol.* **2011**, *7*, 504.
119. Putnam, D. *Nat Mater* **2006**, *5*, 439.
120. Tros de Ilarduya, C.; Sun, Y.; Düzgüneş, N. *Eur. J. Pharm. Sci.* **2010**, *40*, 159.
121. Mellet, C. O.; Fernandez, J. M. G.; Benito, J. M. *Chem. Soc. Rev.* **2011**, *40*, 1586.
122. García Fernández José, M.; Benito Juan, M.; Ortiz Mellet, C. In *Pure Appl. Chem.* **2013**; Vol. 85, p 1825.
123. Lai, W.-F. *Biomaterials* **2014**, *35*, 401.
124. Duval, R. E.; Clarot, I.; Dumarcay-Charbonnier, F.; Fontanay, S.; Marsura, A. *Annales Pharmaceutiques Françaises* **2012**, *70*, 360.
125. Hu, Y.; Yuan, W.; Zhao, N.-N.; Ma, J.; Yang, W.-T.; Xu, F.-J. *Biomaterials* **2013**, *34*, 5411.
126. Croyle, M. A.; Roessler, B. J.; Hsu, C.-P.; Sun, R.; Amidon, G. L. *Pharm. Res.* **1998**, *15*, 1348.
127. Loh, X. J.; Wu, Y.-L. *Chem. Commun.* **2015**, *51*, 10815.
128. Aachmann, F. L.; Aune, T. E. V. *Appl. Microbiol. Biotechnol.* **2009**, *83*, 589.
129. Hu, Y.; Zhao, N.; Yu, B.; Liu, F.; Xu, F.-J. *Nanoscale* **2014**, *6*, 7560.
130. Cryan, S.-A.; Holohan, A.; Donohue, R.; Darcy, R.; O'Driscoll, C. M. *Eur. J. Pharm. Sci.* **2004**, *21*, 625.
131. van de Manakker, F.; Vermonden, T.; van Nostrum, C. F.; Hennink, W. E. *Biomacromolecules* **2009**, *10*, 3157.
132. Yhaya, F.; Gregory, A. M.; Stenzel, M. H. *Aust. J. Chem.* **2010**, *63*, 195.
133. Srinivasachari, S.; Reineke, T. M. *Biomaterials* **2009**, *30*, 928.
134. Huang, H.; Tang, G.; Wang, Q.; Li, D.; Shen, F.; Zhou, J.; Yu, H. *Chem. Commun.* **2006**, 2382.
135. Davis, M. E. *Molecular Pharmaceutics* **2009**, *6*, 659.
136. Reineke, T. M.; Davis, M. E. *Bioconjugate Chem.* **2003**, *14*, 247.
137. Reineke, T. M.; Davis, M. E. *Bioconjugate Chem.* **2003**, *14*, 255.
138. Davis, M. E.; Bellocq, N. C. *J. Incl. Phenom. Macrocycl. Chem.* **2002**, *44*, 17.
139. Huang, H.; Yu, H.; Li, D.; Liu, Y.; Shen, F.; Zhou, J.; Wang, Q.; Tang, G. *Int. J. Mol. Sci.* **2008**, *9*, 2278.
140. Burckbuchler, V.; Wintgens, V.; Leborgne, C.; Lecomte, S.; Leygue, N.; Scherman, D.; Kichler, A.; Amiel, C. *Bioconjugate Chem.* **2008**, *19*, 2311.
141. Davis, M. E.; Pun, S. H.; Bellocq, N. C.; Reineke, T. M.; Popielarski, S. R.; Mishra, S.; Heidel, J. D. *Curr. Med. Chem.* **2004**, *11*, 179.
142. Popielarski, S. R.; Mishra, S.; Davis, M. E. *Bioconjugate Chem.* **2003**, *14*, 672.
143. Pun, S. H.; Bellocq, N. C.; Liu, A.; Jensen, G.; Machemer, T.; Quijano, E.; Schluep, T.; Wen, S.; Engler, H.; Heidel, J.; Davis, M. E. *Bioconjugate Chem.* **2004**, *15*, 831.
144. Redondo, J. A.; Martínez-Campos, E.; Plet, L.; Pérez-Perrino, M.; Navarro, R.; Corrales, G.; Pandit, A.; Reinecke, H.; Gallardo, A.; López-Lacomba, J. L.; Fernández-Mayoralas, A.; Elvira, C. *Macromol. Rapid Commun.* **2016**, *37*, 575.
145. Zhang, M.; Xiong, Q.; Wang, Y.; Zhang, Z.; Shen, W.; Liu, L.; Wang, Q.; Zhang, Q. *Polym. Chem.* **2014**, *5*, 4670.
146. Li, W.; Chen, L.; Huang, Z.; Wu, X.; Zhang, Y.; Hu, Q.; Wang, Y. *Org. Biomol. Chem.* **2011**, *9*, 7799.
147. Arima, H.; Chihara, Y.; Arizono, M.; Yamashita, S.; Wada, K.; Hirayama, F.; Uekama, K. *J. Controlled Release* **2006**, *116*, 64.
148. Arima, H.; Kihara, F.; Hirayama, F.; Uekama, K. *Bioconjugate Chem.* **2001**, *12*, 476.
149. Kihara, F.; Arima, H.; Tsutsumi, T.; Hirayama, F.; Uekama, K. *Bioconjugate Chem.* **2002**, *13*, 1211.
150. Kihara, F.; Arima, H.; Tsutsumi, T.; Hirayama, F.; Uekama, K. *Bioconjugate Chem.* **2003**, *14*, 342.
151. Menuel, S.; Duval, R. E.; Cuc, D.; Mutzenhardt, P.; Marsura, A. *New J. Chem.* **2007**, *31*, 995.

152. Menuel, S.; Fontanay, S.; Clarot, I.; Duval, R. E.; Diez, L.; Marsura, A. *Bioconjugate Chem.* **2008**, *19*, 2357.
153. Tsutsumi, T.; Hirayama, F.; Uekama, K.; Arima, H. *J. Controlled Release* **2007**, *119*, 349.
154. Zhang, W.; Chen, Z.; Song, X.; Si, J.; Tang, G. *Technology in Cancer Research & Treatment* **2008**, *7*, 103.
155. Zinselmeyer, B. H.; Mackay, S. P.; Schatzlein, A. G.; Uchegbu, I. F. *Pharm. Res.* **2002**, *19*, 960.
156. Arima, H.; Motoyama, K.; Higashi, T. *Adv. Drug. Del. Rev.* **2013**, *65*, 1204.
157. Li, J.; Loh, X. J. *Adv. Drug. Del. Rev.* **2008**, *60*, 1000.
158. Shuai, X.; Merdan, T.; Unger, F.; Kissel, T. *Bioconjugate Chem.* **2005**, *16*, 322.
159. Wenz, G.; Han, B.-H.; Müller, A. *Chem. Rev.* **2006**, *106*, 782.
160. Yang, C.; Wang, X.; Li, H.; Goh, S. H.; Li, J. *Biomacromolecules* **2007**, *8*, 3365.
161. Yang, C.; Li, H.; Wang, X.; Li, J. *J. Biomed. Mat. Res. A* **2009**, *89A*, 13.
162. Yang, C.; Wang, X.; Li, H.; Ling Ding, J.; Yun Wang, D.; Li, J. *Polymer* **2009**, *50*, 1378.
163. Ooya, T.; Choi, H. S.; Yamashita, A.; Yui, N.; Sugaya, Y.; Kano, A.; Maruyama, A.; Akita, H.; Ito, R.; Kogure, K.; Harashima, H. *J. Am. Chem. Soc.* **2006**, *128*, 3852.
164. Yamashita, A.; Yui, N.; Ooya, T.; Kano, A.; Maruyama, A.; Akita, H.; Kogure, K.; Harashima, H. *Nat. Protocols* **2007**, *1*, 2861.
165. Yamashita, A.; Kanda, D.; Katoono, R.; Yui, N.; Ooya, T.; Maruyama, A.; Akita, H.; Kogure, K.; Harashima, H. *J. Controlled Release* **2008**, *131*, 137.
166. Yamashita, A.; Choi, H. S.; Ooya, T.; Yui, N.; Akita, H.; Kogure, K.; Harashima, H. *ChemBioChem* **2006**, *7*, 297.
167. Liu, Y.; Yu, L.; Chen, Y.; Zhao, Y.-L.; Yang, H. *J. Am. Chem. Soc.* **2007**, *129*, 10656.
168. Li, Z.; Yin, H.; Zhang, Z.; Liu, K. L.; Li, J. *Biomacromolecules* **2012**, *13*, 3162.
169. Aggelidou, C.; Mavridis, I. M.; Yannakopoulou, K. *Eur. J. Org. Chem.* **2009**, *2009*, 2299.
170. Bennevault-Celton, V.; Urbach, A.; Martin, O.; Pichon, C.; Guégan, P.; Midoux, P. *Bioconjugate Chem.* **2011**, *22*, 2404.
171. Kong, Y.; Li, W.; Mao, Q.; Wang, Y. *Macromol. Chem. Phys.* **2015**, *216*, 1507.
172. Li, J.; Guo, Z.; Xin, J.; Zhao, G.; Xiao, H. *Carbohydr. Polym.* **2010**, *79*, 277.
173. Ma, D.; Zhang, H.-B.; Chen, Y.-Y.; Lin, J.-T.; Zhang, L.-M. *J. Colloid Interf. Sci.* **2013**, *405*, 305.
174. Mourtzis, N.; Eliadou, K.; Aggelidou, C.; Sophianopoulou, V.; Mavridis, I. M.; Yannakopoulou, K. *Org. Biomol. Chem.* **2007**, *5*, 125.
175. Mourtzis, N.; Paravatou, M.; Mavridis, I. M.; Roberts, M. L.; Yannakopoulou, K. *Chem. Eur. J.* **2008**, *14*, 4188.
176. Yang, C.; Li, H.; Goh, S. H.; Li, J. *Biomaterials* **2007**, *28*, 3245.
177. Nakase, I.; Takeuchi, T.; Tanaka, G.; Futaki, S. *Adv. Drug. Del. Rev.* **2008**, *60*, 598.
178. Wender, P. A.; Galliher, W. C.; Goun, E. A.; Jones, L. R.; Pillow, T. H. *Adv. Drug. Del. Rev.* **2008**, *60*, 452.
179. Futaki, S. *Adv. Drug. Del. Rev.* **2005**, *57*, 547.
180. Mitchell, D. J.; Steinman, L.; Kim, D. T.; Fathman, C. G.; Rothbard, J. B. *J. Pept. Res.* **2000**, *56*, 318.
181. Jiménez Blanco, J. L.; Bootello, P.; Benito, J. M.; Ortiz Mellet, C.; García Fernández, J. M. *J. Org. Chem.* **2006**, *71*, 5136.
182. Bilensoy, E.; Hincal, A. A. *Expert Opin. Drug Del.* **2009**, *6*, 1161.
183. Byrne, C.; Sallas, F.; Rai, D. K.; Ogier, J.; Darcy, R. *Org. Biomol. Chem.* **2009**, *7*, 3763.
184. Diaz-Moscoso, A.; Balbuena, P.; Gomez-Garcia, M.; Ortiz Mellet, C.; Benito, J. M.; Le Gourrierec, L.; Di Giorgio, C.; Vierling, P.; Mazzaglia, A.; Micali, N.; Defaye, J.; Garcia Fernandez, J. M. *Chem. Commun.* **2008**, 2001.
185. Gallego-Yerga, L.; González-Álvarez, M. J.; Mayordomo, N.; Santoyo-González, F.; Benito, J. M.; Ortiz Mellet, C.; Mendicuti, F.; García Fernández, J. M. *Chem. Eur. J.* **2014**, *20*, 6622.
186. Martínez, Á.; Bienvenu, C.; Jiménez Blanco, J. L.; Vierling, P.; Mellet, C. O.; García Fernández, J. M.; Di Giorgio, C. *J. Org. Chem.* **2013**, *78*, 8143.
187. Méndez-Ardoy, A.; Guilloteau, N.; Di Giorgio, C.; Vierling, P.; Santoyo-González, F.; Ortiz Mellet, C.; García Fernández, J. M. *J. Org. Chem.* **2011**, *76*, 5882.
188. Méndez-Ardoy, A.; Urbiola, K.; Aranda, C.; Ortiz-Mellet, C.; García-Fernández, J. M.; Tros de Ilarduya, C. *Nanomedicine* **2011**, *6*, 1697.
189. Villari, V.; Mazzaglia, A.; Darcy, R.; O'Driscoll, C. M.; Micali, N. *Biomacromolecules* **2013**, *14*, 811.
190. Walker, S.; Sofia, M. J.; Kakarla, R.; Kogan, N. A.; Wierichs, L.; Longley, C. B.; Bruker, K.; Axelrod, H. R.; Midha, S.; Babu, S.; Kahne, D. *Proceedings of the National Academy of Sciences of the United States of America* **1996**, *93*, 1585.
191. Walker, S.; Sofia, M. J.; Axelrod, H. R. *Adv. Drug. Del. Rev.* **1998**, *30*, 61.
192. O'Mahony, A. M.; Ogier, J.; Darcy, R.; Cryan, J. F.; O'Driscoll, C. M. *PLOS ONE* **2013**, *8*, e66413.
193. Ortega-Caballero, F.; Mellet, C. O.; Le Gourriérec, L.; Guilloteau, N.; Di Giorgio, C.; Vierling, P.; Defaye, J.; García Fernández, J. M. *Org. Lett.* **2008**, *10*, 5143.
194. Hirsch, A. K. H.; Fischer, F. R.; Diederich, F. *Angew. Chem. Int. Ed.* **2007**, *46*, 338.
195. Fujiwara, T.; Hasegawa, S.; Hirashima, N.; Nakanishi, M.; Ohwada, T. *Biochimica et Biophysica Acta (BBA) - Biomembranes* **2000**, *1468*, 396.
196. Ma, M.; Li, D.; Google Patents: **1998**.

197. Li, D.; Ma, M. *Clean Products and Processes* **2000**, *2*, 112.
198. Trotta, F.; SHENDE, P.; BIASIZZO, M.; Google Patents: **2012**.
199. Chilajwar, S. V.; Pednekar, P. P.; Jadhav, K. R.; Gupta, G. J. C.; Kadam, V. J. *Expert Opin. Drug Del.* **2014**, *11*, 111.
200. Trotta, F.; Cavalli, R.; Tumiatti, W.; Zerbinati, O.; Roggero, C.; Vallero, R.; Google Patents: **2006**.
201. Anandam, S.; Selvamuthukumar, S. *J. Porous Mater.* **2014**, *21*, 1015.
202. Castiglione, F.; Crupi, V.; Majolino, D.; Mele, A.; Panzeri, W.; Rossi, B.; Trotta, F.; Venuti, V. *J. Incl. Phenom. Macrocycl. Chem.* **2013**, *75*, 247.
203. Crupi, V.; Fontana, A.; Giarola, M.; Majolino, D.; Mariotto, G.; Mele, A.; Melone, L.; Punta, C.; Rossi, B.; Trotta, F.; Venuti, V. *J. Raman Spectr.* **2013**, *44*, 1457.
204. Swaminathan, S.; Cavalli, R.; Trotta, F. *Wiley Interdisciplinary Reviews: Nanomedicine and Nanobiotechnology* **2016**, *8*, 579.
205. Swaminathan, S.; Vavia, P. R.; Trotta, F.; Cavalli, R.; Tumbiolo, S.; Bertinetti, L.; Coluccia, S. *J. Incl. Phenom. Macrocycl. Chem.* **2013**, *76*, 201.
206. Trotta, F.; Cavalli, R. *Compos. Interfaces* **2009**, *16*, 39.
207. Trotta, F. In *Cyclodextrins in Pharmaceutics, Cosmetics, and Biomedicine*; John Wiley & Sons, Inc.: **2011**, p 323.
208. Swaminathan, S.; Darandale, S.; Vavia, P. R. *Pharmaceutical Formulation and Quality* **2012**, *14*, 12.
209. Trotta, F.; Zanetti, M.; Cavalli, R. *Beilstein J. Org. Chem.* **2012**, *8*, 2091.
210. Trotta, F.; Tumiatti, W.; Google Patents: **2005**.
211. Morin-Crini, N.; Crini, G. *Prog. Polym. Sci.* **2013**, *38*, 344.
212. Arkas, M.; Allabashi, R.; Tsiourvas, D.; Mattausch, E.-M.; Perfler, R. *Environ. Sci. Technol.* **2006**, *40*, 2771.
213. http://www.nanopinion.eu/sites/default/files/therapeutics_april_2009.pdf.
214. Ansari, K. A.; Vavia, P. R.; Trotta, F.; Cavalli, R. *AAPS PharmSciTech* **2011**, *12*, 279.
215. Cavalli, R.; Donalisio, M.; Bisazza, A.; Civra, A.; Ranucci, E.; Ferruti, P.; Lembo, D. In *Methods Enzymol.*; Nejat, D., Ed.; Academic Press: **2012**; Vol. Volume 509, p 1.
216. Swaminathan, S.; Vavia, P. R.; Trotta, F.; Torne, S. *J. Incl. Phenom. Macrocycl. Chem.* **2007**, *57*, 89.
217. Swaminathan, S.; Pastero, L.; Serpe, L.; Trotta, F.; Vavia, P.; Aquilano, D.; Trotta, M.; Zara, G.; Cavalli, R. *Eur. J. Pharm. Biopharm.* **2010**, *74*, 193.
218. Minelli, R.; Cavalli, R.; Ellis, L.; Pettazzoni, P.; Trotta, F.; Ciamporcero, E.; Barrera, G.; Fantozzi, R.; Dianzani, C.; Pili, R. *Eur. J. Pharm. Sci.* **2012**, *47*, 686.
219. Cavalli, R.; Trotta, F.; Tumiatti, W. *J. Incl. Phenom. Macrocycl. Chem.* **2006**, *56*, 209.
220. Lembo, D.; Swaminathan, S.; Donalisio, M.; Civra, A.; Pastero, L.; Aquilano, D.; Vavia, P.; Trotta, F.; Cavalli, R. *Int. J. Pharm.* **2013**, *443*, 262.
221. S, S.; S, A.; Krishnamoorthy, K.; Rajappan, M. *Journal of pharmacy & pharmaceutical sciences : a publication of the Canadian Society for Pharmaceutical Sciences, Societe canadienne des sciences pharmaceutiques* **2012**, *15*, 103.
222. Seglie, L.; Spadaro, D.; Trotta, F.; Devecchi, M.; Gullino, M. L.; Scariot, V. *Postharv. Biol. Technol.* **2012**, *64*, 55.
223. Alongi, J.; Poskovic, M.; P.M, V.; Frache, A.; Malucelli, G. *Carbohydr. Polym.* **2012**, *88*, 1387.
224. Trotta, F.; Cavalli, R.; Martina, K.; Biasizzo, M.; Vitillo, J.; Bordiga, S.; Vavia, P.; Ansari, K. *J. Incl. Phenom. Macrocycl. Chem.* **2011**, *71*, 189.
225. Liang, W.; Yang, C.; Nishijima, M.; Fukuhara, G.; Mori, T.; Mele, A.; Castiglione, F.; Caldera, F.; Trotta, F.; Inoue, Y. *Beilstein J. Org. Chem.* **2012**, *8*, 1305.
226. Laws, D. D.; Bitter, H.-M. L.; Jerschow, A. *Angew. Chem. Int. Ed.* **2002**, *41*, 3096.
227. Conte, P.; Piccolo, A.; van Lagen, B.; Buurman, P.; Hemminga, M. A. *Solid State Nucl. Magn. Reson.* **2002**, *21*, 158.
228. Lo Meo, P.; Lazzara, G.; Liotta, L.; Riela, S.; Noto, R. *Polym. Chem.* **2014**, *5*, 4499.
229. Kolodziejski, W.; Klinowski, J. *Chem. Rev.* **2002**, *102*, 613.
230. Naito, A.; Ganapathy, S.; McDowell, C. A. *Journal of Magnetic Resonance (1969)* **1982**, *48*, 367.
231. Sipin, S. V.; Grachev, M. K.; Vasyanina, L. K.; Nifant'ev, E. E. *Russ. J. Gen. Chem.* **2006**, *76*, 1958.
232. Fernández, M. D.; Fernández, M. J.; Cobos, M. *J. Mater. Sci.* **2016**, *51*, 3628.
233. Pagacz, J.; Raftopoulos, K. N.; Leszczyńska, A.; Pielichowski, K. *J. Therm. Anal. Calorim.* **2016**, *123*, 1225.
234. Brunauer, S.; Emmett, P. H.; Teller, E. *J. Am. Chem. Soc.* **1938**, *60*, 309.
235. Kruk, M.; Antochshuk, V.; Jaroniec, M.; Sayari, A. *J. Phys. Chem. B* **1999**, *103*, 10670.
236. Buchachenko, A. L. *Russian Chemical Reviews* **2003**, *72*, 375.
237. Delgado, J. L.; Herranz, M. a. A.; Martin, N. *J. Mater. Chem.* **2008**, *18*, 1417.
238. Ginger, D. S.; Zhang, H.; Mirkin, C. A. *Angew. Chem. Int. Ed.* **2004**, *43*, 30.
239. Jin, R.; Zeng, C.; Zhou, M.; Chen, Y. *Chem. Rev.* **2016**, *116*, 10346.
240. Resch-Genger, U.; Grabolle, M.; Cavaliere-Jaricot, S.; Nitschke, R.; Nann, T. *Nat Meth* **2008**, *5*, 763.
241. Soler-Illia, G. J. d. A. A.; Sanchez, C.; Lebeau, B.; Patarin, J. *Chem. Rev.* **2002**, *102*, 4093.
242. Feynman, R., *There's Plenty of Room at the Bottom*. Americal Chemical Society meeting Caltech, **29 December 1959**;

243. Alves, A. K.; Berutti, F. A.; Sánchez, F. A. L. In *Nanostructured Materials for Engineering Applications*; Bergmann, C. P., de Andrade, M. J., Eds.; Springer Berlin Heidelberg: Berlin, Heidelberg, **2011**, p 93.
244. Arico, A. S.; Bruce, P.; Scrosati, B.; Tarascon, J.-M.; van Schalkwijk, W. *Nat Mater* **2005**, *4*, 366.
245. Chen, G.; Roy, I.; Yang, C.; Prasad, P. N. *Chem. Rev.* **2016**, *116*, 2826.
246. Chen, G.; Seo, J.; Yang, C.; Prasad, P. N. *Chem. Soc. Rev.* **2013**, *42*, 8304.
247. Su, S.; Wu, W.; Gao, J.; Lu, J.; Fan, C. *J. Mater. Chem.* **2012**, *22*, 18101.
248. Zhang, Q.; Uchaker, E.; Candelaria, S. L.; Cao, G. *Chem. Soc. Rev.* **2013**, *42*, 3127.
249. Zhang, L.; Webster, T. J. *Nano Today* **2009**, *4*, 66.
250. Wang, X.; Summers, C. J.; Wang, Z. L. *Nano Lett.* **2004**, *4*, 423.
251. Burda, C.; Chen, X.; Narayanan, R.; El-Sayed, M. A. *Chem. Rev.* **2005**, *105*, 1025.
252. Rao, C. N. R.; Kulkarni, G. U.; Thomas, P. J.; Edwards, P. P. *Chem. Eur. J.* **2002**, *8*, 28.
253. Ozin;, G. A.; Arsenault;, A.; Cademartiri, L. *Nanochemistry: A Chemical Approach to Nanomaterials : Edition 2* Royal Society of Chemistry, Cambridge, **2008**.
254. Barnes, W. L.; Dereux, A.; Ebbesen, T. W. *Nature* **2003**, *424*, 824.
255. Hutter, E.; Fendler, J. H. *Adv. Mater.* **2004**, *16*, 1685.
256. Liz-Marzán, L. M. *Langmuir* **2006**, *22*, 32.
257. Mulvaney, P. *Langmuir* **1996**, *12*, 788.
258. Thomas, K. G. In *Nanomaterials Chemistry*; Wiley-VCH Verlag GmbH & Co. KGaA: **2007**, p 185.
259. Kelly, K. L.; Coronado, E.; Zhao, L. L.; Schatz, G. C. *J. Phys. Chem. B* **2003**, *107*, 668.
260. Mie, G. *Annalen der Physik* **1908**, *330*, 377.
261. Jain, P. K.; Lee, K. S.; El-Sayed, I. H.; El-Sayed, M. A. *J. Phys. Chem. B* **2006**, *110*, 7238.
262. Link, S.; El-Sayed, M. A. *J. Phys. Chem. B* **1999**, *103*, 4212.
263. Huang, X.; El-Sayed, M. A. *J. Adv. Res.* **2010**, *1*, 13.
264. Abadeer, N. S.; Murphy, C. J. *J. Phys. Chem. C* **2016**, *120*, 4691.
265. Biswas, A.; Bayer, I. S.; Biris, A. S.; Wang, T.; Dervishi, E.; Faupel, F. *Adv. Colloid Interface Sci.* **2012**, *170*, 2.
266. Christian, G.; Erik, D. *J. Optics A: Pure Appl. Optics* **2006**, *8*, S73.
267. In *Compendium of Chemical Terminology*; IUPAC: **2014**, p 1045.
268. Kumar, A.; Joshi, H.; Pasricha, R.; Mandale, A. B.; Sastry, M. *J. Colloid Interf. Sci.* **2003**, *264*, 396.
269. Wu, S.-H.; Chen, D.-H. *J. Colloid Interf. Sci.* **2004**, *273*, 165.
270. Battocchio, C.; Meneghini, C.; Fratoddi, I.; Venditti, I.; Russo, M. V.; Aquilanti, G.; Maurizio, C.; Bondino, F.; Matassa, R.; Rossi, M.; Mobilio, S.; Polzonetti, G. *J. Phys. Chem. C* **2012**, *116*, 19571.
271. Battocchio, C.; Porcaro, F.; Mukherjee, S.; Magnano, E.; Nappini, S.; Fratoddi, I.; Quintiliani, M.; Russo, M. V.; Polzonetti, G. *J. Phys. Chem. C* **2014**, *118*, 8159.
272. Quiros, I.; Yamada, M.; Kubo, K.; Mizutani, J.; Kurihara, M.; Nishihara, H. *Langmuir* **2002**, *18*, 1413.
273. Aslam, M.; Fu, L.; Su, M.; Vijayamohanan, K.; Dravid, V. P. *J. Mater. Chem.* **2004**, *14*, 1795.
274. Koupanou, E.; Ahualli, S.; Glatter, O.; Delgado, A.; Krumeich, F.; Leontidis, E. *Langmuir* **2010**, *26*, 16909.
275. Rao, C. R. K.; Trivedi, D. C. *Mater. Chem. Phys.* **2006**, *99*, 354.
276. Grubbs, R. B. *Polymer Reviews* **2007**, *47*, 197.
277. He, Z.; Alexandridis, P. *PCCP* **2015**, *17*, 18238.
278. Prechtl, M. H. G.; Campbell, P. S.; Scholten, J. D.; Fraser, G. B.; Machado, G.; Santini, C. C.; Dupont, J.; Chauvin, Y. *Nanoscale* **2010**, *2*, 2601.
279. *Dendrimers and Other Dendritic Polymers*; John Wiley & Sons, Ltd, **2002**.
280. Jansen, J. F. G. A.; de Brabander-van den Berg, E. M. M.; Meijer, E. W. *Science* **1994**, *266*, 1226.
281. Balogh, L.; Tomalia, D. A. *J. Am. Chem. Soc.* **1998**, *120*, 7355.
282. Bao, C.; Jin, M.; Lu, R.; Zhang, T.; Zhao, Y. Y. *Mater. Chem. Phys.* **2003**, *81*, 160.
283. Ooe, M.; Murata, M.; Mizugaki, T.; Ebitani, K.; Kaneda, K. *Nano Lett.* **2002**, *2*, 999.
284. *Nanoparticles and Catalysis*; Wiley-VCH Verlag GmbH & Co. KGaA, **2008**.
285. Rothenberg, G. In *Catalysis*; Wiley-VCH Verlag GmbH & Co. KGaA: **2008**, p 127.
286. Rothenberg, G. In *Catalysis*; Wiley-VCH Verlag GmbH & Co. KGaA: **2008**, p 77.
287. Astruc, D.; Lu, F.; Aranzaes, J. R. *Angew. Chem. Int. Ed.* **2005**, *44*, 7852.
288. Astruc, D. *Inorg. Chem.* **2007**, *46*, 1884.
289. Li, G.; Sproviero, E. M.; McNamara, W. R.; Snoeberger, R. C.; Crabtree, R. H.; Brudvig, G. W.; Batista, V. S. *J. Phys. Chem. B* **2010**, *114*, 14214.
290. Reisner, E.; Powell, D. J.; Cavazza, C.; Fontecilla-Camps, J. C.; Armstrong, F. A. *J. Am. Chem. Soc.* **2009**, *131*, 18457.
291. Balanta, A.; Godard, C.; Claver, C. *Chem. Soc. Rev.* **2011**, *40*, 4973.
292. Bej, A.; Ghosh, K.; Sarkar, A.; Knight, D. W. *RSC Advances* **2016**, *6*, 11446.
293. Djakovitch, L.; Köhler, K.; Vries, J. G. d. In *Nanoparticles and Catalysis*; Wiley-VCH Verlag GmbH & Co. KGaA: **2008**, p 303.
294. Wu, X.-F.; Anbarasan, P.; Neumann, H.; Beller, M. *Angew. Chem. Int. Ed.* **2010**, *49*, 9047.
295. Niu, Y.; Yeung, L. K.; Crooks, R. M. *J. Am. Chem. Soc.* **2001**, *123*, 6840.

296. Kabalka, G. W.; Varma, R. S. In *Comprehensive Organic Synthesis*; Fleming, I., Ed.; Pergamon: Oxford, **1991**, p 363.
297. Eising, R.; Signori, A. M.; Fort, S.; Domingos, J. B. *Langmuir* **2011**, *27*, 11860.
298. Gangula, A.; Podila, R.; M, R.; Karanam, L.; Janardhana, C.; Rao, A. M. *Langmuir* **2011**, *27*, 15268.
299. Huang, X.; Xiao, Y.; Zhang, W.; Lang, M. *Appl. Surf. Sci.* **2012**, *258*, 2655.
300. Safari, J.; Enayati Najafabadi, A.; Zarnegar, Z.; Farkhonde Masoule, S. *Green Chem. Lett. Rev.* **2016**, *9*, 20.
301. Saha, S.; Pal, A.; Kundu, S.; Basu, S.; Pal, T. *Langmuir* **2010**, *26*, 2885.
302. Zeng, J.; Zhang, Q.; Chen, J.; Xia, Y. *Nano Lett.* **2010**, *10*, 30.
303. Solanki, J. N.; Murthy, Z. V. P. *Industrial & Engineering Chemistry Research* **2011**, *50*, 7338.
304. Zhou, Q.; Qian, G.; Li, Y.; Zhao, G.; Chao, Y.; Zheng, J. *Thin Solid Films* **2008**, *516*, 953.
305. Cornelio, B.; Rance, G. A.; Laronze-Cochard, M.; Fontana, A.; Sapi, J.; Khlobystov, A. N. *J. Mater. Chem. A* **2013**, *1*, 8737.
306. Giacalone, F.; Campisciano, V.; Calabrese, C.; La Parola, V.; Liotta, L. F.; Aprile, C.; Gruttadauria, M. *J. Mater. Chem. A* **2016**, *4*, 17193.
307. Giacalone, F.; Campisciano, V.; Calabrese, C.; La Parola, V.; Syrgiannis, Z.; Prato, M.; Gruttadauria, M. *ACS Nano* **2016**, *10*, 4627.
308. Taladriz-Blanco, P.; Hervés, P.; Pérez-Juste, J. *Top. Catal.* **2013**, *56*, 1154.
309. Yang, X.; Fei, Z.; Zhao, D.; Ang, W. H.; Li, Y.; Dyson, P. J. *Inorg. Chem.* **2008**, *47*, 3292.
310. Li, Y.; Hong, X. M.; Collard, D. M.; El-Sayed, M. A. *Org. Lett.* **2000**, *2*, 2385.
311. Miyaura, N.; Suzuki, A. *Chem. Rev.* **1995**, *95*, 2457.
312. Pérez-Lorenzo, M. *J. Phys. Chem. Lett.* **2012**, *3*, 167.
313. Amatore, C.; Jutand, A.; Le Duc, G. *Chem. Eur. J.* **2011**, *17*, 2492.
314. Matos, K.; Soderquist, J. A. *J. Org. Chem.* **1998**, *63*, 461.
315. Smith, G. B.; Dezeny, G. C.; Hughes, D. L.; King, A. O.; Verhoeven, T. R. *J. Org. Chem.* **1994**, *59*, 8151.
316. Deraedt, C.; Astruc, D. *Acc. Chem. Res.* **2014**, *47*, 494.
317. Jiang, X. C.; Yu, A. B. *Langmuir* **2008**, *24*, 4300.
318. Kim, B.-H.; Lee, J.-S. *Mater. Chem. Phys.* **2015**, *149–150*, 678.
319. Blosi, M.; Albonetti, S.; Ortelli, S.; Costa, A. L.; Ortolani, L.; Dondi, M. *New J. Chem.* **2014**, *38*, 1401.
320. Gao, Y.; Ding, X.; Zheng, Z.; Cheng, X.; Peng, Y. *Chem. Commun.* **2007**, 3720.
321. Pradhan, N.; Pal, A.; Pal, T. *Colloids Surf. A* **2002**, *196*, 247.
322. Wunder, S.; Polzer, F.; Lu, Y.; Mei, Y.; Ballauff, M. *J. Phys. Chem. C* **2010**, *114*, 8814.
323. Bingwa, N.; Meijboom, R. *J. Mol. Catal. A: Chem.* **2015**, *396*, 1.
324. Kumar, K. V.; Porkodi, K.; Rocha, F. *Catal. Commun.* **2008**, *9*, 82.
325. Lin, F.-h.; Doong, R.-a. *Appl. Catal. A* **2014**, *486*, 32.
326. Pyne, S.; Samanta, S.; Misra, A. *Solid State Sci.* **2013**, *26*, 1.
327. Rodriguez-Acosta, J. W.; Mueses, M.; #xc1; ngel; Machuca-Mart; #xed; nez, F. *Int. J. Photoenergy* **2014**, *2014*, 9.
328. Zhang, J. S.; Delgass, W. N.; Fisher, T. S.; Gore, J. P. *J. Power Sources* **2007**, *164*, 772.
329. Jana, S.; Ghosh, S. K.; Nath, S.; Pande, S.; Praharaj, S.; Panigrahi, S.; Basu, S.; Endo, T.; Pal, T. *Appl. Catal. A* **2006**, *313*, 41.
330. Narayanan, K. B.; Sakthivel, N. *Bioresour. Technol.* **2011**, *102*, 10737.
331. Li, X.; Wang, J.; Zhang, Y.; Li, M.; Liu, J. *Eur. J. Inorg. Chem.* **2010**, *2010*, 1806.
332. Guella, G.; Patton, B.; Miotello, A. *J. Phys. Chem. C* **2007**, *111*, 18744.
333. Koppel, D. E. *J. Chem. Phys.* **1972**, *57*, 4814.
334. Provencher, S. W. *Comput. Phys. Commun.* **1982**, *27*, 213.
335. Provencher, S. W. *Die Makromolekulare Chemie* **1979**, *180*, 201.
336. Lee, K.-S.; El-Sayed, M. A. *J. Phys. Chem. B* **2006**, *110*, 19220.
337. Dong, X.-Y.; Gao, Z.-W.; Yang, K.-F.; Zhang, W.-Q.; Xu, L.-W. *Catal. Sci. Technol.* **2015**, *5*, 2554.
338. Eckhardt, S.; Brunetto, P. S.; Gagnon, J.; Priebe, M.; Giese, B.; Fromm, K. M. *Chem. Rev.* **2013**, *113*, 4708.
339. Stamplecoskie, K. G.; Scaiano, J. C.; Tiwari, V. S.; Anis, H. *J. Phys. Chem. C* **2011**, *115*, 1403.
340. Rycenga, M.; Cobley, C. M.; Zeng, J.; Li, W.; Moran, C. H.; Zhang, Q.; Qin, D.; Xia, Y. *Chem. Rev.* **2011**, *111*, 3669.
341. Stamplecoskie, K. G.; Scaiano, J. C. *Photochem. Photobiol.* **2012**, *88*, 762.
342. Sakamoto, M.; Fujistuka, M.; Majima, T. *J. Photochem. Photobiol. C* **2009**, *10*, 33.
343. Amendola, V.; Meneghetti, M. *PCCP* **2009**, *11*, 3805.
344. Hada, H.; Yonezawa, Y.; Yoshida, A.; Kurakake, A. *J. Phys. Chem.* **1976**, *80*, 2728.
345. Huang, H. H.; Ni, X. P.; Loy, G. L.; Chew, C. H.; Tan, K. L.; Loh, F. C.; Deng, J. F.; Xu, G. Q. *Langmuir* **1996**, *12*, 909.
346. Xu, G.-n.; Qiao, X.-l.; Qiu, X.-l.; Chen, J.-g. *Colloids Surf. A* **2008**, *320*, 222.
347. Scaiano Juan, C.; Billone, P.; Gonzalez Carlos, M.; Marett, L.; Marin, M. L.; McGilvray Katherine, L.; Yuan, N. In *Pure Appl. Chem.* **2009**; Vol. 81, p 635.
348. Jockusch, S.; Landis, M. S.; Freiermuth, B.; Turro, N. J. *Macromolecules* **2001**, *34*, 1619.
349. Stamplecoskie, K. G.; Scaiano, J. C. *J. Am. Chem. Soc.* **2011**, *133*, 3913.

350. Stamplecoskie, K. G.; Scaiano, J. C. *J. Am. Chem. Soc.* **2010**, *132*, 1825.
351. Krajczewski, J.; Joubert, V.; Kudelski, A. *Colloids Surf. A* **2014**, *456*, 41.
352. Lee, G. P.; Shi, Y.; Lavoie, E.; Daeneke, T.; Reineck, P.; Cappel, U. B.; Huang, D. M.; Bach, U. *ACS Nano* **2013**, *7*, 5911.
353. Tang, B.; Sun, L.; Li, J.; Zhang, M.; Wang, X. *Chem. Eng. J.* **2015**, *260*, 99.
354. Wang, H.; Zheng, X.; Chen, J.; Wang, D.; Wang, Q.; Xue, T.; Liu, C.; Jin, Z.; Cui, X.; Zheng, W. *J. Phys. Chem. C* **2012**, *116*, 24268.
355. Yang, L.-C.; Lai, Y.-S.; Tsai, C.-M.; Kong, Y.-T.; Lee, C.-I.; Huang, C.-L. *J. Phys. Chem. C* **2012**, *116*, 24292.
356. Alexander, J. W. *Surgical Infections* **2009**, *10*, 289.
357. Klasen, H. J. *Burns* **2000**, *26*, 117.
358. Huh, A. J.; Kwon, Y. J. *J. Controlled Release* **2011**, *156*, 128.
359. Rai, M. K.; Deshmukh, S. D.; Ingle, A. P.; Gade, A. K. *J. Appl. Microbiol.* **2012**, *112*, 841.
360. Chernousova, S.; Epple, M. *Angew. Chem. Int. Ed.* **2013**, *52*, 1636.
361. Franci, G.; Falanga, A.; Galdiero, S.; Palomba, L.; Rai, M.; Morelli, G.; Galdiero, M. *Molecules* **2015**, *20*, 8856.
362. Jaiswal, S.; Duffy, B.; Jaiswal, A. K.; Stobie, N.; McHale, P. *Int. J. Antimicrob. Agents* **2010**, *36*, 280.
363. Marambio-Jones, C.; Hoek, E. M. V. *J. Nanopart. Res.* **2010**, *12*, 1531.
364. Feng, Q. L.; Wu, J.; Chen, G. Q.; Cui, F. Z.; Kim, T. N.; Kim, J. O. *J. Biomed. Mat. Res.* **2000**, *52*, 662.
365. Jung, W. K.; Koo, H. C.; Kim, K. W.; Shin, S.; Kim, S. H.; Park, Y. H. *Appl. Environ. Microbiol.* **2008**, *74*, 2171.
366. Jose Ruben, M.; Jose Luis, E.; Alejandra, C.; Katherine, H.; Juan, B. K.; Jose Tapia, R.; Miguel Jose, Y. *Nanotechnology* **2005**, *16*, 2346.
367. Lok, C.-N.; Ho, C.-M.; Chen, R.; He, Q.-Y.; Yu, W.-Y.; Sun, H.; Tam, P. K.-H.; Chiu, J.-F.; Che, C.-M. *Journal of Proteome Research* **2006**, *5*, 916.
368. El Badawy, A. M.; Silva, R. G.; Morris, B.; Scheckel, K. G.; Suidan, M. T.; Tolaymat, T. M. *Environ. Sci. Technol.* **2011**, *45*, 283.
369. Mirzajani, F.; Ghassempour, A.; Aliahmadi, A.; Esmaeili, M. A. *Res. Microbiol.* **2011**, *162*, 542.
370. AshaRani, P. V.; Low Kah Mun, G.; Hande, M. P.; Valiyaveettil, S. *ACS Nano* **2009**, *3*, 279.
371. Choi, O.; Deng, K. K.; Kim, N.-J.; Ross Jr, L.; Surampalli, R. Y.; Hu, Z. *Water Res.* **2008**, *42*, 3066.
372. Liu, J.; Hurt, R. H. *Environ. Sci. Technol.* **2010**, *44*, 2169.
373. Liu, J.; Sonshine, D. A.; Shervani, S.; Hurt, R. H. *ACS Nano* **2010**, *4*, 6903.
374. Xiu, Z.-M.; Ma, J.; Alvarez, P. J. J. *Environ. Sci. Technol.* **2011**, *45*, 9003.
375. Xiu, Z.-m.; Zhang, Q.-b.; Puppala, H. L.; Colvin, V. L.; Alvarez, P. J. J. *Nano Lett.* **2012**, *12*, 4271.
376. Li, W.-R.; Xie, X.-B.; Shi, Q.-S.; Duan, S.-S.; Ouyang, Y.-S.; Chen, Y.-B. *BioMetals* **2011**, *24*, 135.
377. Jover, J.; Bosque, R.; Sales, J. *Dalton Transactions* **2008**, 6441.
378. Holt, K. B.; Bard, A. J. *Biochemistry* **2005**, *44*, 13214.
379. Dibrov, P.; Dzioba, J.; Gosink, K. K.; Häse, C. C. *Antimicrob. Agents Chemother.* **2002**, *46*, 2668.
380. Li, W.-R.; Xie, X.-B.; Shi, Q.-S.; Zeng, H.-Y.; OU-Yang, Y.-S.; Chen, Y.-B. *Appl. Microbiol. Biotechnol.* **2010**, *85*, 1115.
381. Park, H.-J.; Kim, J. Y.; Kim, J.; Lee, J.-H.; Hahn, J.-S.; Gu, M. B.; Yoon, J. *Water Res.* **2009**, *43*, 1027.
382. Gordon, O.; Vig Slenters, T.; Brunetto, P. S.; Villaruz, A. E.; Sturdevant, D. E.; Otto, M.; Landmann, R.; Fromm, K. M. *Antimicrob. Agents Chemother.* **2010**, *54*, 4208.
383. Kim, J. S.; Kuk, E.; Yu, K. N.; Kim, J.-H.; Park, S. J.; Lee, H. J.; Kim, S. H.; Park, Y. K.; Park, Y. H.; Hwang, C.-Y.; Kim, Y.-K.; Lee, Y.-S.; Jeong, D. H.; Cho, M.-H. *Nanomedicine: Nanotechnology, Biology and Medicine* **2007**, *3*, 95.
384. Pal, S.; Tak, Y. K.; Song, J. M. *Appl. Environ. Microbiol.* **2007**, *73*, 1712.
385. Hwang, I.-s.; Hwang, J. H.; Choi, H.; Kim, K.-J.; Lee, D. G. *Journal of Medical Microbiology* **2012**, *61*, 1719.
386. Tan, S.; Erol, M.; Attygalle, A.; Du, H.; Sukhishvili, S. *Langmuir* **2007**, *23*, 9836.
387. Govorov, A. O.; Richardson, H. H. *Nano Today* **2007**, *2*, 30.
388. Sondi, I.; Salopek-Sondi, B. *J. Colloid Interf. Sci.* **2004**, *275*, 177.
389. Agnihotri, S.; Mukherji, S.; Mukherji, S. *Nanoscale* **2013**, *5*, 7328.
390. Rai, M.; Kon, K.; Ingle, A.; Duran, N.; Galdiero, S.; Galdiero, M. *Appl. Microbiol. Biotechnol.* **2014**, *98*, 1951.
391. Ruden, S.; Hilpert, K.; Berditsch, M.; Wadhwani, P.; Ulrich, A. S. *Antimicrob. Agents Chemother.* **2009**, *53*, 3538.
392. Fayaz, A. M.; Balaji, K.; Girilal, M.; Yadav, R.; Kalaichelvan, P. T.; Venketesan, R. *Nanomedicine: Nanotechnology, Biology and Medicine*, *6*, 103.
393. Smekalova, M.; Aragon, V.; Panacek, A.; Prucek, R.; Zboril, R.; Kvitek, L. *The Veterinary Journal* **2016**, *209*, 174.
394. Mosselhy, D. A.; El-Aziz, M. A.; Hanna, M.; Ahmed, M. A.; Husien, M. M.; Feng, Q. *J. Nanopart. Res.* **2015**, *17*, 473.
395. Roupas, A.; Pitton, J. S. *Antimicrob. Agents Chemother.* **1974**, *5*, 186.
396. Brown, A. N.; Smith, K.; Samuels, T. A.; Lu, J.; Obare, S. O.; Scott, M. E. *Appl. Environ. Microbiol.* **2012**, *78*, 2768.
397. Daniel, M.-C.; Astruc, D. *Chem. Rev.* **2004**, *104*, 293.

398. Dreaden, E. C.; Alkilany, A. M.; Huang, X.; Murphy, C. J.; El-Sayed, M. A. *Chem. Soc. Rev.* **2012**, *41*, 2740.
399. Jiang, K.; Smith, D. A.; Pinchuk, A. *J. Phys. Chem. C* **2013**, *117*, 27073.
400. Baffou, G.; Quidant, R.; Girard, C. *Appl. Phys. Lett.* **2009**, *94*, 153109.
401. Huang, X.; El-Sayed, I. H.; Qian, W.; El-Sayed, M. A. *J. Am. Chem. Soc.* **2006**, *128*, 2115.
402. Kaneti, Y. V.; Chen, C.; Liu, M.; Wang, X.; Yang, J. L.; Taylor, R. A.; Jiang, X.; Yu, A. *ACS Applied Materials & Interfaces* **2015**, *7*, 25658.
403. Lee, J.; Govorov, A. O.; Kotov, N. A. *Angew. Chem. Int. Ed.* **2005**, *44*, 7439.
404. Richardson, H. H.; Hickman, Z. N.; Govorov, A. O.; Thomas, A. C.; Zhang, W.; Kordesch, M. E. *Nano Lett.* **2006**, *6*, 783.
405. Lee, S. E.; Liu, G. L.; Kim, F.; Lee, L. P. *Nano Lett.* **2009**, *9*, 562.
406. Buchkremer, A.; Linn, M. J.; Reismann, M.; Eckert, T.; Witten, K. G.; Richtering, W.; von Plessen, G.; Simon, U. *Small* **2011**, *7*, 1397.
407. Blankschien, M. D.; Pretzer, L. A.; Huschka, R.; Halas, N. J.; Gonzalez, R.; Wong, M. S. *ACS Nano* **2013**, *7*, 654.
408. Moridi, N.; Corvini, P. F. X.; Shahgaldian, P. *Angew. Chem. Int. Ed.* **2015**, *54*, 14979.
409. Rojas, M. T.; Koeniger, R.; Stoddart, J. F.; Kaifer, A. E. *J. Am. Chem. Soc.* **1995**, *117*, 336.

Acknowledgements

A special heartfelt thanks to Prof. Lo Meo to whom I owe all my esteem and gratitude for having led me up to this point in my academic career. If I have achieved this important goal I owe it largely to him, my Professor, my Academic Father and Friend, who over the years we have worked together has always supported me from both the professional and emotional points of view. Thanks to the deep trust he has had in my capacity for analysis and to his unrivalled scientific preparation, I have had the opportunity to develop my knowledge of Chemistry and learn a lot of tricks of the trade. No words will ever reflect the respect I owe to him.

I would also like to thank all the members, Professors and Colleagues of the Organic Chemistry Section of the STEBICEF Department where this PhD project was born and developed, for providing me with an almost family environment where it was possible to mature from both the scientific and human points of view. In particular, I express my thanks to Prof. Noto and Prof. Gruttadauria for the possibility they have given me in these years to work in their research groups; and to Prof. Pace and Dr. Palumbo Piccionello for providing me with the equipment needed for some experiments and measurements.

During my time at the FHNW University of Basel, I worked closely with Prof. Shahgaldian and his research group. The seven months I spent in this multidisciplinary as well as multicultural context have been highly formative and stimulating. I also wish to thank all the members of the NanoTeam who, during the time we spent together, always made me feel at home. A special thanks to Prof. Shahgaldian and to Dr. Correro for entrusting me with such an innovative project and for the support and readiness to help they have always demonstrated.

Although there are too many people for me to thank individually I would particularly like to express my gratitude towards Prof. Chillura who, in addition to the important technical support for the various analyses needed in the different moments of the laboratory work, has always given me plenteous and valuable advice during my training path; and also towards Prof. Alduina, Dr. Pisciotta and Prof. Gallo, with whom we investigated the potential applications of the **amCD** in biological systems, an experience which allowed me to learn new aspects of biology.